



SAKARYA ÜNİVERSİTESİ

# FEN BİLİMLERİ ENSTİTÜSÜ DERGİSİ

Sakarya University Journal of Science (SAUJS)



SAKARYA  
ÜNİVERSİTESİ

e-issn: 2147-835X

SAÜ Fen Bil Der/SAUJS

Cilt/Volume: 26

Sayı/Issue: 6

Aralık/December 2022

---

---

**Sakarya Üniversitesi Fen Bilimleri Enstitüsü Dergisi**  
**(Sakarya University Journal of Science)**  
**Cilt/Volume: 26 No/ Issue:6 Aralık/December 2022**  
**Editör Kurulu/Editorial Boards**

---

---

---

---

**Owner**

---

---

Hamza Al, Sakarya University (Turkey)

---

---

**Publishing Manager**

---

---

Hüseyin Özkan Toplan, Metallurgical and Materials Engineering, Sakarya University (Turkey)

---

---

**Editor-in-Chief**

---

---

Ömer Tamer, Physics, Sakarya University (Turkey)

---

---

**Associate Editors**

---

---

Ihsan Hakan Selvi, Information Systems Engineering, Sakarya University (Turkey)

---

---

**Editors**

---

---

Abderrahmane Benbrik, M'Hamed Bougara University at Boumerdes (Algeria)

Abdullah Oğuz Kızılcay, Computer Engineering, Zonguldak Bülent Ecevit University (Turkey)

Ali Cemal Benim, Faculty of Mechanical and Process Engineering, Duesseldorf University of Applied Sciences (Germany)

Ali Demir, Mathematics, Kocaeli University (Turkey)

Aligholi Niaei, Chemistry, Tabriz University (Iran)

Aslı Uçar, Faculty of Health Sciences, Nutrition and dietetics, Ankara University (Turkey)

Asude Ateş, Environmental Engineering, Sakarya University (Turkey)

Bahadır Saygı, Physic, Ege University (Turkey)

Barış Yüce, Engineering Management, Exeter University, UK

Belma Zengin Kurt, Chemistry, Bezmiâlem Vakıf University (Turkey)

Benjamin Durakovic, Department of Industrial Engineering, Bosnia International University of Sarajevo (Bosnia and Herzegovina)

Berrin Denizhan, Industrial Engineering, Sakarya University (Turkey)

Can Serkan Keskin, Chemistry, Sakarya University (Turkey)

Caner Erden, International Trade and Finance, Sakarya University of Applied Sciences (Turkey)

Ceren Tayran, Physic, Gazi University (Turkey)

Cansu Akbulut, Biology, Sakarya University (Turkey)

Ece Ümmü Deveci, Environmental Engineering, Niğde Ömer Halisdemir University (Turkey)

Edgar Perez-Esteve, Food Technology, Polytechnic University of Valencia (Spain)

Elif Ağcakoca, Civil Engineering, Sakarya Applied Science University (Turkey)

Elif Eker Kahveci, Mechanical Engineering, Sakarya University (Turkey)

Fahrettin Horasan, Computer Engineering, Kırıkkale University (Turkey)

Faruk Fırat Çalım, Civil Engineering, Alparslan Türkeş University (Turkey)

Feyza Gurbuz, Industrial Engineering, Erciyes University (Turkey)

Francesco de Paulis, Electrical and Electronics Engineering, University of L'Aquila (Italy)

Gökhan Dok, Civil Engineering, Sakarya Applied Science University (Turkey)

Grazyna S Martynkova, Nanotechnology Centre, VŠB-Technical University of Ostrava · Nanotechnology Centre (Czech Republic)

Grzegorz Jaworski, Physics, Heavy Ion Laboratory, University of Warsaw (Poland)

H. F. Nied, Department of Mechanical Engineering and Mechanics, Lehigh University (U.S.A.)

Hakan Alp, Geophysical Engineering, Cerrahpaşa University (Turkey)

Hatice Esen, Industrial Engineering, Kocaeli University (Turkey)

Hüseyin Aksoy, Biology, Sakarya University (Turkey)

Issa Al-Harty, Civil and Architectural Engineering, Sultan Qaboos University (Oman)

İbrahim Bahadır Başyığıt, Electrical and Electronics Engineering, Isparta Applied Science University (Turkey)

İsmail Hakkı Demir, Architecture, Sakarya University (Turkey)

Kamaruzzaman Sopian, Renewable Energy, Universiti Kebangsaan Malaysia (Malaysia)

Khalifa Al-Jabri, Civil and Architectural Engineering, Sultan Qaboos University (Oman)

Luan Thach Hoang, Mathematics, Texas Tech University (U.S.A.)

Luis A. Materon, Biology, The University of Texas Rio Grande Valley (USA)

M. Hilmi Nişancı, Electrical and Electronics Engineering, Sakarya University (Turkey)

Mahmud Tokur, Metallurgical and Materials Engineering, Sakarya University (Turkey)

Mehmet Emin Aydın, Industrial Engineering, University of Bedfordshire (UK)

Mehmet Uysal, Metallurgical and Materials Engineering, Sakarya University (Turkey)

Mesut Baran, Electrical and Computer Engineering, FREEDM Systems Center, North Carolina State University (U.S.A.)

Miraç Alaf, Metallurgical and Materials Engineering, Bilecik Şeyh Edebali University (Turkey)

Mohammad Sukri bin Mustapa, Faculty of Mechanical & Manufacturing Engineering, Universiti Tun Hussein Onn Malaysia (Malaysia)

Muhammed Fatih Adak, Computer Engineering, Sakarya University (Turkey)

Muhammed Maruf Öztürk, Computer Engineering, Süleyman Demirel University (Turkey)

Murat Güzeltepe, Mathematics, Sakarya University (Turkey)

Murat Sarduvan, Mathematics, Sakarya University (Turkey)

Murat Tuna, Chemistry, Sakarya University (Turkey)

Mustafa Akpınar, Software Engineering, Sakarya University (Turkey)

Mustafa Glfen, Chemistry, Sakarya University (Turkey)  
Nahit Gencer, Chemistry, Balıkesir University (Turkey)  
Nazan Deniz Yn Ertuę, Biology, Sakarya University (Turkey)  
Necati Olgun, Mathematics, Gaziantep University (Turkey)  
Nihan Akıncı Kenanoęlu, Biology, anakkale Onsekiz Mart University (Turkey)  
Oęuz Kurt, Biology, Manisa Celal Bayar University (Turkey)  
Ozan Erdin, Electrical and Electronics Engineering, Yıldız Technical University (Turkey)  
Raja Mazuir Raja Ahsan Shah, Aerospace and Automotive Engineering, Coventry University (United Kingdom)  
Rıfkı Terzioęlu, Electrical and Electronics Engineering, Bolu Abant İzzet Baysal University (Turkey)  
S.C. Yao, Mechanical Engineering, Carnegie Mellon University, PA (U.S.A.)  
Sadık Kaka, Mechanical Engineering, TOBB ETU (Turkey)  
Selma zaę, Mathematics, Hacettepe University (Turkey)  
Seong Jin Park, Department of Mechanical Engineering, Pohang University of Science and Technology (Korea)  
Serap Coęansu Akdemir, Food Engineering, Sakarya University (Turkey)  
Syed Nasar Abbas, Food Engineering, Curtin University (Australia)  
Őenay etin Doęruparmak, Environmental Engineering, Kocaeli University (Turkey)  
Tahsin Turęay, Architecture, Sakarya University (Turkey)  
Tauseef Aized, Mechanical Engineering, University of Engineering and Technology (Pakistan)  
Tuba Tatar, Civil Engineering, Sakarya University (Turkey)  
Tuęrul etinkaya, Metallurgical and Materials Engineering, Sakarya University (Turkey)  
Ufuk Durmaz, Mechanical Engineering, Sakarya University (Turkey)  
Urvir Singh, Electrical and Electronics Engineering, Schweitzer Engineering Laboratories: SEL Inc. (U.S.A.)

## **Guest Editor**

---

---

Ertan Bol, Civil Engineering, Sakarya University (Turkey)  
Soley Ersoy, Mathematics, Sakarya University (Turkey)

## **English Language Editor**

---

---

mer Tamer, Physics, Sakarya University (Turkey)

## **Editorial Assistant**

---

---

Ahmet Erhan Tanyeri, Sakarya University (Turkey)  
Evrım Yksel, Sakarya University (Turkey)

SAKARYA ÜNİVERSİTESİ FEN BİLİMLERİ ENSTİTÜSÜ DERGİSİ  
(SAKARYA UNIVERSITY JOURNAL OF SCIENCE)  
İÇİNDEKİLER/CONTENTS  
Cilt/Volume: 26 – No/Issue6: (ARALIK/DECEMBER-2022)

RESEARCH ARTICLES

Title	Authors	Pages
Investigation of The Effect of Feeding Period in Honey Bee Algorithm	Mustafa KAYA	1071-1083
Comparison of Three-Parameter Weibull Distribution Parameter Estimators with the Maximum Likelihood Method	Lazim KAMBERİ, Senad ORHANİ, Mirlinda SHAQİRİ, Sejhan IDRİZİ	1084-1092
Highly Selective and Sensitive Non-enzymatic Glucose Biosensor Based on Polypyrrole-Borophene Nanocomposite	Gülşen BAYTEMİR	1093-1103
Two New Records for the Fish Fauna of Simenlik-Akgöl Lagoon in Yeşilirmak River Basin (Samsun-Turkey)	Melek ÖZPİÇAK, Semra SAYGIN, Savaş YILMAZ, Nazmi POLAT	1104-1110
Investigation of Parametric, Non-Parametric and Semiparametric Methods in Regression Analysis Structures	Esra YAVUZ, Mustafa ŞAHİN	1111-1116
Synthesis and Structural Characterization of Novel 2-Aminomethyl Quinazolin-4(3H)-ones as Organic Building Blocks	Feyzi Sinan TOKALI	1117-1130
Fluid-Structure Interaction Analysis of Carotid Artery Blood Flow with Machine Learning Algorithm and OpenFOAM	Murad KUCUR, Banu KÖRBAHTİ	1131-1141
Traditional Medicinal Plants Used in Dermatologic Disorders in Ardahan, Iğdır and Kars	Songül KARAKAYA, Zehra KIMIŞOĞLU, Serdar Volkan YILMAZ, Özkan AKSAKAL, Yusuf Ziya SÜMBÜLLÜ, Ümit İNCEKARA, Ahmet POLAT	1142-1158
A New Gradient-Based Surface Defect Detection Method for the Ceramic Tile	Murat Alparslan GÜNGÖR	1159-1169
2,4,6-Tris(p-aminoanilino)-1,3,5-triazine: Synthesis and Electron Paramagnetic Resonance (EPR) Analysis	Özgül KARATAŞ, Yusuf CEYLAN, Ziya Erdem KOÇ	1170-1179
Structural Strength Properties of Waste Textile Fiber Reinforced Cementitious Lightweight Composite Mortars	Şevket Onur KALKAN, Lütfullah GÜNDÜZ	1180-1195
Effect of Different Solvents, Pore-Forming Agent and Solubility Parameter Differences on the Properties of PES Ultrafiltration Membrane	Seren ACARER	1196-1208

Investigation of Pharmaceuticals in Sakarya Sewage Wastewater	Berna KIRIL MERT, Cemil YILMAZ, Nihan ÖZENGİN	1209-1223
Synthesis, DPPH and ABTS Activity of Novel Furfuryl-Chalcone Derivatives	Fatih SÖNMEZ, Enes AKGÜN, Zuhâl ŞAHİN	1224-1232
Perturbation Solution for a Cracked Euler-Bernoulli Beam	Lütfi Emir SAKMAN	1233-1243
Frequency Analysis of Rounded Shaped Inductive Metallic Objects in Waveguides via some PEC Approximations and GSM Method	Ahmet AYDOĞAN	1244-1252
A Phased Array Antenna System of a Millimeter-wave FMCW Radar for Blind Spot Detection of Mobile Robots	Hüseyin Şerif SAVCI	1253-1261
A Note On E-Injective Modules	Abuzer GÜNDÜZ, Osama NAJİ	1262-1266
Stability of Partial Differential Equations by Mahgoub Transform Method	Harun BİÇER	1267-1273
The Fatty Acid Compositions and Textural Properties of Dry Clotted Creams Produced in Different Drying Systems	Esmâ ÇAPA, Bedia ŞİMŞEK	1274-1287



SAKARYA ÜNİVERSİTESİ

# FEN BİLİMLERİ ENSTİTÜSÜ DERGİSİ

Sakarya University Journal of Science  
SAUJS

ISSN 1301-4048 e-ISSN 2147-835X Period Bimonthly Founded 1997 Publisher Sakarya University  
<http://www.saujs.sakarya.edu.tr/>

Title: Investigation of The Effect of Feeding Period in Honey Bee Algorithm

Authors: Mustafa KAYA

Received: 2021-12-02 00:00:00

Accepted: 2022-08-23 00:00:00

Article Type: Research Article

Volume: 26

Issue: 6

Month: December

Year: 2022

Pages: 1071-1083

How to cite

Mustafa KAYA; (2022), Investigation of The Effect of Feeding Period in Honey Bee Algorithm. Sakarya University Journal of Science, 26(6), 1071-1083, DOI: 10.16984/saufenbilder.1031673

Access link

<https://dergipark.org.tr/en/pub/saufenbilder/issue/74051/1031673>

New submission to SAUJS

<http://dergipark.gov.tr/journal/1115/submission/start>



## Investigation of The Effect of Feeding Period in Honey Bee Algorithm

Mustafa KAYA\*<sup>1</sup> 

### Abstract

In the study, it was investigated the ejaculation ability and semen quality of drones, according to feeding with pollen in different periods. In the first step of the study, 16 %, 32 %, 47 %, 63 %, 79 %, and 100 % feeding periods were applied to the drones, for investigating the effect on ejaculation ability, and the semen quality of drones was investigated. While investigating these feeding period effects “0-1”, bonded, and unbounded knapsack optimization problems were used. After the most effective feeding period was determined, this period was applied to the traveling salesman and liquid storage tank problems in the second step of the study. In the analysis of the traveling salesman problem, it was determined the shortest way between two cities. Analysis of the liquid storage tank problem, it was determined the minimum connector areas. As a result, the analysis results showed that the performance of the artificial bee colony algorithm is very good while solving too complex engineering optimization problems.

**Keywords:** Bee colony algorithm, feeding period effect, knapsack problems

### 1. INTRODUCTION

One of the most recent bee-based algorithms is the Bees Algorithm (BA). This algorithm (BA) is a population-based metaheuristic algorithm proposed by Pham et al. study [1], which is based on the behavior of honeybees that is observed when they are foraging for food. Fundamentally, the algorithm performs a kind of exploitative local or neighborhood search combined with an exploratory global search. Pham and Ghanbarzadeh [2], and solving timetabling problems (Yuce et al. [3], Abdullah et al. [4]). The artificial bee colony algorithm is one of the SI algorithms that has been developed by using waggle dance and foraging behaviors of real colonies (Lara [5]. Dongli et al. [6], proposed three modified versions of ABC in order to better-quality results for the optimization problems. In the first

modification, the neighborhood structure changes in the solution updating equation of ABC, in the second modification, a new selection equation is proposed for onlooker bees in order to choose an employed bee and the last modified version of ABC is based on modifications 1, and 2. Banharnsakun et. al. [7], presented a modified method for solution update of the onlooker bees in this study. In their method, the best feasible solutions found so far are shared globally among the entire population. Thus, the new candidate solutions are more likely to be close to the current best solution. Finally, they use a more robust calculation to determine and compare the quality of alternative solutions. We empirically assess the performance of our proposed method on two sets of problems: numerical benchmark functions and image registration applications. The results demonstrate that the proposed

\* Corresponding author: mkaya@aksaray.edu.tr

<sup>1</sup> Aksaray University,

ORCID: <https://orcid.org/0000-0003-3368-0796>





method can produce higher quality solutions with faster convergence than the original ABC higher-qualityt state-of-the-art ABC-based algorithm. Anuara et. al. [8], studied on artificial bee colony with the rate of change technique that models the behavior of scout bee to improve the performance of the standard ABC in terms of exploration is introduced. The technique is called artificial bee colony rate of change (ABC-ROC) because the scout bee process depends on the rate of change on the performance graph, replace the parameter limit. The performance of ABC-ROC is analysed on a set of benchmark problems and also on the effect of the parameter colony size. Furthermore, the performance of ABC-ROC is compared with the state of the art algorithms. Brajevic and Tuba [9] introduced an upgraded artificial bee colony (UABC) algorithm for constrained optimization problems. Our UABC algorithm enhances fine-tuning characteristics of the modification rate parameter and employs modified scout bee phase of the Diwold et. al. [10] studied in detail the influence of ABC's parameters on its optimization behavior. It is also investigated whether the use of OBs is always advantageous. Moreover, we propose two new variants of ABC which use new methods for the position update of the artificial bees. Extensive empirical tests were performed to compare the new variants with the standard ABC and several other metaheuristics on a set of benchmark functions. Our findings show that the ideal parameter values depend on the hardness of the optimization goal and that the standard values suggested in the literature should be applied with care. Moreover, it is shown that in some situations it is advantageous to use OBs but in others it is not. In addition, a potential problem of the ABC is identified, namely that it performs worse on many functions when the optimum is not located at the center of the search space. Finally, it is shown that the new ABC variants improve the algorithm's performance and achieve very good performance in comparison to other metaheuristics under the standard as well as hard optimization goals. Erik Cuevas et. al. [11], explored the use of the Artificial Bee

Colony (ABC) algorithm to compute threshold selection for image segmentation. ABC is an evolutionary algorithm inspired by the intelligent behavior of honey bees which has been successfully employed to solve complex optimization problems. In this approach, an image 1-D histogram is approximated through a Gaussian mixture model whose parameters are calculated by the ABC algorithm. In the model, each Gaussian function represents a pixel class and therefore a threshold point. Unlike the Expectation-Maximization (EM) algorithm, the ABC method shows fast convergence and low sensitivity to initial conditions. Remarkably, it also improves complex time-consuming computations commonly required by gradient-based methods. Experimental results over multiple images with different range of complexity validate the efficiency of the proposed technique with regard to segmentation accuracy, speed, and robustness. The paper also includes an experimental comparison to the EM and to one gradient-based method which ultimately demonstrates a better performance from the proposed algorithm. Tsai et al. [12], proposed a model based on ABC, by employing Newtonian law of universal gravitation in the onlooker bee phase of ABC. Alatas [13], proposed an ABC model that uses chaotic maps for parameter adaptation so as to prevent the ABC to get stuck local minimums. The Rosenbrock's rotational direction method which was designed to cope with specific features of "Rosenbrock's banana function" was applied to ABC in order to increase exploitation and local search abilities of the basic AB Kang et al. [14]. Karaboga and Akay [15], adapted the basic ABC for constrained optimization problems by using Deb's Rules and evaluated the performance of the adapted model on the 13 constrained optimizations in the literature. Kiran et al. [16] added directional information to ABC algorithms, instead of updating more design parameters than one. The performance of proposed approach was examined on well known 9 numerical benchmark functions and obtained results are compared with basic ABC Kirran and Gunduz. Omkar et al. [17] presented

vector evaluated ABC for multi objective design optimization of laminated composite components and compared the performance of vector evaluated ABC with other swarm-based methods.

In the first step of the study, 16 %, 32 %, 47 %, 63 %, 79 %, and 100 % feeding periods applied to the drones, and effect on ejaculation ability, and semen quality of drones was investigated. While investigation these feeding period effects “0-1”, bonded, and unbounded knapsack optimization problems used.

After the most effective feeding period was determined, this period applied to the travelling salesman problem (TSP) to determine the minimum way between two cities, and the liquid storage tank problem to determine the minimum connectors areas.

## 2. ARTIFICIALCAL HONEY BEE COLONY

The Artificial Bee Colony (ABC) algorithm is a relatively new member of swarm intelligence and tries to model the natural behavior of real honey bees in food foraging. Honeybees use several mechanisms to optimally locate food sources and search for new ones. This makes them good candidates for developing new intelligent search algorithms.

### 2.1. Coding

The most significant feature that distinguishes the proposed (ABC) from other operators is the use of codes to represent the design variables. The first step in the application of the (ABC) to a problem is the determination of the most appropriate coding type. The 0-1 knapsack problem binary coding was used, but for other problems permutation coding was used.

### 2.2. Formation of Initial Swarm

While the initial swarm is being formed, its members must not be selected the same, since the members must be chosen randomly. The

suitable selection of swarm size significantly affects the performance of the ABC algorithm.

### 2.3. Evaluation

The (ABC) basically finds the maximum of an unconstrained objective function. To solve a constrained objective minimization function, two transformations need to be made. The first transforms the original objective constrained function into an unconstrained objective function, using the concept of the penalty function. In the second transformation, the unconstrained objective function is transformed to the fitness function.

### 2.4. Selection

A sequential selection method was used. In this method, members are set in order by a linearly decreasing function. The members with the lowest fitness value are removed from the swarm in a defined ratio and members with the highest fitness values replace those removed in the same ratio.

## 3. APPLICATIONS

In the first step of the study, 16 %, 32 %, 47 %, 63 %, 79 %, and 100 % feeding periods applied to the “0-1”, bonded, and unbounded knapsack problems. For 0-1 knapsack problems binary coding was used, but for bounded, and unbounded problems permutation coding was used.

In the second step of the study, the most successful feeding period was applied to the traveling salesman problem.

### 3.1. The “0-1” Knapsack Problem

The “0-1” knapsack problem has two options. These options are 0, and 1. If good’s code become 0, this good will not become in the knapsack, else if good’s code become 1, this good will put in the knapsack. In this problem, 16 %, 32 %, 47 %, 63 %, 79 %, and 100 % feeding periods applied to the “0-1” knapsack problem.

The “0-1” knapsack problem removes the restriction of having only one of each good, but restricts the number  $x_i$  of copies of each kind of good to an integer value  $c_i$ . Mathematically the “0-1” knapsack problem can be formulated using Eq. 1.

Table 1 Items will be put in the knapsack “0-1” knapsack problem

Code	Item	Weight (kN)	Value (\$)	Number
1	Map	2.5	5.225	1
2	Compass	3	7.282	1
3	water	15	1.716	1
4	Sandwich	5	1.716	1
5	Glucose	7	5.225	1
6	Tin	3	3.971	1
7	Banana	6.5	2.475	1
8	Apple	4.5	1.969	1
9	Cheese	4	7.469	1
10	Beer	4.5	3.223	1
11	Suntan cream	6.0	6.369	1
13	T-shirt	3.5	12.716	1
14	Trousers	4.0	20.218	1
15	Umbrella	2.5	7.282	1
16	Waterproof trousers	4.5	25.223	1
17	Waterproof clothes	5.5	37.719	1
18	Note-case	3	1.782	1
19	Sunglasses	2	5.225	1
20	Towel	5	3.971	1
21	Socks	2	1.716	1
22	Book	3.5	7.282	1

In this problem, a tourist wants to take a trip. He has a knapsack for carrying his goods, but knows that he can carry maximum 3 kg weight. He creates a list of what he wants to take for the trip, but the total weight of all goods will not become heavier than 3 kg. Then he add columns

to his need list detailing their weights and a numerical value representing how important each good is for the trip (Table 1).

In this problem the total of the weight of the tourist’s knapsack will not exceed 3 kg and their total value should be maximized. Mathematically the “0-1” knapsack problem can be formulated using Eq. 1:

$W(x)$ =Subject to

$$\sum_{i=1}^n w_i \cdot x_i \leq W, \quad x_i \in \{0,1\} \quad (1)$$

$$\phi(s) = W(x)(1 + KC) \quad (2)$$

K: a coefficient selected for the problem taken as 5 in this study.

In the first transformation, the constrained objective function  $\phi(s)$  was transformed into an unconstrained objective function  $\phi(x)$  as shown in Eq. 3.

$$\phi(x) = \sum \phi(s) / \phi(s)_{\max} \quad (3)$$

In the second transformation, the unconstrained objective function was converted to an F(s) fitness function in Eq. 4.

$$F(s) = \phi(x)_{\max} - \phi(x) \quad (4)$$

Using the “0-1” knapsack problem, the highest nectar quality was 0.756 for 79 %, the feeding period, and the average nectar quality was 0.69 for this period. The highest nectar quality was 8.62 % higher than the average nectar quality for this problem. In this analysis, 79 % of this feeding period provided 100 drones, and 16 % feeding period provided only 5 drones in this swarm (Table 2). The good’s maximum price for 0.756 nectar quality was 1918.510 \$, and the goods’ average price was 1818.430 \$. The goods maximum price is 5.50 % higher than their average price.

Table 2 The nectar quality obtained from different feeding periods with pollen for “0-1” knapsack problem

	16 %	32 %	47 %	63 %	79 %	100 %
Run 1	0.572	0.745	0.723	0.756	0.615	0.745
Run 2	0.658	0.615	0.572	0.766	0.702	0.820
Run 3	0.529	0.658	0.756	0.626	0.680	0.723
Run 4	0.442	0.680	0.637	0.680	0.637	0.637
Run 5	0.723	0.734	0.658	0.745	0.723	0.766
Run 6	0.626	0.777	0.691	0.615	0.550	0.507
Run 7	0.680	0.723	0.529	0.518	0.940*	0.572
Run 8	0.399	0.637	0.734	0.777	0.615	0.626
Run 9	0.572	0.658	0.766	0.745	0.756	0.594
Run 10	0.486	0.756	0.6156	0.734	0.745	0.766
Average	0.569	0.698	0.676	0.696	0.693	0.676
Best	0.723	0.734	0.658	0.745	0.940*	0.766
Price (\$)	1897.1	1785.3	1867.9	1918.51*	1787.6	1695.3

### 3.2. The Bounded Knapsack Problem (BKP)

In this problem, 16 %, 32 %, 47 %, 63 %, 79 %, and 100 % feeding periods applied to the bounded knapsack problem.

The BKP places have an upper bound on the number of copies of each kind of goods. Mathematically, the bounded knapsack problem can be formulated using Eq. 9. In this problem, a store boss wants to carry his computer warehouse to another one. He has twenty types, and 12.815 parts (monitors, keyboards, mouse, sound cards, graphics card, TV cards, modem etc.) in his old warehouse. His computer parts total volume 35.72 m<sup>3</sup>, but his new warehouse capacity is only 20 m<sup>3</sup>. As a result, he can carry only 20 m<sup>3</sup> expensive parts to his new warehouse (Table 3).

Table 3 Items in the computer warehouse; bounded knapsack problem

	Name	Number	Volume (cm <sup>3</sup> )	Amount (\$)	Total volume (m <sup>3</sup> )	Total Amount (\$)
1	Monitor	32000	40000	225	7296000	51300
2	Keyboard	960	1200	12	288000	3600
3	Mouse	144	180	10	69120	4800
4	Sound cards	600	750	30	288000	14400
5	Graphic card	600	750	85	324000	45900
6	Modem	600	750	15	432000	10800
7	Speaker	960	1200	20	864000	18000
8	Camera	518	648	30	248640	14400
9	Hard disk	480	600	67	201600	28140
10	DVD drives	1200	1500	38	504000	15960
11	Floppy disk	480	600	20	172800	7200
12	Case	36000	45000	30	17280000	14400
13	Power	2592	3240	10	1555200	6000
14	Motherboard	2400	3000	120	1440000	72000
15	Memory	58	72	15	174000	45000
16	Scanner	8000	10000	40	2640000	13200
17	Flash drive	16	20	20	57600	72000
18	Adaptor	480	600	15	288000	9000
19	Fan	256	320	3	107520	1260
20	Ethernet	136	170	10	57120	4200

$$W(x) = \sum_{i=1}^n w_i \cdot x_i \quad \text{Subject to}$$

$$\sum_{i=1}^n w_i \cdot x_i \leq W, \quad x_i \in \{0, \dots, c_i\} \quad (5)$$

In the first transformation, the constrained objective function  $\phi(s)$  was transformed into an unconstrained objective function  $\phi(x)$  as shown in Eq. 6.

$$\phi(x) = \sum \phi(s) / \phi(s)_{\max} \quad (6)$$

Table 4 The nectar quality obtained from different feeding period with pollen for bounded knapsack problem

	0.025 %	0.050 %	0.1 %	0.25 %	0.5 %	1 %
Run 1	0.462	0.475	0.759	0.745*	0.598	0.773
Run 2	0.551	0.553	0.874	0.672	0.579	0.518
Run 3	0.427	0.444	0.713	0.735	0.722	0.739
Run 4	0.649	0.639	0.885	0.682	0.484	0.612
Run 5	0.293	0.327	0.540	0.577	0.579	0.612
Run 6	0.293	0.327	0.540	0.577	0.579	0.612
Run 7	0.507	0.514	0.816	0.745	0.807	0.391
Run 8	0.703	0.444	0.724	0.567	0.636	0.663
Run 9	0.792	0.530	0.839	0.514	0.465	0.569
Run 10	0.605	0.600	0.598	0.593	0.437	0.450
Average	0.528	0.485	0.729	0.653	0.589	0.594
Best	0.427	0.507	0.551	0.745*	0.676	0.774
Price (\$)	35712.3 5	32927.4 5	34389.4 3	35824.1 7*	35627.1 7	33762.4 5

In the second transformation, the unconstrained objective function  $\phi(x)$  was converted to an  $F(s)$  fitness function in Eq. 7.

$$F(s) = \phi(x)_{\max} - \phi(x) \quad (7)$$

Using the bounded knapsack problem, the highest nectar quality was 0.952 for 63 % feeding period, and the average nectar quality was 0.501 for 16 % feeding period. The highest nectar quality was 16.36 % higher than the average nectar quality for this problem. In this analysis, 63 % of the feeding period provided 50 drones, and 16 % feeding period provided only 5 drones in this swarm (Table 4). For the same knapsack problem, the maximum price of 0,952 nectar quality was 34918.510 \$. The computer part's maximum price was 7.71 % bigger than average price.

### 3.3. The Unbounded Knapsack Problem (UKP)

In this problem, 16 %, 32 %, 47 %, 63 %, 79 %, and 100 % feeding periods applied to the unbounded knapsack problem. The UKP places no upper bound on the number of copies of each kind of goods.

The unbounded knapsack problem (UKP) places no upper bound on the number of copies of each kind of good and can be formulated as above except for that, the only restriction on  $x_i$  is that it is a nonnegative integer. Mathematically the unbounded knapsack problem can be formulated using Eq. 8:

$$W(x) = \sum_{i=1}^n w_i \cdot x_i$$

$$\text{Subject to } \sum_{i=1}^n w_i \cdot x_i \leq W, \quad 0 \leq x_i \leq \infty \quad (8)$$

In this problem; a greengrocer wants to buy fruits with his all money. He has 100,000 USD dollars, and can buy fruits with this money. For the greengrocer fruits kind, weight, or volume does not important, because he wants to buy profitable fruits, with his all money, and want to earn maximum money from this trade (Table 5).

$$\phi(s) = W(x)(1 + KC) \quad (9)$$

K: a coefficient selected for the problem taken as 5 in this study.

In the first transformation, the constrained objective function  $\phi(s)$  was transformed into an unconstrained objective function  $\phi(x)$  as shown in Eq. 10.

$$\phi(x) = \sum \phi(s) / \phi(s)_{\max} \quad (10)$$

In the second transformation, the unconstrained objective function  $\phi(x)$  was converted to an  $F(s)$  fitness function in Eq. 11.

$$F(s) = \phi(x)_{\max} - \phi(x) \tag{11}$$

Using the unbounded knapsack problem, the highest nectar quality was 0.704 for a 63 % feeding period, and the average nectar quality was 0.61 for a 16 % feeding period.

Table 5 Kind of fruits in the greengrocer store; unbounded knapsack problem

	Name	Weight (kg)	Volume (m <sup>3</sup> )	Amount (\$)	Total Amount (\$)
1	Apple	0 ≤ weight < ∞	300	1.5	1.5 ≤ (TA) < 100.000\$
2	Pear	0 ≤ weight < ∞	300	2.2	2.2 ≤ (TA) < 100.000\$
3	Orange	0 ≤ weight < ∞	300	1.6	1.6 ≤ (TA) < 100.000\$
4	Banana	0 ≤ weight < ∞	300	3.5	3.5 ≤ (TA) < 100.000\$
5	Kangerine	0 ≤ weight < ∞	300	1.6	1.6 ≤ (TA) < 100.000\$
6	Kuince	0 ≤ weight < ∞	300	1.5	1.5 ≤ (TA) < 100.000\$
7	Kherry	0 ≤ weight < ∞	300	4.2	4.2 ≤ (TA) < 100.000\$
8	Alligator pear	0 ≤ weight < ∞	300	1.3	1.3 ≤ (TA) < 100.000\$
9	Mango	0 ≤ weight < ∞	300	3.2	3.2 ≤ (TA) < 100.000\$
10	Krapes	0 ≤ weight < ∞	300	1.5	1.5 ≤ (TA) < 100.000\$
11	Blackberry	0 ≤ weight < ∞	300	2.3	2.3 ≤ (TA) < 100.000\$
12	Kiwi	0 ≤ weight < ∞	300	2.4	2.4 ≤ (TA) < 100.000\$
13	Grapefruit	0 ≤ weight < ∞	300	15.0	15.0 ≤ (TA) < 100.000\$
14	Pepino	0 ≤ weight < ∞	300	4.2	4.2 ≤ (TA) < 100.000\$
15	Peach	0 ≤ weight < ∞	300	2.5	2.5 ≤ (TA) < 100.000\$
16	Apricot	0 ≤ weight < ∞	300	2.1	2.1 ≤ (TA) < 100.000\$
17	Plum	0 ≤ weight < ∞	300	1.5	1.5 ≤ (TA) < 100.000\$
18	Pomegranate	0 ≤ weight < ∞	300	1.5	1.5 ≤ (TA) < 100.000\$
19	Raspberry	0 ≤ weight < ∞	300	3.0	3.0 ≤ (TA) < 100.000\$
20	Pineapple	0 ≤ weight < ∞	300	4.0	4.0 ≤ (TA) < 100.000\$

Fruit weight between 0 kg and ∞  
 Total amount (TA) between every unit amount and 100.000\$

The highest nectar quality was 11.71 % higher than the lowest nectar quality for this problem. In this analysis, 63 %, of the feeding period provided only 50 drones, and 16 % feeding period provided only 5 drones in this swarm (Table 6). For the same problem, the fruit maximum price of 0.704 nectar quality was 98.700 \$, and the average was 94.610 \$. Fruits maximum price was 4.32 % bigger than their average price.

Table 6 The nectar quality obtained from different feeding period with pollen for unbounded knapsack problem

	0.025 %	0.050 %	0.1 %	0.25 %	0.5 %	1 %
Run 1	0.508	0.593	0.645	0.699	0.627	0.618
Run 2	0.606	0.691	0.742	0.604	0.607	0.414
Run 3	0.469	0.555	0.606	0.661	0.758	0.591
Run 4	0.713	0.798	0.752	0.613	0.508	0.489
Run 5	0.322	0.408	0.459	0.519	0.607	0.499
Run 6	0.323	0.408	0.459	0.519	0.607	0.467
Run 7	0.557	0.642	0.697	0.704*	0.847	0.312
Run 8	0.773	0.555	0.616	0.510	0.667	0.530
Run 9	0.871	0.662	0.713	0.462	0.488	0.455
Run 10	0.665	0.751	0.508	0.443	0.458	0.366
Average	0.580	0.606	0.619	0.598	0.617	0.474
Best	0.871	0.662	0.713	0.704*	0.488	0.455
Price(\$)	96143.54	89973.73	94385.19	97612.32*	93786.61	89827.72

### 3.4. Travelling Salesman Problem (TSP)

The travelling salesman problem (TSP) is an integer program that gives the shortest route when the distance between the pairs of points is known and each point is visited only once. It is one of the few integer algorithm-based programs described in the literature. The TSP is also a way of collecting and distributing the necessary parts of the objects in the modeling system, thus maximizing the profit while minimizing the cost using the shortest way. In

this problem, a salesman wants to sell his goods in  $n$  number of cities and he wants to visit all the cities using the shortest route. Hence, the salesman has a choice of  $n$  cities of  $\frac{1}{2}(n-1)!$  different routes. The salesman must travel to 32 cities, visiting each city only once, and begin by travelling from city A to city B. This means there are  $8.05 \times 10^{32}$  different routes for 32 cities (Fig. 1.).

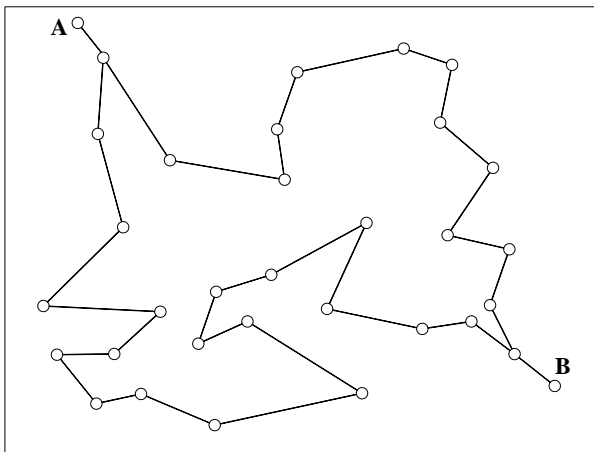


Figure 1 Optimum solution for TSP by using GA

For the TSP the objective function  $W(x)$  is given in Eq. 12

$$\min W(x) = \sum_{k=1}^{nk} L_k \tag{12}$$

Where  $L_k$  is the distance between the two cities.

The constrained objective function was transformed into an unconstrained objective function  $\phi(s)$  as shown in Eq. 16,

$i$ : the number of the first city

$j$ : the number of the second city

$x_i$  and  $y_i$ : the coordinates of the first city

$x_j$  and  $y_j$ : the coordinates of the second city

When the salesman goes to the target city from the starting city then;

If  $x_i > x_j$

$$g(x) = \sqrt{((x_i - x_j)^2 + (y_i - y_j)^2)} \tag{13}$$

Else

$$g(x) = \left[ \sqrt{((x_i - x_j)^2 + (y_i - y_j)^2)} \right] \times 100 \tag{14}$$

$$G = \sum g(x) \tag{15}$$

$$\phi(s) = W(x)(1 + KG) \tag{16}$$

$K$ : a coefficient selected for the problem, taken as 10 in this study.

$g(x)$ : a negligence coefficient thmostas calculated as follows;

In the first transformation, the constrained objective function was transformed into an unconstrained objective function  $\phi(x)$  as given in Eq. 19:

$$\phi(x) = \sum \phi(s) / \phi_{\max} \tag{17}$$

In the second transformation in Eq. 20 the unconstrained objective function  $\phi(x)$  was converted to the fitness function  $F(s)$

$$F(s) = \phi_{\max} - \phi(x) \tag{18}$$

For the travelling salesman problem 79 %, feeding period was used to obtain the shortest way. Because this feeding period had used previous knapsack problems and gave the highest nectar quality. For the travelling salesman problem, the shortest way was found 2718 km, and this way 5.78 % shorter than average way length (Table 7).



Table 7 The result of runs for traveling salesman problem (km)

Run 1	Run 2	Run 3	Run 4	Run 5	Run 6	Run 7	Run 8	Run 9	Run 10
2944	2907	2718	2865	2870	2886	2827	2923	2899	2918
Average way (km): 2885.72 km									
Minimum way (km): 2718 km									

### 3.5. Tsunami Force Effect to The Liquid Storage Tank Problem

The tsunami load effects should be considered in the design of vertical evacuation structures, namely; hydrostatic forces, buoyant forces, hydrodynamic forces, impulsive forces, debris impact forces, debris damming forces, uplift forces, and additional gravity loads from retained water on elevated floors Kang et al. (2011). In this problem minimum liquid storage tank twelve connectors area which connecting storage tank floor to the ground under different height and velocity tsunami waves.

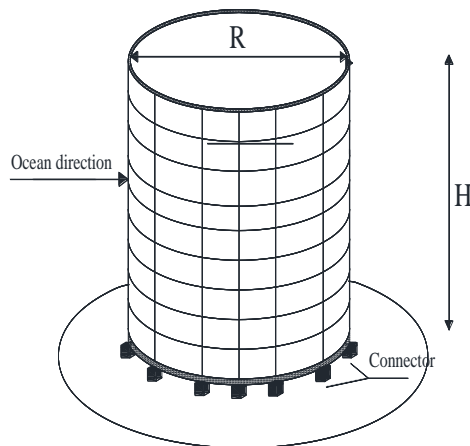


Figure 2 Liquid Storage Tank view

In this problem, it was determined the liquid storage tank's twelve connectors area under debris impact effect, and hydrostatic forces. In the problem, tsunami wave length is 7.30 m, tsunami wave speed is 30-50 km/h, tank diameter is 20 m, and tank height is 40 m (Fig.2).

### 3.5.1. Hydrostatic force

Hydrostatic forces occur when standing or slowly moving water encounters a structure or structural component. This force always acts perpendicular to the surface of the component of interest. It is caused by an imbalance of pressure due to a differential water depth on opposite sides of a structure or component. Hydrostatic forces may not be relevant to a structure with a finite (i.e., relatively short) breadth, around which the water can quickly flow and fill in on all sides. Hydrostatic forces are usually important for long structures such as sea walls and dikes, or for evaluation of an individual wall panel where the water level on one side differs substantially from the water level on the other side FEMA [18].

The horizontal hydrostatic force on a wall panel can be computed using Eq. 19.

$$F_h = P_c \cdot A_w = \frac{1}{2} \rho_s \cdot g \cdot b \cdot h_{max}^2 \quad (19)$$

$$M_h = F_h \cdot \frac{d}{3} \quad (20)$$

Where  $P_c$  is the hydrostatic pressure,  $A_w$  is the wetted area of the panel,  $\rho_s$  is the fluid density including sediment,  $g$  is the gravitational acceleration,  $b$  is the breadth (width) of the wall, and  $h_{max}$  is the maximum water height above the base of the wall at the structure location.

### 3.5.2. Impact force

The impact force from waterborne debris (e.g., floating drift wood, boats, shipping containers, automobiles, buildings) can be a dominant cause of building damage. Unfortunately, it is difficult to estimate this force accurately. The debris impact force can be estimated using Eq. 21.

$$F_i = C_m \cdot U_{max} \sqrt{k \cdot m} \quad (21)$$

$$M_i = F_i \cdot d_i \quad (22)$$

Where  $C_m$  is the added mass coefficient,  $U_{max}$  is the maximum flow velocity carrying the debris at the site, and  $m$  and  $k$  are the mass and the effective stiffness of the debris, respectively. It is recommended that the added mass coefficient be taken as  $C_m = 2.0$ . Unlike other forces, impact forces are assumed to act locally on a single member of the structure at the elevation of the water surface FEMA (2018).

$$\sum M = M_h + M_i \tag{23}$$

$$M_{net} = \sum M - \pi \cdot r^2 \cdot h \cdot \gamma_{oil} \tag{24}$$

In this problem permutation coding type was used. The connectors diameters and their codes were given in Table 8. Individual length is equal to the number of variable groups (connector number) in this problem. Randomly determined an individual was given in Table 9.

Table 8 Connector reinforcement diameters and codes

Diameter	Ø24	Ø28	Ø32	Ø36	Ø40	Ø44	Ø48	Ø52
Code	1	2	3	4	5	6	7	8

Where,  $A_n$  is the reinforcement area,  $\rho$  is the specific gravity of reinforcement,  $l_n$  is the reinforcement length. The constrained objective function was transformed into an unconstrained objective function  $\phi(x)$  as expressed in Eq. 31.

Table 9 Randomly selected an individual sites codes, and connectors diameters

Number	1	2	3	4	5	6	7	8
Site code	7	5	3	8	9 6	2	7	1
Diameters	Ø48	Ø40	Ø32	Ø52	Ø44	Ø28	Ø48	Ø24

$$\min W(x) = \sum_{i=1}^n l_n \cdot A_n \cdot \sigma_n \tag{25}$$

$$g_i(x) = \frac{M_{net}}{\sum_{i=1}^n l_n \cdot A_n \cdot \sigma_n} - 1 \tag{26}$$

$$\text{If } g_i(x) \geq 0 \quad c_i = g_i(x) \tag{27}$$

$$\text{If } g_i(x) < 0 \quad c_i = g_i(x) \cdot 100 \tag{28}$$

$$C = \sum c_i \tag{29}$$

$$\phi(s) = W(x)(1 + KC) \tag{30}$$

K: a coefficient selected for the problem taken to be 10 in this study.

$c_i$ : negligence coefficient and calculated as follows;

In the first transformation, the constrained objective function  $\phi(s)$  was transformed to an unconstrained objective function  $\phi(x)$  as expressed in Eq. 31.

$$\phi(x) = \sum \phi(s) / \phi(s)_{max} \tag{31}$$

Where  $Fe_i$  is the required force met by reinforcements in the x or y direction in the ith zone,  $f_{yd}$  is the yield strength of reinforcement, and  $ns$  is the number of reinforcements in the ith zone.

In the 2nd transformation, the unconstrained objective function  $\phi(x)$  was converted to a fitness function  $F(s)$ . This transformation was achieved using the maximum of the  $i$ th element of the unconstrained objective function. The fitness values of the members were calculated according to Eq. 32 as follows;

$$F(s) = \phi(x)_{max} - \phi(x) \tag{32}$$

For the liquid storage tank problem 79 %, feeding period was used to obtain the lowest total connectors areas. Because this feeding

period had used previous knapsack problems and gave the highest nectar quality.

For the liquid storage tank problem, the minimum 8 connectors area in the tank problem

was 21991.8 mm<sup>2</sup>, and connectors average area was 23508.81mm<sup>2</sup>. Minimum area was 6.45 % less than average area (Table 10).

Table 10 Connector areas determined for liquid storage tank (mm<sup>2</sup>)

	1	2	3	4	5	6	7	8	Total area (mm <sup>2</sup> )
Run 1	1019.03	805.11	1018.63	805.11	1257.27	1521.03	1809.91	3216.63	11452.72
Run 2	1258.47	1258.47	617.91	1258.47	1019.83	1258.47	2464.23	2828.47	11452.72
Run 3	1521.65	1019.25	805.73	805.73	1521.65	1810.53	2124.53	3631.73	11452.72
Run 4	1020.03	1258.67	1020.03	1258.67	1020.03	1811.31	2125.31	2828.67	11452.72
Run 5	1257.95	1019.31	1019.31	805.79	1521.71	1521.71	1810.59	3217.31	11452.72
Run 6	1698.76	1421.19	794.44	1196.36	1497.57	1537.87	2640.76	3394.36	11452.72
Run 7	1259.34	807.18	807.18	1259.34	1523.1	1811.98	2125.98	3633.18	11452.72
Run 8	1021.48	1021.48	619.56	807.96	1260.12	1523.88	1812.76	2830.12	11452.72
Run 9	1523.07	807.15	807.15	1259.31	1259.31	1811.95	1811.95	3218.67	11452.72
Run 10	1258.17	1258.17	806.01	1019.53	1019.53	1521.93	2124.81	3632.01	11452.72

Average liquid storage tank connectors area

#### 4. CONCLUSIONS

In the study, it was investigated to the effect of feeding with pollen in different periods on the ejaculation ability and semen quality of drones. In the first stage of the study "0-1", bounded, and unbounded knapsack problems were used in this comparison. In the analysis, the maximum nectar quality was obtained from Using 79 % fertilization fault ratio for "0-1" knapsack problem, for this fertilization fault ratio drone number is 100, and this drone numbers enough for a 20.000 people swarm. The maximum nectar quality was obtained from 63 % fertilization fault ratio for bounded, and unbounded knapsack problems. For this fertilization fault ratio is 50 drones, and this drone numbers too less for a necessary drone number for a 20.000 people swarm. Using 79 % unfertilization ratio produced successful results in the determination of the highest prices of the goods in the tourist's knapsack, highest prices of the computer parts which the store boss carried them from old warehouse to a new warehouse, and a greengrocer wanted to buy fruits with his all money, and he won the highest money from this trade. In the second

step of the study, while it was determined the travelling salesman problem, and minimum liquid storage tank connectors diameters 79 % fertilization fault ratio were used. Using 79 % fertilization ratio provided higher nectar quality than other fertilization ratios. While determining the shortest way using the same unfertilization ratio, provided the most successful result in traveling salesman problem.

Using a 79 % fertilization ratio provided higher nectar quality than other fertilization ratios. While determining the optimum 8 connectors area for liquid storage tanks using the same unfertilization ratio, provided the most successful result in liquid storage tank connector areas between the tank and ground. It was seen from the analysis, if the fertilization ratio increases, queen and worker bee numbers decrease, but drones number increases. Else if the fertilization fault ratio decreases queen and worker bee numbers increase, but drone number decreases. In this study, the optimum drone number was determined as 100 for this swarm.

**Acknowledgments**

I would like to express our great appreciation to the team during the planning and development of this research.

**Funding**

This study did not receive any specific grant from funding agencies in the public, commercial, or not-for-profit sectors.

**Authors' Contribution**

The author contributed equally to the study.

**The Declaration of Conflict of Interest/  
Common Interest**

No conflict of interest or common interest has been declared by the authors.

**The Declaration of Ethics Committee  
Approval**

This study does not require ethics committee permission or any special permission.

**The Declaration of Research and Publication  
Ethics**

The authors of the paper declare that they comply with the scientific, ethical and quotation rules of SAUJS in all processes of the paper and that they do not make any falsification on the data collected. In addition, they declare that Sakarya University Journal of Science and its editorial board have no responsibility for any ethical violations that may be encountered, and that this study has not been evaluated in any academic publication environment other than Sakarya University Journal of Science.

**REFERENCES**

- [1] D. Pham, A. Ghanbarzadeh, E. Koc, S. Otri, S. Rahim, M. Zaidi, "The Bees Algorithm A Novel Tool For Complex Optimization Problems", Proceedings of the 2nd Virtual International Conference on Intelligent Production Machines and Systems (EPROMS 2006). Elsevier Science Ltd, Cardiff, UK, 2006.
- [2] D. Pham, A. Ghanbarzadeh, "Multiobjective Optimization Using The Bees Algorithm", 3rd International Virtual Conference on Intelligent Production Machines and Systems (EPROMS 2007), Whittles, Dunbeath, Scotland, pp. 111-116, 2007.
- [3] B. Yuce, D. Pham D, M. Packianather, E. Mastrocinque, "An Enhancement To The Bees Algorithm With Slope Angle Computation And Hill Climbing Algorithm And Its Applications In Scheduling And Continuous Type Optimization Problem", Production & Manufacturing Research, vol. 3, pp. 3-19, 2015.
- [4] S. Abdullah, M. Alzaqebah, "A hybrid Self Adaptive Bees Algorithm For Examination Timetabling Problems", Applied Soft Computing, vol. 13, pp. 3608-3620, 2013.
- [5] C. Lara, JJ. Flores, F. Calderón, "Solving A School Timetabling Problem Using A Bee Algorithm", Advances in Artificial Intelligence. Springer, Berlin, Heidelberg, 2008.
- [6] Z. Dongli, G. Xinping, T. Yinggan, T. Yong, "Modified Artificial Bee Colony Algorithms for Numerical Optimization", in Proc. 3rd International Workshop on Intelligent Systems and Applications, 2011, pp. 1-4, 2011.
- [7] A. Banharnsakun, T. Achalakul and B. Sirinaovakul B, "The best-so-far selection in Artificial Bee Colony algorithm", Applied Soft Computing, Vol. 11, no. 2, pp. 2888-2901, 2011.
- [8] S. Anusara, A. Selamatab R. Sallehuddin, "A modified scout bee for artificial bee colony algorithm and its performance on optimization problems", Journal of King Saud University - Computer and

- Information Sciences, vol 28, no. 4, pp. Pages 395-406, 2016.
- [9] I. Brajevic, M. Tuba, "An upgraded artificial bee colony (ABC) algorithm for constrained optimization problems", *Manufacturing*, vol. 24, pp. 729–740, 2013.
- [10] K. Diwold, A. Andrej, A. Scheidler, "Middendorf M, Performance evaluation of artificial bee colony optimization and new selection schemes", *Memetic Computing*, vol. 3, pp. 149-162, 2011.
- [11] E. Cuevas, F. Sención, D. Zaldivar, M. Pérez-Cisneros and H. Sossa, "A multi-threshold segmentation approach based on Artificial Bee Colony optimization", *Applied Intelligence*, vol. 37, pp. 321–336, 2012.
- [12] PW. Tsai, JS. Pan, BY. Liao, SC. Chu (2009), "Enhanced Artificial Bee Colony Optimization", *International Journal of Innovative Computing. Information and Control*, vol. 5, pp. 5081–5092, 2009.
- [13] B. Alatas, "Chaotic Bee Colony Algorithms for Global Numerical Optimization", *Expert System Application*, vol. 37 (2010) pp. 5682–5687, 2010.
- [14] F. Kang, J. Lie, Z. Ma, "Rosenbrock Artificial Bee Colony Algorithm for Accurate Global Optimization of Numerical Functions", *Information Sciences* vol. 181, pp. 3508–3531, 2011.
- [15] D. Karaboga, B. Akay, "A Modified Artificial Bee Colony (ABC) Algorithm for Constrained Optimization Problems", *Applied. Soft Computing*, vol. 11, pp. 3021–3031, 2011.
- [16] MS. Kıran, M. Gündüz, "A Novel Artificial Bee Colony-Based Algorithm for Solving the Numerical Optimization Problems", *International Journal of Innovative Computing. Information and Control*, vol. 9, pp. 6107–6121, 2012.
- [17] SN. Omkar, J. Senthilnath, R. Khandelwal, R. GN. Naik, S. Gopalakrishnan, "Artificial Bee Colony (ABC) for Multi-Objective Design Optimization of Composite Structures", *Applied. Soft Computing*, vol. 11, pp. 489–499, 2011.
- [18] FEMA P646, "Guidelines for Design of Structures for Vertical Evacuation from Tsunamis", (2008).



SAKARYA ÜNİVERSİTESİ

# FEN BİLİMLERİ ENSTİTÜSÜ DERGİSİ

Sakarya University Journal of Science  
SAUJS

ISSN 1301-4048 e-ISSN 2147-835X Period Bimonthly Founded 1997 Publisher Sakarya University  
<http://www.saujs.sakarya.edu.tr/>

Title: Comparison of Three-Parameter Weibull Distribution Parameter Estimators with the Maximum Likelihood Method

Authors: Lazim KAMBERİ, Senad ORHANİ, Mirlinda SHAQİRİ, Sejhan IDRİZİ

Received: 2022-06-29 00:00:00

Accepted: 2022-09-03 00:00:00

Article Type: Research Article

Volume: 26

Issue: 6

Month: December

Year: 2022

Pages: 1084-1092

How to cite

Lazim KAMBERİ, Senad ORHANİ, Mirlinda SHAQİRİ, Sejhan IDRİZİ; (2022), Comparison of Three-Parameter Weibull Distribution Parameter Estimators with the Maximum Likelihood Method. Sakarya University Journal of Science, 26(6), 1084-1092, DOI: 10.16984/saufenbilder.1137262

Access link

<https://dergipark.org.tr/en/pub/saufenbilder/issue/74051/1137262>

New submission to SAUJS

<http://dergipark.gov.tr/journal/1115/submission/start>

## Comparison of Three-Parameter Weibull Distribution Parameter Estimators with the Maximum Likelihood Method

Lazim KAMBERI<sup>2</sup> , Senad ORHANI\*<sup>1</sup> , Mirlinda SHAQİRİ<sup>2</sup> , Sejhan IDRIZI<sup>2</sup> 

### Abstract

Important distributions used to model and analyse data in various real-life sciences such as natural sciences, engineering, and medicine are the Weibull, Weibull exponential, and Weibull Rayleigh distribution. The main objective of this paper is to determine the best evaluators and compare them for the distribution with three-parameters of Weibull, Weibull Rayleigh and Exponential Weibull. The methods under consideration for comparing the parameter estimators for these distributions is that of maximum likelihood using the statistical program R for the application of real data. Based on the results obtained from this study, the maximum likelihood approach used in estimating the parameters is the comparison between these distributions.

**Keywords:** Exponential weibull distribution, maximum likelihood, parameters, weibull distribution, weibull-rayleigh distribution

### 1. INTRODUCTION

In probability theory and statistics, the Weibull distribution is a continuous probability distribution. The widespread interest in study of reliability is due to the fast development of the world, especially in the field of technology. The estimating parameters is the key to the life model, it can predict the life of product accurately in the reliability. The process of estimating three-parameter Weibull distribution is important because of the

difficulty of obtaining the estimated parameters. The estimation process by using the maximum likelihood function requires iterative methods and therefore requires considerable time and effort [1].

In this paper, first describes the Weibull distribution with three-parameters, where further the way of generating certain distributions is given, which is taken as the basic distribution of the Weibull distribution, then for a certain distribution such as Weibull-Rayleigh, the method of generation of the new

\* Corresponding author: senad.orhani@uni-pr.edu

<sup>1</sup> University of Prishtina “Hasan Prishtina”

ORCID: <https://orcid.org/0000-0003-3965-0791>

<sup>2</sup> University of Tetova

E-mail: lazim.kamberi@unite.edu.mk, mirlinda.selami@unite.edu.mk, sejhan.idrizi@unite.edu.mk

ORCID: <https://orcid.org/0000-0001-6995-9189>, <https://orcid.org/0000-0002-9330-8156>, <https://orcid.org/0000-0003-1287-6571>





distribution, then proceeds with the main properties of this distribution such as probability density function, distribution function, confidence interval for estimated parameters, asymptotic behavior of parameter estimators with maximum likelihood method using simulations for generating it data. Estimates of the parameters of these distributions can be found graphically via the probability bar graph, or analytically, using either the smallest squares (linear regression) or the method for calculating the maximum likelihood (MLE). In this paper, we will only use MLE for estimates of Weibull, Weibull-Rayleigh and Exponentiated Weibull Distribution parameters [2].

## 2. MATERIALS AND METHODS

### 2.1. Maximum Likelihood Estimator: Exponentiated Weibull Distribution (EW)

Let  $X_1, X_2, \dots, X_n$  random selection of size  $n$  with observed values  $x_1, x_2, \dots, x_n$  that follows the Exponentiated-Weibull distribution and let  $\Psi = (\alpha, \beta, \theta)^T$  the parameter vector of the model under consideration. The EW distribution has the function of cumulative distribution (CDF) with three- parameters:

$$F(x; \alpha, \beta, \gamma) = (1 - e^{-\beta x^\gamma})^\alpha, x > 0 \quad (1)$$

and probability density function (PDF) with:

$$f(x; \alpha, \beta, \gamma) = \alpha \beta \gamma x^{\beta-1} e^{-\beta x^\gamma} (1 - e^{-\beta x^\gamma})^{\alpha-1}, x > 0 \quad (2)$$

Where,  $\alpha > 0$  and  $\gamma > 0$  are form parameters and  $\lambda > 0$  is the scale parameter.

Gupta and Kundu (1999) considered a special case of EW distribution when  $\gamma = 1$  and referred to it as Generalized Exponential Distribution (GE). GE distribution has received considerable attention in recent years. Readers

refer to a review article by Gupta and Kundu (2001) for a current account on Generalized Exponential Distribution and a book length treatment of the various distributions expressed by Al-Hussaini and Ahsanullah (2015) in their works [3, 4].

Mudholkar et al. (1996) presented a family with three Generalized Weibull (GW) parameters containing unimodal and bath-shaped Hazard Distribution. They showed that distributions in this household are analytical and manageable computationally. Modelling and data analysis using this family of distributions are discussed and illustrated in the analysis section [5].

### 2.2. Maximum Likelihood Estimator: Weibull-Rayleigh Distribution

In this section we have studied the three-parameter Weibull Rayleigh (WR) Distribution [6, 7]. Use  $G(x)$  and  $g(x)$  in in the formula:

$$f(x) = \sum_{i=0}^{\infty} \sum_{j=0}^{\infty} \omega_{i,j} g(x; \zeta) (G(x; \zeta))^{\beta(i+1)+j-1} \quad (3)$$

to be cdf and pdf of

$$g(x, \theta) = \theta x e^{-\frac{\theta}{2}x^2}, x > 0, \theta > 0 \quad (4)$$

$$G(x, \theta) = 1 - e^{-\frac{\theta}{2}x^2}, x > 0, \theta > 0 \quad (5)$$

Cdf of Weibull-Rayleigh Distribution provided by:

$$F(x; \alpha, \beta, \gamma) = 1 - e^{-\alpha \left( e^{\frac{\gamma}{2}x^2} - 1 \right)^\beta}, x > 0 \quad (6)$$

Relevant PDF of the WR Distribution is provided by:

$$f(x; \alpha, \beta, \gamma) = \alpha \beta \gamma x e^{\frac{\gamma}{2}x^2} \left( e^{\frac{\gamma}{2}x^2} - 1 \right)^{\beta-1} e^{-\alpha \left( e^{\frac{\gamma}{2}x^2} - 1 \right)^\beta} \quad (7)$$

### 2.3. Maximum Likelihood Estimator: Weibull Distribution

Weibull Distribution is a generalization of Exponential Distribution and Weibull-Rayleigh Distribution. For random selection  $X_1, X_2, \dots, X_n$  of size  $n$  with the observed values  $x_1, x_2, \dots, x_n$  that follows the Weibull Distribution and let it be  $\Psi = (\alpha, \beta, \theta)^T$  the parameter vector of the model under consideration. The cumulative function (CDF) with three Weibull Distribution parameters and the probability density function (pdf) are [8-10]:

$$F(x, \alpha, \beta, \theta) = 1 - e^{-\alpha \left( e^{\frac{\theta}{2} x^2} - 1 \right)^\beta}, x > 0. \quad (8)$$

and

$$f(x, \alpha, \beta, \theta) = \alpha \beta \theta x e^{\frac{\theta}{2} x^2} \left( e^{\frac{\theta}{2} x^2} - 1 \right)^{\beta-1} e^{-\alpha \left( e^{\frac{\theta}{2} x^2} - 1 \right)^\beta} x > 0, \quad (9)$$

The function of likeness is:

$$L(x_i, \alpha, \beta, \theta) = f(x_1, x_2, \dots, x_n; \alpha, \beta, \theta) = \prod_{i=1}^n \alpha \beta \theta x_i e^{\frac{\theta}{2} x_i^2} \left( e^{\frac{\theta}{2} x_i^2} - 1 \right)^{\beta-1} e^{-\alpha \left( e^{\frac{\theta}{2} x_i^2} - 1 \right)^\beta}$$

Taking the natural logarithm, we have:

$$l = \ln L = n \log \alpha + n \log \beta + n \log \theta + \sum_{i=1}^n \log x_i + \frac{\theta}{2} \sum_{i=1}^n x_i^2 + (\beta - 1) \sum_{i=1}^n \log \left( e^{\frac{\theta}{2} x_i^2} - 1 \right) - \alpha \sum_{i=1}^n \left[ e^{\frac{\theta}{2} x_i^2} - 1 \right]^\beta \quad (10)$$

Deriving (10) based on parameters  $\alpha, \beta$ , and  $\theta$ , as well as equalizing the results to zero, we get the maximum of this function. Partial derivatives of  $L(\phi)$  with respect to each parameter are [11]:

$$U_n(\phi) = \frac{\partial(L)}{\partial \alpha}, \frac{\partial(L)}{\partial \beta}, \frac{\partial(L)}{\partial \theta}$$

where

$$\frac{\partial(L)}{\partial \alpha} = \frac{n}{\alpha} - \sum_{i=1}^n \left[ e^{\frac{\theta}{2} x_i^2} - 1 \right]^\beta = 0, \quad (11)$$

$$\frac{\partial(L)}{\partial \beta} = \frac{n}{\beta} + \sum_{i=1}^n \log \left( e^{\frac{\theta}{2} x_i^2} - 1 \right) - \alpha \sum_{i=1}^n \left[ e^{\frac{\theta}{2} x_i^2} - 1 \right]^\beta \log \left[ e^{\frac{\theta}{2} x_i^2} - 1 \right] = 0 \quad (12)$$

and

$$\frac{\partial(L)}{\partial \theta} = \frac{n}{\theta} + \frac{1}{2} \sum_{i=1}^n x_i^2 + (\beta - 1) \sum_{i=1}^n \frac{x_i^2 e^{\frac{\theta}{2} x_i^2}}{2 \left( e^{\frac{\theta}{2} x_i^2} - 1 \right)} - \frac{\alpha \beta}{2} \sum_{i=1}^n x_i^2 e^{\frac{\theta}{2} x_i^2} \left[ e^{\frac{\theta}{2} x_i^2} - 1 \right]^{\beta-1} = 0 \quad (13)$$

Evaluation of parameters with the method of maximum similarity for parameters  $\alpha, \beta$ , and  $\theta$ , të themi  $\hat{\alpha}, \hat{\beta}$ , and  $\hat{\theta}$  are obtained by solving the equations [12-14]:

$$\frac{\partial(L)}{\partial \alpha} = \frac{\partial(L)}{\partial \beta} = \frac{\partial(L)}{\partial \theta} = 0.$$

$$\begin{pmatrix} \hat{\alpha} \\ \hat{\beta} \\ \hat{\theta} \end{pmatrix} \sim N \left[ \begin{pmatrix} \alpha \\ \beta \\ \theta \end{pmatrix}, \begin{pmatrix} V\alpha\alpha & V\alpha\beta & V\alpha\theta \\ V\beta\alpha & V\beta\beta & V\beta\theta \\ V\theta\alpha & V\theta\beta & V\theta\theta \end{pmatrix} \right] \quad (14)$$

$$V^{-1} = -E \begin{bmatrix} V\alpha\alpha & V\alpha\beta & V\alpha\theta \\ V\beta\alpha & V\beta\beta & V\beta\theta \\ V\theta\alpha & V\theta\beta & V\theta\theta \end{bmatrix} \quad (15)$$

where,

(

$$V_{\alpha\alpha} = \frac{\partial^2 L}{\partial \alpha^2} = -\frac{n}{\alpha^2} \quad (16)$$

$$V_{\beta\beta} = \frac{\partial^2 L}{\partial \beta^2} = -\frac{n}{\beta^2} - \alpha \sum_{i=1}^n (e^{1/2\theta x_i^2} - 1)^\beta (\ln(e^{1/2\theta x_i^2} - 1))^2$$

$$V_{\theta\theta} = \frac{\partial^2 L}{\partial \theta^2} = -\frac{n}{\theta^2} - (\beta - 1) \sum_{i=1}^n \frac{1}{4} \frac{x_i^4 e^{1/2\theta x_i^2}}{(e^{1/2\theta x_i^2} - 1)^2}$$

$$-\frac{\alpha}{4} \sum_{i=1}^n \frac{(e^{1/2\theta x_i^2} - 1)^\beta \beta x_i^4 e^{1/2\theta x_i^2} (\beta e^{1/2\theta x_i^2} - 1)}{(e^{1/2\theta x_i^2} - 1)^2}$$

$$V_{\alpha\beta} = \frac{\partial^2 L}{\partial \alpha \partial \beta} = -\sum_{i=1}^n (e^{1/2\theta x_i^2} - 1)^\beta \ln(e^{1/2\theta x_i^2} - 1)$$

$$V_{\alpha\theta} = \frac{\partial^2 L}{\partial \alpha \partial \theta} = -\frac{1}{2} \sum_{i=1}^n \frac{(e^{1/2\theta x_i^2} - 1)^\beta \beta x_i^2 e^{1/2\theta x_i^2}}{e^{1/2\theta x_i^2} - 1}$$

$$V_{\beta\theta} = \frac{\partial^2 L}{\partial \beta \partial \theta} = \sum_{i=1}^n \frac{1}{2} \frac{x_i^2 e^{1/2\theta x_i^2}}{e^{1/2\theta x_i^2} - 1} - \frac{\alpha}{2} \sum_{i=1}^n \frac{\left( \frac{1}{e^{2\theta x_i^2} - 1} \right)^\beta x_i^2 e^{\frac{1}{2\theta x_i^2}} \left( \beta \ln \left( \frac{1}{e^{2\theta x_i^2} - 1} \right) + 1 \right)}{\frac{1}{e^{2\theta x_i^2} - 1}} \quad (17)$$

Finding the inverse matrix of the above matrix we will obtain the asymptotic values of variance and covariance for the estimators  $\hat{\alpha}$ ,  $\hat{\beta}$ , and  $\hat{\theta}$ . Using (15), we approximate  $100(1 - \gamma)\%$  confidence interval for  $\alpha, \beta$  and  $\theta$  like below:

$$\hat{\alpha} \pm z_{\gamma/2} \sqrt{V_{\alpha\alpha}}, \hat{\beta} \pm z_{\gamma/2} \sqrt{V_{\beta\beta}}, \hat{\theta} \pm z_{\gamma/2} \sqrt{V_{\theta\theta}} \quad (18)$$

where,  $z_{\gamma}$  is  $100\gamma$  standardized normal distribution percentage.

### 3. RESULTS

#### 3.1. Weibull Distribution, Exponential-Weibull and Weibull-Rayleigh Applications with Three- Parameters

In this section we will compare the data [15] adjustment results with Weibull-Rayleigh, Exponential-Weibull and Weibull Distributions. Data are taken from the study conducted by Kamberi, Iljazi and Orhani (2021) [16]. The main purpose of the study is to compare the results of the students who are using information technology in learning with those students who are not using it. Therefore, we here will take the results of student failure before and after the tests developed with the integration of technology and without its use. These data were analysed by means of the R program for our study conducted for the real data. Based on the results obtained from this study, the maximum likelihood approach used in estimating the parameters is the comparison between these distributions. Student data according to failure points are presented as follows:

*Sample 1: Failure results according to the test that students have not used information technology:*

45, 64, 26, 38, 11, 5, 11, 34, 28, 51, 5, 23, 11, 26, 30, 17, 59, 26, 26, 21

*Sample 2: Failure results according to the test that students have used information technology:*

75, 41, 18, 23, 8, 5, 13, 29, 34, 45, 0, 18, 11, 18, 23, 34, 56, 18, 26, 11

In this section, we obtained two sets of data, representing the results of student failure from the reference study. To test the fit of the two data samples for Weibull Distribution with three-parameters, the Kolmogorov-Smirnov

test was used with the resulting values 0.2 and the respective P values is 0.7537. It therefore refers that the three-parameter Weibull Distribution can fit into both data samples.

For the purpose of estimating the reliability function of the three-parameter Weibull Distribution, the methods described in this paper were used. In order to obtain the best estimate, we are presenting the results in the following table:

Table 1 Evaluating maximum likelihood estimation

Model	Parameters	ML – Sample 1	ML – Sample 2
Weibull Distribution	$\hat{\alpha}$	1.775309	1.728758
	$\hat{\beta}$	31.4732	32.86591
	$\hat{\theta}$	-0.120412	-3.89424
Exponentiated Weibull Distribution	$\hat{\alpha}$	1.7251257	1.719023
	$\hat{\beta}$	31.057	32.8991
	$\hat{\theta}$	-0.140	-3.99023
Weibull-Rayleigh Distribution	$\hat{\alpha}$	1.7109	1.7201
	$\hat{\beta}$	31.657	32.8098
	$\hat{\theta}$	-0.121223	-3.70982

Estimating parameters of three-parameter Weibull Distribution, Exponential-Weibull Distribution and Weibull-Rayleigh is an important factor in reliability. The estimation of Weibull Distribution parameters using traditional techniques such as maximum likelihood function is difficult because it is nonlinear functions. Therefore, from the results of the study we are noticing that the Weibull Distribution model for sample 1 shows the findings for the parameters  $\hat{\alpha} = 1.77$ ,  $\hat{\beta} = 31.47$  and  $\hat{\theta} = -0.12$ , whereas for sample 2 displays these findings for the parameters  $\hat{\alpha} = 1.73$ ,  $\hat{\beta} = 31.87$  and  $\hat{\theta} = -3.89$ . On the other hand, from the results of the study we are noticing that the Exponential-Weibull Distribution model for sample 1 shows the findings for the parameters  $\hat{\alpha} = 1.73$ ,  $\hat{\beta} = 31.06$  and  $\hat{\theta} = -0.14$ , whereas for sample 2 displays these findings for the parameters  $\hat{\alpha} = 1.72$ ,  $\hat{\beta} = 32.89$  and  $\hat{\theta} = -3.99$ . And finally, from the results of the study we are noticing that the Weibull-Rayleigh Distribution model for sample 1 shows the findings for the parameters

$\hat{\alpha} = 1.71$ ,  $\hat{\beta} = 31.66$  and  $\hat{\theta} = -0.12$ , whereas for sample 2 displays these findings for the parameters  $\hat{\alpha} = 1.72$ ,  $\hat{\beta} = 32.81$  and  $\hat{\theta} = -3.71$ . From Table 1 we notice that the best estimators for choices 1 and 2 are for  $\hat{\alpha}$  and  $\hat{\beta}$  parameters compared to  $\hat{\theta}$  parameter, since their values are approximate for the three distributions with the maximum depth method. The eight parameter values for choice 1 and 2 are the best estimators, therefore the Weibull-Rayleigh distribution represents the closest distribution to the Weibull distribution, compared to the Exponential Weibull distribution.

Comparing the results from sample 1 and sample 2 for Weibull Distribution, we are noticing that for sample 1 shape is 1.76, standard deviation with 0.31, as well as scale with 31.33 and standard deviation with 4.18. On the other hand, we are noticing that for the sample 2 shape is 1.18, standard deviation with 0.12, as well as scale with 26.4 and standard

deviation with 5.16. These findings are presented below:

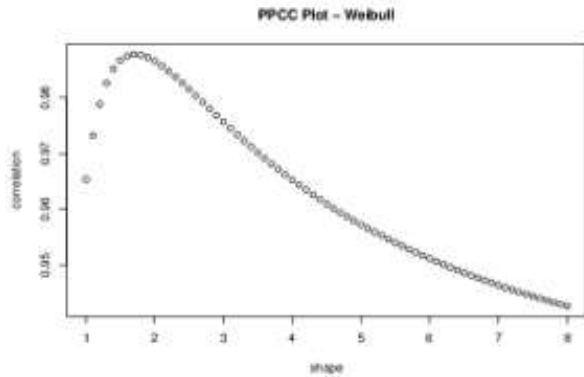


Figure 1 Weibull Distribution for sample 1

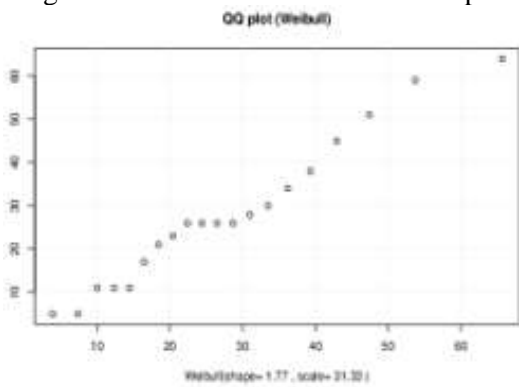


Figure 2 Weibull Distribution for sample 1

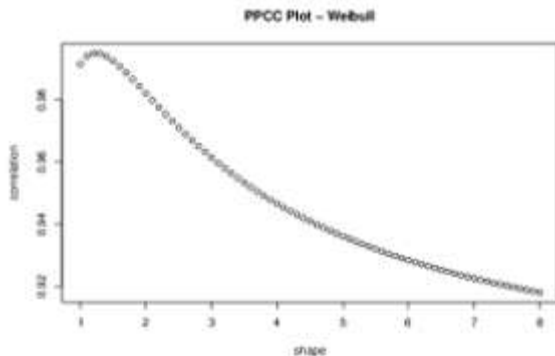


Figure 3 Weibull Distribution for sample 2

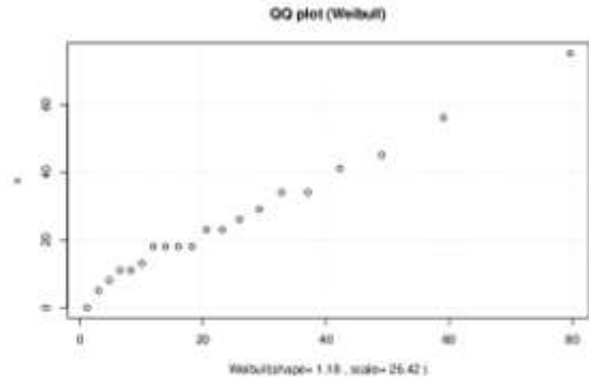


Figure 4 Weibull Distribution for sample 2

Figures 1, 2 and 3, 4 show that the data are distributed approximately with the Weibull distribution. Figure 1, 2 has a distribution that closely approximates the Weibull distribution for the sample 1 data compared to the sample 2 data.

Comparing the results from sample 1 and sample 2 for Exponential-Weibull Distribution, we are noticing that for sample 1 the Estimated Value rate is 0.04 and the standard deviation is 0.008. On the other hand, we are noticing that for sample 2 the rate of Estimated Value is like the result of sample 1 with 0.04 and standard deviation with 0.009. These findings are presented below:

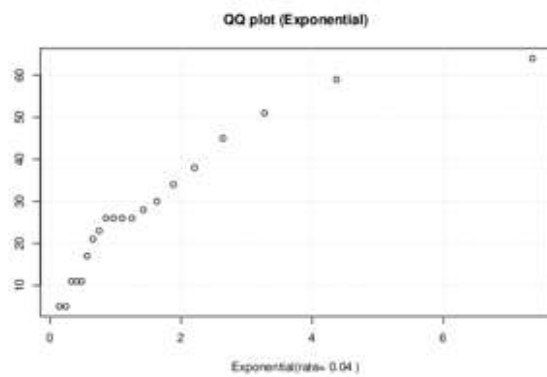


Figure 5 Exponential Weibull Distribution for sample 1

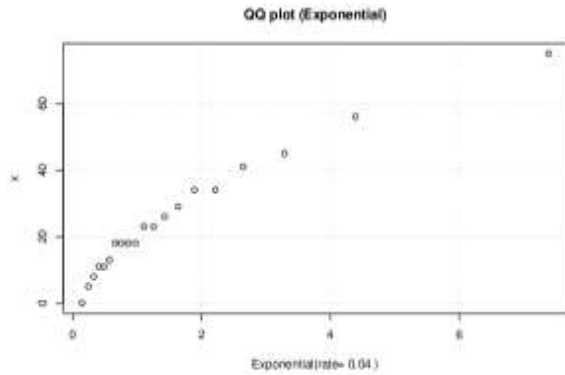


Figure 6 Exponential Weibull Distribution for sample 2

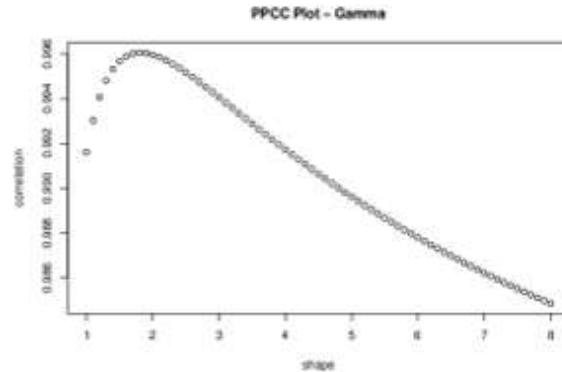


Figure 8 Weibull Rayleigh Distribution for sample 2

On the other hand, Figure 5 and 6 does not give a clear picture of the approximate Weibull Distribution for the data of sample 1 and 2.

However, Figure 7 and 8 gives a better view of the Weibull Distribution for the data in sample 1 and 2, and in particular for sample 2.

The results from sample 1 are showing that for Weibull-Rayleigh Distribution we have for shape a Estimated Value with 2.53 and standard deviation with 0.75, as well as a rate for Estimated Value with 0.09 and a standard deviation with 0.023. On the other hand, the results from sample 2 are showing that for Weibull-Rayleigh Distribution we have for shape an Estimated Value with 1.06 and a standard deviation of 0.29, as well as a rate for Estimated Value with 0.04 and a standard deviation with 0.15. These findings are presented below:

#### 4. CONCLUSION AND DISCUSSION

In this paper are given several types of distributions with three-parameters, starting from that of Weibull Distribution, Exponential-Weibull Distribution and Weibull-Rayleigh Distribution. Basic knowledge about these distributions is given first and the theoretical description of the maximum likelihood method estimating (MLE) for assessment the parameters.

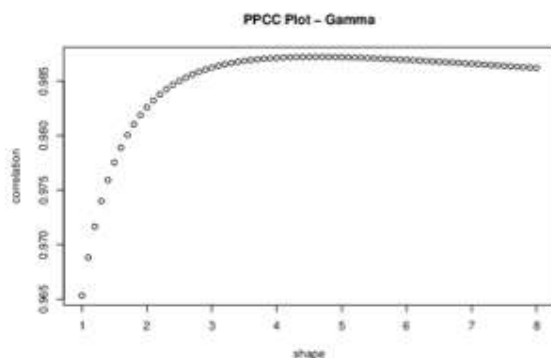


Figure 7 Weibull Rayleigh Distribution for sample 1

Simultaneously in this study the data in the statistical program R were analysed, to see how the statistical parameters are evaluated and depending on it the parameter evaluations were done with the method of maximum likelihood which is shown which distribution is more efficient. Also, an application with real data obtained from the study of the authors Kamberi, Iljazi and Orhani (2021), where it is clearly seen that the distribution of Weibull is one of the distributions that best interprets this data and gives a proper statistical analysis [16, 17].

From the results of Table 1 it is clear that the maximum likelihood (MLE) method is quite clear as a method and can be used efficiently in

practice to estimate the unknown parameters of the Weibull (W), Exponential-Weibull (EW), and Weibull-Rayleigh (WR) models.

In this paper we examined the Weibull distribution for the real data set and also compared it to several sub distributions (models) such as the Exponential-Weibull and Weibull-Rayleigh distributions to show its performance. Therefore, the distributions reviewed provide a very good opportunity in practice for data analysis.

The results of Table 1 were analysed using statistical program R. From the parameter values in the table, we conclude that the Weibull-Rayleigh model provides better estimators for the selection data than other models. Also, the model graphs suggest that the Weibull-Rayleigh model provides better parameter estimators compared to other models according to the maximum likelihood (MLE) method.

#### ***Acknowledgments***

I would like to express our great appreciation to the team during the planning and development of this research.

#### ***Funding***

This study did not receive any specific grant from funding agencies in the public, commercial, or not-for-profit sectors.

#### ***Authors' Contribution***

The authors contributed equally to the study.

#### ***The Declaration of Conflict of Interest/ Common Interest***

No conflict of interest or common interest has been declared by the authors.

#### ***The Declaration of Ethics Committee Approval***

This study does not require ethics committee permission or any special permission.

#### ***The Declaration of Research and Publication Ethics***

The authors of the paper declare that they comply with the scientific, ethical and quotation rules of SAUJS in all processes of the paper and that they do not make any falsification on the data collected. In addition, they declare that Sakarya University Journal of Science and its editorial board have no responsibility for any ethical violations that may be encountered, and that this study has not been evaluated in any academic publication environment other than Sakarya University Journal of Science.

#### **REFERENCES**

- [1] G. T. Basheer, Z. Y. Algamil, "Reliability Estimation of Three Parameters Weibull Distribution based on Particle Swarm Optimization", Pakistan Journal of Statistics and Operation Research, vol. 17, pp. 35-42, 2021.
- [2] A. M. Abd Elfattah, A. S. Hassanand, D.M. Ziedan, "Efficiency of Maximum Likelihood Estimators under Different Censored Sampling Schemes for Rayleigh Distribution", Interstat, 2006.
- [3] R. D. Gupta, D. Kundu, "Exponentiated exponential family: an alternative to gamma and Weibull distributions", Biometrika Journal, vol. 43, pp. 117-130, 2001.
- [4] E. K. AL-Hussaini, M. Ahsanullah, "Exponentiated Distributions", Springer, vol. 5, 2015.
- [5] G. S. Mudholkar, A. D. Hustson, "The exponentiated Weibull family: some properties and a flood data application", Communications in Statistics-Theory and Methods, vol 25, pp. 3059-3083, 1996.



- [6] K. Cooray, "Generalization of the Weibull distribution: the odd Weibull family", *Statistical Modelling*, vol. 6, pp. 265-277, 2006.
- [7] B. Marcelo, R. B. Silva, G. Cordeiro, "The Weibull - G Family of Probability Distributions". *Journal of Data Science*, vol. 12, pp. 53-68, 2014.
- [8] W. Barreto-Souza, A.H.S. Santos, G.M. Cordeiro, "The beta generalized exponential distribution", *Journal of Statistical Computation and Simulation*, vol. 80, pp. 159-172, 2010.
- [9] W. Barreto-Souza, A. L. Morais, G.M. Cordeiro, "The Weibull-geometric distribution", *Journal of Statistical Computation and Simulation*, vol. 81, pp. 645-657, 2011.
- [10] A. L. Morais, W. Barreto-Souza, "A compound class of Weibull and power series distributions", *Computational Statistics and Data Analysis*, vol. 55, pp. 1410-1425, 2011.
- [11] A. Choudhury, "A Simple derivation of moments of the exponentiated Weibull distribution", *Metrika*, vol. 62, pp. 17-22, 2005.
- [12] A. K. Nanda, H. Singh, N. Misra, P. Paul, "Reliability properties of reversed residual lifetime", *Communications in Statistics-Theory and Methods*, vol. 32, pp. 2031-2042, 2003.
- [13] M. M. Nassar, F. H. Eissa, "On the exponentiated Weibull distribution", *Communications in Statistics-Theory and Methods*, vol. 32, pp. 1317-1336, 2003.
- [14] R. Tahmasbi, S. Rezaei, "A two-parameter lifetime distribution with decreasing failure rate", *Computational Statistics and Data Analysis*, vol. 52, pp. 3889-3901, 2008.
- [15] D. F. Andrews, A. M. Herzberg, "Data: A Collection of Problems from Many Fields for the Student and Research Worker", *Springer Series in Statistics*, New York, 1985.
- [16] L. Kamberi, T. Iljazi, S. Orhani, "Statistical Analysis on Information Technology Impact in Quality Learning of Mathematics (for Grades VI-IX)", *Journal of Natural Sciences and Mathematics of UT*, vol. 6, no. 11-12, pp. 123-134, 2021.
- [17] F. Merovci, I. Elbatal, "Weibull Rayleigh Distribution: Theory and Applications", *Appl. Math. Inf. Sci.* Vol. 9, no. 4, pp. 2127-2137, 2015.



SAKARYA ÜNİVERSİTESİ

# FEN BİLİMLERİ ENSTİTÜSÜ DERGİSİ

Sakarya University Journal of Science  
SAUJS

ISSN 1301-4048 e-ISSN 2147-835X Period Bimonthly Founded 1997 Publisher Sakarya University  
<http://www.saujs.sakarya.edu.tr/>

Title: Highly Selective and Sensitive Non-enzymatic Glucose Biosensor Based on Polypyrrole-Borophene Nanocomposite

Authors: Gülsen BAYTEMİR

Received: 2022-06-06 00:00:00

Accepted: 2022-09-18 00:00:00

Article Type: Research Article

Volume: 26

Issue: 6

Month: December

Year: 2022

Pages: 1093-1103

How to cite

Gülsen BAYTEMİR; (2022), Highly Selective and Sensitive Non-enzymatic Glucose Biosensor Based on Polypyrrole-Borophene Nanocomposite . Sakarya University Journal of Science, 26(6), 1093-1103, DOI: 10.16984/saufenbilder.1126859

Access link

<https://dergipark.org.tr/en/pub/saufenbilder/issue/74051/1126859>

New submission to SAUJS

<http://dergipark.gov.tr/journal/1115/submission/start>

## Highly Selective and Sensitive Non-enzymatic Glucose Biosensor Based on Polypyrrole-Borophene Nanocomposite

Gülşen BAYTEMİR\*<sup>1</sup> 

### Abstract

In this study, a non-enzymatic glucose sensor composed of two-dimensional (2D) borophene-decorated polypyrrole (PPy) nanocomposites (NCs) was developed. The PPy-borophene NCs were prepared using a low-cost sonication method. The sensing performance of the PPy-borophene NCs was investigated by the cyclic voltammetry (CV) technique against various biomolecules such as glucose, maltose, lactose, fructose, and urea. According to the electrochemical results, it was observed that in the glucose concentration range of 1.5 to 24 mM within a voltammetric cycle of 1 min, the PPy-based sensor and PPy-borophene NCs-based sensor exhibited sensitivities of  $11.88 \mu\text{AmM}^{-1} \text{cm}^{-2}$  and  $213.42 \mu\text{AmM}^{-1} \text{cm}^{-2}$ , respectively. The detection limits of the PPy-based and PPy-borophene NCs-based sensors were determined to be 0.5  $\mu\text{M}$  and 0.04  $\mu\text{M}$ , respectively. Furthermore, selectivity measurement results revealed that the proposed non-enzymatic biosensor has remarkably good sensitivity and high selectivity, indicating that common biomolecules (glucose, maltose, lactose, fructose, and urea) could be captured by the sensor. Consequently, it was proven that the proposed biosensor could be a potential device for diabetes diagnosis.

**Keywords:** Non-enzymatic electrochemical biosensor, borophene, polypyrrole, glucose.

### 1. INTRODUCTION

Diabetes is a global health problem that affects millions of people. In 2030, the prevalence of diabetes is estimated to be 4.4% for all age groups worldwide [1, 2]. It is believed that the reasons for the rapid increase in the number of diabetes patients are accelerating obesity, sedentary lifestyles and unhealthy diets. Diabetes is a metabolic disease that occurs when the pancreas is not able to produce enough insulin or the body can not effectively use the insulin it produces. Since the cells cannot absorb

the blood sugar (glucose) required for the energy they need due to insulin deficiency, the level of glucose in the blood rises. If not treated or controlled, diabetes can damage blood vessels and cause a variety of complications when glucose concentrations exceed 10–12 mM [2-9]. Therefore, accurate monitoring of glucose concentration is crucial.

Conventional glucose biosensors make use of enzymes such as glucose oxidase and glucose hydrogenase due to their simplicity, high sensitivity and selectivity to glucose. The signal

\* Corresponding author: gulsenbaytemir@gmail.com

<sup>1</sup> Maltepe University, Faculty of Engineering

ORCID: <https://orcid.org/0000-0002-1143-0730>



is obtained from the oxidation of hydrogen peroxide produced as a result of the reaction of these enzymes. However, although the development of enzyme-modified electrodes has advanced considerably, these enzymatic sensors often suffer from stability issues due to the nature of enzymes. In order to overcome this problem, it is attractive to produce non-enzymatic sensors that can directly oxidize glucose at the electrode surface [10-15]. In general, metal/metaloxides [16-21] such as platinum (Pt), gold (Au), platinum-lead (Pt-Pb), nickel (Ni), copper (Cu), nickel-titanium (Ni-Ti), nickel-copper (Ni-Cu), transition metal oxides [22-26] such as tricobalt tetroxide ( $\text{Co}_3\text{O}_4$ ), nickel oxide (NiO), nickel hydroxide ( $\text{Ni}(\text{OH})_2$ ), and copper hydroxide ( $\text{Cu}(\text{OH})_2$ ) etc., can be used as sensing materials for the detection of glucose sensor. However, these electrodes have some disadvantages, such as low sensitivity, poor selectivity, and poisoning by chloride ions. Carbon and carbon-based nanomaterials (carbon nanotubes, carbon fibers, carbon dots, and graphene) have recently received increasing attention due to their unique physical and chemical properties. In particular, graphene, which is a two-dimensional (2D) material, attracts attention as a glucose sensing material due to its high surface area, chemical stability, and biocompatibility [27-29]. In addition, since conductive polymers such as polypyrrole (PPy) [30], polyaniline (PANI) [31], poly-o-aminophenol (POAP) [32] have similar electrical and optical properties to metal or inorganic semiconductor materials, they are of interest for chemical sensor, biosensor, and supercapacitor studies. In particular, PPy has been reported as being suitable for the design of various sensors since it is a good substrate for the immobilization of nanomaterials. For instance, the electrochemical sensor fabricated for the determination of D-glucose using a polypyrrole-N-phenylboronic acid modified Pt electrode has been reported to exhibit a low detection limit [33]. In another study, glucose was detected over a wide dynamic detection range of 0.001-4.863 mM using overoxidized polypyrrole nanowire electrodes (nf-

$\text{Ni}(\text{OH})_2@o\text{PPyNW}$ ) modified with nickel hydroxide nanoflakes. The proposed electrode exhibits a low detection limit of 0.3  $\mu\text{M}$ , making it suitable for a sensitive, selective, and stable electrochemical sensor [34]. In another study, it has been shown that the limit of detection of the hybrid  $\text{NF}/\text{NiCo}_2\text{O}_4@Ppy$  electrochemical sensor created by fabricating  $\text{NiCo}_2\text{O}_4@$ polypyrrole nanowires on a nickel foam (NF) substrate for glucose sensing was 0.22  $\mu\text{M}$  [35]. An enzyme-free sensor developed for glucose detection based on chemical oxidative polymerization of pyrrole monomers on the surface of  $\text{CuFe}_2\text{O}_4$  nanoparticles exhibited a limit detection of 0.1  $\mu\text{M}$  for low glucose concentrations and 0.47  $\mu\text{M}$  for high glucose concentrations [36]. In a study examining an enzyme-free biosensor modified with cobalt(II) phthalocyanine tetrasulfonate ( $\text{CoPcTS}$ )-based on the electrodeposition of over-oxidized polypyrrole nanofiber on a pencil graphite electrode, excellent performance was observed for glucose sensing with a wide linear range (0.25–20 mM) and highly reproducible response. In addition, the calculated limit of detection was 0.1 mM [37]. Li et al. worked on an enzyme-free glucose biosensor based on Au nanoparticles ( $\text{Au}/\text{PPyNFs}$ ) supporting polypyrrole nanofibers. It has been shown that with a non-enzymatic glucose sensor based on  $\text{Au}/\text{PPyNFs}$ , 0.2-13 mM of glucose can be detected [38].

In recent years, borophene as a two-dimensional nanomaterial has been the subject of many studies due to its unique physical, chemical, and electronic properties. In 2015, in the first theoretical studies of borophene, its chemical stability at room temperature was reported. As of 2018, borophene has started to be prepared by wet chemical methods, but there are still a limited number of papers. In these studies, it is reported that the performance of supercapacitors and sensors is improved with the addition of prepared borophene to conductive polymers [39-44]. Here, the addition of borophene to conductive polymers increases the electrical conductivity of conductive polymer-borophene

nanocomposite-based devices. Therefore, it can be predicted that the PPy-borophene NCs obtained with the addition of borophene will improve the redox interaction between glucose and the nanocomposite in a non-enzymatic electrochemical sensor.

In this study, PPy-based and PPy-borophene NCs-based non-enzymatic sensors were prepared and their glucose sensing properties were investigated. It was demonstrated that borophene improves the glucose sensing properties of the sensor. The novelty of this work is that the glucose sensing mechanism of the PPy-borophene NCs-based electrochemical sensor has been reported for the first time. In addition, the prepared sensors have been tested to detect urea, fructose, lactose, and maltose, and it has been shown that the sensors are more selective towards glucose.

## 2. EXPERIMENTAL

Borophene nanosheets were prepared by physical exfoliation of boron microparticles (1.5  $\mu\text{m}$  particle size) in dimethylformamide (DMF) as previously described [45-47]. High resolution transmission electron microscopy (HRTEM) and X-ray diffraction (XRD) techniques were performed to elucidate the crystalline structure and morphology of the borophene. Then, PPy and borophene were mixed at a ratio of 1:1, and the solution was sonicated at 200 W for 15 min. Scanning electron microscopy (SEM) and Fourier-transform infrared (FTIR) analysis of the PPy-borophene NCs were performed.

Glucose analytes with 1.5 mM, 3 mM, 6 mM, 12 mM and 24 mM concentrations were prepared in phosphate buffer solution (PBS). PPy and PPy-borophene solutions were coated on the gold (Au) electrochemical transducers by drop casting and dried at 40  $^{\circ}\text{C}$  to obtain the sensors. Measurements for each glucose concentration were carried out by the 3-electrode cyclic voltammetry method. In addition, I-V characteristics of the sensor for each glucose concentration in the range of [-1, +1] V were obtained in real-time measurements. Since the current response is based on the reduction and

oxidation reactions, the sensitivities of the sensors were thus determined.

## 3. RESULT AND DISCUSSION

The HRTEM images and XRD pattern of borophene were given in Figure 1. The HRTEM micrographs of the borophene show that borophene, prepared using the ultrasonic method, has excellent structural morphology. As seen in Figure 1-a, borophene has a uniform nanosheet structure with hexagonal boron crystals. The nanosheets have a crystalline structure with a 0.41 nm stripe pitch, and this matches the characteristics of a  $\beta$ -rhombohedral boron structure [48]. Moreover, the Fast Fourier Transform (FFT) diffraction pattern of an individual borophene nanosheet is also given in the inset of Figure 1-b. The XRD pattern given in Figure 1-c, in which the phase and crystallinity of the nanosheets were examined, corresponds to the centrosymmetric (0001) plane of  $\beta$ -rhombohedral borophene (0001) plane (unit cell parameters:  $a=10.925\text{\AA}$ ,  $b=10.925\text{\AA}$  and  $c=23.814\text{\AA}$ ). The XRD pattern was indexed to the crystal system of the  $\beta$ -borophene was R-3 m (166) [49]. The results of HRTEM and XRD techniques are compatible with each other.

The surface morphology of the ultrasonically prepared PPy-borophene NCs was also identified. SEM images of borophene and PPy-borophene NCs are given in Figure 2 (a-b). The SEM image of the PPy-borophene NCs at higher magnification is also given in the inset of Figure 2-b. According to the experimental results of the PPy-borophene NCs, it has a random nanofringe structure. The results of the FTIR used to determine the chemical functional groups of borophene and PPy-borophene NCs are presented in Figure 2-c. In the previous studies of our group, it was reported that the characteristic peaks of borophene were observed at 3479  $\text{cm}^{-1}$  (O-H), 2929  $\text{cm}^{-1}$  (B-B), 2861  $\text{cm}^{-1}$  (B-H), 1653  $\text{cm}^{-1}$  (C=O), 1496  $\text{cm}^{-1}$  (B-H), 1385  $\text{cm}^{-1}$  (B-O), 1255  $\text{cm}^{-1}$  (B-O), and 1091  $\text{cm}^{-1}$  (B-O-B vibrations), 865  $\text{cm}^{-1}$  (B-

OH stretching vibration), and 659 (B–O–B stretching vibration) [31]. The characteristic peaks of the prepared PPy-borophene NCs were observed at  $3272\text{ cm}^{-1}$  (O–H vibrational stretching),  $1634\text{ cm}^{-1}$  (C=C stretching),  $1126\text{ cm}^{-1}$  (C–H in-plane bending vibration), and  $1037\text{ cm}^{-1}$  (–C–O–C) [50]. According to the FTIR results, it was concluded that borophene sheets were encapsulated in the polymer matrix (PPy).

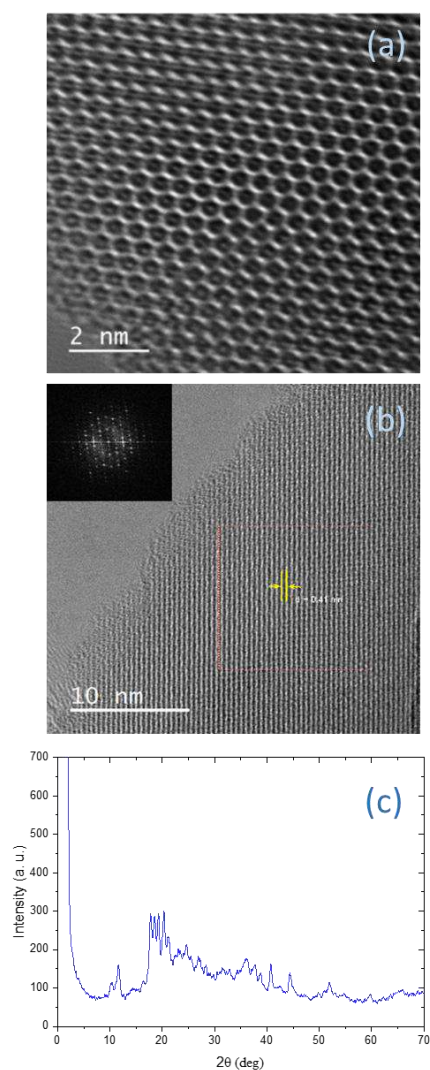


Figure 1 HRTEM images of the  $\beta$ -rhombohedral borophene at (a) high magnification, (b) low magnification. The inset of (b) is the FFT diffraction pattern of an individual borophene nanosheet. (c) XRD pattern of the  $\beta$ -rhombohedral borophene.

Electrochemical measurements of the PPy and PPy-borophene NCs based biosensors were carried out in the  $[-1, +1]$  V range with a  $50\text{ mV/s}$  scan rate. The sensors were tested to detect glucose in the  $1.5\text{--}24\text{ mM}$  concentration range. The measurements started with  $1.5\text{ mM}$  glucose concentration, and the glucose was added continually to  $24\text{ mM}$ . The current density-voltage graphs of the sensors for each glucose concentration were presented in Figure 3 a-b. The peak current measured during voltammetry varied depending on the analyte concentration. The response of the sensors to the changes in the glucose concentrations is represented by an increase in the output current.

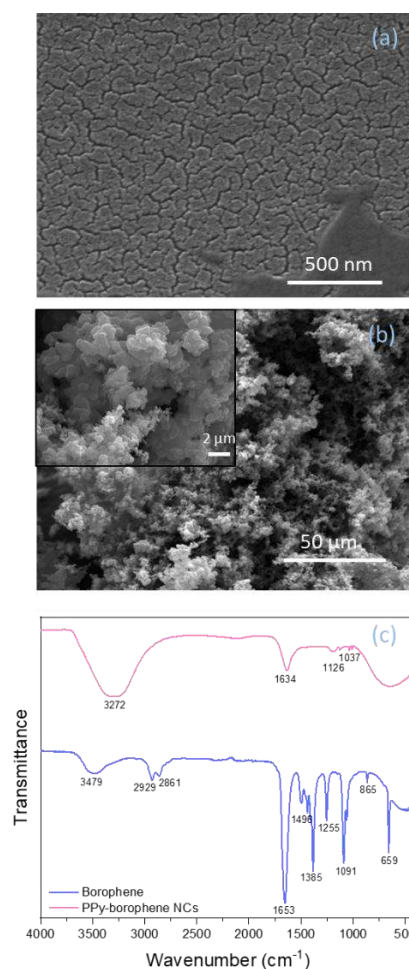


Figure 2 SEM images of (a) borophene, (b) PPy-borophene NCs. (Higher magnification is given as inset) (c) FTIR analysis of the borophene and PPy-borophene NCs.



The current peaks arise from redox reactions of glucose with the PPy and PPy-borophene NCs. The current density-voltage curves of the PPy-borophene NCs-based sensor indicated a highly prominent redox peak for the 1.5-24 mM glucose concentration range. The results show that the PPy-borophene nanocomposite-based sensor detects glucose with higher sensitivity due to the enhanced redox mechanism resulting from the borophene additive. The sensitivities of the PPy and PPy-borophene NCs based sensors were obtained by calculating the slope of the current density versus glucose concentration curves shown in Figure 3-c. PPy-based and PPy-borophene NCs-based sensors detected glucose in 1.5-24 mM concentration range with a sensitivity of  $11.88 \mu\text{AmM}^{-1} \text{cm}^{-2}$  and  $213.42 \mu\text{AmM}^{-1} \text{cm}^{-2}$  within 1 min voltammetric cycle, respectively (Figure 3-c).

The detection limit of the sensors were calculated by the

$$LOD = 3S_{y/x}/b$$

equation where  $S_{y/x}$  is the standard deviation of the background current and  $b$  is the slope of the calibration curve [51]. PPy-based sensor was calculated as  $0.5 \mu\text{M}$ , while that of the PPy-borophene NCs-based sensor was calculated as  $0.04 \mu\text{M}$ . Table 1 shows the characteristics of the non-enzymatic, nanomaterial-modified PPy electrochemical biosensors used for glucose detection and their limit of detection values.

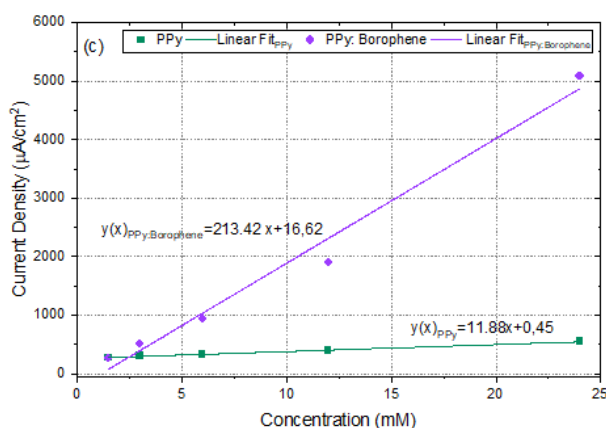
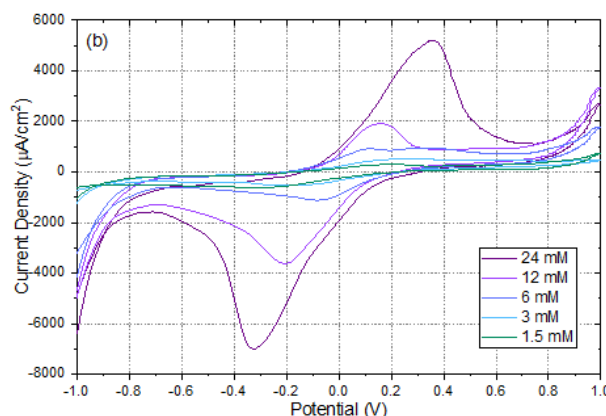


Figure 3 (a) Current density-voltage graph of PPy-based sensor against glucose, (b) PPy-borophene NCs-based sensor for varying glucose concentration, (c) The sensitivities of the sensors

Furthermore, Figure 4 shows the comparison of current density-voltage curves of PPy and PPy-borophene NCs-based sensors for glucose, maltose, lactose, fructose, and urea at 24 mM concentration. According to the results given in Figure 4 a-b, both of the sensors are remarkably selective for glucose. In the literature, there is no report on the PPy-borophene NCs-based glucose sensor. This is the first report on the preparation, structural characterization, and measurements of the PPy-borophene NCs-based glucose sensor. The measurements were performed 3 times, and obtaining similar results shows that the sensor has repeatability and stability. In light of the above, it can be said that the sensor is a potential device for rapid, cost-effective, selective, and sensitive diagnosis of diabetes

Table 1 The performances of various nanomaterials modified PPy non-enzymatic biosensors for glucose detection

Electrode	Concentration Range	Limit of Detection	Detection method	Ref.
PPy-phenylboronic acid	0.05–0.52 mM	80 $\mu$ M	Voltammetry	[33]
Over-oxidized PPy nanowires modified with Ni(OH) <sub>2</sub> nanoflakes	0.001-4.863 mM	0.3 $\mu$ M	Amperometry	[34]
NiCo <sub>2</sub> O <sub>4</sub> @PPy nanowires on nickel foam substrate	0.001–20 mM	0.22 $\mu$ M	Voltammetry	[35]
Core-shell–CuFe <sub>2</sub> O <sub>4</sub> /PPy nanocompo	20 $\mu$ M-5.6 mM	0.1 $\mu$ M for low concentrations 0.47 $\mu$ M for high concentrations	Voltammetry	[36]
Overoxidized PPy nanofiber electrode modified with CoPc tetrasulfonate	0.25–20 mM	0.1 mM	Amperometry	[37]
PPy nanofibers supporting Au nanoparticles (Au/PPyNFs)	0.2–13 mM	0.2 mM	Amperometry	[38]
PPy	1.5-24 mM	0.5 $\mu$ M	Voltammetry	This work
PPy-borophene NCs		0.04 $\mu$ M		

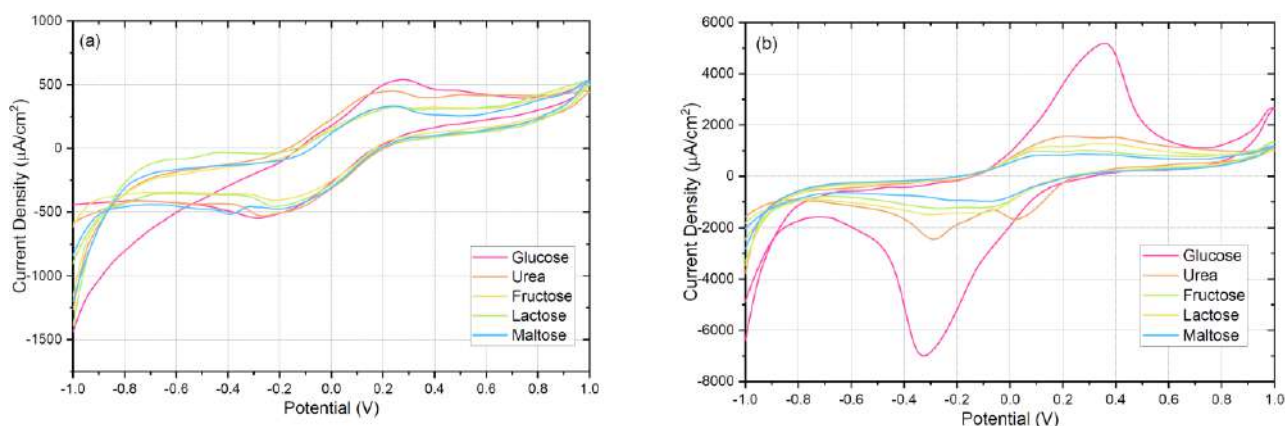


Figure 4 Selectivity of (a) PPy-based sensor (b) PPy-borophene NCs -based sensor.

#### 4. CONCLUSION

Borophene with a uniform transparent nanosheet structure and PPy-borophene NCs with a random

nanofringe structure were prepared by the ultrasonic method. After that, PPy and PPy-borophene NCs-based non-enzymatic electrochemical sensors were prepared to investigate glucose detection and the selectivity of



the sensors to glucose, maltose, lactose, fructose, and urea. In the 1.5 to 24 mM glucose concentration range, the sensitivity of the PPy-based sensor was  $11.88 \mu\text{AmM}^{-1} \text{cm}^{-2}$  and the sensitivity of the PPy-borophene NCs-based sensor was  $213.42 \mu\text{AmM}^{-1} \text{cm}^{-2}$ . The detection limits of the PPy-based and PPy-borophene NCs-based sensors were determined to be 0.5  $\mu\text{M}$  and 0.04  $\mu\text{M}$ , respectively. These results revealed that both of the sensors were remarkably selective for glucose. The PPy-borophene NCs-based sensor detected glucose with higher sensitivity and lower detection limit due to the enhanced redox mechanism arising from the borophene additive. Moreover, current density-voltage curves of PPy and PPy-borophene NCs-based sensors for glucose, maltose, lactose, fructose, and urea at 24 mM concentration show that both of the sensors are remarkably selective for glucose. In addition, the measurements were performed 3 times and similar results were observed. In the light of the above, it can be concluded that the PPy-borophene NCs-based sensor has high sensitivity, high selectivity, and stability. Since this is the first report on the preparation, structural characterization, and measurements of the the PPy-borophene NCs-based glucose sensor it could be further developed in the future as a potential device for the diagnosis of diabetes.

#### **Funding**

The author has not received any financial support for the research, authorship or publication of this study.

#### **Authors' Contribution**

The author confirms sole responsibility for the following: study conception, data collection, interpretation of results, and manuscript preparation.

#### **The Declaration of Conflict of Interest/ Common Interest**

The author of the paper declares that there are no competing financial and non-financial interest.

#### **The Declaration of Ethics Committee Approval**

This study does not require ethics committee permission or any special permission.

#### **The Declaration of Research and Publication Ethics**

The author of the paper declares that they comply with the scientific, ethical and quotation rules of SAUJS in all processes of the paper and that they do not make any falsification on the data collected. In addition, they declare that Sakarya University Journal of Science and its editorial board have no responsibility for any ethical violations that may be encountered, and that this study has not been evaluated in any academic publication environment other than Sakarya University Journal of Science.

### **REFERENCES**

- [1] S. Wild, G. King, Roglic Anders, Green Richard, "Sicree Hilary, Estimates for the year 2000 and projections for 2030," Diabetes Care, vol. 27 pp. 1047–1053, 2004.
- [2] F. J. Garcia-Garcia, P. Salazar, F. Yubero, A. R. González-Elipe, "Non-enzymatic Glucose electrochemical sensor made of porous NiO thin films prepared by reactive magnetron sputtering at oblique angles." Electrochimica Acta. Vol. 201 pp. 38-44, 2016.
- [3] B. L. Allen, P. D. Kichambare, A. Star, "Carbon nanotube field-effect-transistor-based biosensors," Advanced Materials vol. 19 pp. 1439–1451, 2007.
- [4] K. Besteman, J. O. Lee, F. G. M. Wiertz, H .A. Heering, C. Dekker, "Enzyme-coated carbon nanotubes as single-molecule biosensors," Nano Letters, vol. 3 pp. 727–730, 2003.
- [5] A. Esmaeeli, A. Ghaffarinejad, A. Zahedi, O. Vahidi, "Copper oxide-

- polyaniline nanofiber modified fluorine doped tin oxide (FTO) electrode as non-enzymatic glucose sensor,” *Sensors and Actuators B: Chemical* vol. 266 pp. 294–301, 2018.
- [6] Y. H. Lin, F. Lu, Y. Tu, Z.F. Ren, “Glucose biosensors based on carbon nanotube nanoelectrode ensembles,” *Nano Letters* vol. 4 pp. 191–195, 2004.
- [7] L. N. Jia, X.B. Wei, L. L. Lv, X. X. Zhang, X. X. Duan, Y. Xu, K. L. Liu, J. Wang, “Electrodeposition of hydroxyapatite on nickel foam and further modification with conductive polyaniline for non-enzymatic glucose sensing”, *Electrochimica Acta* 280 315–322, 2018.
- [8] L. Wang, X. Lu, C. Wen, Y. Xie, L. Miao, S. Chen, H. Li, P. Li, Y. Song, “One-step synthesis of Pt–NiO nanoplate array/reduced graphene oxide nanocomposites for non-enzymatic glucose sensing,” *Journal of Materials Chemistry A* vol. 3 pp. 608–616, 2015.
- [9] M. Bogun M, S .E Inzucchi, “Inpatient management of diabetes and hyperglycemia,” *Clinical Therapeutics* vol. 35 pp. 724–33, 2013.
- [10] A. Gaoa, X. Zhang, X. Penga, H. Wua, L. Bai, W. Jina, G. Wua, R. Hanga, P. K. Chua, “In situ synthesis of Ni(OH)<sub>2</sub>/TiO<sub>2</sub> composite film on NiTi alloy for non-enzymatic glucose sensing,” *Sensors and Actuators B* vol. 232 pp. 150-157, 2016.
- [11] R. Wang, X. Liang, H. Liu, L. Cui, X. Zhang, C. Liu, “Non-enzymatic electrochemical glucose sensor based on monodispersed stone-like PtNi alloy nanoparticles,” *Microchimica Acta* vol. 185 p.339, 2018.
- [12] K. K. Lee, P. Y. Loh, C. H. Sow, W. S. Chin, “CoOOH nanosheets on cobalt substrate as a non-enzymatic glucose sensor,” *Electrochemistry Communications*, vol. 20 pp. 128-132, 2012.
- [13] S. SoYoon, A. Ramadoss, B. Saravanakumar, S. J. Kim, “Novel Cu/CuO/ZnO hybrid hierarchical nanostructures for non-enzymatic glucose sensor application,” *Journal of Electroanalytical Chemistry* vol. 717-718 pp. 90-95, 2014.
- [14] G. He, L. Tian, Y. Cai, S. Wu, Y. Su, H. Yan, W. Pu, J. Zhang, L. Li, “Sensitive Non-enzymatic Electrochemical Glucose Detection Based on Hollow Porous NiO,” *Nanoscale Research Letters* vol. 13 p. 3 2018.
- [15] N. Taştaltın, E. Aydın, S. Karakuş, A. Kilislioğlu, “K-carrageenan/PVA/nano-eggshell biocomposite-based non-enzymatic electrochemical biosensor for low-level urea detection,” *Applied Physics A* vol. 126:827, 2020.
- [16] X. Bo, J. Bai, L. Yang, L. Guo, “The nanocomposite of PtPd nanoparticles/onion-like mesoporous carbon vesicle for nonenzymatic amperometric sensing of glucose,” *Sensor and Actuators B: Chemical* vol. 157 pp. 662–668, 2011.
- [17] Y. Sun, H. Yang, X. Yu, H. Meng, X. Xu, “A novel non-enzymatic amperometric glucose sensor based on hollow Pt-Ni alloy nanotubes array electrode with enhanced sensitivity,” *RSC Advances* vol. 5 pp. 70387–70394, 2015.
- [18] Y. Sun, H. Buck, T.E. Mallouk, “Combinatorial discovery of alloy electrocatalysts for amperometric glucose

- sensors,” *Analytical Chemistry* vol. 73 pp. 1599–1604, 2001.
- [19] S. Park, T. D. Chung, H. C. Kim, “Nonenzymatic glucose detection using mesoporous platinum,” *Analytical Chemistry* vol. 75 pp. 3046–3049, 2003.
- [20] M. Jafarian, F. Forouzandeh, I. Danaee, F. Gobal, M. G. Mahjani, “Electrocatalytic oxidation of glucose on Ni and NiCu alloy modified glassy carbon electrode,” *Journal of Solid State Electrochemistry* vol.13 pp. 1171–1179, 2009.
- [21] P. F. Luo, T. Kuwana, “Nickel-titanium alloy electrode as a sensitive and stable LCEC detector for carbohydrates,” *Analytical Chemistry* vol. 66 pp. 2775–2782, 1994.
- [22] Y. Ding, Y. Wang, L. Su, M. Bellagamba, H. Zhang, Y. Lei, “Electrospun  $\text{Co}_3\text{O}_4$  nanofibers for sensitive and selective glucose detection,” *Biosensors and Bioelectronics* Vol. 26 pp. 542–548, 2010.
- [23] J. Yang, M. Cho, Y. Lee, “Synthesis of hierarchical  $\text{Ni}(\text{OH})_2$  hollow nanorod via chemical bath deposition and its glucose sensing performance,” *Sensor and Actuators B: Chemical* vol. 222 pp. 674–681, 2016.
- [24] M. M. Rahman, A. J. S. Ahammad, J. H. Jin, S. J. Ahn, J. J. Lee, “A comprehensive review of glucose biosensors based on nanostructured metal-oxides,” *Sensors* vol.10 pp. 4855–4886, 2010.
- [25] Y. Ren, W. K. Chim, S. Y. Chiam, J.Q. Huang, C. Pi, J. S. Pan, “Formation of nickel oxide nanotubes with uniform wall thickness by low-temperature thermal oxidation through understanding the limiting effect of vacancy diffusion and the Kirkendall phenomenon,” *Advanced Functional Materials* vol. 20 pp. 3336–3342, 2010.
- [26] L. C. Jiang, W. De Zhang, “A highly sensitive nonenzymatic glucose sensor based on CuO nanoparticles-modified carbon nanotube electrode,” *Biosens and Bioelectronics* vol. 25 pp. 1402–1407, 2010.
- [27] D.-W. Hwang, S. Lee, M. Seo, T. D. Chung, “Recent advances in electrochemical non-enzymatic glucose sensors- A review,” *Analitica Chimica Acta* vol. 1033 pp. 1–34, 2018.
- [28] S. K. Krishnan, E. Singh, P. Singh, M. Meyyappan, H. S. Nalwa, A review on graphene-based nanocomposites for electrochemical and fluorescent biosensors,” *RSC Advances* vol. 9 pp. 8778–8881, 2019.
- [29] M. Mathew, S. Radhakrishnan, A. Vaidyanathan, B. Chakraborty, C. S. Rout, “Flexible and wearable electrochemical biosensors based on two-dimensional materials: Recent developments,” *Analytical and Bioanalytical Chemistry* vol. 413 pp. 727–762, 2021.
- [30] A. Yavuz, S. Aktaş, S. Duru, “Polypyrrole Modified Graphite Electrode for Supercapacitor Application: The Effect of Cycling Electrolytes,” *Sakarya University Journal of Science* vol. 3 pp. 462-471, 2019.
- [31] C. Tasaltın, T. A. Türkmen, N. Tasaltın, S. Karakus, “Highly sensitive non-enzymatic electrochemical glucose biosensor based on PANI:  $\text{B}_{12}$  Borophene,” *Journal of Materials Science: Materials in Electronics* vol. 32 pp. 10750–10760, 2021.

- [32] S. Aytac, F. Kuralaya, I. H. Boyacı, C. Unaleroglu, "A novel polypyrrole-phenylboronic acid based electrochemical saccharide sensor," *Sensors and Actuators B* vol. 160 pp. 405–411, 2011.
- [33] R. Ojani, J. B. Raoof, S. Fathi, "Electrocatalytic oxidation of some carbohydrates by nickel/poly(o-aminophenol) modified carbon paste electrode," *Electroanalysis*. Vol. 20 pp. 1825-1830, 2008.
- [34] J. Yang, M. Cho, C. Pang, Y. Lee, "Highly sensitive non-enzymatic glucose sensor based on over-oxidized polypyrrole nanowires modified with Ni(OH)<sub>2</sub> nanoflakes," *Sensors and Actuators B* vol. 211 pp. 93-101, 2015.
- [35] X. Duan, K. Liu, Y. Xu, M. Yuan, T. Gao, J. Wang, "Nonenzymatic electrochemical glucose biosensor constructed by NiCo<sub>2</sub>O<sub>4</sub>@Ppy nanowires on nickel foam substrate," *Sensors and Actuators B: Chemical* vol. 292 pp. 121-128, 2019.
- [36] Z. Shahnavaaz, F. Lorestani, W. P. Meng, Y. Alias, "Core-shell-CuFe<sub>2</sub>O<sub>4</sub>/PPy nanocomposite enzyme-free sensor for detection of glucose," *Journal of Solid State Electrochemistry* vol. 19 pp. 1223–1233, 2015.
- [37] L. Ozcan, Y. Sahin, H. Türk, "Non-enzymatic glucose biosensor based on overoxidized polypyrrole nanofiber electrode modified with cobalt (II) phthalocyanine tetrasulfonate," *Biosensors and Bioelectronics* vol. 24 pp. 512–517, 2008.
- [38] C. Li, Y. Su, X. Lv, H. Xia, H. Shi, X. Yang, J. Zhang, Y. Wang, "Controllable anchoring of gold nanoparticles to polypyrrole nanofibers by hydrogen bonding and their application in nonenzymatic glucose sensors," *Biosensors and Bioelectronics* vol. 38 pp. 402–406, 2012.
- [39] Z. Zhang, Y. Yang, G. Gao, B. I. Yakobson, "Two-dimensional boron monolayers mediated by metal substrates," *Angewandte Chemie International Edition*, vol. 127 pp. 13214-13218, 2015.
- [40] Z. Zhang, S. N. Shirodkar, Y. Yang, B. I. Yakobson, "Gate-voltage control of borophene structure formation," *Angewandte Chemie International Edition*, vol. 129 pp. 15623-15628, 2017.
- [41] L. Liu, Z. Zhang, X. Liu, X. Xuan, B. I. Yakobson, M. C. Hersam, W. Guo, "Borophene concentric superlattices via self-assembly of twin boundaries," *Nano Letters*, vol. 20(2), pp. 1315-1321, 2020.
- [42] Z. Zhang, A. J. Mannix, X. Liu, Z. Hu, N. P. Guisinger, M. C. Hersam, B. I. Yakobson, "Near-equilibrium growth from borophene edges on silver," *Science Advances*, vol. 5 eaax0246, 2019.
- [43] Z. Zhang, Y. Yang, E. S. Penev, B. I. Yakobson, "Elasticity, flexibility, and ideal strength of borophenes," *Advanced Functional Materials* vol. 27(9) p. 605059, 2017.
- [44] Z. Zhuhua, E. S. Penev, B. I. Yakobson, "Two-dimensional boron: structures, properties and applications," *Chemical Society Reviews* vol. 46(22) pp. 6746-6763, 2017.
- [45] T. A. Türkmen, N. Taşaltın, C. Taşaltın, G. Baytemir, S. Karakuş, "PEDOT:PSS/β12 borophene nanocomposites as an inorganic-organic hybrid electrode for high performance supercapacitors,"

- Inorganic Chemistry Communications vol. 139, 109329 2022.
- [46] S. Güngör, C. Taşaltın, İ. Gürol, G. Baytemir, S. Karakus, N. Tasaltın, "Copper phthalocyanine-borophene nanocomposite-based non-enzymatic electrochemical urea biosensor," Applied Physics A vol. 128 p.89 2022.
- [47] G. Baytemir, İ. Gürol, S. Karakuş, C. Taşaltın, N. Taşaltın, "Nickel phthalocyanine-borophene nanocompositebased electrodes for non-enzymatic electrochemical detection of glucose," Journal of Materials Science: Materials in Electronics vol. 33 pp. 16586- 16596 2022.
- [48] M. Ou, X. Wang, L. Yu, C. Liu, W. Tao, X. Ji, L. Mei, "The Emergence and Evolution of Borophene," Advanced Science vol. 8 pp. 1-29, 2021.
- [49] C. Tasaltın, "Glucose sensing performance of PAN:  $\beta$ -rhombohedral borophene based non-enzymatic electrochemical biosensor," Inorganic Chemistry Communications vol. 133, 108973, 2021.
- [50] Y. Wang, X. Pan, Y. Chen, Q. Wen, C. Lin, J. Zheng, W. Li, H. Xu, L. Qi "A 3D porous nitrogen-doped carbon nanotube sponge anode modified with polypyrrole and carboxymethyl cellulose for high-performance microbial fuel cells," Journal of Applied Electrochemistry vol. 50 pp. 1281–1290, 2020.
- [51] M. Guzinski, E. Lindner, B. Prendley, E. Chaum, "Electrochemical sensor for tricyclic antidepressants with low nanomolar detection limit: Quantitative Determination of Amitriptyline and Nortriptyline in blood," Talanta, vol. 239, p. 123086, 2022.



SAKARYA ÜNİVERSİTESİ

# FEN BİLİMLERİ ENSTİTÜSÜ DERGİSİ

Sakarya University Journal of Science  
SAUJS

ISSN 1301-4048 e-ISSN 2147-835X Period Bimonthly Founded 1997 Publisher Sakarya University  
<http://www.saujs.sakarya.edu.tr/>

Title: Two New Records for the Fish Fauna of Simenlik-Akgöl Lagoon in Yeşilırmak River Basin (Samsun-Turkey)

Authors: Melek ÖZPİÇAK, Semra SAYGIN, Savaş YILMAZ, Nazmi POLAT

Received: 2022-07-05 00:00:00

Accepted: 2022-09-20 00:00:00

Article Type: Research Article

Volume: 26

Issue: 6

Month: December

Year: 2022

Pages: 1104-1110

How to cite

Melek ÖZPİÇAK, Semra SAYGIN, Savaş YILMAZ, Nazmi POLAT; (2022), Two New Records for the Fish Fauna of Simenlik-Akgöl Lagoon in Yeşilırmak River Basin (Samsun-Turkey). Sakarya University Journal of Science, 26(6), 1104-1110, DOI: 10.16984/saufenbilder.1141017

Access link

<https://dergipark.org.tr/en/pub/saufenbilder/issue/74051/1141017>

New submission to SAUJS

<http://dergipark.gov.tr/journal/1115/submission/start>

## Two New Records for the Fish Fauna of Simenlik-Akgöl Lagoon in Yeşilirmak River Basin (Samsun-Turkey)

Melek ÖZPİÇAK\*<sup>1</sup> , Semra SAYGIN<sup>1</sup> , Savaş YILMAZ<sup>1</sup> , Nazmi POLAT<sup>1</sup> 

### Abstract

In this study, two new freshwater fish species, *Gambusia holbrooki* Girard, 1859 and *Petroleuciscus borysthenicus* (Kessler, 1859) were reported from Simenlik-Akgöl Lagoon in Yeşilirmak Basin (Samsun). Turkey has a rich biodiversity in terms of freshwater fish. Because of climate change, periodic ichthyofauna monitoring and updating of fish fauna are critical. *Gambusia holbrooki*, Eastern mosquitofish, is an invasive fish species and has a widespread range because of biological struggle against mosquitoes in many water sources. However, simultaneously feeding with fish eggs presents a significant threat to biodiversity. And also, *Petroleuciscus borysthenicus*, Dnieper chub, is a small bodied-fish from the genus *Petroleuciscus* with a wide range. Dnieper chub and Eastern mosquitofish were assessed as Least Concern (LC) species according to the IUCN criteria. The minimum and maximum total lengths of *P. borysthenicus* and *G. holbrooki* are 4.5 cm-5.7 cm and 2.5 cm-5.3 cm, respectively. The results of this study reveal that the existence of new fish species has been recorded for the fish fauna of Simenlik-Akgöl Lagoon, and the distribution area of both these fish species have reached a different location in Yeşilirmak Basin.

**Keywords:** New record, Yeşilirmak River Basin, *Gambusia holbrooki*, *Petroleuciscus borysthenicus*

### 1. INTRODUCTION

Historical natural processes have produced biodiversity [1]. This means that the identification of biological units, such as species, that are the product of evolutionary processes is the first step in any logical approach to protecting biodiversity [2]. Turkey has a rich biodiversity and endemism in terms

of freshwater fish, because of having both European- and Asian origin species [3]. The species whose range crosses Turkey throughout different geological epochs settle in these locations and establish local colonies there [4]. And also, Black Sea rivers could have acted as glacier refuges during the creation of freshwater ichthyofauna [5, 6]. As a result, many researchers were interested in the detailed

\* Corresponding author: melek.zengin@omu.edu.tr

<sup>1</sup> Ondokuz Mayıs University

E-mail: semra.saygin@omu.edu.tr, savas.yilmaz@omu.edu.tr, npolat@omu.edu.tr

ORCID: <https://orcid.org/0000-0003-3506-4242>, <https://orcid.org/0000-0002-3249-5074>, <https://orcid.org/0000-0003-2859-4886>, <https://orcid.org/0000-0001-9785-9927>



examination of Turkey's ichthyofauna and the finding of faunal components [7-16].

Palearctic leuciscid genus *Petroleuciscus* was first described by [17]. This genus is phenotypically and genetically distinct from sister group *Squalius* [6, 18]. In this genus, *Petroleuciscus borysthenicus* is distributed in Eurasia: Eastern, northern, and western, Black Sea and Azov Sea basins, from eastward in Europe to northwestern Turkey [19]. Due to its extensive distribution and high abundance, this fish was given the IUCN designation of Least Concern (LC) species [20].

The mosquitofish, *Gambusia holbrooki* Girard 1859, one of the worst invasive fish in the world, small fishes of the family Poeciliidae only native to freshwater basins of the east coast of the U.S.A. and Mexico but has been introduced into more than 50 countries [21] in order to control mosquito populations and hence malaria [22]. They were introduced into Turkey for the biological control of malaria between the years 1920-1929 [23]. *G. holbrooki* exhibit strong sexual dimorphism, with females being noticeably bigger than males and males having an anal fin transformed into a gonopodium [24]. The conservation status of *G. holbrooki* was classified as Least Concern (LC) according to the IUCN Red List Criteria [25].

The aim of this study is to record the presence of *Petroleuciscus borysthenicus* and *Gambusia holbrooki* of the families Leuciscidae and Poeciliidae which were not recorded in previous studies of Simenlik-Akgöl Lagoon located within the borders of Yeşilirmak River Basin.

## 2. MATERIALS AND METHODS

Samples were collected from Simenlik-Akgöl Lagoon following coordinates, 41°16' 41.952"

N - 36°56'29.868" E using SAMUS 725 MP electroshocker (Figure 1).

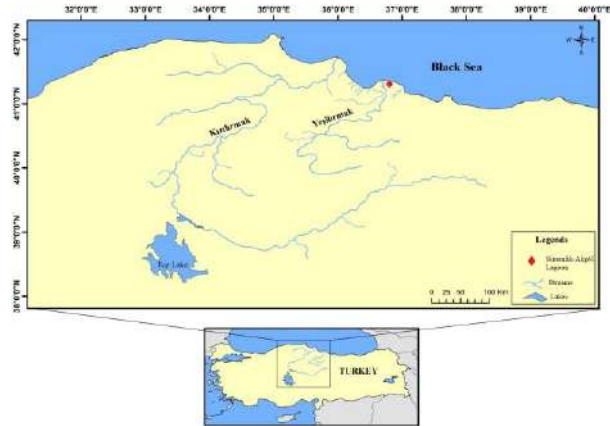


Figure 1 The map of Simenlik-Akgöl Lagoon

*Petroleuciscus borysthenicus* and *Gambusia holbrooki* samples were immediately fixed in 4% formaldehyde in the field and stored permanently in 70% ethanol. Identification of the specimens was based on the morphological characters following [10, 13, 20].

Samples were measured for total length (TL), fork length (FL) and standard length (SL) (0.01 cm.). Individual weights (W) were taken using a digital balance with a precision of 0.01 g. Meristical counts such as Dorsal fin rays (D), Anal fin rays (A), Pectoral fin rays (P), and Ventral fin rays (V) were performed for each sample. Linealateral scales were counted on the left side of the fish samples. Sex was determined by macroscopic examination of the gonads.

## 3. RESULTS AND DISCUSSION

A total of 20 *Petroleuciscus borysthenicus* (12 female, 8 male) individuals and 31 *Gambusia holbrooki* (15 female, 16 male) individuals were sampled from Simenlik-Akgöl Lagoon. The minimum and maximum total lengths and weights of *P. borysthenicus* and *G. holbrooki* individuals are 4.5-5.7 cm and 2.5-5.3 cm, and 0.90-1.98 g and 0.15-1.95 g respectively. And



also, morphological data were offered in Table 1. Meristic characters of the *P. borysthenicus* samples were counted as D: III-IV/8-10; A: III-IV/9-10, V: I-II/8-9; P: I/9-11 and also, D: I-II/5-6; A: II-III 7-8, V: I-II/4-5; P: I/7 for *G. holbrooki*. Scales on lineae lateral are counted as 33-40 and 29-32 for *P. borysthenicus* and *G. holbrooki*, respectively.

Table 1 Descriptive statistics of morfometric measurements for *P. borysthenicus* and *G. holbrooki*

Variables	<i>P. borysthenicus</i>	<i>G. holbrooki</i>
	Min-Max (Mean±SD)	Min-Max (Mean±SD)
Total Length (cm)	4.50-5.70 (5.07±0.4)	2.50-5.30 (4.19±0.9)
Fork Length (cm)	3.90-5.30 (4.64±0.3)	-
Standard Length (cm)	3.60-4.80 (4.16±0.3)	1.90-4.40 (3.34±0.7)
Weight (g)	0.90-1.98 (1.31±0.3)	0.15-1.84 (0.95±0.5)

SD: Standard deviation, Min: Minimum, Max: Maximum.

In the province of Samsun, Simenlik-Akgöl Lagoon Lake is located 25 kilometers from the center of Terme. The boundaries of Yeşilirmak Delta include this region. When the literature is examined, it has been found that there are different studies carried out with the aim of determining the fish fauna of the Yeşilirmak Delta [26-31]. There are some studies about fish fauna of Simenlik-Akgöl Lagoon in literature. *Mugil cephalus*, *Mugil saliens*, *Esox lucius*, *Carassius gibelio*, *Tinca tinca* and *Abramis brama* were recorded from Simenlik by [32]. In addition, *Syngnathus abaster*, *Platichthys flesus*, *Atherina boyeri*, *Gasterosteus aculeatus*, *Neogobius melanostomus* and *Proterorhinus marmoratus* were added to fish fauna of Simenlik-Akgöl Lagoon Lake [26, 33]. However, a recent study [33] recorded an endemic fish species, *Anatolichthys marassentensis* from Simenlik-Akgöl Lagoon.

It is essential to regularly update the fish fauna and monitor the ichthyofauna due to climate change. *Petroleuciscus borysthenicus* was first declared to belong to the genus *Squalius* [8]. It has been accepted later as valid species belonging to the new genus *Petroleuciscus* by many scientists and authorities [17, 20, 34]. *P. borysthenicus* was detected in the Karaboğaz Lagoon [26, 35] and [36] in Miliç River in Samsun Province. *P. borysthenicus* is a small bodied-fish a wide range. This small-bodied fish tolerates a variety of habitats, including marshes, lakes, and montane streams, and favors shallow places with sluggish currents [37- 39].

Also, *G. holbrooki* reported in in this study clearly corroborate with several data obtained by [40] from the Kızılırmak River, Taflan, and Yurtluk Streams and [36] from Miliç River. *G. holbrooki* is among the most invasive fish worldwide, with well documented ecological impacts on ecosystem functioning [41]. The detection of this species in a new location in the Yeşilirmak Basin will contribute to the determination of any potential effects on the local fish fauna. There is no record of *P. borysthenicus* and *G. holbrooki* from Simenlik-Akgöl Lagoon.

#### 4. CONCLUSION

In this study, we report two new records of *P. borysthenicus* and *G. holbrooki* from Simenlik-Akgöl Lagoon. The results of this study reveal that the existence of these fish species has been recorded for the fish fauna of Simenlik-Akgöl Lagoon. In particular, the fact that one of the caught species is an invasive species is important for carrying out more comprehensive studies in this area.

It is important to look into the effects of invasive fish species that have colonized the inland waters of Turkey, either naturally or as a result of human activity, and have established

long-term populations there. Particular attention should be paid to endemic species that live in these habitats. It is essential for scientists, decision-makers, resource managers, and the general public to comprehend the variety of the freshwater ichthyofauna of any nation in order to more accurately assess how human activities affect the freshwater fishes there.

### ***Funding***

The author (s) has no received any financial support for the research, authorship or publication of this study.

### ***Authors' Contribution***

The authors contributed equally to the study.

### ***The Declaration of Conflict of Interest/ Common Interest***

No conflict of interest or common interest has been declared by the authors.

### ***The Declaration of Ethics Committee Approval***

This study does not require ethics committee permission or any special permission.

### ***The Declaration of Research and Publication Ethics***

The authors of the paper declare that they comply with the scientific, ethical and quotation rules of SAUJS in all processes of the paper and that they do not make any falsification on the data collected. In addition, they declare that Sakarya University Journal of Science and its editorial board have no responsibility for any ethical violations that may be encountered, and that this study has not been evaluated in any academic publication environment other than Sakarya University Journal of Science.

## **REFERENCES**

- [1] C. R. Darwin, On the origin of species by means of natural selection: or the preservation of favoured races in the struggle for life. J. Murray, London, 1859.
- [2] R. L. Mayden, Wood R. M., "Systematics, species concepts, and the evolutionarily significant unit in biodiversity and conservation biology" in Evolution And The Aquatic Ecosystem: Defining Unique Units In Population Conservation. J. L. Nielsen, editor. Symposium 17. American Fisheries Society, Bethesda, Maryland, 1995, pp. 58-113.
- [3] A. S. Tarkan, S. M. Marr, F. G. Ekmekçi, "Non-native and translocated freshwater fish," FiSHMED Fishes in Mediterranean Environments, vol. 3, pp. 1-28, 2015.
- [4] S. Ugurlu, N. Polat, "Fish Fauna of the Karaabdal Stream (Samsun-Turkey)," Turkish Journal of Fisheries and Aquatic Sciences, vol. 8, pp. 121-124, 2008.
- [5] P. Kotlík, N. G. Bogutskaya, F. G. Ekmekci, "Circum Black Sea phylogeography of *Barbus* freshwater fishes: divergence in the Pontic glacial refugium," Molecular Ecology, vol. 13, no. 1, pp. 87-95, 2004.
- [6] S. Perea, M. Bohme, P. Zupancic, J. Freyhof, R. Sanda, M. Ozulug, A. Abdoli, I. Doadrio, "Phylogenetic relationships and biogeographical patterns in Circum-Medi-terranean subfamily Leuciscinae (Teleostei, Cyprinidae) in-ferred from both mitochondrial and nuclear data," BMC Evolutionary Biology, vol. 10, pp. 1-27, 2010.

- [7] K. E. Abbolt, "Letter accompanying a collection from Trebizond and Erzeroun," *Proceedings of the Zoological Society of London*, vol. 3, pp. 89-92, 1835.
- [8] N.G. Bogutskaya, "Contribution to the knowledge of leuciscine fishes of Asia Minor. Part 1. Morphology and taxonomic relationships of *Leuciscus borysthenicus* (Kessler, 1859), *L. smyrnaeus* Boulenger, 1896 and *Ladigesocypris ghigii* (Gianferrari, 1927)," *Publicaciones especiales del Instituto Español de Oceanografía*, vol. 21, pp. 25-44, 1996.
- [9] M. Kuru, "Türkiye iç su balıklarının son sistematik durumu," *Gazi Üniversitesi Eğitim Fakültesi Dergisi*, vol. 24, pp. 1-21, 2004.
- [10] R. Geldiay, S. Balık, "Türkiye tatlısu balıkları," 5. Baskı, Ege Üniversitesi Basımevi, Bornova-İzmir, 644 p, 2007.
- [11] R. Fricke, M. Bilecenoglu, H.M. Sari, "Annotated checklist of fish and lamprey species (Gnathostomata and Petromyzontomorphi) of Turkey, including a Red List of threatened and declining species," *Stuttgarter Beiträge zur Naturkunde, Serie A (Biologie)*, vol. 706, pp. 1-172, 2007.
- [12] M., Bilecenoglu, M. Kaya, B. Cihangir, E. Çiçek, "An updated checklist of the marine fishes of Turkey," *Turkish Journal of Zoology*, vol. 38, pp. 901-929, 2014.
- [13] E. Cicek, S. Sungur, R. Fricke, "Freshwater lam-preys and fishes of Turkey; a revised and updated annotated checklist 2020," *Zootaxa*, vol. 4809, no. 2, pp. 241-270, 2020.
- [14] D. Giannetto D. Innal, "Status of endemic freshwater fish fauna inhabiting major lakes of Turkey under the threats of climate change and anthropogenic disturbances: A review," *Water*, vol. 13, no. 11, pp. 1534, 2021.
- [15] D. Turan, M. Kottelat, C. Kaya, "The trouts of the upper Kura and Aras rivers in Turkey, with description of three new species (Teleostei: Salmonidae)," *Zootaxa*, vol. 5150, no. 1, pp. 43-64, 2022.
- [16] E. Çiçek, S. Eagderi, B. Secer, S. Sungur, "Taxonomic Status of the Genus *Sabanejewia* (Cobitidae) from Kura-Aras River System (Turkey)," *Transylvanian Review of Systematical and Ecological Research*, vol. 24, pp. 83-94, 2022.
- [17] N.G. Bogutskaya, "*Petroleuciscus* a new genus for the *Leuciscus borysthenicus* species group (Teleostei: Cyprinidae)," *Zoosystematica Rossica*, vol. 11, no. 1, pp. 235-237, 2002.
- [18] S. Schönhuth, J. Vukić, R. Šanda, L. Yang, R.L. Mayden, "Phylogenetic relationships and classification of the Holarctic family Leuciscidae (Cypriniformes: Cyprinoidei)," *Molecular Phylogenetics and Evolution*, vol. 127, pp. 781-799, 2018.
- [19] G. Kalaycı, "Molecular Phylogeny and Historical Biogeography of *Petroleuciscus* (Teleostei: Leuciscidae) Species in Turkey," *Journal of Anatolian Environmental and Animal Sciences*, vol. 7, no. 1, pp. 88-95, 2022.
- [20] J. Freyhof, M. Kottelat, "*Petroleuciscus borysthenicus*. The IUCN Red List of Threatened Species, 2008, e.T61395A12461180". 28.06.2022

- [Online]. Available <https://dx.doi.org/10.2305/IUCN.UK.2008.RLTS.T61395A12461180>. en.
- [21] E. García-Berthou, C. Alcaraz, Q. Pou-Rovira, L. Zamora, G. Coenders, and C. Feo, "Introduction pathways and establishment rates of invasive aquatic species in Europe," *Canadian Journal of Fisheries and Aquatic Sciences*, vol. 62, pp. 453–463, 2005.
- [22] G. H. Pyke, "A review of the biology of *Gambusia affinis* and *G. holbrooki*," *Reviews in Fish Biology and Fisheries*, vol. 15, pp. 339–365, 2005.
- [23] W. E. Walton, J. A. Henke, A. M. Why, "*Gambusia affinis* (Baird & Girard) and *Gambusia holbrooki* Girard (mosquitofish)," in *A Handbook of Global Freshwater Invasive Species*, New York: Earthscan, R. A. Francis, 2012, pp. 261-272.
- [24] M. B. Cabrera, S. Bogan, P. Posadas, G. M. Somoza, J. I. Montoya-Burgos, and Y. P. Cardoso, "Risks associated with introduction of poeciliids for control of mosquito larvae: first record of the non-native *Gambusia holbrooki* in Argentina," *Journal of Fish Biology*, vol. 91, no. 2, pp. 704-710, 2017.
- [25] NatureServe, "*Gambusia holbrooki*. The IUCN Red List of Threatened Species 2013: e.T202394A18232445". July, 4 2022, [Online]. Available:<https://dx.doi.org/10.2305/IUCN.UK.2013-1.RLTS.T202394A18232445>.en.
- [26] S. Uğurlu, N. Polat, Ş. Kandemir, "Fish fauna of lagoons within the Kızılırmak and Yeşilirmak Deltas (Samsun-Turkey)," *Journal of Fisheries Sciences*, vol. 2, no. 3, pp. 475-483, 2008.
- [27] M. Zengin, S. U. Tiril, M. Dağtekin, M. Gül, H. Eryildirim, "Preliminary study on the status of sturgeon populations (*Acipenser* sp.) in the South Eastern Black Sea Coast (Kızılırmak-Yeşilirmak Basin) in the early 21st century," in *EIFAC Symposium On Interactions Between Social, Economic And Ecological Objectives Of Inland Commercial And Recreational Fisheries And Aquaculture*, 2010, pp. 44-55.
- [28] B. Yogurtcuoglu, G. F. Ekmekci, "New Records of Kızılırmak Toothcarp, *Aphanius marassantensis* from Central Yeşilirmak River Basin (Turkey)," *Turkish Journal of Fisheries and Aquatic Sciences*, vol. 17, pp. 205-208, 2007.
- [29] S. Benzer "New record of the Kizilirmak killifish (*Aphanius marassantensis* Pflaederer, Geiger & Herder, 2014) from Süreyyabey Dam Lake in Yeşilirmak basin," *Mugla Journal of Science and Technology*, vol. 4, no. 1, pp. 41-45, 2018.
- [30] S. Benzer, "First Record of the Sand Smelt *Atherina boyeri* Risso, 1810 in the Süreyyabey Dam Lake, Yeşilirmak Basin, Turkey". *Annals of Biological Science*, vol. 6, no. 2, pp. 38-42.
- [31] M. Ozpicak, M., S. Saygin, S. Yilmaz, N. Polat, "Additional record of *Anatolichthys marassantensis* from Simenlik-Akgöl Lagoon in lower Yeşilirmak Drainage (Türkiye)," *Aquatic Research*, vol. 5, pp. 230-237, 2022.
- [32] S. (Helli) Uğurlu, N. Polat, "An investigation on fish fauna in Lake Simenit (Terme-SAMSUN)," *Science*

- and Engineering Journal of Firat University, vol. 15, no. 4, pp. 485-494, 2003.
- [33] N. Polat, S. Uğurlu, “Samsun İli Tatlı Su Balık Faunası,” Ceylan Ofset, 2011, 272, Samsun. ISBN: 978-605-87638-0-7.
- [34] E. V. Romanov, S. Luna, *Petroleuciscus borysthenicus* (Kessler, 1859), Dnieper chub, Aug., 6 2017, [Online]. Available: <http://www.fishbase.org/summary/25956>
- [35] S. Uğurlu, N. Polat, Ş. Kandemir, “First records for the ichthyofauna of Samsun (Turkey),” Journal of Applied Biological Sciences, vol. 3, no. 3, pp. 81-84, 2009.
- [36] S. Saygun, F. Saygun, C. Önel, “Five New Records for the Ichthyofauna of Miliç River in Turkey,” Ordu University Journal of Science and Technology, vol. 7, no. 2., pp.183-195, 2017.
- [37] M. Kottelat, J. Freyhof. Handbook of European Freshwater Fishes. Berlin, Germany, 2007.
- [38] G. Saç, M. Özuluğ, “Effects of environmental variables on the distribution of fish assemblages in an endorheic stream (Istanbul, Turkey),” Fresenius Environmental Bulletin, vol. 26, no. 12, pp. 7150–7159, 2017.
- [39] S. Ağdamar, G. Saç “Growth and feeding ecology of Dnieper chub *Petroleuciscus borysthenicus* (Kessler, 1859) in Şahinkaya Reservoir, an artificial water body of an island ecosystem (Gökçeada, Turkey),” Çanakkale Onsekiz Mart University Journal of Advanced Research in Natural and Applied Sciences, vol. 8, no. 1, pp. 76-85, 2022.
- [40] S. Uğurlu, N. Polat, “Exotic fish species inhabiting in freshwater sources within the province of Samsun,” Journal of Fisheries Sci., vol. 1, no. 3, pp. 139–151, 2007.
- [41] C. Alcaraz, E. García-Berthou, “Life history variation of an invasive fish (*Gambusia holbrooki*) along a salinity gradient,” Biological Conservation, vol. 139, pp. 83-92, 2007.



SAKARYA ÜNİVERSİTESİ

# FEN BİLİMLERİ ENSTİTÜSÜ DERGİSİ

Sakarya University Journal of Science  
SAUJS

ISSN 1301-4048 e-ISSN 2147-835X Period Bimonthly Founded 1997 Publisher Sakarya University  
<http://www.saujs.sakarya.edu.tr/>

Title: Investigation of Parametric, Non-Parametric and Semiparametric Methods in Regression Analysis Structures

Authors: Esra YAVUZ, Mustafa ŞAHİN

Received: 2022-07-22 00:00:00

Accepted: 2022-09-22 00:00:00

Article Type: Research Article

Volume: 26

Issue: 6

Month: December

Year: 2022

Pages: 1111-1116

How to cite

Esra YAVUZ, Mustafa ŞAHİN; (2022), Investigation of Parametric, Non-Parametric and Semiparametric Methods in Regression Analysis Structures. Sakarya University Journal of Science, 26(6), 1111-1116, DOI: 10.16984/saufenbilder.1147135

Access link

<https://dergipark.org.tr/en/pub/saufenbilder/issue/74051/1147135>

New submission to SAUJS

<http://dergipark.gov.tr/journal/1115/submission/start>

## Investigation of Parametric, Non-Parametric and Semiparametric Methods in Regression Analysis

Esra YAVUZ\*<sup>1</sup> , Mustafa ŞAHİN<sup>2</sup> 

### Abstract

Regression analysis is known as statistical methods applied to model and analyze the relationship between variables. Regression method can be examined as parametric, non-parametric and semiparametric regression methods. The parametric regression method assumes that the dependent variable is in a linear relationship with the independent variables and that the shape of the relationship is known. If these assumptions are not met, non-parametric regression methods are applied. However, these methods cause difficulties especially in the interpretation part due to the problem of multidimensionality when there is more than one independent variable. Thus, when there is more than one independent variable, some of the independent variables may be in a linear relationship with the dependent variable, while the other part may be in a nonlinear relationship. Thus, in order to model these relationships, semiparametric regression methods, which are the additive combination of parametric and non-parametric regression methods, are used. In this study, parametric regression method, definition of non-parametric regression method and assumption conditions are given. It has been shown that the semiparametric regression method can be applied in cases where these assumptions are not met. Thus, in the study, regression methods were examined in three different parts, and parametric, non-parametric and semiparametric regression methods were examined theoretically.

**Keywords:** Parametric, non-parametric, semiparametric, regression

### 1. INTRODUCTION

Regression analysis, one of the most important subjects of statistics, is an analysis method applied to measure the relationship between two or more variables.

Regression analysis gives information about the existence of a relationship between dependent and independent variables and, if there is, about the type and strength of that relationship [1]. In general, regression analysis investigates whether there is an effect of another variable on a variable.

\* Corresponding author: yavuz7346@gmail.com

<sup>1</sup> Şırnak University

ORCID: <https://orcid.org/0000-0002-5589-297X>

<sup>2</sup> Kahramanmaraş Sütçü İmam University

E-mail: ms66@ksu.edu.tr

ORCID: <https://orcid.org/0000-0003-3622-4543>



Here, while the dependent variable is one, the variables that affect it (independent variables) can be one or more. A regression model with one independent variable is called simple linear regression, and a regression model with more than one independent variable is called multiple linear regression analysis. Regression analysis is based on the assumptions that the independent variables affect the dependent variable linearly, that the relationship between dependent and independent variables is known, and that the dependent variable has a normal distribution.

However, in many estimation problems, some of the independent variables do not affect the dependent variable linearly. Thus, the need to examine regression models that include nonlinear or more complex variables arises. For this reason, regression analysis is examined in three different groups as parametric, non-parametric and semiparametric regression [2].

In the parametric regression model, it is assumed that the shape of the regression function is known beforehand. At the same time, it is assumed that the error variances are constant for all independent variables, there is no autocorrelation between the error terms, the variables are normally distributed, and there is no multicollinearity problem between the independent variables [3]. If these conditions are not met, the estimations made for the regression function lead to incorrect results and interpretations. In cases where the assumptions are not met, these estimations will not be a good estimation result, so a non-parametric regression model that can stretch the linearity assumption in the parametric regression model is needed. While strong assumptions are required in the parametric regression model, these assumptions are not required in the non-parametric regression model [4].

In the non-parametric regression model, the shape of the function is not predetermined and there are no assumptions provided in the parametric regression model. The only part of the assumption requirement is that the mean of the error terms is zero and the variance is finite. Thus, flexibility is created in the emergence of the relationship between the variables. In non-parametric regression, it is known for the ability of the data to express itself [5]. In addition to its advantages in non-parametric regression, it also has some difficulties. One of these challenges is the need for a large amount of data. Another challenge is the complexity of operations and the need for intensive computer use. In cases where the number of independent variables is more than two, alternative methods are needed because it is difficult to apply the analyzes with non-parametric regression method and to interpret the graphs [6]. Thus, semiparametric regression model can be applied in cases where parametric and non-parametric regression methods are not used. In semiparametric regression models, time dependent and chance variables are included in the model with non-parametric methods, while continuous independent variables are included in the model with parametric methods [7].

Semiparametric regression method is also known as partial linear regression method due to the additive combination of parametric and non-parametric regression. In the semiparametric regression method, if the independent variables are unrelated, the coefficients of the parametric variables are estimated by the least squares method, and the non-parametric variables are estimated by methods such as spline [8]. The fact that the semiparametric regression method is less restrictive than parametric and non-parametric methods has led to the use of this method more. In addition, since the sample size is less important in this method, especially in applications consisting of small samples, the researcher has the opportunity to continue the



practice even if he or she has no knowledge about the parameter and variable. One of the most important features that distinguishes the semiparametric method from other methods is that the research continues even if the assumptions are not fulfilled [9].

Recently, in addition to parametric and non-parametric regression methods, the need for semiparametric regression method has increased. The aim of this study is to use semiparametric regression method in addition to these methods in cases where parametric and non-parametric regression methods are insufficient [10].

## 2. METHODS

### 2.1. Regression Methods

The regression method is a method applied to measure the relationship between two or more variables that have a cause-effect relationship between them. In the regression, the existence of the relationship between the variables, and if there is a relationship, estimations and predictions about the strength of the relationship are made. In the regression method, one of the variables is applied as the dependent variable and the others as the independent variable [11].

where  $x$  is the independent variable and  $y$  is the relationship between the dependent variable,

$$y = f(x) \quad (1)$$

shown in the form.

The purpose of the regression method is to examine the existence of the relationship between the independent variables on the dependent variable and to estimate the values that the dependent variable can take [12]. The regression method is shown in three different

groups as parametric, non-parametric and semiparametric regression [13].

#### 2.1.1. Parametric regression method

The method of examining the mean relationship between dependent and independent variables with a mathematical function and determining the parameters in this function clearly is called parametric regression [14]. Parameters are measures such as mean, variance and ratio of the population. In the parametric regression method, the  $x_1, x_2, \dots, x_p$  arguments are assumed to be linear.  $X = (x_1, x_2, \dots, x_p)$  represents the mean of  $y$  dependent variable versus the change in independent variables [15],

$$y = X\beta + \varepsilon_i \quad (2)$$

shown in the form.

The parametric regression method is based on assumptions. It assumes that the functional shape between the independent variables,  $X\beta$ , is considered linear and that the  $\beta$  parameters are finite [15].

#### 2.1.2. Nonparametric regression method

Non-parametric regression model created with the dependent variable ( $y$ ) and the independent variable ( $x$ ), whose relationship with the dependent variable is unknown,

$$y_i = f(x_i) + \varepsilon_i, \quad i = 1, 2, \dots, n \quad (3)$$

shown in the form. In the non-parametric regression method, besides estimating the parameters, it aims to estimate the unknown mean function  $f(x_i)$ .

Although there are no limiting assumptions when estimating in non-parametric regression, some features must be provided. When the number of independent variables is large, it

becomes increasingly difficult to make an estimation. Thus, the interpretation of the resulting graphics becomes more complicated [16]. Thus, it causes the problem of dimensionality. In addition to these situations, it is difficult to apply discrete independent variables in the non-parametric regression method and to interpret the effects of the y variable with the increase in the number of independent variables. As a result of these difficulties, the application of the semiparametric regression method provides an advantage [17].

### 2.1.3. Semiparametric regression method

Semiparametric regression method, in which some of the variables in the model are considered as parametric and the other part as non-parametric regression,

$$y_i = \alpha + x_1\beta_1 + \dots + x_j\beta_j + f_1(x_{j+1}) + \dots + f_k(x_k) + \varepsilon \quad (4)$$

is expressed as. In this model,  $j$  variables have a linear effect on the dependent variable  $y$  and represent the parametric part of the model. It creates a non-linear effect on the dependent variable  $y$  of other variables and represents the non-parametric part of the model. Since more than one variable is considered in the non-parametric regression part, the problems that occur in the non-parametric regression method are also valid for these models. In order to eliminate the problems that occur, the variables in the non-parametric part of the model are included in the model additively, and a new model is created. In addition, there may be dummy variables in the parametric part of the model [18].

At the stage of model creation, first of all, the variables are determined. Then, the functional or mathematical shape of the model should be determined. While creating the mathematical figure, first of all, the graphics should be interpreted. By interpreting the graphs created

with the dependent variable and the independent variables, information is given about the structure of the relationship between the variables. After examining the graphs of the variables, a semiparametric regression model is applied in which some of the independent variables are suitable for parametric and the other part is suitable for non-parametric relationships. The parametric part of the semiparametric regression method creates the linear relationship, and the non-parametric part creates the nonlinear relationship. For this reason, the semiparametric regression method is also called semi-linear methods.

Iterative algorithms are generally applied in the estimation of semiparametric regression methods. These algorithms are many algorithms used for estimation of methods and these algorithms are analyzed in many computer programs. The most preferred programs in the analysis of these algorithms are R software, SAS software and Stata software [15].

When the independent variables in the semiparametric regression model are unrelated, the coefficients of the variables in the parametric part of the model are analyzed with the least squares method, and the non-parametric variables are analyzed with the estimations of non-parametric methods such as spline. However, in the semiparametric regression method, the parametric and non-parametric parts of the model may be related to each other [13]. Algorithms are needed in which the relationships between the variables are taken into account when relevant. The most preferred among these algorithms are the backward fit algorithm, the Newton-Raphdon algorithm, the Speckman approach and the partial spline approaches [16].

### 3. CONCLUSIONS AND DISCUSSION

When there is more than one independent variable in the regression analysis, some of the independent variables may be in a linear relationship with the dependent variable, while the other part may be in a nonlinear relationship. In addition, in cases where the number of independent variables is more than two, it becomes difficult to apply non-parametric regression analyzes and interpret graphs. In order to model such relationships, semiparametric regression methods, which are a combination of parametric and non-parametric regression methods, are used.

In this study, first of all, parametric regression method, definition of non-parametric regression method and assumption conditions are given. It has been shown that the semiparametric regression method can be applied in cases where these assumptions are not met. Thus, in the study, regression methods were examined in three different parts, and parametric, non-parametric and semiparametric regression methods were examined theoretically.

#### *Acknowledgments*

This study was presented at the "IFSCOM2022 8th International IFS and Contemporary Mathematics Conference".

#### *Funding*

The author (s) has no received any financial support for the research, authorship or publication of this study.

#### *Authors' Contribution*

The authors contributed equally to the study.

#### *The Declaration of Conflict of Interest/ Common Interest*

No conflict of interest or common interest has been declared by the authors.

#### *The Declaration of Ethics Committee Approval*

This study does not require ethics committee permission or any special permission.

#### *The Declaration of Research and Publication Ethics*

The authors of the paper declare that they comply with the scientific, ethical and quotation rules of SAUJS in all processes of the paper and that they do not make any falsification on the data collected. In addition, they declare that Sakarya University Journal of Science and its editorial board have no responsibility for any ethical violations that may be encountered, and that this study has not been evaluated in any academic publication environment other than Sakarya University Journal of Science.

### REFERENCES

- [1] G. Aneiros-Pérez, P. Vieu, "Nonparametric time series prediction: A semi-functional partial linear modeling", *Journal of Multivariate Analysis*, vol. 99, no 5, pp. 834-857, 2008.
- [2] M. Aytaç, "Applied non-parametric statistical tests", Uludag University Press, Bursa, Turkey, 1991.
- [3] J. Begun, W. Hall, W. Huang, J. Wellner, "Information and asymptotic efficiency in parametric-nonparametric models", *The Annals of Statistics*, vol. 11, pp. 432-452, 1983.
- [4] M. Çitil, F. Tuğrul, "Some New Equalities On the Intuitionistic Fuzzy Modal Operators", *Sakarya University Journal of Science*, vol. 22, no 6, pp. 1524-1531 2018.

- [5] J. Harezlak, D. Ruppert, M. P. Wand, "Semiparametric regression with R", New York: Springer, 2018.
- [6] L. Keele, "Semiparametric Regression For The Social Sciences", Chichester: John Wiley & Sons, 2008.
- [7] R. Li, H. Liang, "Variable selection in semiparametric regression modeling", *Annals of statistics*, vol. 36, no 1, p. 261, 2008.
- [8] D. Y. Lin, L. J. Wei, I. Yang, Z. Ying, "Semiparametric regression for the mean and rate functions of recurrent events", *Journal of the Royal Statistical Society: Series B (Statistical Methodology)*, vol. 62, no 4, pp. 711-730, 2000.
- [9] J. Liu, R. Zhang, W. Zhao, "A robust and efficient estimation method for single index models". *Journal of Multivariate Analysis*, vol. 122, pp. 226-238, 2013.
- [10] M. Mammadov, A. F. Yüzer, D. Aydın, "Splayn correction regression and correction parameter selection", 4th Statistics Congress proceedings and poster abstracts book, Belek-Antalya, September 25-28, pp: 148-149, 2005.
- [11] X. Shi, "Applications of nonparametric and semiparametric methods in economics and finance". PhD Thesis, Economics in the Graduate School of Binghamton University, New York, 2009.
- [12] D. Ruppert, M. P. Wand, R. J. Carroll, "Semiparametric regression" (No. 12). Cambridge university press, 2003.
- [13] X. Shi, "Applications of nonparametric and semiparametric methods in economics and finance". PhD Thesis, Economics in the Graduate School of Binghamton University, New York, 2009.
- [14] N. Tezcan, "Non-parametric regression analysis". *Atatürk University Journal of Economics and Administrative Sciences*, vol. 25, pp. 341-352, 2011.
- [15] S. Toprak, "Semi-parametric regression models with measurement errors". PhD Thesis, Dicle University, Institute of Science, Department of Mathematics, Diyarbakır, Turkey, pp: 98, 2015.
- [16] A. Yatchew, "Semiparametric regression for the applied econometrician". Cambridge University Pres, Cambridge, UK, pp: 213, 2003.
- [17] E. Yavuz, M. Şahin, "Semiparametric Regression Models and Applicability in Agriculture". *Black Sea Journal of Agriculture*, 9-10, 2022.
- [18] M. Turan, S. Bağdatlı, "Semiparametric Regression". *Suggestion Journal*, vol. 9, no 35, pp. 207-213, 2011.



SAKARYA ÜNİVERSİTESİ

# FEN BİLİMLERİ ENSTİTÜSÜ DERGİSİ

Sakarya University Journal of Science  
SAUJS

ISSN 1301-4048 e-ISSN 2147-835X Period Bimonthly Founded 1997 Publisher Sakarya University  
<http://www.saujs.sakarya.edu.tr/>

Title: Synthesis and Structural Characterization of Novel 2-Aminomethyl  
Quinazolin-4(3H)-ones as Organic Building Blocks

Authors: Feyzi Sinan TOKALI

Received: 2022-03-09 00:00:00

Accepted: 2022-09-29 00:00:00

Article Type: Research Article

Volume: 26

Issue: 6

Month: December

Year: 2022

Pages: 1117-1130

How to cite

Feyzi Sinan TOKALI; (2022), Synthesis and Structural Characterization of Novel  
2-Aminomethyl Quinazolin-4(3H)-ones as Organic Building Blocks. Sakarya  
University Journal of Science, 26(6), 1117-1130, DOI:  
10.16984/saufenbilder.1085086

Access link

<https://dergipark.org.tr/en/pub/saufenbilder/issue/74051/1085086>

New submission to SAUJS

<http://dergipark.gov.tr/journal/1115/submission/start>

## Synthesis and Structural Characterization of Novel 2-Aminomethyl Quinazolin-4(3H)-ones as Organic Building Blocks

Feyzi Sinan TOKALI\*<sup>1</sup> 

### Abstract

Quinazoline and quinazolinone derivatives display an extensive application in organic and pharmaceutical chemistry, and they have been used as natural and synthetic materials for medicinal chemistry purposes. Here I reported an investigation of a new series of quinazolinone ring derivatives. In this context, starting from the methyl anthranilate, six quinazolinone derivatives (**4a-f**) with various aminomethyl moieties at position 2 were synthesized (89-80%). The structures of compounds **4a-f** were identified using FTIR and NMR Spectroscopy (<sup>1</sup>H NMR - <sup>13</sup>C NMR). The data obtained from the all spectra clearly identify the structures of the compounds.

**Keywords:** Quinazoline, quinazolinone, synthesis, building blocks, NMR

### 1. INTRODUCTION

Heterocyclic compounds are very important building blocks in drug discovery studies. They are found in structure of many drugs as synthetic or natural products (Figure 1). Quinazolines and quinazolinones are some of the common chemical building blocks, which belong to the family of heterocyclic nitrogen compounds. Quinazolines are heterocyclic compounds that contain a fused pyrimidine and benzene ring in their structure. Quinazolinones are the saturated form of the quinazolines and classified according to the position of carbonyl group (2(1H), 4(3H), and 2,4(1H,3H) quinazolinindiones). 4(3H) derivatives have attracted the attention of scientists due to their accessibility, ease of synthesis methods, easy availability of starting

materials and their biological activities. This class of compounds that known natural and synthetic derivatives have investigated by many scientists for their antitumor [1, 2], anticancer [3-6], anti-inflammatory [7], antimicrobial [8-10], anticonvulsant [11, 12], antifungal [13], anticholinesterase [14, 15], anti-HIV [16], anti-diabetic [17, 18], dihydrofolate reductase inhibition [19], and kinase inhibition [20] properties. Quinazolinones are generally derived from the 2-position. Studies on quinazolinones with some alkyl [21-26] and aryl group [27-30] at the 2 position are frequently encountered in the literature. However, quinazolinones with an aminomethyl moiety at position 2 are rarely encountered. The ones synthesized from these compounds either do not have an experimental procedure or their structures have not been characterized [31].

\* Corresponding author: feyzitokali@gmail.com

<sup>1</sup> Kafkas University

ORCID: <https://orcid.org/0000-0001-5532-8802>



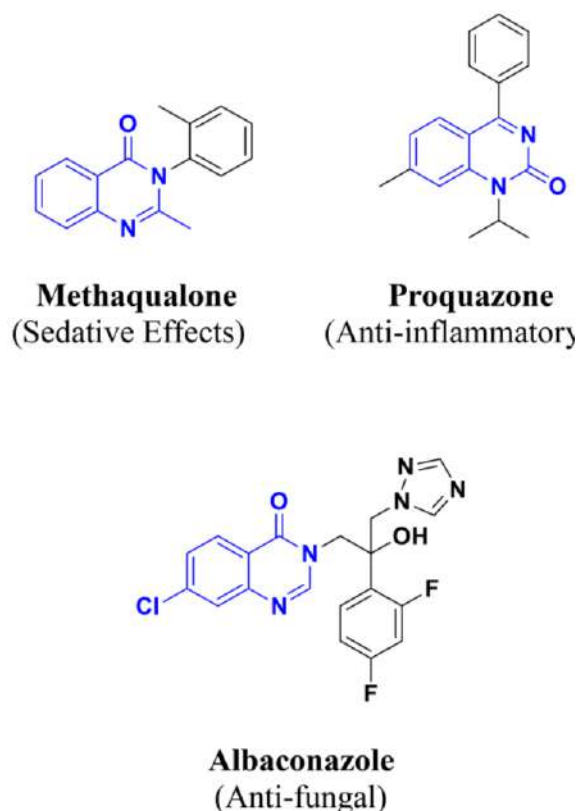


Figure 1 Some drugs containing quinazolinone ring

In this study, it was aimed to synthesize 2-aminomethyl derivatives of quinazolinones, which have great importance in organic, pharmaceutical, and medicinal chemistry for the scientist wants to study the biological activity of quinazolinone derivatives and to characterize their structures.

## 2. MATERIALS AND METHODS

### 2.1. Materials

The starting materials used in this synthesis study were purchased from various suppliers and used without any treatment. WRS-2A Meltingpoint Apparatus was used for determine melting points of the compounds. The FTIR spectra of the compounds were recorded using Alpha-P Bruker FTIR spectrophotometer.  $^1\text{H}$  NMR spectras were recorded on Bruker (400 MHz) and  $^{13}\text{C}$  NMR spectras were recorded on Bruker (100 MHz) spectrometer.

Deuterated chloroform ( $\text{CDCl}_3$ ) was used as solvent.

### 2.2. Methods

#### 2.2.1. Synthesis of compounds 4a-f

Methyl-2-amino benzoate (methyl anthranilate) (**1**) (1,512 g, 10mmol) was dissolved in 20 mL dichloromethane. Sodium bicarbonate (1,68 g, 20mmol) was added to this solution and stirred for 20 minutes at  $0-5^\circ\text{C}$ . Chloroacetyl chloride (1,13 g, 10mmol) was added by dropwise and stirred for an hour at room temperature. After completion (checked by thin layer chromatography; PE:EtOAc – 9:1), the mixture was filtered off and the solvent was removed. *N*-chloroacetyl methyl anthranilate (**2**) (2,28 g, 10mmol) was added to a solution of secondary amine (10mmol) (primer amine for compound **3f**) and  $\text{K}_2\text{CO}_3$  (2,07 g, 15mmol) in acetonitrile (30 mL) at room temperature. Potassium iodide (catalytic amount) was added and refluxed for an hour. After completion (checked by thin layer chromatography; PE:EtOAc – 7:3), the mixture was filtered off and the solvent was removed. The crude product (**3a-f**) (10mmol) was dissolved in absolute ethanol (20 mL) and  $\text{N}_2\text{H}_4\cdot\text{H}_2\text{O}$  (1,6 mL, 25mmol, w/w: 80%) was added. The solution was refluxed for 12 hours. After completion (checked by thin layer chromatography; PE:EtOAc – 1:1), 50% of solvent was removed and ether (20 mL) was added. Formed white crystals were filtered off. The crude products (**4a-f**) were recrystallized from ethanol:ether - 1:2 (Figure 2).

##### 2.2.1.1. 2-(Morpholinomethyl)-3-aminoquinazolin-4(3H)-one (4a)

White crystals, yield 89% (2,32 g), mp:  $126-128^\circ\text{C}$ . FTIR ( $\text{cm}^{-1}$ ):  $\nu_{\text{max}}$  3312, 3262, 3070, 2953, 1662, 1598, 768.  $^1\text{H}$  NMR (400 MHz,  $\text{CDCl}_3$ )  $\delta$  8.20 (d,  $J= 8.0$  Hz, 1H, ArH), 7.64 – 7.62 (m, 2H, ArH), 7.42 (t,  $J= 7.3$  Hz, 1H, ArH), 6.16 (brs, 2H,  $\text{NH}_2$ ), 3.74



(s, 2H, N-CH<sub>2</sub>), 3.63 (t, *J* = 4.0, 4H, CH<sub>2</sub>-O-CH<sub>2</sub>), 2.56 (t, *J* = 4.0, 4H, CH<sub>2</sub>-N-CH<sub>2</sub>). <sup>13</sup>C-NMR (100 MHz, CDCl<sub>3</sub>): δ 159.3 (C=O), 150.3 (N=C), 146.1, 133.9, 127.5, 126.9, 126.4, 120.0 (ArC), 66.9 (CH<sub>2</sub>-O-CH<sub>2</sub>), 61.9 (N-CH<sub>2</sub>), 53.4 (CH<sub>2</sub>-N-CH<sub>2</sub>).

### 2.2.1.2. 2-[(4-Methylpiperazin-1-yl)methyl]-3-amino-quinazolin-4(3H)-one (4b)

White crystals, yield 80% (2,18 g), mp: 136-138 °C. FTIR (cm<sup>-1</sup>): ν<sub>max</sub> 3323, 3249, 3106, 2956, 1668, 1593, 776. <sup>1</sup>H NMR (400 MHz, CDCl<sub>3</sub>) δ 8.28 (d, *J* = 7.8 Hz, 1H, ArH), 7.81 – 7.65 (m, 2H, ArH), 7.49 (t, *J* = 6.3 Hz, 1H, ArH), 6.36 (brs, 2H, NH<sub>2</sub>), 3.82 (s, 2H, N-CH<sub>2</sub>), 2.67 (s, 4H, CH<sub>2</sub>-N-CH<sub>2</sub>), 2.44 (s, 4H, CH<sub>2</sub>-N-CH<sub>2</sub>), 2.29 (s, 3H, N-CH<sub>3</sub>). <sup>13</sup>C NMR (101 MHz, CDCl<sub>3</sub>) δ 159.1 (C=O), 150.5 (N=C), 146.2, 133.8, 127.5, 126.8, 126.3, 120.0 (ArC), 61.5 (N-

CH<sub>2</sub>), 55.1(CH<sub>2</sub>-N-CH<sub>2</sub>), 52.9 (CH<sub>2</sub>-N-CH<sub>2</sub>), 46.0 (N-CH<sub>3</sub>).

### 2.2.1.3. 2-[(4-Phenylpiperazin-1-yl)methyl]-3-amino-quinazolin-4(3H)-one (4c)

White crystals, yield 85% (2,86 g), mp: 156-158 °C. FTIR (cm<sup>-1</sup>): ν<sub>max</sub> 3326, 3239, 3024, 2937, 1662, 1592, 771. <sup>1</sup>H NMR (400 MHz, CDCl<sub>3</sub>) δ 8.21 (d, *J* = 7.7 Hz, 1H, ArH), 7.75 – 7.55 (m, 2H, ArH), 7.42 (t, *J* = 8.2 Hz, 1H, ArH), 7.18 (t, *J* = 8.0 Hz, 2H, ArH), 6.89 – 6.73 (m, 3H, ArH), 6.22 (brs, 2H, NH<sub>2</sub>), 3.80 (s, 2H, N-CH<sub>2</sub>), 3.11 (t, *J* = 4.0, 4H, CH<sub>2</sub>-N-CH<sub>2</sub>), 2.72 (t, *J* = 4.0, 4H, CH<sub>2</sub>-N-CH<sub>2</sub>). <sup>13</sup>C NMR (100 MHz, CDCl<sub>3</sub>): δ 159.3 (C=O), 151.0 (ArC), 150.5 (N=C), 146.2, 133.9, 129.2, 127.5, 126.9, 126.4, 120.1, 120.0, 116.3 (ArC), 61.6 (N-CH<sub>2</sub>), 53.1 (CH<sub>2</sub>-N-CH<sub>2</sub>), 49.3 (CH<sub>2</sub>-N-CH<sub>2</sub>).

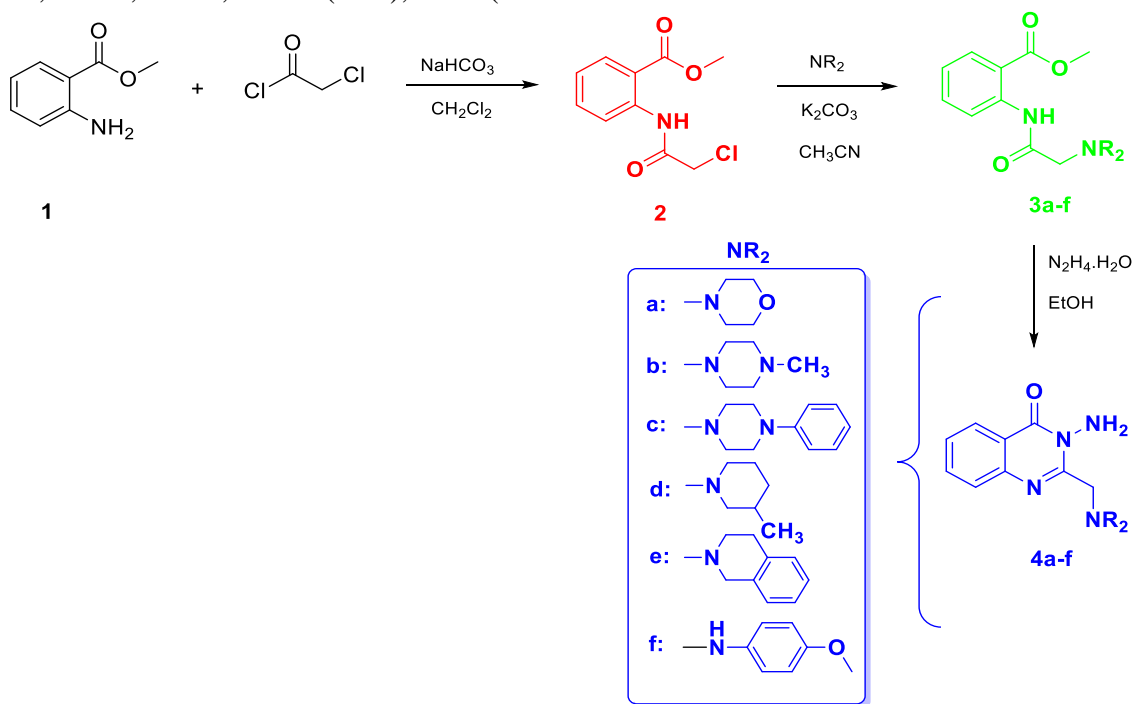


Figure 2 Synthesis of compounds 4a-f

### 2.2.1.4. 2-[(3-Methylpiperidin-1-yl)methyl]-3-amino-quinazolin-4(3H)-one (4d)

White crystals, yield 80% (2,19 g), mp: 85-87 °C. FTIR (cm<sup>-1</sup>): ν<sub>max</sub> 3306, 3236, 2947, 1674, 1599, 779. <sup>1</sup>H NMR (400 MHz,

CDCl<sub>3</sub>) δ 8.29 (d, *J* = 7.6 Hz, 1H, ArH), 7.78 – 7.68 (m, 2H, ArH), 7.51 – 7.47 (m, 1H, ArH), 6.56 (brs, 2H, NH<sub>2</sub>), 3.76 (s, 2H, N-CH<sub>2</sub>), 2.83 (t, *J* = 12.0 Hz, 2H, N-CH<sub>2</sub>), 2.15 (t, *J* = 10.1 Hz, 1H), 1.87 (t, *J* = 10.6 Hz, 1H), 1.74 – 1.57 (m, 3H), 1.52 – 1.48 (m, 1H) (Protons of piperidine ring), 1.00 –



0.88 (m, 1H, CH), 0.86 (d,  $J = 6.6$  Hz, 3H, CH<sub>3</sub>). <sup>13</sup>C NMR (101 MHz, CDCl<sub>3</sub>)  $\delta$  158.9 (C=O), 150.7 (N=C), 146.2, 133.6, 127.4, 126.7, 126.3, 120.0 (ArC), 62.3, 61.6, 53.8 (N-CH<sub>2</sub>), 32.5 (CH<sub>2</sub>), 31.4 (CH), 25.5 (CH<sub>2</sub>), 19.4 (CH<sub>3</sub>).

#### 2.2.1.5. 2-[(3,4-Dihydroisoquinolin-2(1H)-yl)methyl]-3-amino-quinazolin-4(3H)-one (4e)

White crystals, yield 89% (2,73 g), mp: 107-109 °C. FTIR (cm<sup>-1</sup>):  $\nu_{\max}$  3241, 3066, 2934, 1658, 1594, 757. <sup>1</sup>H NMR (400 MHz, CDCl<sub>3</sub>)  $\delta$  8.19 (d,  $J = 8.0$  Hz, 1H, ArH), 7.66 (d,  $J = 3.6$  Hz, 2H, ArH), 7.40 (m, 1H, ArH), 7.09 – 6.97 (m, 3H, ArH), 6.91 (d,  $J = 6.6$  Hz, 1H, ArH), 6.26 (brs, 2H, NH<sub>2</sub>), 3.89 (s, 2H, N-CH<sub>2</sub>), 3.72 (s, 2H, N-CH<sub>2</sub>), 2.84 (t,  $J = 4.0$ , 2H, CH<sub>2</sub>), 2.82 (t,  $J = 4.0$ , 2H, CH<sub>2</sub>). <sup>13</sup>C-NMR (100 MHz, CDCl<sub>3</sub>):  $\delta$  159.1 (C=O), 150.6 (N=C), 146.2, 133.8, 133.7, 128.9, 127.5, 126.6, 126.4, 120.1 (ArC), 61.4, 55.7, 50.6 (N-CH<sub>2</sub>), 29.1 (CH<sub>2</sub>).

#### 2.2.1.6.2-[(4-Methoxyphenyl)amino]methyl}-3-amino-quinazolin-4(3H)-one (4f)

Beige solid, yield 87% (2,58 g), mp: 125-127 °C. FTIR (cm<sup>-1</sup>):  $\nu_{\max}$  3394, 3340, 3200, 3049, 2935, 1673, 1595, 771. <sup>1</sup>H NMR (400 MHz, CDCl<sub>3</sub>)  $\delta$  8.09 (d,  $J = 7.8$  Hz, 1H, ArH), 7.65 – 7.57 (m, 2H, ArH), 7.34 (t,  $J = 7.3$  Hz, 1H, ArH), 6.69 (m, 4H, ArH), 4.74 (brs, 3H, NH<sub>2</sub> and NH), 4.37 (s, 2H, N-CH<sub>2</sub>), 3.64 (s, 3H, OCH<sub>3</sub>). <sup>13</sup>C NMR (101 MHz, CDCl<sub>3</sub>)  $\delta$  161.5 (C=O), 154.1 (ArC), 152.5 (N=C), 146.4, 141.4, 134.3, 127.3, 126.7, 126.4, 120.2, 114.9, 114.7 (ArC), 55.7 (OCH<sub>3</sub>), 46.7 (NH-CH<sub>2</sub>).

### 3. RESULTS AND DISCUSSION

#### 3.1. Synthesis

In this study, six 2-aminomethyl quinazolin-4(3H)-one derivatives (**4a-f**) were synthesized with good purity and

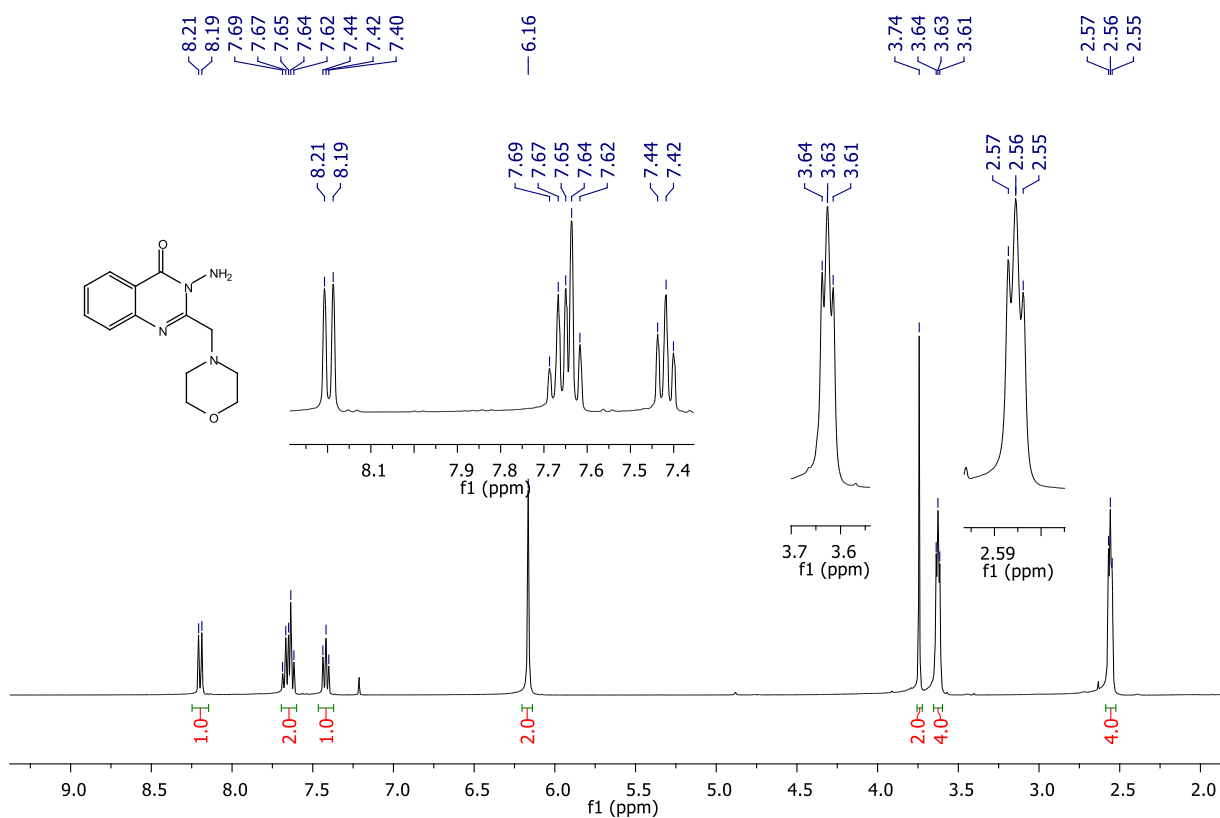
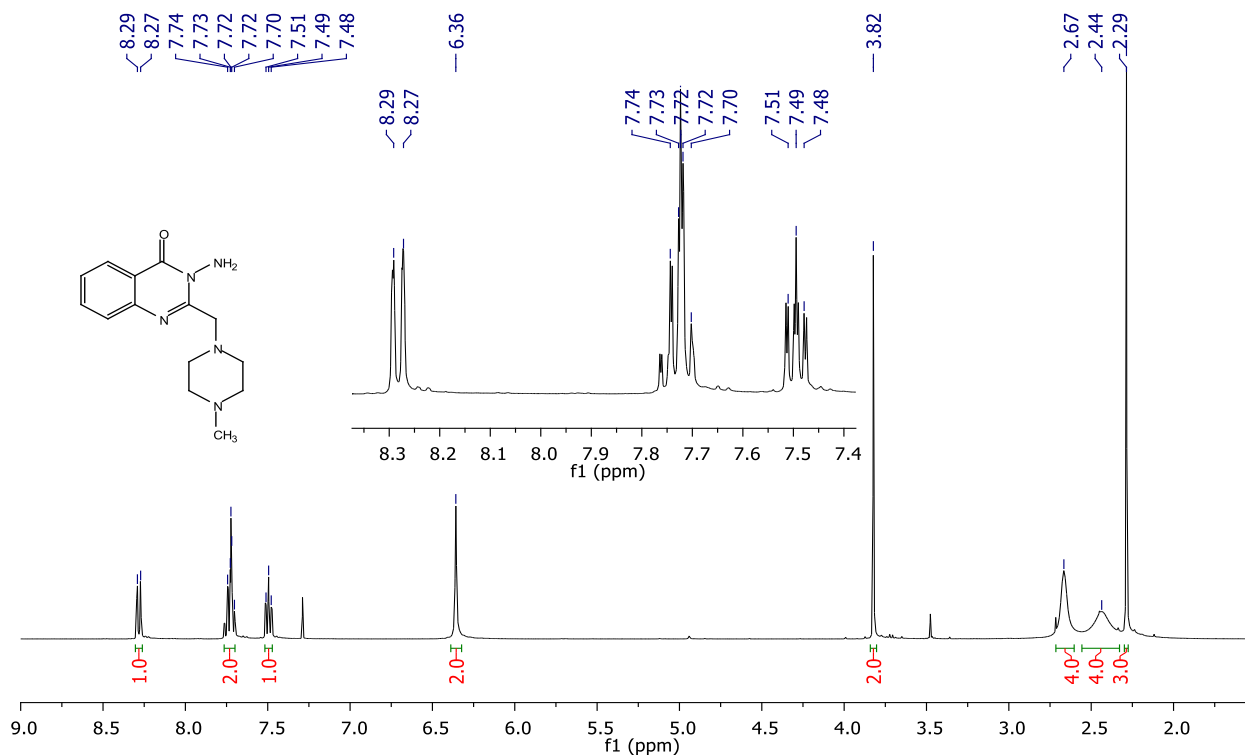
yields. (Figure 2). The reactants and the solvents used in this synthesis study were supplied from various suppliers and used without any treatment. Compounds **4a-f** were obtained starting from the methyl anthranilate (**1**) in three steps with good yields (89-80%). The purity of the all compounds synthesized in this study was checked using TLC. FTIR and NMR (<sup>1</sup>H - <sup>13</sup>C) spectroscopies were applied for the characterization of the synthesized compounds.

#### 3.2. Structural Characterization

In the FTIR spectra of compounds **4a-f**, the stretching bands of the NH<sub>2</sub> group were observed at 3340 – 3200 cm<sup>-1</sup>. Aromatic and aliphatic C-H stretching bands were seen at 3106 – 3024 cm<sup>-1</sup> and 2956 – 2934 cm<sup>-1</sup>, respectively. The stretching bands of the C=O and C=N bonds were observed at 1674 – 1658 cm<sup>-1</sup> and 1599 – 1592 cm<sup>-1</sup>, respectively.

<sup>1</sup>H NMR spectra of the compounds **4a-f** are seen in Figure 3-8. Peaks of the aromatic protons are seen at  $\delta$  8.29 – 6.69 ppm as a set of signals (multiplet, triplet or doublet) relative to their chemical environment. Peaks of the NH<sub>2</sub> protons at position 3 of the quinazolinone ring, are seen as a broad singlet at  $\delta$  6.56 – 6.16 ppm. For compound **4f**, peaks of the NH<sub>2</sub> protons and the NH proton at position 2 were overlapped and seen as a broad singlet at  $\delta$  4.74 ppm (Figure 8). The characteristic peaks of the aminomethyl protons (N-CH<sub>2</sub>) were observed at  $\delta$  3.82 – 3.74 ppm. For compound **4f**, this peak was observed as a singlet at  $\delta$  4.37 ppm. Peaks of the aliphatic protons are seen at  $\delta$  3.63 – 0.88 ppm as a set of signals (multiplet, triplet, doublet or singlet) relative to their chemical environment. Finally, peaks of the OCH<sub>3</sub> protons (for compound **4f**) and CH<sub>3</sub> (for compound **4b**) are seen as a singlet at  $\delta$  3.64 ppm and  $\delta$  2.29 ppm, respectively (Figure 4 and 8). The spectroscopic data mentioned above are in accordance with the

structure of molecules and the data in the literature [16, 32].

Figure 3  $^1\text{H}$  NMR (4a)Figure 4  $^1\text{H}$  NMR (4b)

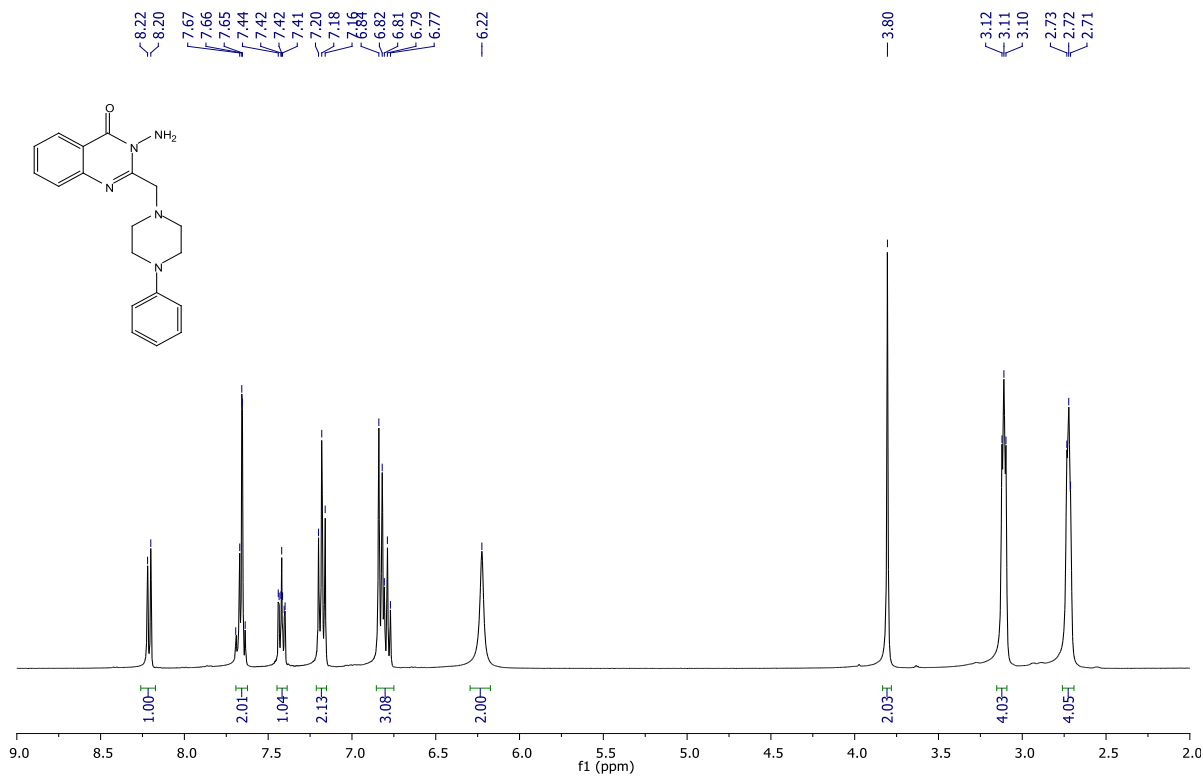


Figure 5 <sup>1</sup>H NMR (4c)

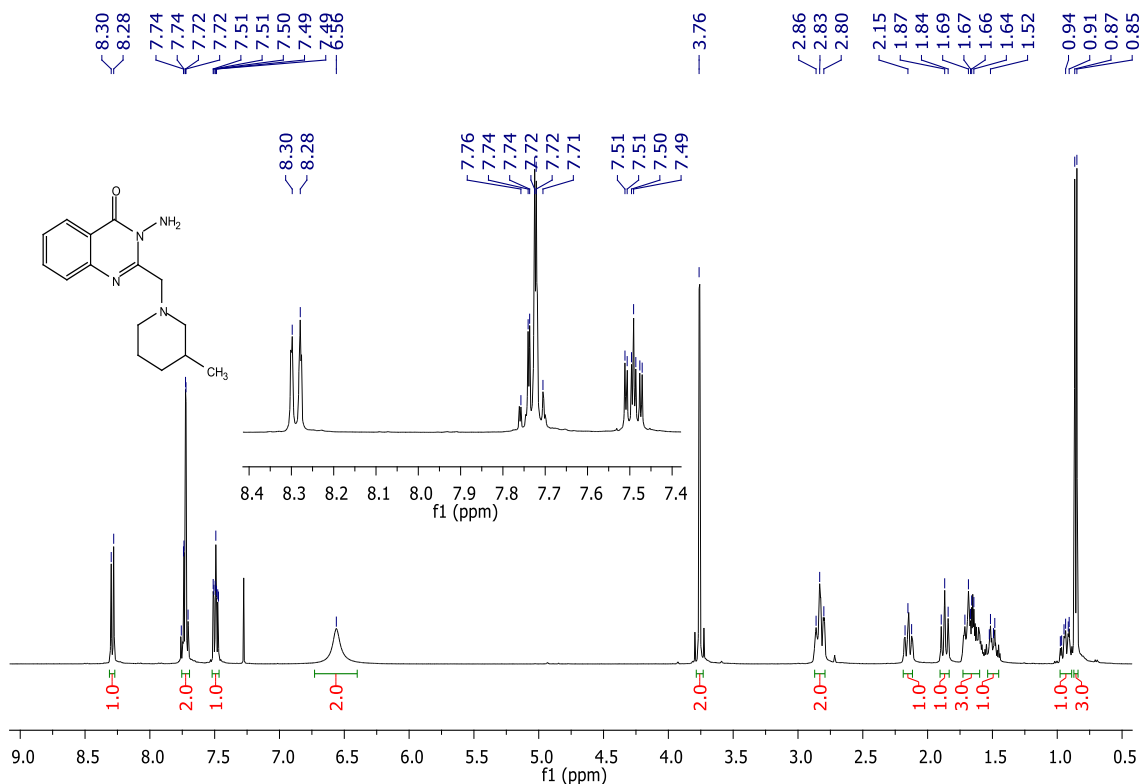


Figure 6 <sup>1</sup>H NMR (4d)

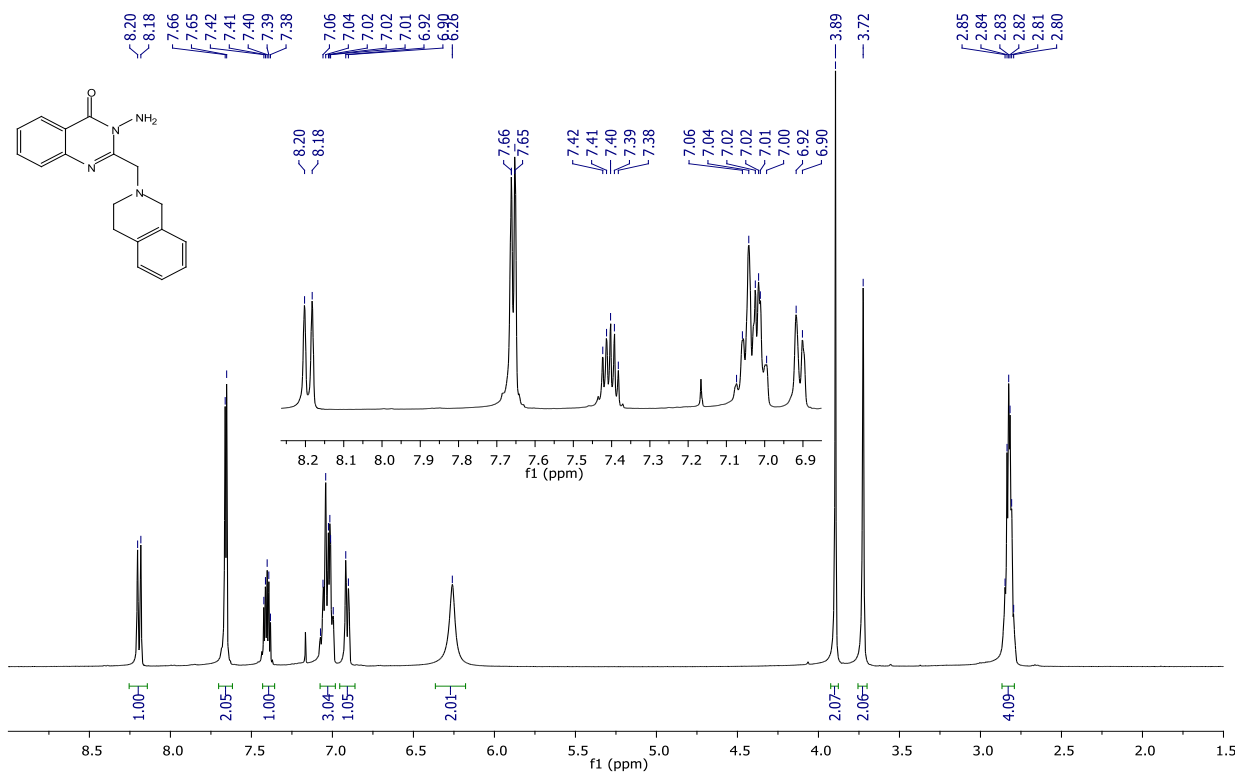


Figure 7  $^1\text{H}$  NMR (4e)

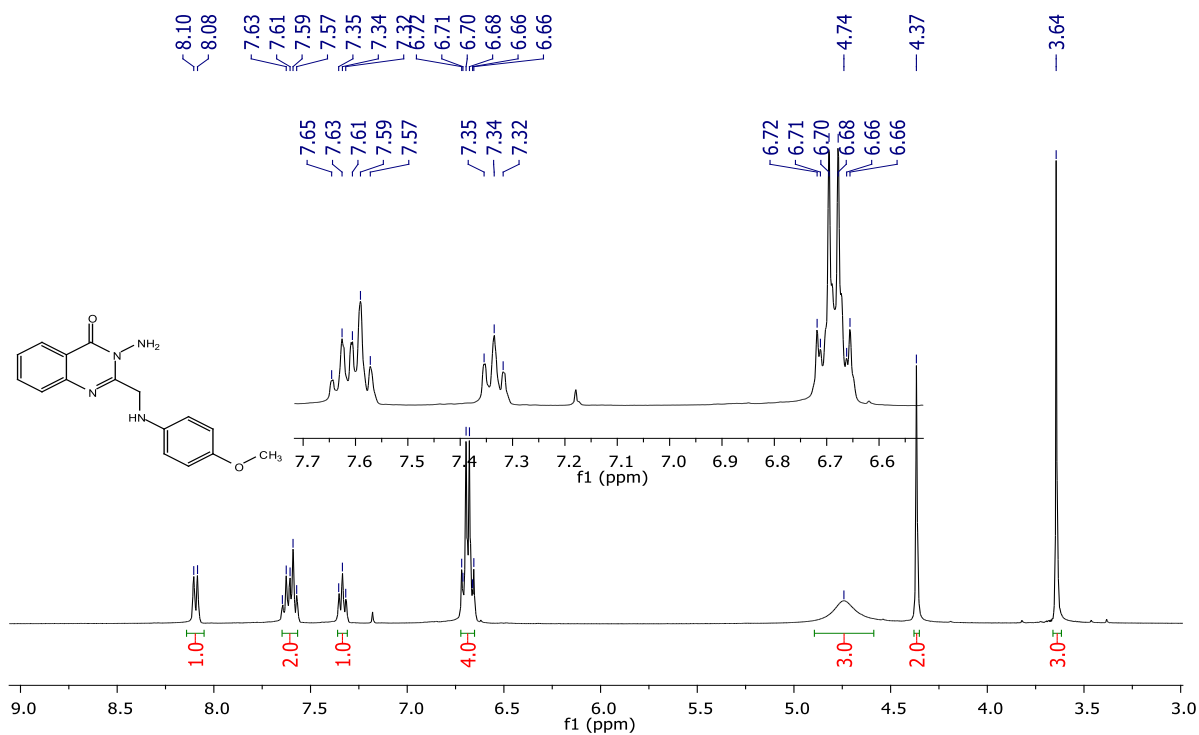
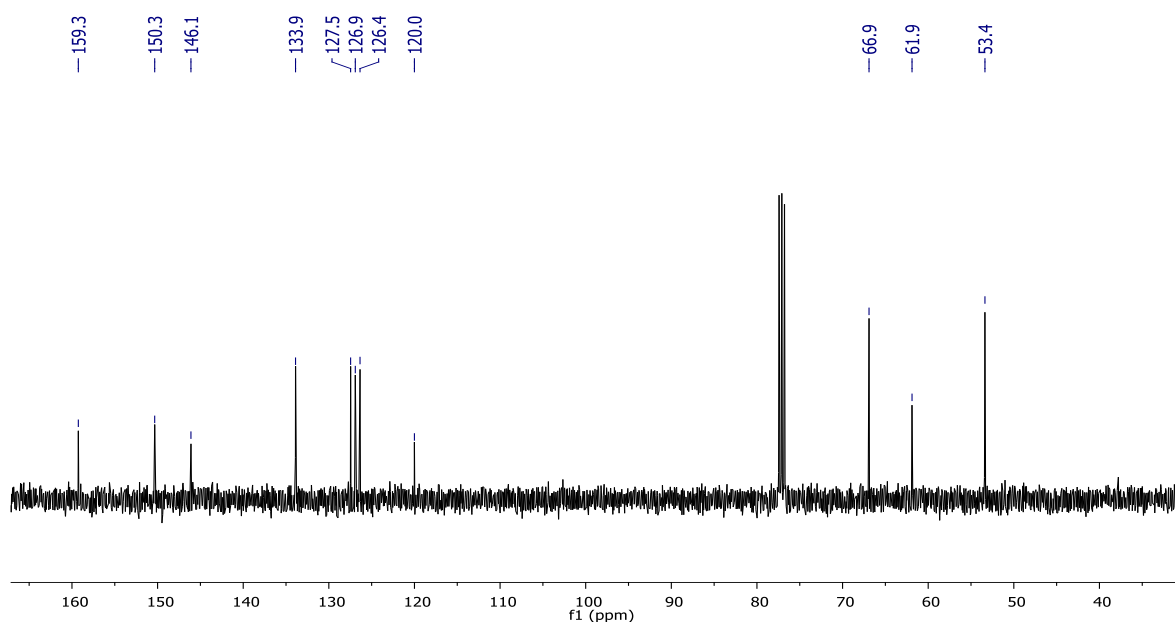
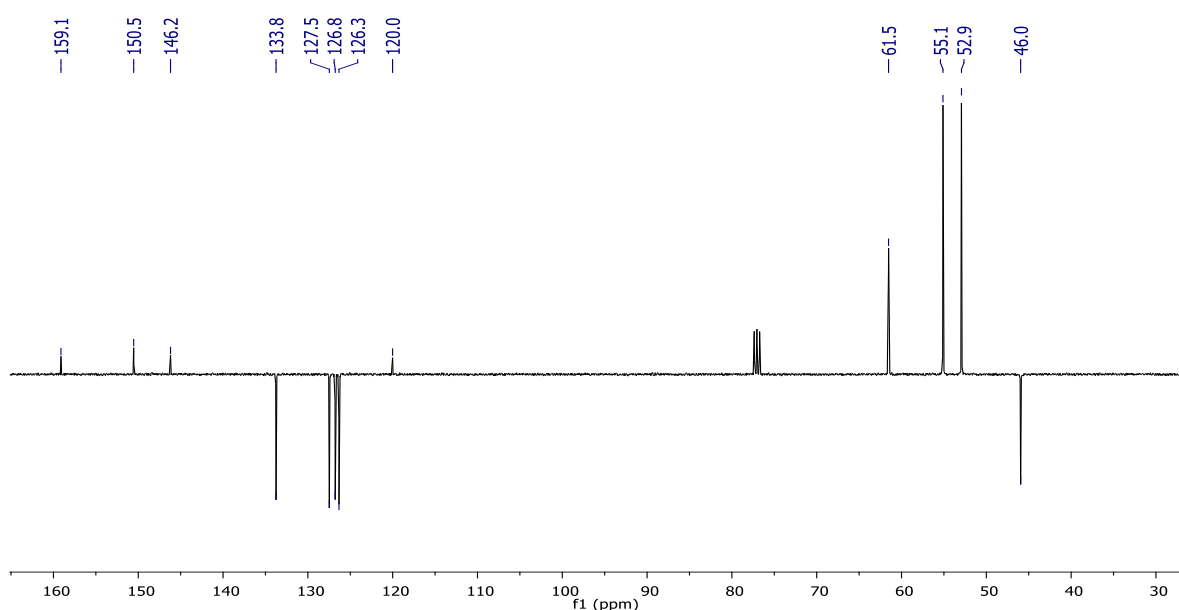


Figure 8  $^1\text{H}$  NMR (4f)

Figure 9  $^{13}\text{C}$  NMR (**4a**)

When the  $^{13}\text{C}$  NMR spectra of the compounds **4a-f** were analysed (Figure 9-14), peaks of the carbonyl carbons (C4) are seen at  $\delta$  161.5 – 158.9 ppm. Peaks of carbons at the 2 position of quinazoline ring are observed at  $\delta$  152.5 – 150.3 ppm. Aromatic carbons are seen at  $\delta$  154.1 – 116.3 ppm. The characteristic peaks of the aminomethyl carbons (N-CH<sub>2</sub>) were seen  $\delta$

61.9 – 61.4 ppm. For compound **4f**, this peak was observed at  $\delta$  46.7 ppm (Figure 14). For all compounds, peaks of the aliphatic carbons were seen at  $\delta$  66.9 – 19.4 ppm. Finally, for compound **4f**, peak of the OCH<sub>3</sub> carbon was observed at  $\delta$  55.7 ppm (Figure 14). The spectroscopic data mentioned above are in accordance with the structure of molecules and the data in the literature [16, 32].

Figure 10  $^{13}\text{C}$  NMR (**4b**)

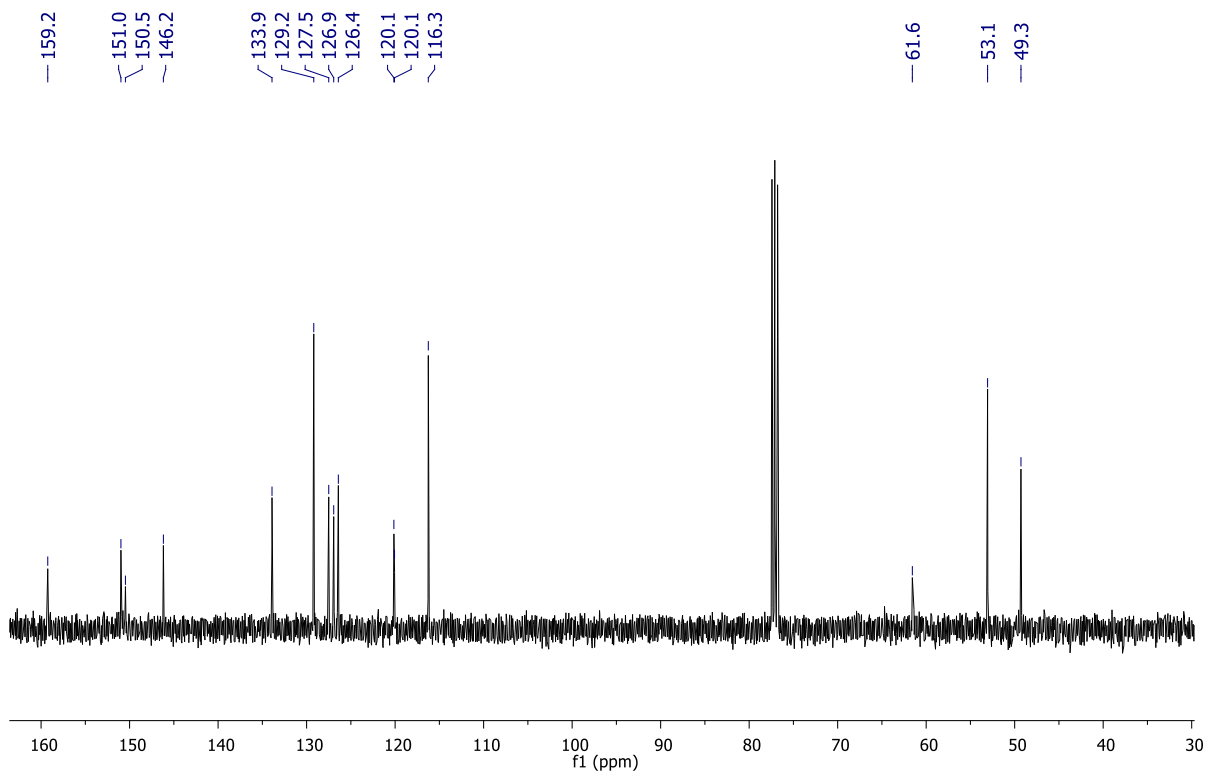


Figure 11 <sup>13</sup>C NMR (4c)

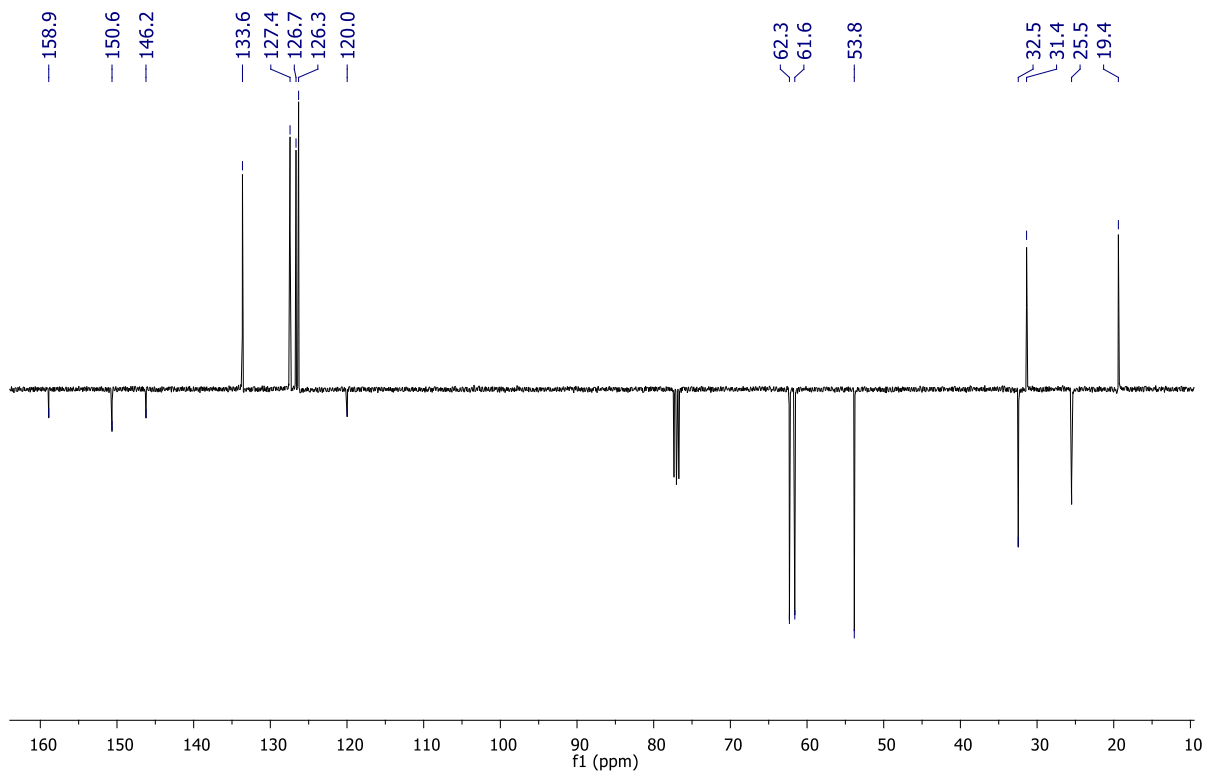
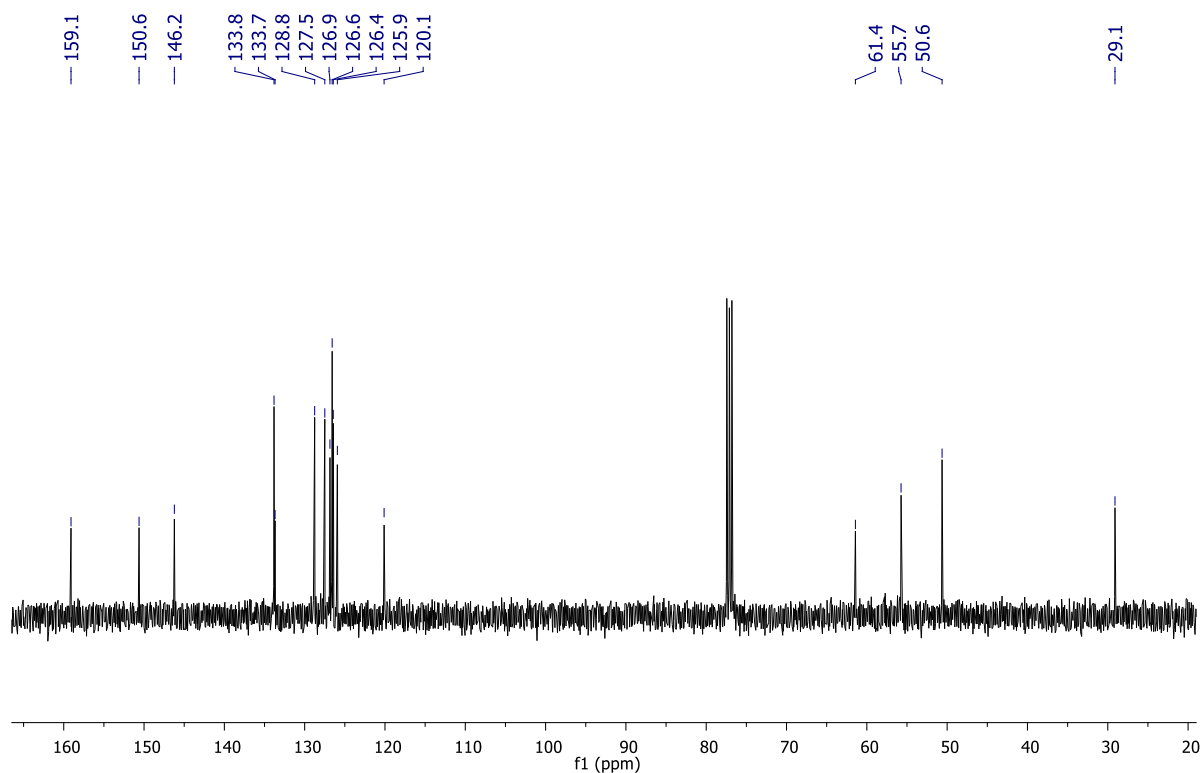
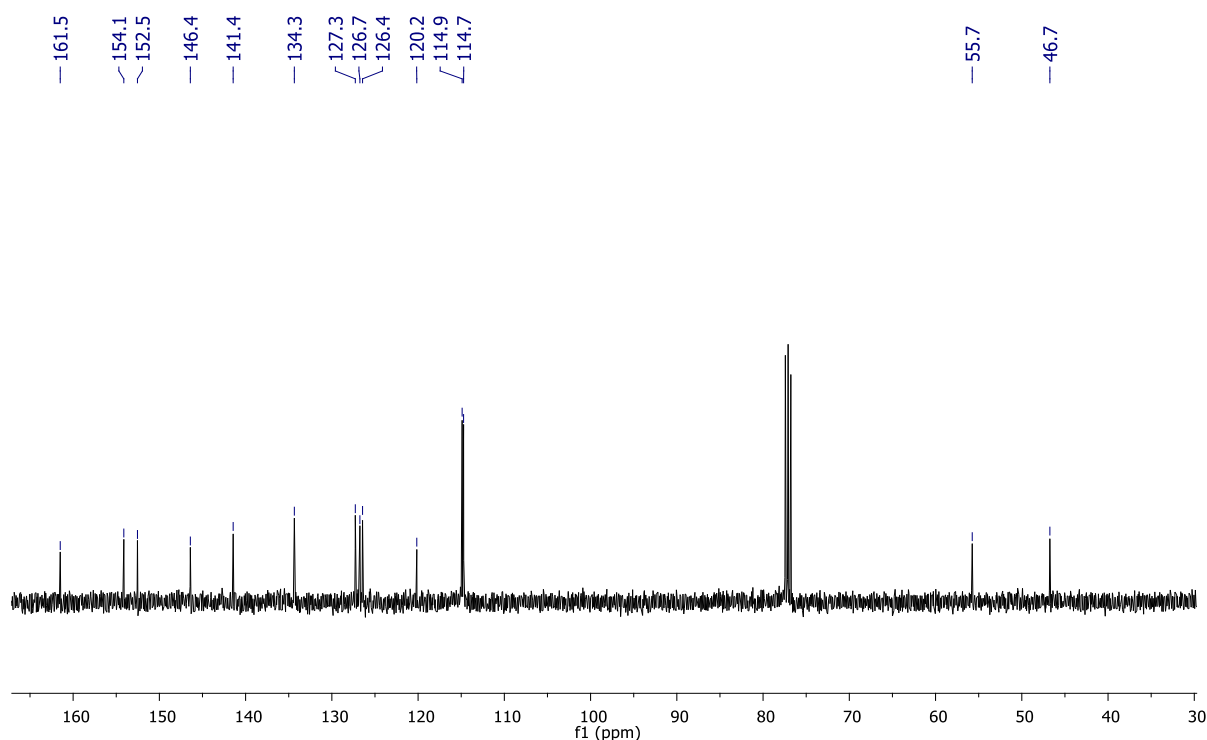


Figure 12 <sup>13</sup>C NMR (4d)

Figure 13  $^{13}\text{C}$  NMR (4e)Figure 14  $^{13}\text{C}$  NMR (4f)

#### 4. CONCLUSION

In this study, the synthesis of new members of quinazolin-4(3H)-ones with

aminomethyl moiety at 2 positions were carried out, successfully (according to the data from the spectra). The structures of the compounds were identified and some physical properties were determined. New ligands or building blocks have been

synthesized for scientists interested in the chemical and pharmaceutical properties of quinazolines. Because these molecules contain an aminomethyl group in their structure, they behave like Mannich Bases, which have many uses in various fields of chemistry [33]. In addition, it is possible to synthesize many new molecules by easily derivatizing the molecules over the free NH<sub>2</sub> at the 3 position. NH<sub>2</sub> group at the 3 position of the ring has the character of aromatic primary amine in chemical reactions. Therefore, Schiff Bases with aldehydes, amides with acyl chlorides, and sulfonamide derivatives with sulfonyl chlorides can be easily synthesized. These classes of compounds are mentioned because they are frequently used in pharmaceutical chemistry, medicinal chemistry and biochemistry. Because the molecules have a polar aminomethyl group in their structure, their solubility is quite good in polar solvents (including hot water). Molecules are compounds that can be stored at room temperature and are not affected by heat, light and moisture. Therefore, the molecules are excellent ligands for scientists who want to study the pharmaceutical properties of quinazolinones and their derivatives.

***The Declaration of Conflict of Interest/ Common Interest***

No conflict of interest or common interest has been declared by the author.

***The Declaration of Ethics Committee Approval***

This study does not require ethics committee permission or any special permission.

***The Declaration of Research and Publication Ethics***

The author of the paper declares that he complies with the scientific, ethical, and quotation rules of SAUJS in all processes of the paper and that they do not make any falsification on the data collected. In addition, he declare that Sakarya University

Journal of Science and its editorial board have no responsibility for any ethical violations that may be encountered, and that this study has not been evaluated in any academic publication environment other than Sakarya University Journal of Science.

**REFERENCES**

- [1] R. J. Abdel-Jalil, H. M. Aldoqum, M. T. Ayoub, W. Voelter, "Synthesis and Antitumor Activity of 2-aryl-7-fluoro-6-(4-methyl-1-piperazinyl)-4(3H)-quinazolinones," *Heterocycles-Sendai Institute Heterocyclic Chemistry*, vol.65, pp.2061-2070, 2005.
- [2] A. S. El-Azab, K. E. El-Tahir, "Design and Synthesis of Novel 7-Aminoquinazoline Derivatives: Antitumor and Anticonvulsant Activities," *Bioorganic and Medicinal Chemistry Letters*, vol.22, pp.1879-1885, 2012.
- [3] V. M. Sharma, P. Prasanna, K. A. Seshu, B. Renuka, C. L. Rao, G. S. Kumar, C. P. Narasimhulu, P. A. Babu, R. Puranik, D. Subramanyam, "Novel Indolo [2, 1-b] quinazoline Analogues as Cytostatic Agents: Synthesis, Biological Evaluation and Structure-activity Relationship," *Bioorganic and Medicinal Chemistry Letters*, vol.12 pp.2303-2307, 2002.
- [4] H. J. Park, Y-S. Kim, J. S. Kim, E-J. Lee, Y-J. Yi, H. J. Hwang, M-E. Suh, C-K. Ryu, S. K. Lee, "6-Arylamino-7-chloro-quinazoline-5,8-diones as Novel Cytotoxic and DNA Topoisomerase Inhibitory Agents," *Bioorganic and Medicinal Chemistry Letters*, vol.14, pp.3385-3388, 2004.
- [5] Z. Ma, Y. Hano, T. Nomura, Y. Chen, "Novel Quinazoline-quinoline Qlkaloids with Cytotoxic and DNA Topoisomerase II Inhibitory Activities," *Bioorganic and Medicinal*



- Chemistry Letters, vol.14, pp.1193-1196, 2004.
- [6] N. Malecki, P. Carato, B. T. Rigo, J-F. Goossens, R. Houssin, C. Bailly, J-P, Hénichart, "Synthesis of Condensed Quinolines and Quinazolines as DNA Ligands," *Bioorganic and Medicinal Chemistry*, vol.12 pp.641-647, 2004.
- [7] E. Manivannan, S. Chaturvedi, "Analogue-based Design, Synthesis and Molecular Docking Analysis of 2,3-Diaryl Quinazolinones as Non-ulcerogenic Anti-inflammatory Agents," *Bioorganic and Medicinal Chemistry*, vol.19, pp.4520-4528, 2011.
- [8] A. Gangjee, O. O. Adair, M. Pagley, S. F. Queener, "N9-substituted 2,4-diaminoquinazolines: Synthesis and Biological Evaluation of Lipophilic Inhibitors of Pneumocystis Carinii and Toxoplasma Gondii Dihydrofolate Reductase," *Journal of Medicinal Chemistry*, vol.51, pp.6195-6200, 2008.
- [9] J. Chevalier, A. Mahamoud, M. Baitiche, E. Adam, M. Viveiros, A. Smarandache, A. Militaru, M. L. Pascu, L. Amaral, J-M, Pagès, "Quinazoline Derivatives are Efficient Chemosensitizers of Antibiotic Activity in Enterobacter Aerogenes, Klebsiella Pneumoniae and Pseudomonas Aeruginosa Resistant Strains," *International Journal of Antimicrobial Agents*, vol.36, pp.164-168, 2010.
- [10] A. Mahamoud, J. Chevalier, M. Baitiche, E. Adam, J-M, Pages, "An Alkylaminoquinazoline Restores Antibiotic Activity in Gram-negative Resistant Isolates," *Microbiology*, vol.157, pp.566-571, 2011.
- [11] K. Bajaj, V. K. Srivastava, A. Kumar, "Newer Substituted Benzoxazepinyl quinazolinones as Potent Antipsychotic and Anticonvulsant Agents," *ArzneimittelForschung*, vol.53, pp.480-485, 2003.
- [12] M. Amir, I. Ali, M. Z. Hassan, "Design and Synthesis of Some New Quinazolin-4-(3H)-ones as Anticonvulsant and Antidepressant Agents," *Archives of Pharmacal Research*, vol.36, pp.61-68, 2013.
- [13] M. Shivananda, B. S. Holla, "Antifungal Activity Studies of Some Quinazolinone Derivatives," *Journal of Chemical and Pharmaceutical Research*, vol.3, pp.83-86, 2011.
- [14] M. Decker, "Novel Inhibitors of Acetyl and Butyrylcholinesterase Derived from the Alkaloids Dehydroevodiamine and Rutaecarpine," *European Journal of Medicinal Chemistry*, vol.40, pp.305-313, 2005.
- [15] F. S. Tokalı, P. Taslimi, İ. H. Demircioğlu, M. Karaman, M. S. Gültekin, K. Şendil, İ. Gülçin, "Design, Synthesis, Molecular Docking, and Some Metabolic Enzyme Inhibition Properties of Novel Quinazolinone Derivatives," *Archiv der Pharmazie (Weinheim, Germany)*, vol.354, no.5, pp.2000455, 2021.
- [16] A. Gürsoy, N. Karalı, "Synthesis and Primary Cytotoxicity Evaluation of 3-[[3-Phenyl-4(3H)-quinazolinone-2-yl]mercaptoacetyl] hydrazono]-1H-2-indolinones," *European Journal of Medicinal Chemistry*, vol.38, pp.633-643, 2003.
- [17] M. S. Malamas, J. Millen, "Quinazolineacetic Acids and Related Analogs as Aldose Reductase

- Inhibitors,” *Journal of Medicinal Chemistry*, vol.34 pp.1492-1503, 1991.
- [18] F. S. Tokalı, Y. Demir, İ. H. Demircioğlu, C. Türkeş, E. Kalay, K. Şendil, Ş. Beydemir, “Synthesis, *in silico* docking study and biological evaluation of novel library sulfonates containing quinazolin-4(3H)-one derivatives as potential aldose reductase inhibitors,” *Drug Development Research*, vol.83, no.3, pp.586-604 2022.
- [19] A. Gangjee, M. Kothare, R. L. Kisliuk, “The Synthesis of Novel Nonclassical Reversed Bridge Quinazoline Antifolates as Inhibitors of Thymidylate Synthase,” *Journal of Heterocyclic Chemistry*, vol.37, pp.1097-1102, 2000.
- [20] R-D. Li, X. Zhang, Q-Y. Li, Z-M. Ge, R-T. Li, “Novel EGFR Inhibitors Prepared by Combination of Dithiocarbamic Acid Esters and 4-Anilinoquinazolines,” *Bioorganic and Medicinal Chemistry Letters*, vol.21, pp.3637-3640, 2011.
- [21] J. P. Patil, S. V. Amrutkar, M. S. Ranawat, “Microwave Assisted Synthesis of Quinazolinone Using Different Bases,” *Journal of Pharmaceutical Sciences and Research*, vol.1, no.3, pp.52-54, 2009.
- [22] S. G. Davies, K. B. Ling, R. M. Roberts, A. J. Russell, J. E. Thomson, P. A. Woods, “The Stereodivergent Aziridination of Allylic Carbamates, Amides and Sulfonamides,” *Tetrahedron*, vol.66, no.34, pp.6806-6813, 2010.
- [23] A. M. F. Eissa, A. M. El-Metwally, M. A. El-Hashash, A. M. F. El-Gohary, “Synthesis and Biological Evaluation of Some New 2-Propyl-4(3H)-quinazolinone Derivatives as Anti-bacteria,” *Journal of the Korean Chemical Society*, vol.52, no.3, pp.328-337, 2008.
- [24] A. F. M. Fahmy, M. A. El-Hashash, M. M. Habashy, S. A. El-Wannise, “Some Reactions of 2-Isopropyl-[4H]-3,1-benzoxazin-4-one,” *Revue Roumaine de Chimie*, vol.23, no.11-12, pp.1567-1573, 1978.
- [25] V. Alagarsamy, V. Rajasolomon, R. Meena, K. V. Ramseshu, “Synthesis and Analgesic, Anti-inflammatory and Antibacterial Activities of Some Novel 3-substituted 2-butylquinazolin-4(3H)-ones,” *Biological & Pharmaceutical Bulletin*, vol.28, no.6, pp.1091-1094, 2005.
- [26] M. A. El-Sherbeny, “Synthesis, Antitumor Activity, and Anti-HIV-1 Testing of Certain Heterocyclic Systems Containing an Adamantane Nucleus,” *Archiv der Pharmazie (Weinheim, Germany)*, vol.333, no.10, pp.323-328, 2000.
- [27] P. Kumar, B. Shrivastava, S. N. Pandeya, J. P. Stables, “Design, Synthesis and Potential 6 Hz Psychomotor Seizure Test Activity of Some Novel 2-(Substituted)-3-{{substituted}amino}quinazolin-4(3H)-one,” *European Journal of Medicinal Chemistry*, vol.46, no.4, pp.1006-1018, 2011.
- [28] C. K. Reddy, P. S. N. Reddy, C. V. Ratnam, “A New Synthesis of 2-Aryl-3,4-dihydro-5H-1,3,4-benzotriazepin-5-ones,” *Indian Journal of Chemistry, Section B: Organic Chemistry Including Medicinal Chemistry*, vol.24B, no.9, pp.902-904, 1985.
- [29] H. Patel, R. Pawara, S. Surana, “Resolving the Mystery of Ring Opening in the Synthesis of Benzo[d][1, 3]oxazin-4-one and

- Quinazolin-4(3H)-one,” Letters in Organic Chemistry, vol.16, no.11, pp.898-905, 2019.
- [30] L. M. Deck, S. D. Turner, J. A. Deck, E. P. Papadopoulos, “ Synthesis of Derivatives of Thiophene Using Methyl 2-isothiocyanatobenzoate,” Journal of Heterocyclic Chemistry, vol.38, no.2, pp.343-347, 2001.
- [31] F. Sauter, P. Stanetty, U. Jordis, “New 3-Aminoquinazolinones,” Archiv der Pharmazie (Weinheim, Germany), vol.310, no.8, pp.680-682, 1977.
- [32] F. S. Tokalı, P. Taslimi, İ. H. Demircioğlu, K. Şendil, B. Tüzün, İ. Gülçin, “Novel Phenolic Mannich Base Derivatives: Synthesis, Bioactivity, Molecular Docking, and ADME-Tox Studies,” Journal of the Iranian Chemical Society, vol.19, pp.563–577, 2022.
- [33] G. Roman, “Mannich bases in medicinal chemistry and drug design,” European Journal of Medicinal Chemistry, vol. 89, pp. 743 – 816, 2015.



SAKARYA ÜNİVERSİTESİ

# FEN BİLİMLERİ ENSTİTÜSÜ DERGİSİ

Sakarya University Journal of Science  
SAUJS

ISSN 1301-4048 e-ISSN 2147-835X Period Bimonthly Founded 1997 Publisher Sakarya University  
<http://www.saujs.sakarya.edu.tr/>

Title: Fluid-Structure Interaction Analysis of Carotid Artery Blood Flow with Machine Learning Algorithm and OpenFOAM

Authors: Murad KUCUR, Banu KÖRBAHTİ

Received: 2022-09-12 00:00:00

Accepted: 2022-10-08 00:00:00

Article Type: Research Article

Volume: 26

Issue: 6

Month: December

Year: 2022

Pages: 1131-1141

How to cite

Murad KUCUR, Banu KÖRBAHTİ; (2022), Fluid-Structure Interaction Analysis of Carotid Artery Blood Flow with Machine Learning Algorithm and OpenFOAM. Sakarya University Journal of Science, 26(6), 1131-1141, DOI: 10.16984/saufenbilder.1173983

Access link

<https://dergipark.org.tr/en/pub/saufenbilder/issue/74051/1173983>

New submission to SAUJS

<http://dergipark.gov.tr/journal/1115/submission/start>

## Fluid-Structure Interaction Analysis of Carotid Artery Blood Flow with Machine Learning Algorithm and OpenFOAM

Murad KUCUR\*<sup>1</sup> , Banu KÖRBAHTI<sup>1</sup> 

### Abstract

In this study, a patient-specific carotid artery model was analyzed with an open source program foam-extend. The research includes the effect of arterial wall deformation by fluid-structure analysis. Pulsatile velocity cycle is trained for 144 patients with different hemodynamic parameters, by machine learning algorithm using blood flow velocity measured from 337 points of the carotid artery. Data used for training is obtained from an open source in the literature. Here, the machine learning algorithm was created by the help of an open source code Phyton. Then, using trained values of machine learning, and the known systole and diastole blood pressures for a specific chosen patient, the patient-specific pulsatile velocity cycle was estimated. The estimated pulsatile velocity cycle was then fitted to Fourier series. This pulsatile velocity cycle is used as the input boundary condition for the model analyzed in foam-extend. The outlet boundary condition, pulsatile pressure cycle is found by 4-Element Windkessel algorithm. Wall shear stresses and time averaged wall shear stresses were obtained for both the rigid and fluid structure interaction models, and variation of displacement throughout the pulsatile cycle was found for the FSI model. Wall shear stresses, velocity, and displacements were obtained high at peak systole, consistent with pulsatile cycles. Like the wall shear stresses, the time averaged wall shear stresses for the FSI model were also found lower than the rigid model. The wall shear stresses showed an increase towards the exit of internal and external carotid artery.

**Keywords:** Open-FOAM, machine learning, carotid artery, blood flow

### 1. INTRODUCTION

Hemodynamic studies have an important place in the field of biomechanics. The changing behavior of blood flow, especially in narrowing and expanding vessels, poses an important problem for human health. In this emerging

problem, it is vital to be able to predict the plaque formation and wall shear stresses that will occur as a result of the atherosclerosis, narrowing, and expansion of the vessels.

Machine learning methods are used in hemodynamics for prediction of wall shear

\* Corresponding author: [kucur@iuc.edu.tr](mailto:kucur@iuc.edu.tr)

<sup>1</sup> Istanbul University-Cerrahpaşa, Engineering Faculty, Mechanical Engineering Department, Istanbul, Turkey.

E-mail: [korbahti@iuc.edu.tr](mailto:korbahti@iuc.edu.tr)

ORCID: <https://orcid.org/0000-0002-0356-0359>, <https://orcid.org/0000-0002-2579-5255>

stresses, hypertension, pulsatile velocity, and pressure cycles. These investigations focus on carotid artery as well as aortic branches. Mostly, the prediction of pulsatile velocity and pressure cycles are made from the experimentally obtained Ultrasonic Doppler data [1, 2].

The researches conducted in the literature on carotid artery cover experimental and numerical works widely. The main aim in these investigations is determining the wall shear stresses (WSS), time averaged wall shear stresses (TWSS), oscillatory shear index (OSI), and relative residence time (RRT).

Many investigations have studied the effect of taking the flow as steady or pulsatile, and assuming the fluid is Newtonian or Non-Newtonian [3-6]. Among the various models available to study non-Newtonian flow, the Carreau-Yasuda, Power law, Carreau, and Casson models are mostly used. But the opinion is that, if the blood cells are small according to the vessel diameter, and blood vessel are large enough the fluid behaves like Newtonian [7]. The early studies considered the geometry of the carotid artery as 2-Dimensional [8], but after in the opinion of that the 3-Dimensional models can simulate the secondary flows in a better way, 3- Dimensional computer aided designed models are started to use. Nowadays, to take a realistic geometry, the researchers are using solid models based on patient-specific data of the carotid artery. The geometrical differences of the carotid artery also effect the flow characteristics. At that point, many investigations were carried out to see the effect of the bifurcation angle of the carotid artery and sinus region location. Because low shear stresses are responsible from the plaque formation, and these regions are the places where the low shear stresses occur.

Last years the investigations mostly focus on fluid-structure interactions (FSI) of the fluid

and vessel wall. The studies showed that taking the vessel walls as rigid over-estimates the wall shear stresses slightly but this amount is still negligible. Lopes et al. [9] have carried out such research to show the difference between rigid and elastic wall approaches. They have concluded that rigid wall approach, overestimates the wall shear stresses, the higher elastic modulus produce lower displacement of the carotid artery walls. Lopes et al. [10] also have investigated the effect of the blood viscosity with FSI approach by taking the fluid as Newtonian and using Carreau-Yasuda viscosity model. They have found the WSS values higher, with Carreau-Yasuda model than, by taking the blood as Newtonian fluid. However, the displacement of the artery wall was not affected from the viscosity model. Wong et al. [11], have made FSI study with a geometry previously used by Tada et al. [12]. They have tried to establish a relationship between blood pressure, stenotic compression, and deformation. With their results, they have showed that a high level of compression and maximum WSS occurs in the stenotic apex and may be responsible from plaque formation. Kumar et al. [13], have carried out a 3-Dimensional FSI study using a patient carotid artery created by converting 2-Dimensional scan images from CT Angio data into a 3-Dimensional model using MIMICS. To better understand the formation and progression of atherosclerotic plaques in the carotid artery bifurcation, computer simulations were performed with different blood pressures, first normal and then indicative of hypertension. They have showed that the deformation of the artery, wall shear stress and especially oscillatory shear index highly affected from blood pressure variation. Lee et al. [14] also has performed 3-Dimensional FSI analysis with a carotid artery model reconstructed from patient specific clinical data. They have considered the effect of blood viscosity and have predicted the WSS values.

This research has focused on blood flow in the carotid artery, where stenosis and atherosclerosis are most commonly seen. The carotid artery model used here is patient-specific model that is taken from literature [15]. Computational Fluid Dynamics (CFD) analysis was done with foam-extend [16] (based on OpenFOAM) in order to get the wall shear stresses and displacement. Pulsatile velocity cycle as input boundary condition, and pulsatile pressure cycle as output boundary condition were obtained by machine learning algorithm and 4-Element Windkessel algorithm, respectively. The training data used in machine learning were taken from open source data in the literature [17, 18].

This study showed that using known systole and diastole blood pressures for a given patient, patient-specific pulsatile velocity cycle can be predicted with trained values of machine learning algorithm. In addition, the effect of the flexible structure of the vessel walls on the wall shear stresses was revealed by the fluid-structure interaction analysis on a patient-specific artery model.

## 2. PROBLEM FORMULATION AND METHODS

In this study, 3-Dimensional patient-specific solid model [15] of the arterial geometry was drawn from the dicom dataset by using VMTK program [19] and shown in Figure 1.

Carotid artery splits into two branches as internal carotid and external carotid artery. In this study, the diameter of the internal carotid artery (ICA) is 4.5 mm, and the diameter of external carotid artery (ECA) is 4.15 mm. The length and wall thickness of the artery is 81.6771 mm and 0.55 mm, respectively. The carotid artery was modelled as a linear elastic isotropic material and the mechanical properties of the vessel are taken as  $\rho_w = 1160 \text{ kg/m}^3$ ,  $\nu = 0.45$ , and  $E = 1.106 \times 10^6 \text{ Pa}$ . Here

$\rho_w$  is artery's wall density,  $\nu$  is Poisson ratio and  $E$  is elasticity modulus.

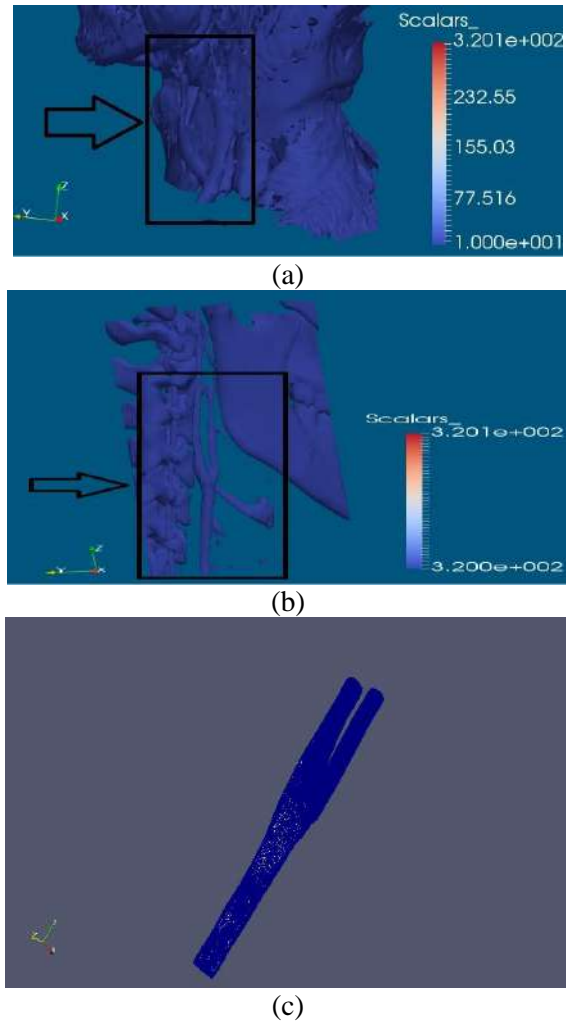


Figure 1 Carotid artery main geometry

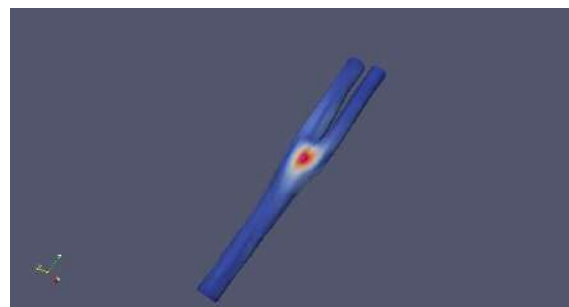


Figure 2 Mesh independency point

Mesh independency analysis was conducted for the displacement and velocity at the point shown at Figure 2 with tetrahedral elements ranging from 0.2 to 1 million, to determine the

accuracy of the solution. According to the results of the mesh independency study as shown in Figure 3, it was decided that the mesh structure constructed with 339872 elements for the solid domain and 934376 elements for fluid domain is sufficient.

Fluid structure interaction (FSI) simulations were made using the Foam-extend which is based on OpenFoam [16]. In simulations made with foam-extend, the solid model and the fluid model should fit together structurally. The absence of any gaps at the interfaces of the geometries is a necessary condition for simulation. The mesh structures of the geometries that interact correctly with each other structurally must also be compatible for simulation. For the fluid model with a higher mesh structure, the values after a certain mesh structure are also valid for the solid model.

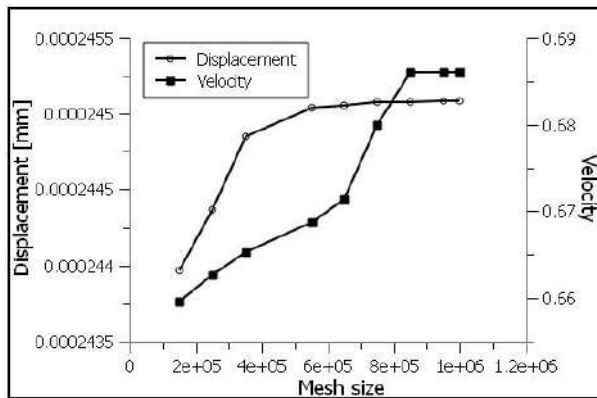


Figure 3 Mesh independency

Here, the blood flow in the carotid artery assumed as incompressible, laminar, and Newtonian. Blood density is taken as  $\rho_f = 1060 \text{ kg/m}^3$  and the dynamic viscosity is  $\mu = 3.71 \times 10^{-3} \text{ kg/m s}$ . The governing equations for the problem solved here are continuity and momentum equations.

Continuity equation is;

$$\nabla \cdot \mathbf{u} = 0 \quad (1)$$

Momentum equation is;

$$\rho_f \left( \frac{\partial \mathbf{u}}{\partial t} + \mathbf{u} \cdot \nabla \mathbf{u} \right) = -\nabla P + \mu \nabla^2 \mathbf{u} \quad (2)$$

here  $\mathbf{u}$ ,  $P$ , and  $\rho_f$  is used as the velocity vector, static pressure, and fluid density, respectively. At the walls, the boundary conditions are no-slip so  $\mathbf{u}=\mathbf{v}=0$ .

The governing equation for artery wall deformation is the linear momentum equation expressed as [9,10],

$$\rho_s \left( \frac{\partial^2 \mathbf{w}}{\partial t^2} - \vec{\mathbf{b}} \right) - \nabla \sigma = 0 \quad (3)$$

Here,  $\rho_s$  is the structure density and  $w$  is the displacement of the arterial wall,  $b$  is body force and  $\sigma$  is the Cauchy stress tensor. Assuming linear isotropic structure, stress tensor can be represented as [9,10],

$$\sigma = 2 \mu_L \varepsilon + \lambda_L \text{tr}(\varepsilon) I \quad (4)$$

$\mu_L$  and  $\lambda_L$  is the first and second Lamé parameters respectively,  $\varepsilon$  is strain tensor,  $\text{tr}$  is trace function and  $I$  is identity matrix. Lamé parameters are defined as functions of elasticity modulus and Poisson ratio [9,10].

$$\lambda_L = \frac{\nu E}{(1+\nu)(2\nu-1)} \quad (5)$$

$$\mu_L = \frac{E}{2(1+\nu)} \quad (6)$$

Wall shear stress is the frictional force per unit area applied by the blood on the surface of the arteries. In this study wall shear stresses are calculated as;

$$\vec{\tau}_w = \mu \cdot (\omega_{wall} \cdot \vec{n}) \quad (7)$$

here,  $\omega_{wall}$  and  $\vec{n}$  is the vorticity at the wall and the normal unit vector to the artery wall, respectively. Time averaged wall shear stresses (TWSS) during a pulsatile cycle are calculated as;



$$TWSS = \frac{1}{T} \int_0^T |\overline{\tau_w}| dt \quad (8)$$

where, T is the period of the pulsatile cycle.

The Support Vector Machine (SVC) [20] is an algorithm for learning effectively from a limited number of data. In this study, 144 patient's data from a small number of data sets were processed using the Support Vector Machine algorithm from the data file downloaded from the relevant web page [17, 18]. Systolic blood pressure, SBP; Diastolic blood pressure, DBP; Mean blood pressure, MBP; stroke volume, SV; and cardiac output, CO were taken as the hemodynamic properties of these patients. Pulsatile velocity cycle was trained by taking 337 velocity points for each 144 patients from the open source literature [17, 18]. Using the machine learning algorithm, 337 velocity points were taught depending on these five hemodynamic parameters that differ according to each patient. First of all, the accuracy of the machine learning result was checked by considering the 14th patient in the existing file. Here, the score of the learning algorithm (accuracy score) was obtained as 1. The rbf kernel function is used in the SVC algorithm.

Table 1 Hemodynamic specifications of 14th patient [17, 18]

SV [ml]	66.277
CO [L/min]	4.826
SBP [mmHg]	117.12
DBP [mmHg]	70.823
MBP [mmHg]	86.257
HR [bpm]	75
Tcardiac [s]	0.8

Table 1 shows the hemodynamic parameters for 14th patient. According to these parameters, by machine learning algorithm pulsatile velocity cycle is obtained for 14th patient and was compared with the original cycle that can be

obtained from the open access data set [17, 18] and shown in Figure 4.

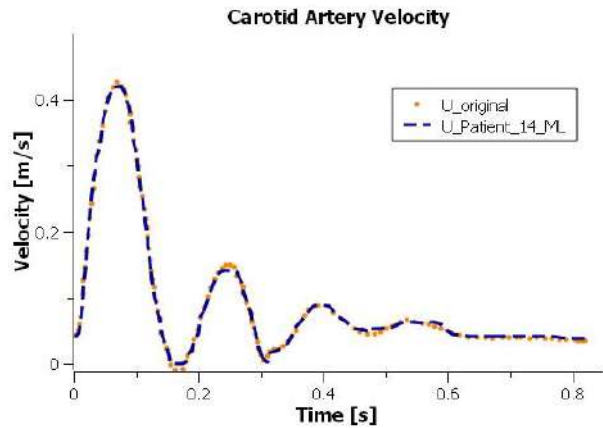


Figure 4 Velocity estimation results for 14th patient

Figure 4 shows a very good agreement between the original values and the predicted values for 14th patient.

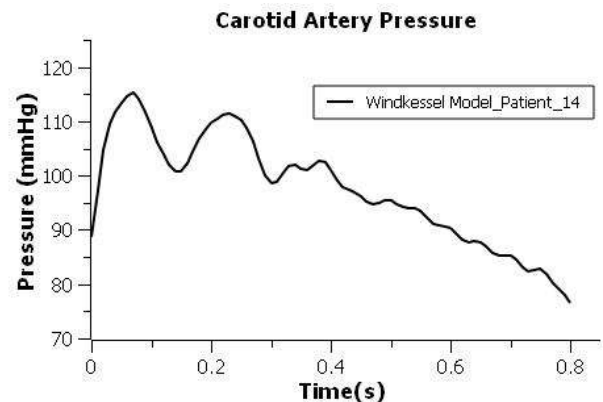


Figure 5 Pulsatile pressure cycle for 14th patient

Pressure pulse cycle is obtained by using 4-Element Windkessel model and shown in Figure 5.

After these validations for the learning result, the hemodynamic parameter values were determined for a completely different selected patient, and the velocity profile that would emerge for this patient with the previous learning was obtained. The hemodynamic values of this specially selected patient are given in Table 2, and the pulsatile velocity and

pulsatile pressure cycles are shown in Figure 6 and Figure 7, respectively.

Table 2 Hemodynamic values of a patient

SV [ml]	62
CO [L/min]	4.5
SBP [mmHg]	120
DBP [mmHg]	75
MBP [mmHg]	90
HR [bpm]	75
Tcardiac [s]	0.8

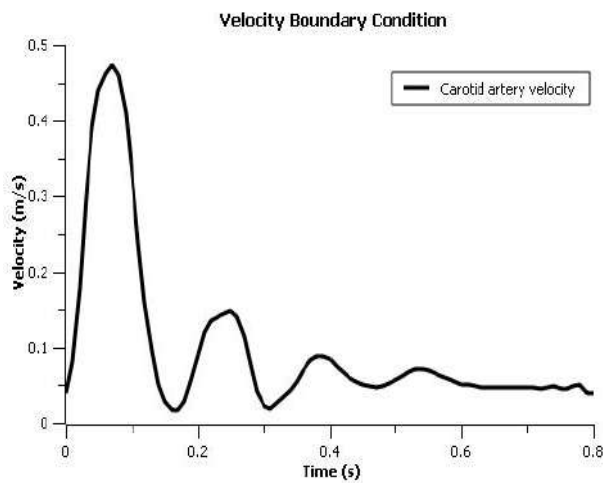


Figure 6 The pulsatile velocity cycle

The pulsatile velocity cycle in Figure 6 was used as inlet boundary condition for CFD analysis.

Also, the pulsatile velocity and pressure cycles are expressed as Fourier series in Equation 9 and 10, respectively. The coefficients of the series are given in Table 3. The frequency,  $\omega$  for both equations is 7.85398.

$$V = a_0 + \sum_{n=1}^{20} a_n \cos n\omega t + \sum_{n=1}^{20} b_n \sin n\omega t \quad (9)$$

$$P = a_0 + \sum_{n=1}^{15} a_n \cos n\omega t + \sum_{n=1}^{15} b_n \sin n\omega t \quad (10)$$

Table 3 Parameters for pulsatile velocity and pressure cycles

Coefficients	Velocity	Pressure cycle
<b>a</b> <sub>0</sub>	0.101388	96.78016
<b>a</b> <sub>1</sub>	0.058847	-2.12215
<b>a</b> <sub>2</sub>	0.027928	-0.87664
<b>a</b> <sub>3</sub>	0.00765	0.48207
<b>a</b> <sub>4</sub>	-0.02192	0.706841
<b>a</b> <sub>5</sub>	-0.06202	-1.46143
<b>a</b> <sub>6</sub>	-0.02518	-2.42601
<b>a</b> <sub>7</sub>	-0.01349	-1.08502
<b>a</b> <sub>8</sub>	-0.01019	-1.20661
<b>a</b> <sub>9</sub>	-0.00288	-0.76442
<b>a</b> <sub>10</sub>	-0.00355	-0.28466
<b>a</b> <sub>11</sub>	-0.0045	-0.36057
<b>a</b> <sub>12</sub>	-0.00209	-0.36565
<b>a</b> <sub>13</sub>	-0.00506	-0.05564
<b>a</b> <sub>14</sub>	-0.00418	-0.96011
<b>a</b> <sub>15</sub>	-0.00033	-0.82192
<b>a</b> <sub>16</sub>	-0.00126	-
<b>a</b> <sub>17</sub>	-0.00094	-
<b>a</b> <sub>18</sub>	0.000103	-
<b>a</b> <sub>19</sub>	0.000225	-
<b>a</b> <sub>20</sub>	0.000125	-
<b>b</b> <sub>1</sub>	0.051645	11.5202
<b>b</b> <sub>2</sub>	0.062584	4.754548
<b>b</b> <sub>3</sub>	0.060867	3.21535
<b>b</b> <sub>4</sub>	0.059719	3.637598
<b>b</b> <sub>5</sub>	0.02457	4.601801
<b>b</b> <sub>6</sub>	-0.0153	1.281552
<b>b</b> <sub>7</sub>	-0.00544	1.00616
<b>b</b> <sub>8</sub>	-0.00743	0.870868
<b>b</b> <sub>9</sub>	-0.00482	0.165459
<b>b</b> <sub>10</sub>	-0.00141	0.43652
<b>b</b> <sub>11</sub>	-0.00184	0.663278
<b>b</b> <sub>12</sub>	-0.00154	0.31772
<b>b</b> <sub>13</sub>	-0.00024	0.86716
<b>b</b> <sub>14</sub>	-0.00453	0.823721
<b>b</b> <sub>15</sub>	-0.00344	-0.06602
<b>b</b> <sub>16</sub>	-0.00159	-
<b>b</b> <sub>17</sub>	-0.00242	-
<b>b</b> <sub>18</sub>	-0.00211	-
<b>b</b> <sub>19</sub>	-0.00108	-
<b>b</b> <sub>20</sub>	-2.6E-05	-

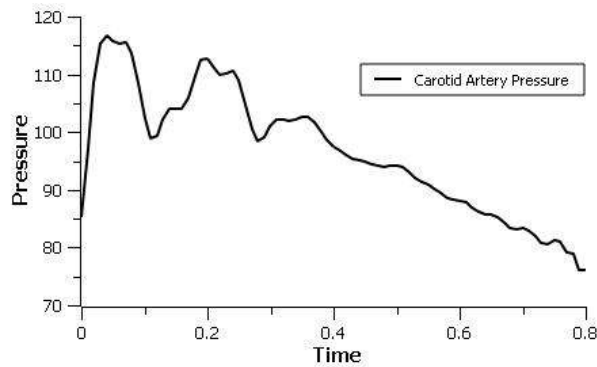


Figure 7 The pulsatile pressure cycle

### 3. RESULTS AND DISCUSSION

In the fluid-structure interaction analysis performed in this study, the displacements and the wall shear stresses were acquired throughout the pulsatile cycle. Wall shear stresses were obtained both for rigid and FSI model, and then compared at the peak of systole, and diastole.



Figure 8 The planes for wall shear stresses

Figure 8 shows the planes where the wall shear stresses are obtained.

Average wall shear stresses throughout the pulsatile cycle for rigid and FSI models are shown in Figure 9 and Figure 10, respectively. WSS are slightly higher in rigid model than FSI. In both cases, at all planes the maximum WSS appears at systolic peak. WSS during systolic peak and diastole increases towards outlet of ICA and ECA. Table 4 gives this

comparison. The WSS variation shows similar trend for both cases.

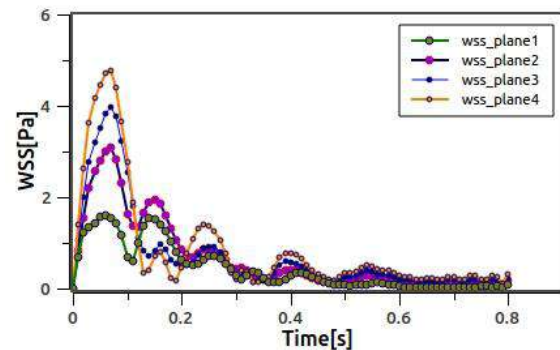


Figure 9 Wall shear stresses variation for rigid model

Table 4 Comparison of wall shear stresses for FSI and rigid model at systolic peak, and diastole

	Systolic Peak		Diastole	
	FSI model WSS [Pa]	Rigid model WSS [Pa]	FSI model WSS [Pa]	Rigid model WSS [Pa]
Plane 1	1.298	1.532	0.0551	0.0872
Plane 2	2.599	3.072	0.1911	0.2183
Plane 3	3.585	3.975	0.2190	0.2977
Plane 4	4.097	4.769	0.3429	0.3895

Figure 11 and 12 represents the time averaged wall shear stresses for FSI and rigid models, respectively. For both cases TWSS is high at the bifurcation point because of separation of flow at that point, velocity gradients are high so due to this TWSS is high at that region.

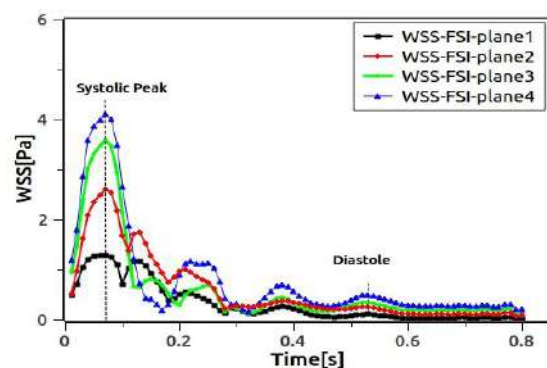


Figure 10 Wall shear stresses variation for FSI model

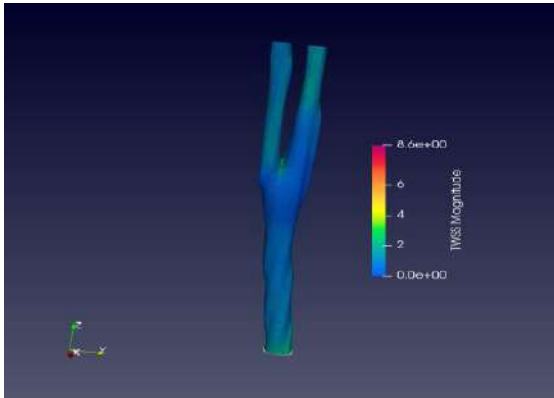


Figure 11 TWSS variation for FSI model

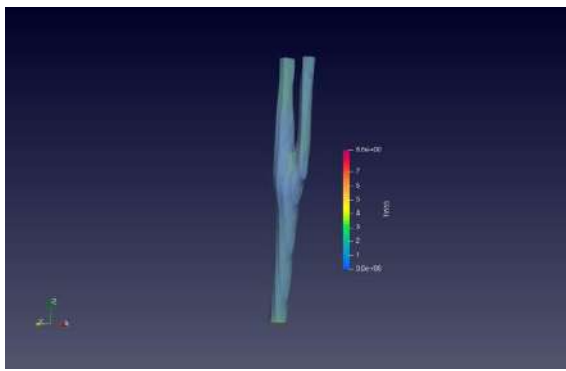


Figure 12 TWSS variation for rigid model

Table 5 shows a comparison of TWSS values between rigid and FSI models. Like the WSS values, TWSS values for the FSI model are lower than for the rigid model, and TWSS also increases towards the outlet of ICA and ECA.

Table 5 Comparison of time averaged wall shear stresses for FSI and rigid model

	FSI model TWSS [Pa]	Rigid model TWSS [Pa]
Plane 1	0.11665	0.32298
Plane 2	0.12188	0.36912
Plane 3	0.16003	0.46383
Plane 4	0.66452	0.77702

Figure 14 gives the variation of velocity at the location shown in Figure 13, Figure 16 gives the variation of WSS at the location shown in Figure 15 for both rigid and FSI models.

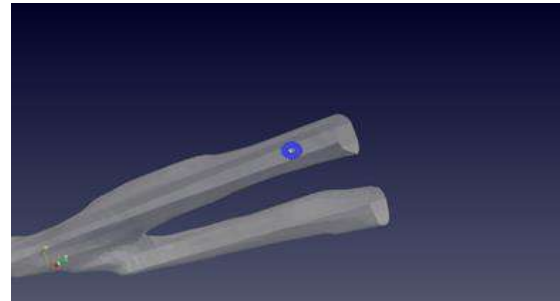


Figure 13 The location of velocity point

Wall shear stresses take their highest values during the pulsatile cycle near the peak of systole. Subsequently, after the peak of systole the wall shear stresses tend to decrease. Like WSS, velocity is also higher throughout all the pulsatile cycle for rigid model.

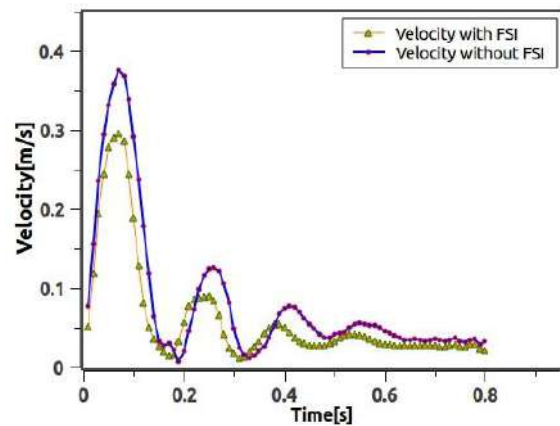


Figure 14 Variation of velocity for rigid and FSI models



Figure 15 The location of wall shear stress point

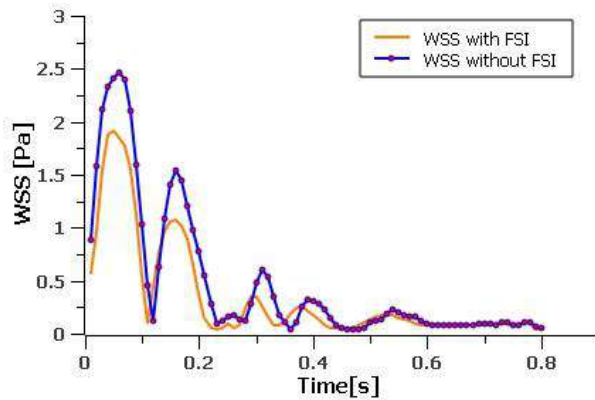


Figure 16 Variation of WSS for rigid and FSI models

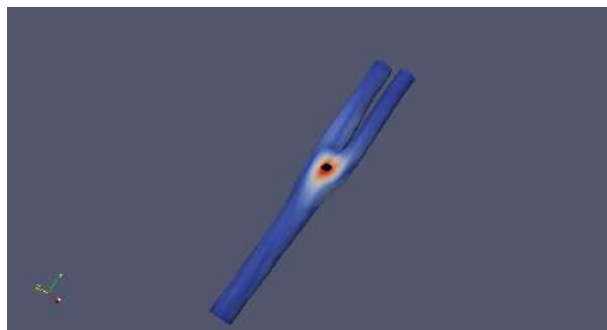


Figure 17 The location of displacement point

Figure 18 gives the variation of displacement at the location shown in Figure 17 for FSI model. The displacement decreases during the pulsatile cycle, maximum displacement appears at systolic peak. This is consistent with the pressure cycle, pressure is also high at systolic peak.

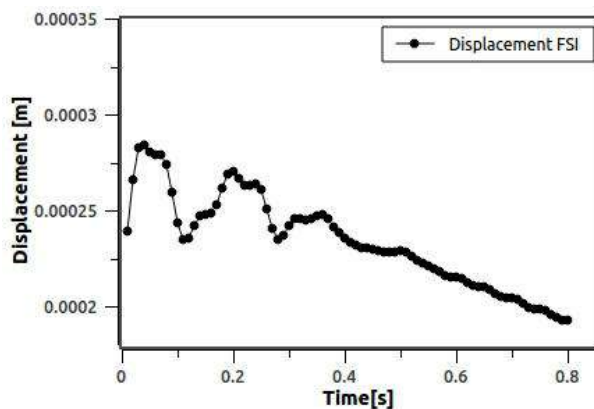


Figure 18 Variation of displacement

## 4. CONCLUSION

Areas of low wall shear stresses are responsible for the formation of atherosclerosis. In this study, the variation of wall shear stresses and displacements during the pulsatile cycle were investigated by considering the fluid structure interaction. Here, the input boundary condition, the pulsatile velocity cycle, was obtained for an independent patient by teaching the data from the literature with machine learning method.

In accordance with the studies in the literature, in this study, the rigid model revealed higher wall shear stresses than the FSI model. Wall shear stresses along the branches of the carotid artery decrease in both the rigid and FSI models. Wall shear stresses, velocity, and displacements are highest at the peak of systole consistent with the pulsatile cycles.

### *Funding*

The author (s) has no received any financial support for the research, authorship, or publication of this study.

### *Authors' Contribution*

The authors contributed equally to the study.

### *The Declaration of Conflict of Interest/ Common Interest*

No conflict of interest or common interest has been declared by the authors.

### *The Declaration of Ethics Committee Approval*

This study does not require ethics committee permission or any special permission.

### *The Declaration of Research and Publication Ethics*

The authors of the paper declare that they comply with the scientific, ethical and quotation rules of SAUJS in all processes of the paper and that they do not make any falsification on the data collected. In addition,

they declare that Sakarya University Journal of Science and its editorial board have no responsibility for any ethical violations that may be encountered, and that this study has not been evaluated in any academic publication environment other than Sakarya University Journal of Science.

## REFERENCES

- [1] P. Çeltikçi, Ö. Eraslan, M. A. Atıcı, I. Conkbayır, O. Ergun, H. Durmaz, E. Çeltikçi, “Application of machine learning algorithms for predicting internal carotid stenosis and comparing their value to duplex Doppler ultrasonography criteria,” *Pamukkale Medical Journal*, vol. 15, no. 2, pp. 213-222, 2022.
- [2] S. Savaş, N. Topaloğlu, Ö. Kazıcı, P. N. Koşar, “Comparison of deep learning models in carotid artery Intima-Media thickness ultrasound images: CAIMTUSNet,” *Bilişim Teknolojileri Dergisi*, vol. 15, no. 1, pp. 1-11, 2022.
- [3] K. Perklot, M. Resch, H. Florian, “Pulsatile Non-Newtonian flow characteristics in a three-dimensional human carotid bifurcation model,” *Journal of Biomechanical Engineering, Transactions of the ASME*, vol. 113, pp. 464-475, 1991.
- [4] F. Yubo, J. Wentao, Z. Yuanwen, L. Jinchuan, C. Junkai, D. Xiaoyan, “Numerical Simulation of Pulsatile Non-Newtonian Flow in the Carotid Artery Bifurcation,” *Acta Mechanica Sinica*, vol. 25, no. 249, pp. 249-255, 2009.
- [5] J. Moradicheghamahi, J. Sadeghiseraji, M. Jahangiri, “Numerical solution of the pulsatile, Non-Newtonian and turbulent flow in a patient specific elastic carotid artery,” *International Journal of Mechanical Sciences*, vol. 150, pp. 393-403, 2019.
- [6] N. Kumar, S. M. Abdul Khader, R. B. Pai, P. Kyriacou, S. Khan, K. Prakashini, R. Srikanth, “Effect of Newtonian and Non-Newtonian flow in subject specific carotid artery,” *Journal of Engineering Science and Technology*, vol. 14, no. 4, pp.2746-2763, 2020.
- [7] D. N. Ku, “Blood flow in arteries,” *Annual Review of Fluid Mechanics*, vol. 29, pp. 399-434, 1997.
- [8] B. K. Bharadvaj, R. F. Mabon, D. P. Giddens, “Steady flow in a model of the human carotid bifurcation part I- flow visualization,” *Journal of Biomechanics*, vol. 15, pp. 349-362, 1982.
- [9] D. Lopes, H. Puga, J. C. Teixeira, S. F. Teixeira, “Influence of arterial mechanical properties on carotid blood flow: comparison of CFD and FSI studies,” *International Journal of Mechanical Sciences*, vol. 160, pp. 209-218, 2019.
- [10] D. Lopes, H. Puga, J. C. Teixeira, S. F. Teixeira, “Fluid-Structure interaction study of carotid blood flow: Comparison between viscosity models,” *European Journal of Mechanics/ B Fluids*, vol. 83, pp. 226-234, 2020.
- [11] K. K. L. Wong, P. Thavornpattanapong, S. C. P. Cheung, J. Y. Tu, “Biomechanical investigation of pulsatile flow in a three-dimensional atherosclerotic carotid bifurcation model,” *Journal of Mechanics in Medicine and Biology*, vol. 13, pp.1-21, 2013.

- [12] S. Tada, M. Tarbell, "A Computational study flow in a compliant carotid bifurcation-stress phase angle correlation with shear stress," *Annals of Biomedical Engineering*, vol. 33, no. 9, pp.1202-1212, 2005.
- [13] N. Kumar, S. M. Abdul Khader, R. Pai, S. H. Khan, P. A. Kyriacou, "Fluid structure interaction study of stenosed carotid artery considering the effects of blood pressure," *International Journal of Engineering Science*, vol. 154, pp.1-14, 2020.
- [14] S. H. Lee, S. Kang, N. Hur., S. Jeong, "A Fluid-Structure interaction analysis on hemodynamics in carotid artery based on patient specific clinical data," *Journal of Mechanical Science and Technology*, vol. 26, pp. 3821-3831, 2012.
- [15] Dr. M. Itagaki. (2019, September.30). The Biomedical 3D Printing Community, Available : <http://www.embodi3d.com/files/file/8523-head-and-neck-ct-dicom-dataset-for-teaching/>.
- [16] B. Gschaider, H. Rusche, H. Jasak, H. Nilsson, M. Beaudoin, V. Skuric. (2013, December.30). Sourceforge, Available : <http://sourceforge.net/p/foamextend/wiki/Home>.
- [17] P. H. Charlton, M. H. Jorge, V. Samuel, L. Ye, A.Jordi. (2019, April.10). Available : <http://doi.org/10.528/zenodo.3275625>
- [18] P. H. Charlton, M. H. Jorge, V. Samuel, L. Ye, A. Jordi, "Modelling arterial pulse waves in healthy aging: a database for in silico evaluation of hemodynamics and pulse wave indexes," *American Journal of Physiology-Heart and Circulatory Physiology*, vol. 317, no. 5, pp. 1062-1085, 2019.
- [19] [19] L. Antiga, D. Steinman, S. Manini, R. Izzo. (2018, March.20). *Vascular Modeling Toolkit*, Available : <http://www.vmtk.org>.
- [20] [20] C. Cortes, V. Vapnik, "Support-vector networks," *Machine Learning*, vol. 20, pp. 273-297, 1995.





SAKARYA ÜNİVERSİTESİ

# FEN BİLİMLERİ ENSTİTÜSÜ DERGİSİ

## Sakarya University Journal of Science SAUJS

ISSN 1301-4048 e-ISSN 2147-835X Period Bimonthly Founded 1997 Publisher Sakarya University  
<http://www.saujs.sakarya.edu.tr/>

Title: Traditional Medicinal Plants Used in Dermatologic Disorders in Ardahan, Iğdır and Kars

Authors: Songül KARAKAYA, Zehra KIMIŞOĞLU, Serdar Volkan YILMAZ, Özkan AKSAKAL, Yusuf Ziya SÜMBÜLLÜ, Ümit İNCEKARA, Ahmet POLAT

Received: 2022-06-21 00:00:00

Accepted: 2022-10-09 00:00:00

Article Type: Research Article

Volume: 26

Issue: 6

Month: December

Year: 2022

Pages: 1142-1158

How to cite

Songül KARAKAYA, Zehra KIMIŞOĞLU, Serdar Volkan YILMAZ, Özkan AKSAKAL, Yusuf Ziya SÜMBÜLLÜ, Ümit İNCEKARA, Ahmet POLAT; (2022), Traditional Medicinal Plants Used in Dermatologic Disorders in Ardahan, Iğdır and Kars. Sakarya University Journal of Science, 26(6), 1142-1158, DOI: 10.16984/saufenbilder.1133853

Access link

<https://dergipark.org.tr/en/pub/saufenbilder/issue/74051/1133853>

New submission to SAUJS

<http://dergipark.gov.tr/journal/1115/submission/start>



## Traditional Medicinal Plants Used in Dermatologic Disorders in Ardahan, Iğdır and Kars

Songül KARAKAYA\*<sup>1</sup>, Zehra KIMIŞOĞLU<sup>1</sup>, Serdar Volkan YILMAZ<sup>1</sup>, Özkan AKSAKAL<sup>1</sup>, Yusuf Ziya SÜMBÜLLÜ<sup>2</sup>, Ümit İNCEKARA<sup>1</sup>, Ahmet POLAT<sup>1</sup>

### Abstract

Ethnobotany is briefly defined as a "human-plant relationship". Mankind has used plants as a food source since ancient times, resorted to healing and accumulated their experiences. About 12.000 plant species grow in Turkey. The World Health Organization (WHO) has determined the number of herbal medicines as approximately 1900 and it has been determined that approximately 20,000 plants are grown in Turkey, 600 of which are used for therapeutic purposes. This investigation was conducted to document the species, family, and local names, usage types and localities of medicinal plants utilized by people living in and around Ardahan, Iğdır and Kars provinces between 2020-2021 for dermatologic disorders. To that end, medicinal plant species utilized by the local mankind for therapeutic aims were collected and detected. The visitations were organised to the investigation regions at regular intervals, and survey investigations were realized by interviewing and talking with the local people one-on-one. 82 medicinal plant taxa belonging to 31 plant families utilized in dermatologic disorders were collected from Ardahan, Iğdır and Kars provinces and their surroundings. Of these, 68 species are wild and 14 are cultivated plants. It has been reported that the most commonly utilized medicinal plant families in dermatologic disorders are Asteraceae (12), Scrophulariaceae (7), Boraginaceae (5), Fabaceae (5), and Salicaceae (5). As a conclusion, despite the deep-rooted history in such regions, the transmission and use of traditional knowledge have remained limited.

**Keywords:** Ardahan, Iğdır, Kars, dermatologic.

\* Corresponding author: songul.karakaya@atauni.edu.tr

<sup>1</sup> Atatürk University

E-mail: zehra\_kimisoglu@hotmail.com, svyilmaz92@gmail.com, ozkanaksakal@atauni.edu.tr,

uincekara@atauni.edu.tr, ahmetpolat@atauni.edu.tr

ORCID: <https://orcid.org/0000-0002-3268-721X>, <https://orcid.org/0000-0003-2029-9321>, <https://orcid.org/0000-0001-7139-6127>, <https://orcid.org/0000-0003-0760-7502>, <https://orcid.org/0000-0002-3283-5841>,

<https://orcid.org/0000-0002-5172-9753>

<sup>2</sup> Erzurum Technical University

E-mail: yzsumbullu@erzurum.edu.tr

ORCID: <https://orcid.org/0000-0002-7062-9109>



## 1. INTRODUCTION

Throughout history, people have benefited from plants grown in their region for various purposes. Mankind started cultivating the plants he collected from nature frequently for the first time [1]. The term ethnobotany was firstly used by the American botanist Dr John William Hershberger and was used to describe his research, which he described as his work on "plants produced by primitive and indigenous peoples" during a conference in Philadelphia in 1895. Ethnobotany is briefly defined as "human-plant relationship". Ethnobotany is also the study of interactions and relationships between plants and humans in time and space. Mankind has used plants as a source of food since ancient times, resorted to their healing and accumulated their experiences. About 12.000 plant species grow in Turkey. It has been reported that more than 50,000 of the approximately 4.22 million flowering plants found in the world are used for medicinal purposes. The World Health Organization (WHO) said that 80% of the world's population is mainly dependent on indigenous medicines and most traditional treatments involve using plant extracts. According to WHO, three-quarters of the world's population cannot afford modern medicines and rely on traditional herbal medicines. Until the middle of the 19th century, herbs were the main therapeutic agents used by humans, and their role in medicine is still valid today. In the late 19th century, ethnobotany began to develop as a science offering new tools for pharmaceutical research. Public institutions such as WHO and private pharmaceutical companies have started investing in ethnobotanical discoveries. Medicinal plants are an important element of local medicinal systems around the world. Ethnobotanical accumulation is accepted as a part of the "traditional" knowledge of a culture. For many years, Europe benefited from the ancient accumulation of local cultures, especially in newly discovered regions, and most of the modern drug molecules and some phytotherapeutic preparations used today are

derived from plants included in the traditional knowledge of indigenous cultures. Eighteenth-century explorers, British Richard Spruce and German Alexander von Humboldt, detailing the use of plants by indigenous communities, studied in detail the preparation of curare, which was used as an arrow poison in South America and later became famous as an important muscle relaxant. The role of ethnobotany in the search for new drugs remained important until the second half of the 20th century, when other approaches became more 'fashionable'. In recent years, the use of such information in medicinal plant research has again attracted great interest in the media and some parts of the scientific community. In addition, 'Western' use of such information has come under increasing scrutiny and national and indigenous rights to these resources have been recognized by most academic and industrial researchers. WHO has determined the number of herbal medicines as approximately 1900 and it has been determined that approximately 20,000 plants are grown in Turkey, 600 of which are used for therapeutic purposes. Most of the living in the Eastern Anatolia Region make their living from agriculture and animal husbandry. The fact that the plant diversity in the region is high also reinforces the closeness of the people of the region to the plants [2-5].

The Eastern Anatolia Region (EWA) covers an area of approximately 170.000 km<sup>2</sup>, 20% of Turkey, and is located in the Iran-Turanian phytogeographical region. More than 3000 plants are grown in the region and the region is among the richest regions of our country in terms of endemism, with a rate of 25%. Due to the geographical conditions of the region, the distance of the villages from the city centres, and the cold and long winter months, herbal treatment is still quite common today. Due to different ecological conditions, various climatic types and vegetation history, it has been observed that EAB has a rich flora. The region, which has a rich cultural heritage, also has a wide wealth of information in terms of

ethnobotany, but due to the migration from rural areas to cities and advancing technology, the youngest generations do not know the value of this treasure and this treasure is facing loss [6].

Although skin diseases are not life-threatening, unlike other organ diseases, they affect the external appearance of the person; they can negatively affect their psychosocial status, personal relationships and daily activities. For this reason, it is important to determine the effects of the diseases on life apart from the clinical severity, to understand how the patients perceive the disease, and to determine the changes in the psychosocial status of the treatment results. "Good quality of life" is more relevant to dermatology than any other medical field, because the most of dermatology patients have chronic and incurable diseases. The effects of these diseases are subjective and depend on the person's circumstances [7].

Complementary and alternative medicine (CAM) is defined by the American National Center for Complementary and Alternative Medicine as a "complementary standard medical treatment" in various health care systems, practices and is referred to as "products". CAM, which is used all over the world today; alternative medical systems (homoeopathy, or traditional Chinese medicine), treatment methods based on the mind-body relationship (meditation, prayer, dance, art, music), biological-based treatments (herbal treatments, dietary supplements), manipulative and body-based treatments (chiropractic medicine, massage), energy-focused therapies (Ki gong, Reiki, touch) are classified under 5 main groups. The frequency of CAM use in dermatology has been reported as 35-69% due to studies conducted in different countries [8].

This research was carried out to document the parts and preparation methods of medicinal plants used in skin diseases by people living in

and around Ardahan, Iğdır and Kars provinces between 2020 and 2021.

## 2. MATERIALS AND METHODS

### 2.1. Study Areas

The Eastern Anatolia Region has the largest surface area in Turkey and is the region with the lowest population density. The average altitude of the region is 2000 m. and three quarters of the region's land is approximately 1500-2500 m. is in the range. The Eastern Anatolia Region is located in the east of our country and it is a region that has borders with the Black Sea, Mediterranean, Southeastern Anatolia and Central Anatolia Regions and draws attention with its length of land border with neighboring countries. The region has borders with five neighboring countries (Nakhchivan (Azerbaijan), Iraq, Georgia, Armenia and Iran). Severe continental climate is seen in most of the region and low temperature values and long and snowy winter months dominate in the region [9] (Figure 1).

### 2.2. Data Collecting

Within the scope of the study, the information was compiled by face-to-face interview method in the field studies carried out in 120 villages (Ardahan-40, Iğdır-30 and Kars-50). In order to identify people with traditional knowledge, general information about the project was given by contacting the reeves beforehand, and information was obtained about people with traditional knowledge. In addition, interview-based interviews in the form of questions and answers were held with people in village coffee shops, mosques, village/district solidarity/association associations, public education centers, agricultural chambers, and cooperatives. As much as possible, women over the age of 60, midwives, shepherds, people referred to as "cookers" or "healers" were interviewed. Before starting the fieldwork, a "Question List" was created regarding the questions to be asked to the interlocutors during

the fieldwork, taking into account the following main headings and the detailed headings in the standard information forms. Thus, it was ensured that a fast and fluent compilation was made without skipping any title. Of the informants, 149 (35.82%) were women, while the remaining 267 were men.

### 2.3. Plant Samples

The plants were collected from the villages of Ardahan, Iğdır and Kars regions in 2020-2021. Identification of the collected plants was made by Prof. Dr. Özkan Aksakal.

### 3. RESULTS

The demographic characteristics of the participants were recorded through face-to-face interviews. 94 participants (36 women, 58 men) were interviewed in Ardahan. It was observed that 18.92% of the participants were illiterate. A total of 144 participants (50 women, 94 men) were interviewed in Iğdır. It was observed that 18.66% of the participants were illiterate. A total of 178 participants (63 women, 115 men) were interviewed in Kars. It was seen that 12.09% of the participants were illiterate.

82 medicinal plant taxa belonging to 31 plant families utilized in dermatologic disorders were collected from Ardahan, Iğdır and Kars provinces and their surroundings. Of these, 68 species are wild and 14 are cultivated plants. It has been reported that the most commonly utilized medicinal plant families in dermatologic disorders are Asteraceae (12), Scrophulariaceae (7), Boraginaceae (5), Fabaceae (5), and Salicaceae (5). The most commonly used plants were *Achillea biebersteinii* (as a blood stopper for wounds), *Achillea millefolium* (as a blood stopper for wounds), *Onosma armena* (for wounds), *Alkanna tinctoria* (for burns and wounds), *Alkanna orientalis* (for burns and wounds), *Euphorbia iberica* (for warts and eczema), *Astragalus microcephalus* (for cracks of the hands), *Medicago sativa* (as a blood stopper for wounds), *Malva neglecta* (as a wound healer),

*Pinus sylvestris* (as a wound healer), *Plantago major* (as a wound healer), *Plantago lanceolata* (as a wound healer), *Rumex crispus* (as a wound healer), *Salix fragilis* (for "Demiro"), *Salix armenorossica* (for eczema), *Verbascum agrimoniifolium* (for fungus foot), *Tamarix smyrnensis* (for scabies), and *Ulmus minör* (as a wound healer). The 82 plants identified in the area were prepared according to the alphabetical order of the families and their botanical names are given in Table A1.

### 4. DISCUSSION

Ethnobotanical studies on the use of plants by the public increased, especially in the 90s and 2000s, in our country as well as all over the world, and as a result, the number of ethnobotanical studies has increased. Almost all of the research on the determination of traditional knowledge based on biodiversity in Ardahan, Iğdır and Kars environs have an ethnobotanical content, and most of the qualified studies belong to the recent past. As a result of the literature review, the most of ethnobotanical studies on Ardahan, Iğdır and Kars regions cover Eastern Anatolia. As in the studies carried out in Ardahan, Iğdır and Kars, it has been observed that *Achillea millefolium*, *Eryngium campestre*, *Achillea biebersteinii*, *Arctium platylepis*, *Cichorium intybus*, *Glycyrrhiza glabra*, *Medicago sativa*, *Mentha longifolia*, *Malva neglecta*, *Plantago lanceolata*, *Rumex crispus*, *Galium verum*, *Ulmus minör*, *Urtica dioica*, *Juglans regia*, *Fumaria officinalis*, *Morus alba*, and *Pinus sylvestris* are used for similar purposes [3, 10-13]. Factors such as the difficulty of the climatic conditions in the region, the difficulty in reaching modern methods due to the distance from the district and city centers, and the economic inadequacy have positively affected the use of existing traditional methods. However, this situation continued until the 1990s. With the death of people called "cooks" or "healers", whom rural people often refer to for all kinds of problems, a large part of the experiences based on traditional knowledge

could not be transferred to new generations. In almost every village, the words "if you had come 20-30 years ago" were said to the project team, "if you had come when my healer-cooker grandfather, grandmother, midwife were alive". In addition, very precious traditional information with high potential to be used and popularized in the future has been recorded from the field.

The Eastern Anatolia Region is a mountainous and high region that is rich in terms of physical geography due to the mountains extending in the east-west direction and the basins between these mountains. While fertile agricultural areas are found in intermountain basins and tectonic depressions, high mountains are important grassland areas. In this context, the region can be considered as an important agriculture and animal husbandry area of our country. The region has difficult conditions, especially with its climatic and geographical structure. The reflection of environmental conditions on the cultural process and the traceability of this reflection through the data to be obtained through the studies to be carried out are of great importance [14, 15].



Figure 1 Ardahan, Iğdır and Kars Provinces Traditional Information Recorded Villages (Circled)

Numerical data on the use of medicinal plants in Ilıca (Erzurum) were evaluated and it was reported that the rate of plants used in skin problems was 14.5% [16]. Numerical data on the use of medicinal plants in Iğdır were

evaluated and it was reported that the rate of plants used in skin diseases was 11.05% [17].

## 5. CONCLUSION

Although it has a deep-rooted history, limited data have been reached in villages where the number of households has decreased due to various reasons, especially immigration. Those who settled in the villages, which are cultural transition areas, through migration, left a significant part of their traditional knowledge, manners and experiences in the places they came from. On the other hand, they had difficulty in learning and assimilating much of the traditional knowledge of the region they came from. For this reason, despite the deep-rooted history in such villages, the transmission and use of traditional knowledge have remained limited. Despite the deep-rooted history in such villages, the transmission and use of traditional knowledge have remained limited.

### *Funding*

We would like to thank the "Republic of Türkiye Ministry of Agriculture and Forestry General Directorate of Nature Conservation and National Parks, 13. Regional Directorate Ardahan Branch Office, 13. Regional Directorate Iğdır Branch Office and 13. Regional Directorate Kars Branch Office." for supporting the project "Kars-Ardahan-Iğdır İl Şube Müdürlüklerinin Sınırları İçerisinde Bulunan Köylerde Biyolojik Çeşitliliğe Dayalı Geleneksel Bilginin Kayıt Altına Alınması".

### *The Declaration of Conflict of Interest/ Common Interest*

The authors have declared no conflict of interest.

### *Authors' Contribution*

Concept: S.K., Z.K., S.V.Y., Ö.A., Y.Z.S., Ü.İ., A.P., Design: S.K., Z.K., Ö.A., Ü.İ., Data Collection or Processing: S.K., Z.K., S.V.Y., Ö.A., Y.Z.S., Ü.İ., A.P., Analysis or Interpretation S.K., Z.K., S.V.Y., Ö.A., Y.Z.S.,

Ü.İ., A.P., Literature Search: S.K., Z.K., Ü.İ.,  
Writing: S.K., Z.K., Ü.İ.

### ***The Declaration of Ethics Committee Approval***

This study was carried out within the scope of the project named “Biyolojik Çeşitliliğe Dayalı Geleneksel Bilginin Kayıt Altına Alınması”. Field studies in the related project were carried out under the coordination of the relevant village headmen, with the assignment of the Ministry of Agriculture and Forestry and the knowledge of the governorships.

### ***The Declaration of Research and Publication Ethics***

The authors of the paper declare that they comply with the scientific, ethical and quotation rules of SAUJS in all processes of the paper and that they do not make any falsification on the data collected. In addition, they declare that Sakarya University Journal of Science and its editorial board have no responsibility for any ethical violations that may be encountered, and that this study has not been evaluated in any academic publication environment other than Sakarya University Journal of Science.

## **REFERENCES**

- [1] H. Akan, M. M. Korkut, M. M. Balos, “Arat Dağı ve Çevresinde (Birecik, Şanlıurfa) Etnobotanik Bir Araştırma.”. Fırat Üniversitesi Mühendislik Bilimleri Dergisi, vol. 20, no. 1, pp. 67-81, 2008.
- [2] U. R. Inayat, A. Aftab, I. Zafar, I. Farhana, A. Niaz, S. Muzammil, U. Sana, W. B. Rainer, “Historical perspectives of ethnobotany.”. Clinics in Dermatology, vol. 37, pp. 382-388, 2019.
- [3] M. Heinrich, “Ethnobotany and its Role in Drug Development.”. Phytotherapy Research, vol. 14, pp. 479-488, 2000.
- [4] H. Akan, Y. B. Sade, “Kâhta (Adıyaman) Merkezi ve Narince Köyü’nün Etnobotanik Açısından Araştırılması.” Bitlis Eren Üniversitesi Fen Bilimleri Dergisi, vol 4, no. 2, pp. 219-248, 2015.
- [5] G. Akgül, “Çıldır (Ardahan) ve çevresinde bulunan bazı doğal bitkilerin yerel adları ve etnobotanik özellikleri.” OT Sistematik Botanik Dergisi, vol. 14, no. 1, pp. 5-88, 2008.
- [6] Z. Kadioğlu, K. Çukadar, A. Kandemir, N. N. Kalkan, H. Vurgun, V. Dönderalp, “Kars İlinde Sebze Olarak Tüketilen Yabani Bitki Türlerinin Tespiti ve Kullanım Şekilleri.” Anadolu Ege Tarımsal Araştırma Enstitüsü Dergisi, vol. 30, no. 1, pp. 11-32, 2020.
- [7] E. Acıöz, G. Gökdemir, A. Köşlü, “Dermatolojide Yaşam Kalitesi.” Turkish Archives of Dermatology and Venereology, vol. 37, no. 1, pp. 16-23. 2003.
- [8] G. T. Demirci, İ. Altunay, A. Küçükünal, E. Mertoğlu, S. Sarıkaya, G. Atış, B. Ateş, “Complementary and Alternative Medicine Usage in Skin Diseases and the Positive and Negative Impacts on Patients.”. Türk Dermatoloji Dergisi, vol. 6, pp. 150-154, 2012.
- [9] O. Coşkun, “Doğu Anadolu Bölgesi'nde Kentleşme ve Kentsel Gelişim.” Eastern Geographical Review, vol. 30, pp. 239-256, 2013.
- [10] E. Sezik, E. Yeşilada, M. Tabata, G. Honda, T. Yoshihisa, F. Tetsuro, T. Toshihiro, T. Yoshio, “Traditional Medicine in Turkey VIII. Folk Medicine in East Anatolia; Erzurum, Erzincan, Ağrı, Kars, Iğdır Provinces.” Economic Botany, vol. 51, no. 3, pp. 195-211, 1997.

- [11] F. Özgökçe, H. Ozelik, "Ethnobotanical Aspects of Some Taxa in East Anatolia.," *Economic Botany*, vol. 58, no. 4, pp. 697-704, 2004.
- [12] E. Altundağ, "Iğdır İlinin (Doğu Anadolu Bölgesi) Doğal Bitkilerinin Halk Tarafından Kullanımı.," PhD, İstanbul: İstanbul Üniversitesi. 2009.
- [13] N. Özhatay, F. Güneş, "An Ethnobotanical Study From Kars (Eastern) Turkey.," *Biological Diversity and Conservation*, vol. 4, pp. 30-41, 2011.
- [14] A. Baysal, "Doğu Anadolu Arkeolojisinde Göçebelik Ve Yaylacılık Kültürü (M.Ö. İi. Bin): Veriler Işığında Yeni Düşünceler.," *U.Ü. Fen-Edebiyat Fakültesi Sosyal Bilimler Dergisi*, vol. 13, pp. 255-268, 2012.
- [15] M. Çelik, İ. Kopar, H. Bayram, "Doğu Anadolu Bölgesi'nin Mevsimlik Kuraklık Analizi.," *Atatürk Üniversitesi Sosyal Bilimler Enstitüsü Dergisi Eylül*, vol. 22, no. 3, pp. 1741-1761. 2018.
- [16] R. Polat, U. Çakılcıoğlu, F. Ertuğ, F. Satıl, "An evaluation of ethnobotanical studies in Eastern Anatolia.," *Biological Diversity and Conservation*, vol. 5, pp. 23-40, 2012.
- [17] M. Ozturk, E. Altundağ, S. J. Ibadullayeva, V. Altay, B. Aslanipour, "A comparative analysis of medicinal and aromatic plants used in the traditional medicine of Iğdır (Turkey), Nakhchivan (Azerbaijan), and Tabriz (Iran).," *Pakistan Journal of Botany*, vol, 50, no. 1, pp. 337-343, 2018.

**Table A1.** Plants Used in Skin Diseases in Ardahan, Iğdır and Kars Provinces and Surroundings.

NO	Species Name	Family Name	Local Name	Usage Types	Localite
1.	<i>Allium sativum</i> L.*	Amaryllidaceae	Sarımsak	Garlic is crushed in the oil. A little salt is added. It is applied to “Demiro” skin disease.	Iğdır
2.	<i>Eryngium campestre</i> L. var. <i>virens</i> Link	Apiaceae	Devetabanı	Garlic is used by crushing for the sty. Fresh leaves are crushed and put on wounds.	Iğdır Iğdır
3.	<i>Achillea biebersteinii</i> Afan.	Asteraceae	Kılıç otu, Sarı civanperçemi, Oymaderem, Zımkaner	After the leaves of the plant are lightly beaten, they are placed on the cut area and wrapped in order to stop the bleeding.	Iğdır
4.	<i>Achillea millefolium</i> L.	Asteraceae	Kılıç otu, Pisik otu, Gılıç otu	After the flowering aerial parts of the plant are boiled, the foot with fungus is washed with this water.	Kars
				After the leaves of the plant are crushed, they are placed on the cuts as a blood stopper.	Iğdır
				The fresh aerial parts of the plant are crushed and applied to the bleeding area.	Kars
				The leaves of the plant are crushed and used as an astringent.	Kars
5.	<i>Cichorium intybus</i> L.	Asteraceae	Cıtlanguş, Çıtlı öz	After the leaves of the plant are lightly beaten, they are placed on the cut area and wrapped in order to stop the bleeding.	Iğdır
				After the plant’s leaves of are lightly beaten, they are placed on the cut area and wrapped in order to stop the bleeding.	Ardahan
				The plant’s leaves are dried and powdered and used on wounds.	Kars
				After the plant’s leaves are lightly beaten, they are placed on the cut area to stop the bleeding and wrapped.	Iğdır
5.	<i>Cichorium intybus</i> L.	Asteraceae	Cıtlanguş, Çıtlı öz	The resin of <i>Pinus sylvestris</i> and aerial parts of the plant are crushed into a paste. It is applied to the bleeding part.	Ardahan
				The plant’s leaves are crushed and used as a blood stopper.	Kars
				The plant’s leaves are crushed and mixed with lard oil and used as a wound healer.	Kars
				After the plant’s leaves are crushed, they are mixed with butter and used in bruises after they become an ointment.	Kars
5.	<i>Cichorium intybus</i> L.	Asteraceae	Cıtlanguş, Çıtlı öz	It is used to treat burns after the aerial parts are burned.	Iğdır
				The aerial parts are cooked with eggs and used in sty treatment.	Iğdır
				Stems are burned for inflammatory wounds and boils; The resulting ash is placed on the wound until the inflammation dries up. Each time ash is added to the wound, and the previous deposits are not deleted. This ash is also used for scabies.	Kars



6.	<i>Xanthium spinosum</i> L.	Asteraceae	Pitrak	The stems are crushed and put on the wound.	Iğdır
7.	<i>Lactuca serriola</i> L.	Asteraceae	Artok	Plant's aerial part is boiled and is applied to the area with alopecia. Plant aerial part juice is used for foot fungus. The aerial parts of the plant are boiled. The area with foot fungus is washed with this water. The aerial part of the plant is boiled against eczema and its water is used. The whole plant is boiled and the person with scabies is washed with its juice.	Iğdır Iğdır Iğdır Iğdır
8.	<i>Scorzonera cana</i> (C.A.Mey.) O.Hoffm.	Asteraceae	Sıping	The latex obtained from the plant's roots is used in the treatment of warts.	Iğdır
9.	<i>Arctium platylepis</i> (Boiss. & Bal.) Sosn. ex Grossh.	Asteraceae	Garahort	The plant's leaves are crushed and put on wounds.	Iğdır
10.	<i>Tragopogon aureus</i> Boiss.	Asteraceae	Sıping	The latex obtained from the roots of the plant is applied in the itching.	Kars
11.	<i>Cichorium glandulosum</i> Boiss. & A.Huet	Asteraceae	Çakçak	After the plant's roots are burned and mixed with butter, it is applied to the wounds.	Kars
12.	<i>Helichrysum plicatum</i> DC.	Asteraceae	Altınbaş	The plant's flowers are boiled with garlic until they have the consistency of an ointment and applied to the wounds.	Kars
13.	<i>Achillea tenuifolia</i> Lam.	Asteraceae	Kiliç otu	The plant's leaves are crushed and used as a blood stopper.	Kars
14.	<i>Tanacetum punctatum</i> (Desr.) Grierson	Asteraceae	Sandal	The plant is added to the bath water. It is used for hair.	Ardahan
15.	<i>Betula alba</i> L.	Betulaceae	Kayın	The plant tar is applied directly to the area with fungus foot, 1-2 drops.	Ardahan
16.	<i>Betula pendula</i> Roth	Betulaceae	Huş	Plant bark tar is used as a healer in eczema wounds.	Ardahan
17.	<i>Echium vulgare</i> L.	Boraginaceae	Havaciva	The aerial parts are boiled and the water is applied to the burns.	Ardahan
18.	<i>Onosma armena</i> DC.	Boraginaceae	Havaotu, Yara yaprağı, Hevaju, Havaju, Enlik	The plant's leaves are wetted with hot water. The softened leaves are closed on the wound. Roots are roasted in a pan. When the roots are roasted, the oil comes out. That oil is rubbed into the wounds. The plant's roots are roasted in a pan and the oil is extracted. It is used as a wound healer. The water obtained by boiling the root is used for eczema. This water is used until eczema dries up.	Kars Kars Kars Kars
19.	<i>Alkanna tinctoria</i> (L.) Tausch	Boraginaceae	Havajo, Havaciva, Hevaco	The plant's roots are cooked with butter and used for red cream burns. The plant's root, which is roasted in oil to the consistency of ointment, is applied to the wound after it takes this state.	Iğdır Kars
				The plant's root are boiled until they reach the consistency of ointment and this ointment is applied to the circumcision wounds.	Kars

					The plant's root is roasted and used to treat of burn wounds.	Kars
					The plant's root are collected, roasted in butter, wax is put on it and fried a little more, the prepared mixture is kept at room temperature and applied to wounds and cracks.	Ardahan
20.	<i>Anchusa azurea</i> Mill.	Boraginaceae	Havajo, Havaciva		The plant's root is roasted in butter with beeswax. When it becomes an ointment, it is applied directly to the wounds.	Ardahan
					The plant's root are cooked with butter and rubbed into the wounds.	Kars
					The root is boiled and mixed with unsalted butter and applied to burns and wounds.	Kars
21.	<i>Alkanna orientalis</i> Boiss.	Boraginaceae	Havaciva, Hevaco, Havajo, Havago, Havejo,		The plant's root are cooked with butter and used as a wound healer.	Kars
					The plant's roots are cooked with butter and used to treat burns.	Kars
					The plant's root are cooked with butter and used for burns.	Kars
					It is combined with rosin, olive oil, the root of the plant, lime, white wax, beeswax, garlic, and 5 g of each. These crushed components are applied to the burned area like a cream.	Kars
					The plant's root are cooked with butter and used for burns.	Kars
					The poultice obtained after the roots of the plant are cooked with butter is used as a wound healer.	Iğdır
					30-40 g of plant root, which is put in 100 g of butter, is roasted until it reaches the consistency of ointment. The resulting arrangement is applied to the injured area.	Kars
22.	<i>Cephalaria procera</i> Fisch. & Avé-Lall.	Caprifoliaceae	Cipreş		The plant's aerial parts are crushed and used as a wound healer.	Kars
23.	<i>Cuscuta campestris</i> Yunck.	Convolvulaceae	Kevze		The whole plant is applied directly to the bleeding site.	Ardahan
24.	<i>Elaeagnus angustifolia</i> L.	Elaeagnaceae	İğde		Fruit peels are used for skin diseases and psoriasis.	Iğdır
25.	<i>Euphorbia iberica</i> Boiss.	Euphorbiaceae	Sütlegen, Hulişirk (Sütlegen), Sütübiyan, Südyan		For warts, 1-2 drops of plant milk are dripped.	Ardahan
					Its latex is used to dry fungal diseases or acne.	Iğdır
					The latex of the plant is used to cure eczema and warts.	Iğdır
					The latex of the plant is applied directly to the eczema and "Demiro" areas.	Iğdır
					Its latex is dripped onto the wounds on the skin. It dries the wound.	Kars

26.	<i>Euphorbia orientalis</i> L.	Euphorbiaceae	Sütligen	The latex on the body of the plant dries the wart.	Kars
27.	<i>Euphorbia virgata</i> Waldst. et Kit.	Euphorbiaceae	Topuştupuğu	The milk of the plant is mixed with some water. The milk of this plant is good for skin wrinkles.	Kars
28.	<i>Trifolium campestre</i> Schreb.	Fabaceae	Üç yaprak yonca	The leaves of the plant are dried, ground into powder and mixed with <i>Cichorium intybus</i> . It is poured into watery wounds. It dries the wound.	Iğdır
29.	<i>Medicago lupulina</i> L.	Fabaceae	Kara yonca, Yabani yonca	The aerial parts of the plant are used as a blood thinner. It is applied by crushing lightly.	Iğdır
30.	<i>Glycyrrhiza glabra</i> L.*	Fabaceae	şirinbiyan	The resin obtained from the roots of the plant is used in foot wounds.	Iğdır
31.	<i>Astragalus microcephalus</i> Willd.	Fabaceae	Geven, Guni	The liquid obtained by squeezing the roots of the plant is applied externally to treat swelling and bruises caused by sprains.	Ardahan
				The root oil of the plant is applied to the cracks of the hands.	Iğdır
				The plant's root oil is applied to the cracks of the hands.	Ardahan
				The gum obtained from plant roots is used as a wound healer.	Kars
				The gum obtained from the roots of the plant is mixed with barley flour and applied as a wound healer.	Kars
				The root oil of the plant is applied to the cracks of the hands.	Kars
				The gum obtained from the roots of the plant is used as a wound healer.	Kars
32.	<i>Medicago sativa</i> L.	Fabaceae	Kara yonca, Yabani yonca, Oncarej	The plant is chewed a little in the mouth and pressed on the bleeding place.	Ardahan
				The leaves of the plant are chewed and tied to the bleeding wound.	Iğdır
				The aerial part of the plant is chewed and tied to the bleeding wound.	Iğdır
				The aerial part of the plant is lightly chewed and wrapped as a blood thinner on cut wounds.	Iğdır
				The leaves of the plant, and the root of <i>Salix</i> sp. are pounded in a stony mortar and then clay is added. This mixture is suitable for mouth sores.	Iğdır
				The leaves of the plant are applied as a boil remover by chewing lightly in the mouth.	Iğdır
33.	<i>Fagus orientalis</i> Lipsky	Fagaceae	Kayın	The resin of the plant is used directly as a wound healer.	Ardahan
34.	<i>Gentiana lutea</i> L.	Gentianaceae	Camışkıran, Egzema otu	The person with scabies takes a bath with the boiled water of the plant's roots.	Ardahan
				The flowering plant is boiled above ground and drunk for eczema.	Kars
35.	<i>Hypericum venustum</i> Fenzl	Hypericaceae	Kantaron	The plant's aerial part of the is kept in olive oil for more than 40 days in the sun and is used as a wound healer.	Kars
36.	<i>Salvia verticillata</i> L.	Lamiaceae	Dermanigali	The aerial part of the plant is crushed and used when fresh as a blood thinner and a wound healer.	Kars

37.	<i>Teucrium orientale</i> L.	Lamiaceae	Mayasıl otu	Aerial parts with flowers are boiled and fungus feet are washed with water.	Kars
38.	<i>Mentha longifolia</i> Host	Lamiaceae	Yarpuz	Powdered leaves are used for aphthae. It is added to bath water and used to relieve itching.	Iğdır Ardahan
39.	<i>Juglans regia</i> L.*	Juglandaceae	Ceviz	Walnuts are crushed, and ezvay ( <i>Aloe</i> sp.) is pounded and mixed. Henna is added to this mixture. This mixture is wrapped around the person's hair. If it is applied 2-3 times, hair loss stops. Henna and walnut inner membrane are crushed and applied to the area with fungus foot.	Iğdır Kars
40.	<i>Malva neglecta</i> Wallr.	Malvaceae	Dolık, Ebegümeci, Dolig, Dolık, Dolig, Dalık	The leaves of the plant are boiled in water, mixed with chopped onion, some barley flour is added, mixed and applied to the boil. The aerial parts of the plant are crushed and used for burns. The aerial parts of <i>M. neglecta</i> and <i>Plantago major</i> are crushed and mixed with linseed oil and used as a wound healer. After the leaves of the plant are lightly boiled, it is used as a wound healer. After the plant leaves are crushed, it is used as a wound healer. The plant's leaf is mixed with <i>Galium</i> sp. and used for burns. The leaves of the plant are boiled with red wheat flour, the dough is made and placed on the wounds for 3 days. After the aerial parts of the plant are crushed, they are mixed with milk and honey. On the 1st day, it is applied to the crushed and injured area. On the 2nd day, after the plant is crushed again, barley flour and milk are mixed and applied to the same area. The leaves are crushed and mixed with soft soap. It is applied to the furuncles.	Ardahan Iğdır Iğdır Iğdır Iğdır Kars Kars Iğdır Kars
41.	<i>Alcea calvertii</i> (Boiss.) Boiss.	Malvaceae	Hırılgülü	After the roots and flowers are crushed, it is cooked with milk and used externally on inflamed wounds.	Iğdır
42.	<i>Alcea striata</i> (DC.) Alef. subsp. <i>rufescens</i> (Boiss.) Cullen	Malvaceae	Hiro	The aerial parts of the plant are crushed and boiled. Its water is filtered and the pulp is placed on the wound.	Iğdır
43.	<i>Gossypium hirsutum</i> L.*	Malvaceae	Pamuk	Papillomas are cured by burning with cotton.	Iğdır
44.	<i>Ficus carica</i> L.*	Moraceae	İncir	The latex of the fig leaf is applied directly to the wart.	Iğdır
45.	<i>Morus nigra</i> L.*	Moraceae	Karadut	The latex of the fruit or leaf dries warts. The fruits of the plant are eaten against mouth sores.	Iğdır Iğdır
46.	<i>Orobanche minor</i> Sm.	Orobanchaceae	Pişikotu	The aerial parts of the plant are boiled and the water is rubbed into the rash.	Kars

47.	<i>Fumaria officinalis</i> L.	Papaveraceae	Egzema otu	After the aerial parts of the plant are boiled, the places with eczema are washed.	Kars
48.	<i>Pinus sylvestris</i> L.	Pinaceae	Sarıçam	The resin of the plant is mixed with “Raspberry (Pisik otu)”. It is applied to bleeding wounds.	Ardahan
				The plant’s resin is used as a healer for cracks in the hand.	Ardahan
				The tar of the plant is used as a wound healer.	Ardahan
				The plant’s resin is mixed with wax and lime in a one-to-one ratio, turned into an ointment and applied to burns.	Ardahan
				The plant’s resin is wrapped around the wounds by being slightly heated.	Ardahan
				After the rotten dust of pine (called “putur ağaç”) is finely sieved, its dust is applied to the circumcision wounds.	Ardahan
				The powder of the rotten plant tree is applied over the circumcision wound by passing it through cheesecloth.	Ardahan
				<i>Alkanna orientalis</i> root, the plant's tar and butter are roasted. The resulting cream is used as a wound healer.	Ardahan
				The tar of the plant is used as a healer in eczema wounds.	Ardahan
				Pine tar is rubbed directly into the wounds.	Ardahan
				Pine tar is rubbed into hand cracks.	Ardahan
				Plant tar is used as a healer for hand cracks.	Ardahan
				Plant tar is used as a healer in eczema wounds.	Ardahan
				The fine dust of rotten trees is used as a healer for the circumcision wound.	Kars
				Rotten wood dust is applied to the circumcision wound as a blood thinner.	Ardahan
				Plant tar is used as a healer in eczema wounds.	Ardahan
49.	<i>Pinus nigra</i> Aiton	Pinaceae	Karaçam	Karaçam reçinesi çıban tedavisi için yara üzerine tatbik edilir.	Ardahan
50.	<i>Abies nordmanniana</i> (Steven) Spach	Pinaceae	Kökнар	The resin of the plant is roasted with butter and applied directly to the cracks of the hands.	Ardahan
51.	<i>Plantago major</i> L.	Plantaginaceae	Bağa yaprağı, Yara otu, Boz otu, Boğa yaprağı, Belhevis, Yara yaprağı	The leaf of the plant is wrapped directly on the finger with the entanglement.	Ardahan
			Pelheves, Pelhevesek, Pelhevis, Belhevis, Belgeheves, Belhavis, Belgeheves, Belgevis	The leaves of the plant are boiled and wrapped around the swellings in the body.	Ardahan
				The leaves of the plant are wrapped around the wound, either directly or by slightly crushing them.	Ardahan
				The leaf of the plant is directly attached to the non-tipped boils.	Ardahan
				The leaves of the plant are slightly crushed and wrapped around the finger.	Kars
				The leaves are boiled and the pulp is wrapped in wounds.	Kars
				For whittle, the leaf of the plant is directly coiled.	Kars
				After the leaves of the plant are slightly crushed, it is used externally in the treatment of fungus.	Kars
				Fresh leaves of the plant are put on the wound.	Kars
				The leaves of the plant are crushed and placed on the boil.	Kars

				After the leaves of the plant are crushed, they are put on the wounds.	Kars
				The leaves of the plant are crushed and put on wounds.	Kars
				The leaves of the plant are placed in hot water, after adding granulated sugar, it is put on the wounds.	Kars
				The aerial parts of the plant are dried and ground into powder. This powder is left on the open skin wound for 3 days. Fresh leaves can also be used by covering the open wound directly. If the dry leaf is to be placed directly, the leaf is wetted and then placed on the wound.	Kars
				The leaf of the plant is lightly crushed and wrapped on a boil.	Kars
				The fresh leaves of the plant clean the wound and expel the secretions.	Ardahan
				The fresh leaves of the plant clean the wound and expel the secretions.	Ardahan
				The fresh leaves of the plant are slightly crushed and put on the wound or boil and bandaged.	Ardahan
				The fresh leaves of the plant are used as wound healing.	Iğdır
				The fresh leaves of the plant take the swelling of the wounds.	Iğdır
				Fresh leaves are crushed and put on boils and pimples.	Iğdır
				The fresh leaves are used for boils.	Iğdır
				The leaves of the plant are crushed and put on the wound as a wound healer.	Iğdır
				The leaves of the plant are slightly crushed and put in place of wounds or boils and bandaged.	Iğdır
				After the leaves of the plant are crushed, it is used as a desiccant.	Iğdır
52.	<i>Plantago lanceolata</i> L.	Plantaginaceae	Kılıç otu, Zilleganer Pisik kuyruğu, Kaynak otu, Belgeheves, Kılıç otu, Bağa yaprağı,	Fresh leaves are used as a wound healer.	Iğdır
				The fresh leaves of the plant are used as an anti-inflammatory.	Kars
				The fresh leaf of the plant is wrapped directly over the bleeding cut.	Kars
				The leaves of the plant are dried in the shade and ground. It is sprinkled on the bleeding places as a blood suppressant.	Ardahan
				The leaves of the plant are slightly crushed and put in place of wounds or boils and bandaged.	Iğdır
				The leaves of the plant are slightly crushed and put in place of wounds or boils and bandaged.	Ardahan
				The leaves of the plant are crushed into deep cuts and wounds.	Iğdır
				The fresh leaf of the plant is used directly as a blood thinner.	Iğdır
				After the fresh leaves of the plant are crushed, they are placed on the cuts as a blood stopper.	Iğdır
53.	<i>Lolium perenne</i> L.	Poaceae	Çimen	The person with the itching rolls naked in the wet grass.	Ardahan
54.	<i>Oryza sativa</i> L.*	Poaceae	Pirinç	They use the oil obtained from the plant for temre.	Iğdır

55.	<i>Triticum aestivum</i> L.*	Poaceae	Buğday	The wheat is roasted in a pan and the oil is extracted. It is applied to the area with ringworm.	Kars
56.	<i>Hordeum vulgare</i> L.*	Poaceae	Arpa	Barley oil is extracted by roasting. It is applied to the psoriasis area.	Kars
57.	<i>Rumex acetosella</i> L.	Polygonaceae	Evelik	The seeds are used for psoriasis.	Ardahan
58.	<i>Rumex crispus</i> L.	Polygonaceae	Evelik, Ğala, Evelik	Dry leaves are boiled with milk, powdered onions are added, and then cooked with flour and oil. The mixture is used in burn treatment. The leaves of the plant are applied directly to the boil, by crushing or slightly boiling. It causes the boil to burst by tipping. The root of the plant is cut into small pieces, mixed with yogurt, left in the sun for 1 day and applied to the scabies area for 3 days.	Iğdır Ardahan Ardahan
59.	<i>Armeniaca vulgaris</i> Lam.*	Rosaceae	Kayıı	The stems of the plant are peeled and the liquid inside is removed. This liquid is applied to children with a rash.	Iğdır
60.	<i>Rosa canina</i> L.	Rosaceae	Şilan	The tar obtained by dry distillation of the stems of the plant is used in "Demiro" skin disease.	Kars
61.	<i>Prunus cerasifera</i> Ehrh.*	Rosaceae	Alca, Erik	The fruits of the plant are crushed, mixed with vinegar, and applied directly to the areas with eczema.	Iğdır
62.	<i>Galium verum</i> L.	Rubiaceae	Sim otu	After crushing the flowers, linseed oil is added. This mixture is applied to reddened and swollen areas.	Kars
63.	<i>Salix fragilis</i> L.	Salicaceae	Civirsöğüt, Çivirsöğüt, Çivrebi Söğüt, Yabani söğüt	Dry branches of the plant are heated. The oil that comes out is rubbed into the area with ringworm.	Iğdır
				The fresh branch of the plant is heated, 1-2 drops are applied from the dripping water to the "Demiro" area.	Iğdır
				The fresh branches of the plant are kept close to the fire and heated, and the water dripping from the tip is applied directly to the areas with "Demiro" disease.	Iğdır
				The medicine prepared from the root of the plant is used for temre.	Iğdır
				For temre disease, the root of the plant is crushed and applied directly.	Iğdır
64.	<i>Salix alba</i> L.	Salicaceae	Söğüt, Yabani söğüt	The leaves of the plant are crushed in vinegar, the mixture is applied directly to the area with ringworm.	Iğdır
				For foot fungus, the branch of the plant is heated. The water that comes out is applied directly to the area with fungus foot.	Iğdır
65.	<i>Salix armenorossica</i> A. SKV.	Salicaceae	Duzik, Söğüt	Tar obtained from the wood of the plant is used in eczema.	Kars
				The leaf of the plant is boiled before the daylight strikes and the child is washed with that water against sunstroke (ğun çalgını).	Kars
				The plant's branches are put on the wart after waiting for a while on the fire.	Kars

66.	<i>Salix pseudomedemii</i> E.Wolf	Salicaceae	Kara söğüt ağacı	When the outer bark of the plant is placed on the fire, it gives its sap. This water is applied to places with eczema once a day for 1 week.	Kars
67.	<i>Salix babylonica</i> L.	Salicaceae	Salkım söğüt	The branches and leaves of the plant are boiled and used externally for itching.	Kars
68.	<i>Verbascum georgicum</i> Benth.	Scrophulariaceae	Öküzkuşu, Sığırkuyruğu	The aerial parts of the plant are boiled in water. It is mixed with flour and turned into a slurry. This mixture is applied to the boiled area. The aerial part of the plant is boiled. The area with foot fungus is washed with this water.	Ardahan Ardahan
69.	<i>Verbascum transcaucasicum</i> E.Wulff	Scrophulariaceae	Sığırkuyruğu	The leaf of the plant is put on the sole of the shoe. It heals the fungus.	Iğdır
70.	<i>Verbascum orephilum</i> C.Koch var. joannis	Scrophulariaceae	Mejok	The base leaves of the plant are placed in the area of the foot fungus.	Iğdır
71.	<i>Verbascum agrimoniifolium</i> (K.Koch) Hub.-Mor.	Scrophulariaceae	Şahmerhemi, Sığırkuyruğu, Majork, Mayork, Marjek, Majalk	The root is boiled. The person with scabies is washed with this water. 200-300 g of fresh oxtail is boiled. In the warm water, the feet with fungus are kept in the water for 30 minutes. The leaves of the plant are put directly between the fingers against fungus foot. The leaves and roots are boiled, a paste is made with the water obtained. The dough is wrapped on the inflamed swelling. The swelling goes down. The root of the plant is boiled. The person with scabies is washed with water. Tea made from its leaves is drunk by people for fungal diseases.	Iğdır Kars Kars Iğdır Iğdır
72.	<i>Verbascum speciosum</i> Schrad. <i>Verbascum speciosum</i>	Scrophulariaceae	Sığırkuyruğu, Mejok, Majork Mejok	The aerial part of the plant is boiled, the person with scabies is washed with its water. The aerial part of the plant is boiled and the fungus foot is washed with its water. The fresh base leaves of the plant are placed in the area of the foot fungus. The aerial part of plant is boiled and used against foot fungus.	Kars Kars Iğdır Iğdır
73.	<i>Verbascum orephilum</i> C.Koch var. joannis	Scrophulariaceae	Mejok	The fresh base leaves of the plant are placed in the area of the foot fungus.	Iğdır
74.	<i>Verbascum songaricum</i> Schrenk	Scrophulariaceae	sığırkuyruğu	The flowers of the plant are boiled and the hand with eczema is washed with its juice.	Iğdır
75.	<i>Solanum nigrum</i> L.*	Solanaceae	Siyah baldırcan	Roasted eggplants are used for skin wounds and inflammations.	Iğdır
76.	<i>Lycopersicon esculentum</i> Mill.*	Solanaceae	Süper domates	Tomatoes are sliced, wrapped around the calloused area, and socks are put on. For foot fungus, tomato juice is squeezed and feet are washed.	Iğdır Iğdır
77.	<i>Solanum tuberosum</i> L.*	Solanaceae	Kartol	The super tomato is sliced and tied to the callus. A raw potato is placed on the burned part to heal the burn.	Iğdır Iğdır
78.	<i>Tamarix tetrandra</i> Pall. ex M.Bieb.	Tamaricaceae	Ilgın	The branches of the tree of the plant are heated. Dripping water is applied to the area with ringworm.	Iğdır



79.	<i>Tamarix tetrandra</i> Pall. ex M.Bieb.	Tamaricaceae	Ilgın	For temre disease, the branches of the plant are heated. The dripping water is applied directly to the relevant area. The fresh branches of the plant are brought close to the fire and the water is removed. The water is applied directly to the area with scabies. The fresh branches of the plant are brought close to the fire and the water is removed, which is applied directly to the area with the temre.	Iğdır Iğdır Iğdır
80.	<i>Tamarix smyrnensis</i> Bunge	Tamaricaceae	İlgın, Kırmızı ılgın, Ilgın, Boz ılgın	When the plant is exposed to fire, it is watered and this water is applied to the temre. The branches of the plant are heated, the water that comes out is applied directly to the area with ringworm. The tar obtained by burning wood is used for scabies. The branches of the plant are heated. Dripping water is applied directly for ringworm disease. The branches of the plant are heated, the water that comes out is applied directly to the wart area. The branches of the plant are heated. Dripping water is directly dripped onto the wart area.	Iğdır Iğdır Iğdır Iğdır Iğdır Iğdır
81.	<i>Ulmus minor</i> Mill.	Ulmaceae	Karaağaç	The ointment is made from the bark of the stem to heal wounds. The root bark of the plant and the onion are boiled together. It is made into an ointment. If it is applied to the boils, it will burst the boil and the pus will fall out. The root bark is boiled with water and used on wounds. The roots are boiled and used on wounds. The barks are boiled with milk and flour and oil are added. It is applied to open wounds. The plant's roots is crushed by pounding and applied directly to the non-spiky boil.	Iğdır Iğdır Iğdır Iğdır Kars
82.	<i>Urtica dioica</i> L.	Urticaceae	Isırgan, Gezgezik	The aerial part of the plant, green clover, barley flour, mallow are boiled together. The resulting water is rubbed on the swollen area.  After boiling the aerial parts of the plant, its water is used as a hair thickener.	Kars  Kars

\* Cultivated plants



SAKARYA ÜNİVERSİTESİ

# FEN BİLİMLERİ ENSTİTÜSÜ DERGİSİ

Sakarya University Journal of Science  
SAUJS

ISSN 1301-4048 e-ISSN 2147-835X Period Bimonthly Founded 1997 Publisher Sakarya University  
<http://www.saujs.sakarya.edu.tr/>

Title: A New Gradient-Based Surface Defect Detection Method for the Ceramic Tile

Authors: Murat Alparslan GÜNGÖR

Received: 2021-12-17 00:00:00

Accepted: 2022-10-10 00:00:00

Article Type: Research Article

Volume: 26

Issue: 6

Month: December

Year: 2022

Pages: 1159-1169

How to cite

Murat Alparslan GÜNGÖR; (2022), A New Gradient-Based Surface Defect Detection Method for the Ceramic Tile. Sakarya University Journal of Science, 26(6), 1159-1169, DOI: 10.16984/saufenbilder.1038022

Access link

<https://dergipark.org.tr/en/pub/saufenbilder/issue/74051/1038022>

New submission to SAUJS

<http://dergipark.gov.tr/journal/1115/submission/start>

## A New Gradient-Based Surface Defect Detection Method for the Ceramic Tile

Murat Alparslan GÜNGÖR\*<sup>1</sup> 

### Abstract

Ceramic tiles are controlled to detect surface defects after production because many defects may occur on their surface during production. The detection of ceramic tile surface defects is usually performed by human observations in most factories. In this paper, an image processing method was proposed to detect the defects. In the proposed method, first, the user selects the homogenous region in the image. Then the gradient-based image processing algorithm is applied. We conducted our study using simulated and real images to which we applied the conventional image processing methods and our proposed method. Performance of the proposed method was evaluated with quality metric and subjective evaluation. The obtained results demonstrate that the proposed method has very good performance and is very promising for ceramic tile application.

**Keywords:** Ceramic tile, surface defect, defect detection, image processing

### 1. INTRODUCTION

Nowadays, the ceramic tile (CT) industry is a very important sector, but in the production of CTs, many surface defects occur such as cracks, edges, holes, and pinholes [1, 2]. Human vision control can be used for the detection of defective products. This depends on human experience and expertise. Thus, using image processing in the CT industry becomes very important for an effective, objective, and repetitive evaluation. This is done by computers automatically without or with little human intervention [3].

The block diagram of the defect detection algorithm is shown in Fig. 1 [4]. The first stage in the pre-processing step is image acquisition. In this stage, the CT image is captured from the real-world source and stored into a computer for further processing. The captured image is in the RGB format and is converted to gray-scale format. Then various operations such as contrast stretching, noise reduction, and image cropping are performed to realize a more effective defect detection algorithm [3, 5, 6]. Finally, the defect detection methods are applied.

Up to now, various methods have been proposed to detect surface defects. One of the

\* Corresponding author: [alparslangunor@hitit.edu.tr](mailto:alparslangunor@hitit.edu.tr)

<sup>1</sup> Hitit University, Faculty of Engineering, Department of Electrical and Electronics Engineering

ORCID: <https://orcid.org/0000-0001-7446-7808>



methods is selecting an appropriate threshold. Ng [7] proposed a thresholding approach based on the Otsu method. The proposed method is effective, simple and fast for defect detection. Hocenski et al. [8] focused on detecting one kind of defect, and highly contrasted dot shaped formation of pixels. To find highly contrasted dot shaped formations, they proposed the convolution-based method with local intensity difference analysis. The presented method shows better performance than similar methods but is less accurate than any complex morphology analysis-based method. Shire et al. [6] compared reference and test images to decide the defect after pre-processing operations but the proposed method is useful only for plain ceramic tiles. Sioma [9] presented 3D image analysis to evaluate defects on the surface of ceramic tiles and successful results were obtained for quick defect detection in automated control systems installed on production lines. Latif-Amet et al. [10] used wavelet transform for texture defect detection. Considering computational complexity and reliability, their approach is feasible for real-time applications. In [4], the Rotation Invariant Measure of Local Variance operator was employed for surface defect detection. The proposed system has high accuracy and can be used for the detection and classification of ceramic tile defects that occurred in firing unit. Sobel, Prewitt and Canny edge detectors are gradient-based edge detection methods used to find the edge pixel in an image. These detectors have been employed in many studies for the surface defect detection of ceramic tiles [3, 11-13].

In this paper, a new gradient-based surface defect detection method for ceramic tile was proposed. In the proposed method, one or more homogeneous regions in the image are selected first. According to the selected regions, a threshold value and mean pixel value are calculated. Then, the gradient-based algorithm is applied using these values. We present, in detail, the proposed method and the materials used to assess the performance of the proposed method in Section 2. The

proposed method is evaluated in Section 3 and our conclusions are presented in Section 4.

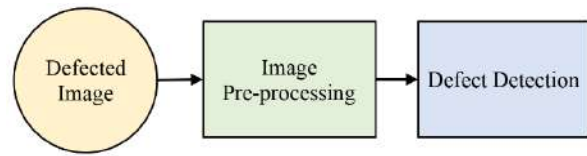


Figure 1 Block diagram of the defect detection algorithm

## 2. MATERIALS AND METHOD

The proposed method was applied to CT images having surface defects and compared with the existing gradient-based methods. The performance of the proposed method was evaluated with image quality metric and subjective evaluation.

### 2.1. Image Quality Metric and CT Images

In our study, we used real and simulated CT images. Performance was evaluated both objectively and subjectively. For objective evaluation, the first type of image used in this paper was the real CT images (these images were also used in [4]) shown in Fig. 2. The images in Fig. 2 are in the RGB format and they were converted to gray-scale format based on the NTSC conversion formula as Eq. (1), used in the image processing toolbox of MATLAB [14].

$$rgb2gray = 0.2989R + 0.587G + 0.114B \quad (1)$$



Figure 2 Real CT images for objective evaluation

The obtained gray level images are shown in Fig. 3. We named the images in Fig. 3a, Fig.3b and Fig. 3c as RI1, RI2 and RI3 (RI=Real Image), respectively. As shown in the images, all of them have one or more defective regions.

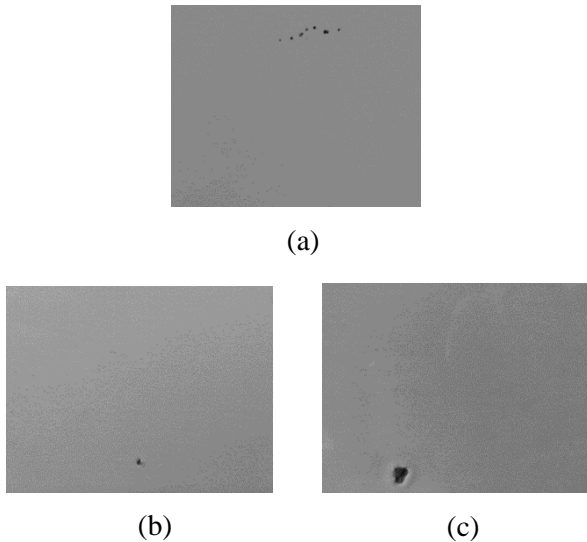


Figure 3 The gray level CT images (a) RI1 (b) RI2 (c) RI3

The second type of image used in this paper was the simulated image shown in Fig. 4 for objective evaluation. We named the images in Fig. 4a, Fig.4b and Fig. 4c as SI1, SI2 and SI3 (SI=Simulated Image), respectively. The SIs were created using MATLAB [14]. The pixel values of the SIs are 210 except in the defective regions. The pixel values of the defective regions are zero in the SIs.

Any surface defect detection method aims to find pixels in the defective regions. The quality metric, the detection accuracy rate (%) (DAR) [4], is used for objective evaluation of the method, defined by:

$$DAR = \frac{A+D}{A+B+C+D} * 100 \quad (2)$$

where A is the number of the defective pixels, which are detected as defective pixels; D is the number of the non-defective pixels, which are detected as non-defective pixels; B is the number of the pixels detected as defect, but these are non-defective pixels; C is the number of the pixels detected as non-defect,

but these are defective pixels. The DAR value is between 0 and 100. The higher this value, the better the performance of the applied method.

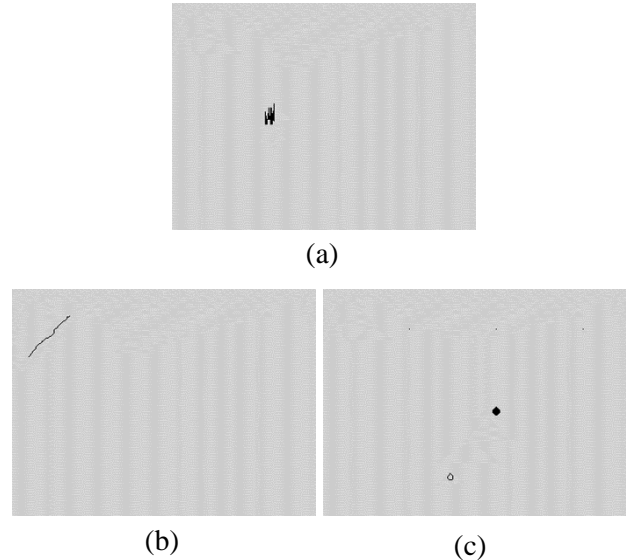


Figure 4 The simulated images (a) SI1 (b) SI2 (c) SI3

## 2.2. Existing Gradient-Based Methods for Defect Detection

In this paper, we developed a new gradient-based surface defect detection method for ceramic tile. Sobel [15], Prewitt [16] and Canny [17] edge detectors which are gradient-based methods have been employed in many studies for defect detection. Canny implements a multi-step algorithm, while Sobel and Prewitt usually use 3\*3 masks for the detection of edges. The purpose of these methods is to obtain the edges of the defective regions.

After the edges of the defective regions of the CT are determined using edge detection methods, a morphological operator is used to fill in the detected regions [3, 4, 13]. In all the morphological processes, structuring elements are used. There are different structuring elements such as diamond, disk, and octagon [18]. Each structuring element has its own parameter. A proper structuring element and parameter selection is important.

The structuring elements and parameters used in this paper are shown in Table 1.

Table 1 The structuring elements and parameters used in this paper

Structuring Element	Parameter
diamond	R
disk	R
octagon	R
line	LEN, DEG
square	W

The parameter R shown in Table 1, specifies the distance for the diamond and octagon, and the radius for the disk. For the line, the parameters LEN and DEG specify length and angle, respectively. The parameter W specifies the width for the square. We used the closing morphology operator. The morphological closing of I by S, denoted  $I \bullet S$ , is defined by Eq. (3) [18].

$$I \bullet S = (I \oplus S) \ominus S \quad (3)$$

where I is a binary image, and S is a matrix of 0s and 1s that specifies the structuring element. The closing morphology operator is a dilation followed by an erosion as shown in Eq. (3). While the dilation operator fills the intra borders of defective regions, erosion operator eliminates the extra borders of defective regions.

### 2.3. Derivation of the Proposed Method

This paper provided the derivation of a new gradient-based surface defect detection (GBSDD) method for CT images. In this method, one or more homogeneous regions in the image are selected first. According to the selected regions, a threshold value and mean pixel value are calculated. Then, a reference pixel is determined in the CT image. By comparing the reference pixel with the relevant pixel in the CT image, it is determined whether the relevant pixel is defective. The GBSDD method has two steps: 1- Determination of threshold and mean pixel values. 2- Obtaining the defective pixels in the CT image using these values.

#### 2.3.1. Determination of Threshold and Mean Pixel Values

To calculate the threshold value (T) and the mean pixel value ( $P_{\text{mean}}$ ), first, a homogeneous region is selected in the CT image as shown in Fig. 5.

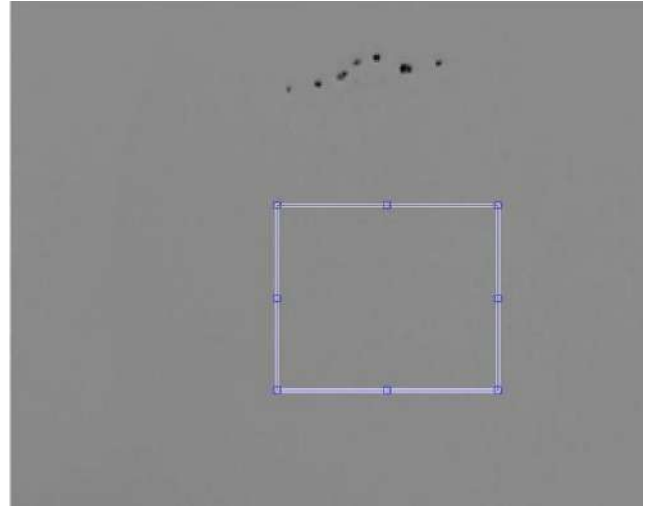


Figure 5 Selected homogenous region in the gray level image

The row and column numbers of the selected part of the image are  $m_s$  and  $n_s$ , respectively. Then, Eq. (4) is computed for each pixel in the first row of the selected region

$$T_x = |I(x) - I(x + 1)| \quad \text{for } x = 1, 2, 3, \dots, n_s - 1 \quad (4)$$

where “ $I(x) - I(x+1)$ ” indicates the difference between the two horizontally adjacent pixels. After calculating the threshold values for the first row,  $(n_s-1)$  number of threshold values are obtained. For each row in the selected region, Eq. (4) is repeated. Finally, the maximum value ( $T_{x\text{max}}$ ) is selected among  $((n_s-1) * m_s)$  number of threshold values for the horizontal direction.

Then, Eq. (5) is computed separately for each column in the selected region

$$T_y = |I(y) - I(y + 1)| \quad \text{for } y = 1, 2, 3, \dots, m_s - 1 \quad (5)$$

where “ $I(y) - I(y+1)$ ” indicates the difference between the two vertically adjacent pixels. After calculating all the threshold values, the maximum value ( $T_{y_{max}}$ ) is selected among  $((m_s-1) * n_s)$  number of threshold values for the vertical direction.

If the number of selected homogeneous regions ( $h$ ) is  $z$ , then  $z$  number of  $T_{x_{max}}$  ( $T_{x_{max}1}, T_{x_{max}2}, T_{x_{max}3}, \dots, T_{x_{max}z}$ ) and  $z$  number of  $T_{y_{max}}$  ( $T_{y_{max}1}, T_{y_{max}2}, T_{y_{max}3}, \dots, T_{y_{max}z}$ ) values are obtained. After eliminating  $\max \{T_{x_{max}1}, T_{x_{max}2}, T_{x_{max}3}, \dots, T_{x_{max}z}\}$  and  $\max \{T_{y_{max}1}, T_{y_{max}2}, T_{y_{max}3}, \dots, T_{y_{max}z}\}$ , the mean value of the remaining values is calculated ( $T_m$ ).

Finally,  $T$  is calculated by Eq. (6)

$$T = T_m + dp \quad (6)$$

where  $dp$  is the defect parameter.  $dp$  determines the sensitivity of the defective detected. Larger values of  $dp$  decrease the sensitivity.

The second parameter,  $P_{mean}$ , is obtained by calculating the mean value of the pixels in the selected region. If more than one region is selected, the mean of the obtained  $P_{mean}$  values is calculated. As the number of selected homogeneous regions increases, the accuracy of the proposed method increases, but the processing time also increases.

### 2.3.2. Obtaining Defective Pixels in the CT Image

The detailed block diagram of the proposed defect detection algorithm is shown in Fig. 6. First, the proposed algorithm shown in Fig. 6 is applied for the first row. The first pixel in the row is determined as the reference pixel ( $I(r)$ ). The reference pixel is compared with the pixel just to the right. The aim is to determine whether the compared pixel ( $I(c)$ ) is defective. If the following two conditions are met,  $I(c)$  is determined as defective.

$$|I(r) - I(c)| > T$$

and

$$I(c) > (P_{mean} + T) \text{ or } I(c) < (P_{mean} - T)$$

If  $I(c)$  is defective, the pixel just to the right of the  $I(c)$  becomes the new pixel to be compared ( $I(c) = I(c+1)$ ). Then  $I(r)$  is compared with the  $I(c)$  to determine whether the  $I(c)$  is defective. When  $I(c)$  is not defective, the compared pixel becomes the new reference pixel. Then the obtained reference pixel is compared with the pixel just to the right. This process continues until the last pixel in the corresponding row is involved in the process. For each row in the CT image, the above algorithm is repeated. As a result, a defective binary image is obtained according to the detected defective and non-defective pixels. The pixel in the obtained image is “1” if it is defective, otherwise, it is “0”.

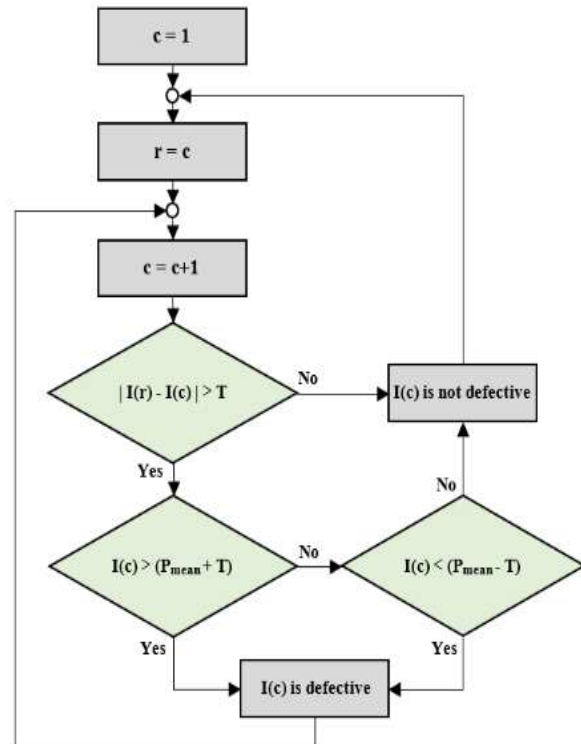


Figure 6 Block diagram of the proposed defect detection algorithm

Let's show a CT image by using pixels as in Fig. 7.



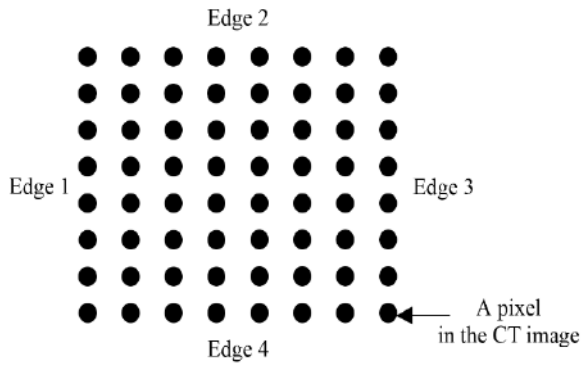


Figure 7 CT image represented by pixels

A CT has four edges, and each edge was numbered as shown in Fig. 7: Edge 1, Edge 2, Edge 3 and Edge 4. The defect detection algorithm mentioned above is repeated four times, with each edge selected as the starting edge. The starting edge is Edge 1 for Fig. 7. Fig. 8 shows when the starting edges are Edge 2, Edge 3 and Edge 4.

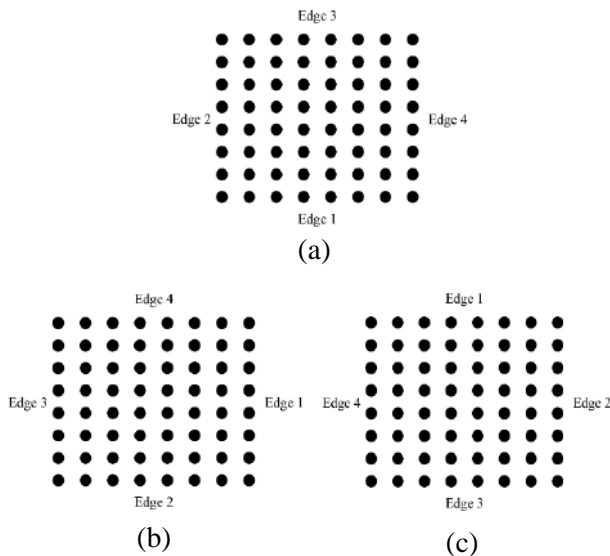


Figure 8 The starting edge is (a) Edge 2 (b) Edge 3 (c) Edge 4

Thus, four defective binary images are obtained for the four starting edges. For the final defective binary image, the obtained four defective binary images are combined according to Eq. (7).

$$I(i, j) = (I_{e1}(i, j) | I_{e3}(i, j)) \& (I_{e2}(i, j) | I_{e4}(i, j))$$

$$\text{for } i = 1, 2, 3, \dots, N \text{ and } j = 1, 2, 3, \dots, M \quad (7)$$

where  $I_{e1}(i, j)$ ,  $I_{e2}(i, j)$ ,  $I_{e3}(i, j)$  and  $I_{e4}(i, j)$  are the pixels at position  $(i, j)$  in the defective binary images when the starting edges are Edge 1, Edge 2, Edge 3 and Edge 4, respectively.  $I(i, j)$  is the pixel at position  $(i, j)$  in the final defective binary image,  $M$  and  $N$  are the sizes of the CT image. According to Eq. (7), if at least one of the  $I_{e1}(i, j)$  and  $I_{e3}(i, j)$  values and at least one of the  $I_{e2}(i, j)$  and  $I_{e4}(i, j)$  values are “1”, the value of  $I(i, j)$  in the defective binary image is “1”, otherwise its value is “0”.

A CT image and its defective binary image are shown in Fig. 9.

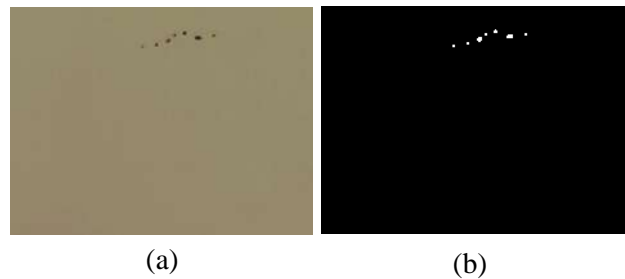


Figure 9 (a) Original CT image (b) defective binary image

The defective binary image shown in Fig. 9b was obtained from the original image shown in Fig. 9a using the GBSDD method. The non-defective and defective pixels are shown as black and white in Fig. 9b, respectively.

The proposed method cannot be applied to tiles with defects on the edges. It is accepted that there is no defective pixel on the edge of the CT image. Besides that, if the image has regions containing edge, these regions can be identified as a defect after the proposed method. These regions are image specific and known, so these edge regions are eliminated before the defect detection method is applied.

### 3. RESULTS AND DISCUSSION

To evaluate the GBSDD method, we used the existing gradient-based methods: Sobel, Prewitt and Canny, both with and without the morphological operator, six CT images which



were RI1, RI2, RI3, SI1, SI2, SI3 for objective evaluation and four CT images for subjective evaluation. We applied the structuring elements and the different values of the parameters, shown in Table 1, when the morphological operator was used. Table 2 gives the obtained best results using the existing methods for RI1, RI2 and RI3.

Table 2 The best results obtained with the existing method for RI1, RI2 and RI3

Images	DAR and its parameters	The type of method with the best result
RI1	99.9547 A=72, B=4, C=22, D=57254	Prewitt+Square (W=3)
RI2	99.4997 A=21, B=448, C=50, D=99027	Prewitt
RI3	99.577 A=312, B=337, C=100, D=102571	Prewitt+Line (LEN=14, DEG=45)

Among the existing gradient-based methods for RIs, Table 2 shows that the best performance was Prewitt. While the best results were obtained by using the morphological operator for RI1 and RI3, the best results were obtained for RI2 without the morphological operator. The defective binary images corresponding to the best results for all three images are shown in Fig. 10.

For RIs, the obtained results and defective binary images using the proposed method are given in Table 3 and Fig. 11, respectively.

For the proposed method, eight homogeneous regions were selected. Then  $T$  and  $P_{\text{mean}}$  were calculated by selecting different  $dp$  values for the three images. When the results obtained after applying the proposed method are compared with the results shown in Table 2, the proposed method gives better results than the existing methods for all three images. Comparing Fig. 10 with Fig. 11, the proposed method better identifies both defective and non-defective regions.

For SIs, the obtained results and images for both the existing and the proposed methods are given in Tables 4-5 and Figs. 12-13.

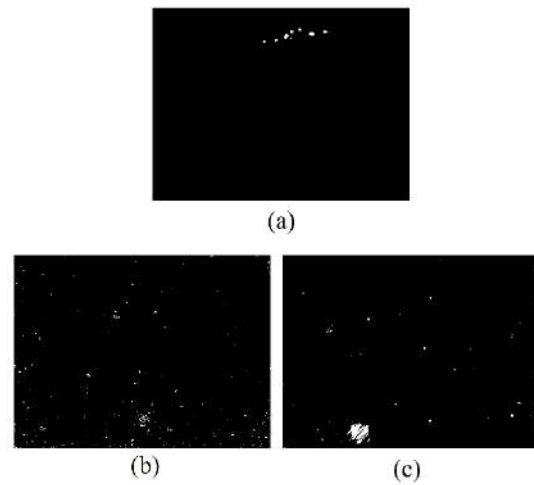


Figure 10 Obtained defective binary images using existing methods corresponding to the best results for (a) RI1 (b) RI2 (c) RI3

Table 3 The obtained results with the GBSDD method for RI1, RI2 and RI3

Images	DAR and its parameters	The proposed method parameters
RI1	99.9983 A=93, B=0, C=1, D=57258	$dp=4, h=8$
RI2	99.9879 A=61, B=2, C=10, D=99473	$dp=1, h=8$
RI3	99.9642 A=385, B=10, C=27, D=102898	$dp=1, h=8$

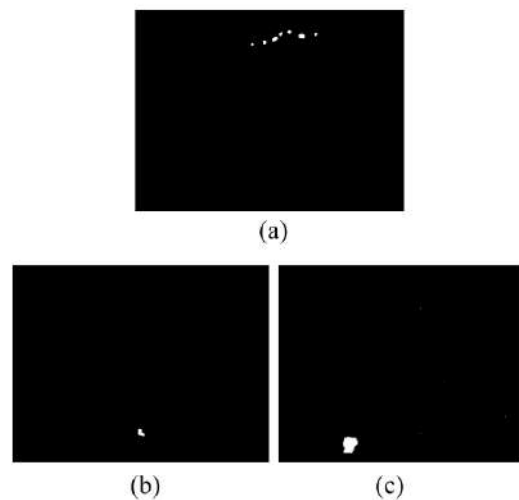


Figure 11 The obtained defective binary images using the GBSDD method for (a) RI1 (b) RI2 (c) RI3

Table 4 The best results obtained with the existing method for SI1, SI2 and SI3

Images	DAR and its parameters	The type of method with the best result
SI1	99.8949 A=152, B=103, C=0, D=97745	Sobel+Disk (R=4)
SI2	99.8776 A=60, B=120, C=0, D=97820	Sobel+Disk (R=3)
SI3	99.9255 A=89, B=73, C=0, D=97838	Sobel+Diamond (R=4)

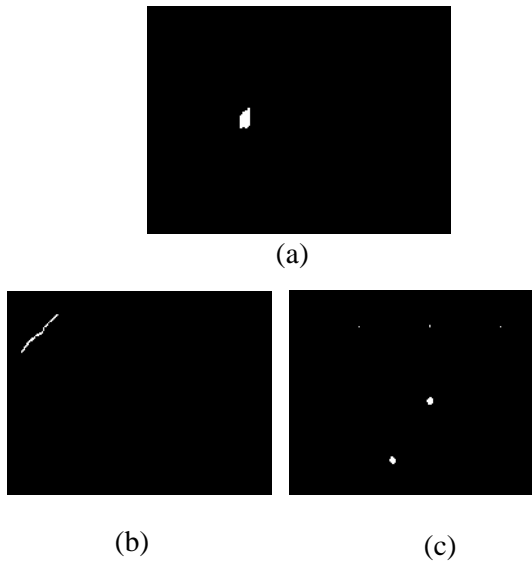


Figure 12 Obtained defective binary images using existing methods corresponding to the best results for (a) SI1 (b) SI2 (c) SI3

Images	DAR and its parameters	The proposed method parameters
SI1	100 A=152, B=0, C=0, D=97848	dp=0, h=8
SI2	100 A=60, B=0, C=0, D=97940	dp=0, h=8
SI3	100 A=89, B=0, C=0, D=97911	dp=0, h=8

Table 5 The obtained results with the GBSDD method for SI1, SI2 and SI3

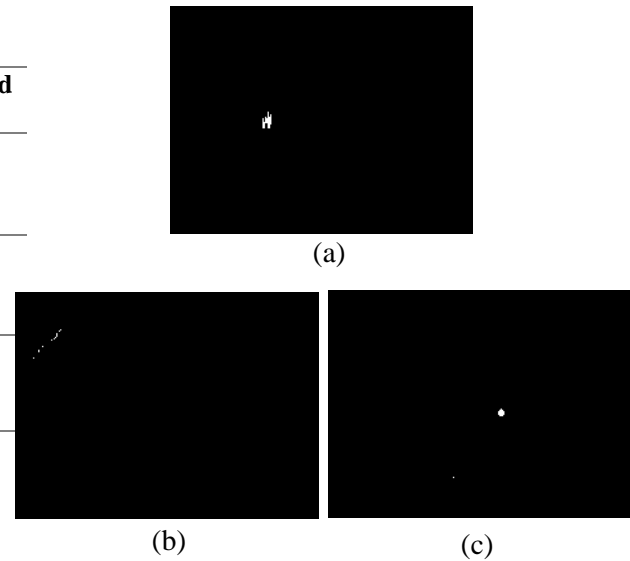


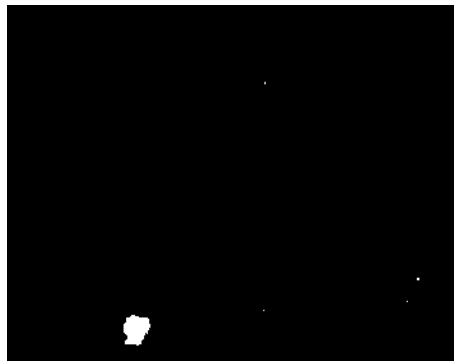
Figure 13 The obtained defective binary images using the GBSDD method for (a) SI1 (b) SI2 (c) SI3

As in the RIs, eight homogeneous regions were selected within the SIs. Table 4 shows that the best performance was Sobel among the existing gradient-based methods for SIs. As shown in Table 4, parameter B negatively affected the results. Table 5 shows the proposed method gives excellent results for SIs. There is no wrongly identified pixel for the output images of the proposed method. If we compare Fig. 4 with Figs. 12 and 13, it is understood that the GBSDD method has a better performance than the existing methods.

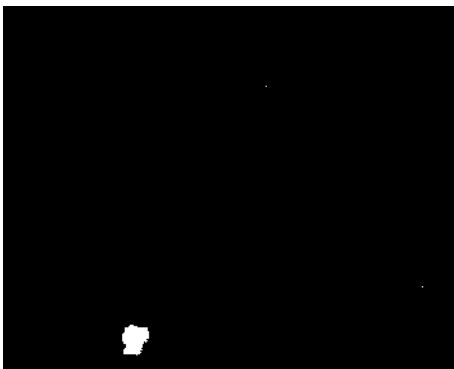
Table 5 shows the values of the dp were determined as zero for all SIs. For the RIs, different dp values were determined as shown in Table 3. If the values of dp in Eq. (6) are selected as zero for all RIs, the obtained DAR values were 99.9686, 99.9859 and 99.9555 for RI1, RI2 and RI3, respectively. If we compare these DAR values with DAR values in Table 2, the values obtained for dp = 0 are bigger than the best results obtained with the existing method. For improving the defective binary image, the value of the dp parameter is important. The DAR values shown in Table 3 are bigger than the DAR values obtained for dp = 0. For example, Fig. 14 shows the reference and the defective binary images obtained using the GBSDD method for RI3 when dp=0 and dp=1.



(a)



(b)



(c)

Figure 14 The reference and defective binary images obtained using the GBSDD method for the RI3 (a) reference image (b)  $dp = 0$  (c)  $dp = 1$

When Fig. 14a is examined, there are very small defective pixels. Comparing Fig. 14b with Fig. 3c, invisible defects by people can be determined by the proposed method. Moreover, a better defective binary image can be obtained as shown in Fig. 14c by increasing the  $dp$  value. Increasing the  $dp$  value too much can cause these pixels to disappear.

Finally, the tests were carried out with some real CT images, shown in Fig. 15, for subjective evaluation. There is no reference image for these images. The obtained

defective binary images using the GBSDD method are shown in Fig. 16. By comparing Fig. 15 and Fig. 16, it can be seen that the GBSDD method has good defect detection capability.

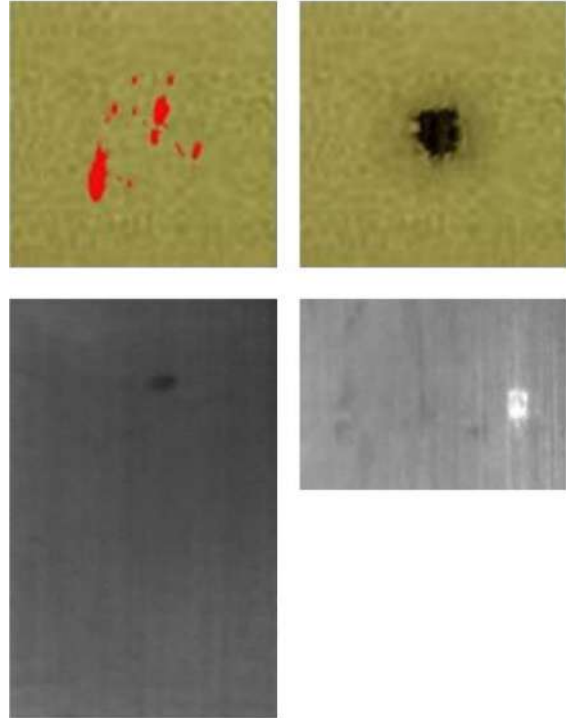


Figure 15 Real CT images for subjective evaluation

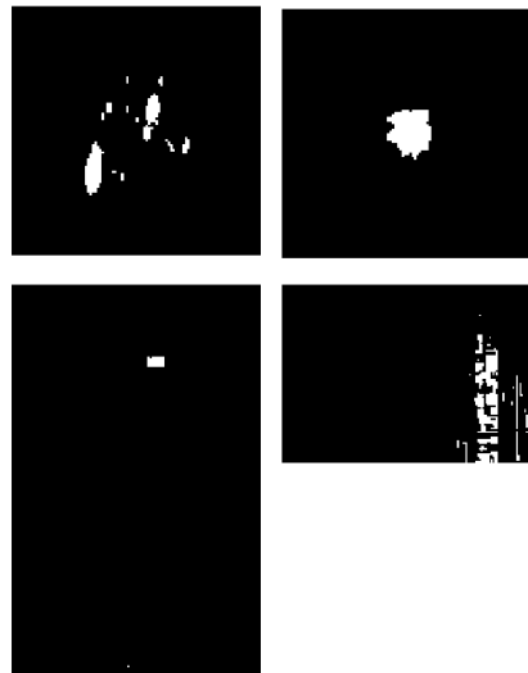


Figure 16 Defective binary images of the CT images shown in Fig. 15

Image processing methods have been used in the ceramic industry for various purposes [19]. Our target is to detect the surface defects for the CT using the image processing method we developed. The tests carried out on the CT images show that the proposed method assures a good performance.

#### 4. CONCLUSIONS

In this paper, we proposed a new method, GBSDD, as a way to detect the surface defects of CTs. For this purpose, one or more homogeneous regions in the CT image are selected. After calculating the threshold and mean pixel values, the reference pixel is compared to another pixel in the image to determine whether the compared pixel is defective. If the compared pixel is defective, the same reference pixel is compared with another pixel. When the compared pixel is not defective, the reference pixel changes. Thus, the defective binary image showing defective and non-defective regions of the CT image is obtained. The obtained results show us that the proposed method assures a good performance, and as such, we recommend it as a useful method.

#### *Acknowledgments*

The author thanks S. H. Hanzaei, A. Afshar and F. Barazandeh for providing the real CT images.

#### *Funding*

The author has no received any financial support for the research, authorship or publication of this study.

#### *The Declaration of Conflict of Interest/ Common Interest*

No conflict of interest or common interest has been declared by the authors.

#### *The Declaration of Ethics Committee Approval*

This study does not require ethics committee permission or any special permission.

#### *The Declaration of Research and Publication Ethics*

The authors of the paper declare that they comply with the scientific, ethical and quotation rules of SAUJS in all processes of the paper and that they do not make any falsification on the data collected. In addition, they declare that Sakarya University Journal of Science and its editorial board have no responsibility for any ethical violations that may be encountered, and that this study has not been evaluated in any academic publication environment other than Sakarya University Journal of Science.

#### REFERENCES

- [1] M. H. Karimi, D. Asemani, "Surface defect detection in tiling Industries using digital image processing methods: Analysis and evaluation", ISA transactions, vol. 53, no. 3, pp. 834-844, 2014.
- [2] T. Czimmermann, G. Ciuti, M. Milazzo, M. Chiurazzi, S. Roccella, C. M. Oddo, P. Dario, "Visual-Based Defect Detection and Classification Approaches for Industrial Applications—A SURVEY", Sensors, vol. 20, no. 5, pp. 1459, 2020.
- [3] G. M. Rahaman, M. Hossain, "Automatic defect detection and classification technique from image: a special case using ceramic tiles", International Journal of Computer Science and Information Security, vol. 1, no. 1, pp. 22-30, 2009.
- [4] S. H. Hanzaei, A. Afshar, F. Barazandeh, "Automatic detection and classification of the ceramic tiles' surface defects", Pattern Recognition, vol. 66, pp. 174-189, 2017.
- [5] A. Mohan, S. Poobal, "Crack detection using image processing: A critical review and analysis", Alexandria Engineering Journal, vol. 57, no. 2, pp. 787-798, 2018.

- [6] A. N. Shire, M. M. Khanapurkar, R. S. Mundewadikar, "Plain ceramic tiles surface defect detection using image processing", in 2011 Fourth International Conference on Emerging Trends in Engineering & Technology, pp. 215-220, November 2011.
- [7] H. F. Ng, "Automatic thresholding for defect detection", *Pattern recognition letters*, vol. 27, no. 14, pp. 1644-1649, 2006.
- [8] Z. Hocenski, T. Keser, A. Baumgartner, "A simple and efficient method for ceramic tile surface defects detection", in 2007 IEEE International Symposium on Industrial Electronics, pp. 1606-1611, June 2007.
- [9] A. Sioma, "Automated Control of Surface Defects on Ceramic Tiles Using 3D Image Analysis", *Materials*, vol. 13, no.5, pp. 1250, 2020.
- [10] A. Latif-Amet, A. Ertüzün, A. Erçil, "An efficient method for texture defect detection: sub-band domain co-occurrence matrices", *Image and Vision computing*, vol. 18, no. 6-7, pp. 543-553, 2000.
- [11] S. Vasilic, Z. Hocenski, "The edge detecting methods in ceramic tiles defects detection", in 2006 IEEE International Symposium on Industrial Electronics, pp. 469-472, July 2006.
- [12] Z. Hocenski, T. Keser, "Failure detection and isolation in ceramic tile edges based on contour descriptor analysis", in 2007 Mediterranean Conference on Control & Automation, pp. 1-6, June 2007.
- [13] Y. C. Samarawickrama, C. D. Wickramasinghe, "Matlab based automated surface defect detection system for ceramic tiles using image processing", in 2017 6th National Conference on Technology and Management (NCTM), pp. 34-39, January 2017.
- [14] Matlab, *Image Processing Toolbox*.
- [15] I. Sobel, "Camera models and perception", Ph.D. thesis, Stanford University, CA, 1970.
- [16] J. Prewitt, "Object Enhancement and Extraction. Picture Processing and Psychopictorics", NY, Academic Pres., 1970.
- [17] J. Canny, "A Computational approach to edge detection", *IEEE Transactions on Pattern Analysis and Machine Intelligence*, vol. 8, pp. 679-700, 1986.
- [18] R. C. Gonzalez, R. E. Woods, S. L. Eddins, "Digital Image Processing Using MATLAB", Saddle River, NJ, Pearson Prentice Hall., 2004.
- [19] S. Chowdhury, D. Dhara, S. Chowdhury, P. Haldar, K. Chatterjee, T. K. Bhattacharya, "A novel approach toward microstructure evaluation of sintered ceramic materials through image processing techniques", *International Journal of Applied Ceramic Technology*, vol. 18, no. 3, pp. 773-780, 2021.



SAKARYA ÜNİVERSİTESİ

# FEN BİLİMLERİ ENSTİTÜSÜ DERGİSİ

Sakarya University Journal of Science  
SAUJS

ISSN 1301-4048 e-ISSN 2147-835X Period Bimonthly Founded 1997 Publisher Sakarya University  
<http://www.saujs.sakarya.edu.tr/>

Title: 2,4,6-Tris(p-aminoanilino)-1,3,5-triazine: Synthesis and Electron Paramagnetic Resonance (EPR) Analysis

Authors: Özgül KARATAŞ, Yusuf CEYLAN, Ziya Erdem KOÇ

Received: 2022-06-24 00:00:00

Accepted: 2022-10-10 00:00:00

Article Type: Research Article

Volume: 26

Issue: 6

Month: December

Year: 2022

Pages: 1170-1179

How to cite

Özgül KARATAŞ, Yusuf CEYLAN, Ziya Erdem KOÇ ; (2022),  
2,4,6-Tris(p-aminoanilino)-1,3,5-triazine: Synthesis and Electron Paramagnetic  
Resonance (EPR) Analysis. Sakarya University Journal of Science, 26(6),  
1170-1179, DOI: 10.16984/saufenbilder.1135112

Access link

<https://dergipark.org.tr/en/pub/saufenbilder/issue/74051/1135112>

New submission to SAUJS

<http://dergipark.gov.tr/journal/1115/submission/start>



## 2,4,6-Tris(p-aminoanilino)-1,3,5-triazine: Synthesis and Electron Paramagnetic Resonance (EPR) Analysis

Özgül KARATAŞ<sup>\*1</sup> , Yusuf CEYLAN<sup>2</sup> , Ziya Erdem KOÇ<sup>2</sup> 

### Abstract

A significant group of compounds arise from substituted s-triazine derivatives that have tripodal heterocyclic compound. Compounds classified as heterocyclic possible created the largest and most diverse family of organic compounds. In this study, we reported that a new template has been syntheses from a cyanuric chloride and its diamine derivative. The desired triamine a tripodal 2, 4, 6-tris (p-aminoanilino)-1, 3, 5-triazine (C<sub>21</sub>H<sub>21</sub>N<sub>9</sub>), called to be TRIPOD, has been obtained from cyanuric chloride with 3 eq of p-phenylenediamine reaction in acetone. After synthesis, TRIPOD sample which was polycrystal form was irradiated by cobalt-gamma source. The electron paramagnetic resonance spectra of TRIPOD were recorded using X-band EPR spectrometer at room temperature in three axes (x, y, z) which are perpendicular at 10° intervals. The EPR spectrum was simulated using computer program and by using the spectrum. The radical structure was determined in the sample.

**Keywords:** EPR, S-triazine, radical, synthesis, irradiation effects

### 1. INTRODUCTION

It is known that 1,3,5-Triazine (or s-triazines) derivatives attract mainly great attention because of their applications in different fields. These compounds have commonly used such as explosives, pesticides, dyestuffs, polymer photostabiliser, optical bleaches and surface-active agents [1-11]. Looking at the past studies, it is seen that this compounds group has been studied quite a lot [12-19]. The 1,3,5-triazine ring has been shown to be an appropriate structural element to be assembled into thermotropic liquid crystals.

The s-triazine derivatives can be simply prepared with cyanuric chloride (C<sub>3</sub>N<sub>3</sub>Cl<sub>3</sub>), 2,4,6-(trichloro)-1,3,5-triazine (1) which is inexpensive and easily existing. [20-21]. Cyanuric chloride is a fantastic starting compound for preparation of a very well multitopic molecule. Any nucleophile reactant can substitute every 2,4,6-trichloro-1,3,5-triazine chloride atom (Figure 1.) [22]. When looking on the tripodal-s-triazine derivatives preparation, the first substitution step was exothermic, so, the mixture of reaction temperature was kept at 0°C. Then, at room temperature the second one step is

<sup>1</sup> \* Corresponding author: ozgulkaratass@gmail.com

<sup>1</sup> Konya Technical University

ORCID: <https://orcid.org/0000-0003-3848-5800>

<sup>2</sup> Selçuk University

E-mail: yceylan@selcuk.edu.tr, okaratas@ktun.edu.tr

ORCID: <https://orcid.org/0000-0003-0588-1188>, <https://orcid.org/0000-0002-5875-9779>



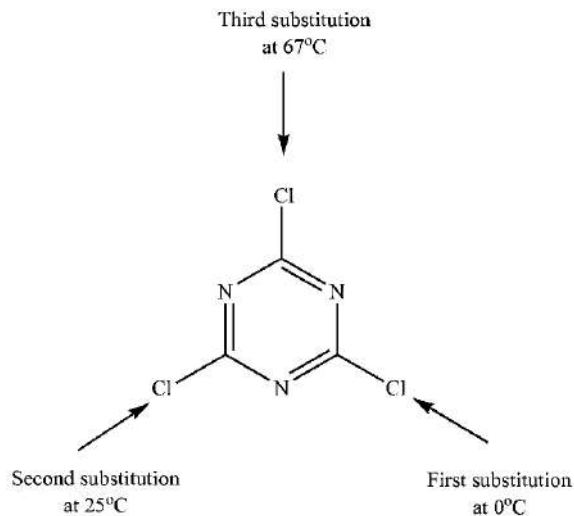


Figure 1 Tripodal-s-triazine derivatives preparation process

chloride and the third step was operationalized under with refluxing solvent. Consequently, the synthesis of 2,4,6-trisubstituted-triazines was obtained with the temperature control during the substitution reactions and sequential addition of grignard reagents, amines, thiols, or alcohols. The performance of every substitution step generally exceeded 95%. Also, the symmetric trisubstituted derivatives could even be obtained in a one pot synthesis [23].

Irradiation has an important role to change of chemical and physical characteristics of materials. It is in preference for chemistry fields for different usage purposes such as sterilization or pathogen killing etc. [24-29]. The electron paramagnetic resonance (EPR) is the most effective method for determination of free radicals formed in various crystalline materials by gamma irradiated [30-34]. Furthermore, this method is widely used for providing information about the paramagnetic defect centers and detail description for structures [35-40].

To understand chemical reaction, it is necessary to investigate the electronic

structure of molecules. In this study, we aimed to synthesize of 2,4,6-tris(*p*-aminoanilino)-1,3,5-triazine ( $C_{21}H_{21}N_9$ ), TRIPOD, understanding its chemical reaction after gamma irradiation by using EPR method.

## 2. MATERIALS AND METHODS

The chemicals were used in the study. The 2,4,6-trichloro-1,3,5-triazine was used like a connection agent and provided commercially from Aldrich. The pure cyanuric chloride by recrystallizations was used for providing the pure petroleum ether (60–90°C) [41].

Measurements as follow: Carlo Erba 1106 elemental analyzer was used for elemental analyses; Perkin Elmer 1600 model FT-IR spectrophotometer was used for recording the IR spectra; Varian MAT 711 spectrometer was used for examination of metal contents; Bruker 200 MHz spectrometer was used for obtained the  $^1H$ -NMR spectra in  $\delta 6$ -DMSO; MMM-Medcenter and Einrichtungen GmbH Vacucell 22 were used as Vacuum Cabinets; Buchi SMP-20 melting point apparatus was used for measuring the melting points; Arex Velp Sci. as Heating Magnetic stirrer equipped with a contact Vetex thermostat connection was used for direct control of the temperature of the stirred liquid; Jeol JES-FA 300 X-Band ESR spectrometer was used for EPR measurements.

### 2.1 The 2,4,6-tris(*p*-aminoanilino)-1,3,5-triazine Synthesis

Firstly, acetone (75 mL) was used for dissolving the cyanuric chloride (1) (1.84 g, 10 mmol). Then,  $NaHCO_3$  (6.30 g, 75 mmol) in water (100 mL) which was saturated with  $N_2$  was added and three necked round bottomed flask was cooled to 0°C. *p*-Phenylenediamine (3.24 g, 30 mmol) was



added gradually. When the addition was complete, the suspension mix was warmed to room temperature and then heated under reflux for 48 h. The residual was suspended in water (100 mL) and the acetone was removed by vacuum. The water phase was extracted three times with dichloromethane and the precipitate was removed by filtration. Powder solid product was washed with cold water (3x100 mL) to remove the sodium bicarbonate and collected by filtration. The CHN analyse results of the compound were similar the molecular formula  $C_{21}H_{21}N_9$ . (Elemental analysis was obtained as: C, 63.94; H, 5.34; N, 31.68 %). Calc.: C, 63.14; H, 5.30; N, 31.56. FT-IR ( $cm^{-1}$ ) 3335–3290 (NH), 2835 (CH), 1589–1484 (triazine C=N).  $^1H$  NMR ( $\delta_6$ -DMSO) 6.73 ( $\delta$ , 6H), 7.32 ( $\delta$ , 6H).

## 2.2 The EPR Measurement

Polycrystalline form of sample was obtained as the TRIPOD was synthesized. This polycrystalline sample was irradiated for 72h at room temperature. For irradiation, cobalt-gamma irradiator which has 0.985 kGy/h dose speed was used. After that, all EPR spectra of this sample were recorded in the magnetic fields for three perpendicular planes at room temperature. The spectrometer conditions were set as following: microwave power of 5mW, modulation amplitude of 0.4mT, center field of 325mT, modulation frequency of 100kHz.

## 3. RESULTS AND DISCUSSION

The results showed that, a new synthetic route was enhanced for versatile ligands prepared using 2,4,6-trichloro-1,3,5-triazine as core. The reaction contained the selective substitutions of p-phenylenediamine onto three chlorides of the triazine ring via a stepwise manner at 1:1, 1:2, or 1:3 eq. and 0,

25, 130°C, respectively. An effective synthesis of a new class of versatile molecules was enhanced with high efficiency chloride substitution steps of 2,4,6-trichloro-1,3,5-triazine by amines. The versatile molecules which were mono-new 1,3,5-triazine derived were synthesized and characterized by means of elemental analysis,  $^1H$  NMR, FT-IR spectroscopy (Figure.2 and Figure.3).

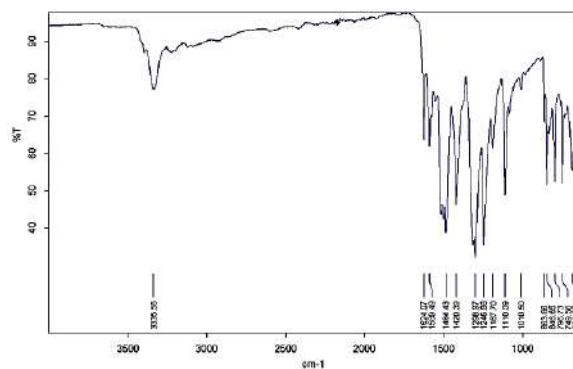


Figure 2 FT-IR spectrum of 2,4,6-tris(p-aminoanilino)-1,3,5-triazine

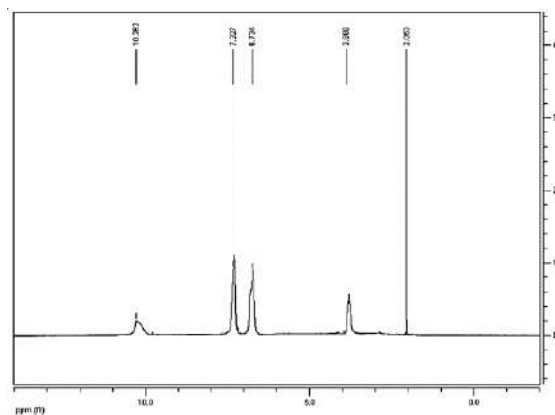


Figure 3  $^1H$  NMR spectrum of 2,4,6-tris(p-aminoanilino)-1,3,5-triazine

These analyzes showed that replacement of the chloro by the amine group induced lowering of the energy of the  $NH_2$  stretch in the FT-IR spectrum and a shift to higher field of the  $NH$  proton signal in the  $^1H$ -NMR spectrum.

The particularity of amine substitution over three chlorides of cyanuric chloride and the optimization of reaction temperatures were studied using *p*-phenylenediamine as the initial amine. The *p*-phenylenediamine has only a single -NH<sub>2</sub> functional group for substitution on the triazine ring. During the reaction, the different reaction temperatures and molar ratios of triazine to amine at 1:3 eq. were used for confirmation the particularity mode for the substitutions of three chlorides (Figure 4.).

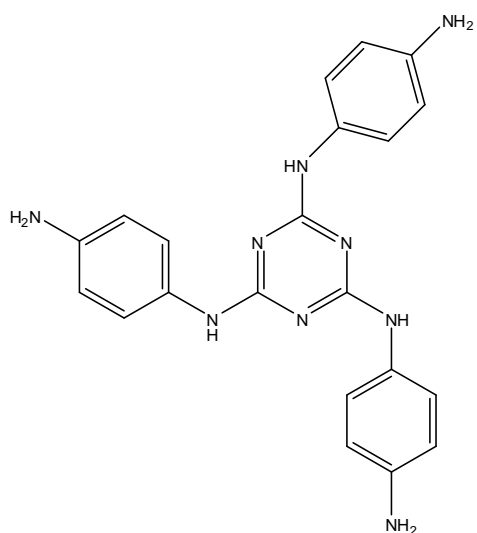


Figure 4 Reactions of cyanuric chloride with *p*-phenylenediamine

The <sup>1</sup>H-NMR spectra were obtained in DMSO- $\delta_6$ . <sup>1</sup>H-NMR spectra were also correlated with the synthesized compounds structures. <sup>1</sup>H-NMR, FT-IR, of the product *p*-phenylenediamine and cyanuric chloride established that each a NH group of *p*-phenylenediamine had reacted with triazine ring. This was confirmed by Fujiwara test [23,41]. This *s*-triazine compound was easily converted to the amine derivative and the yield of the conversion reaction was very high 82%. In the <sup>1</sup>H NMR spectra of compounds 2,4,6-tris(*p*-aminoanilino)-1,3,5-triazine, the signals were detected at about 10.28 and 3.88 ppm, respectively. All

signals appeared as broad singlets and were attributed to the N–H in the tripodal-*s*-triazine. The chemical shifts of the aromatic protons are in a range of 6.73 and 7.32 ppm respectively [42-46]. The presence of N–H was also identified by FT-IR spectroscopy as a sharp band at about 3325–3290 cm<sup>-1</sup>. Also, the vibrations of the triazine C=N of compounds *s*-triazine ring were observed at 1589–1484 cm<sup>-1</sup> range, respectively [47].

According to the EPR measurements, there were not detected any EPR signal on non-irradiated TRIPOD polycrystalline sample. But, after the sample was irradiated using gamma irradiator with about 70 kGy dose, by using EPR spectrometre the obtained spectra results showed that free radical occurred over the sample (Figure 3.).

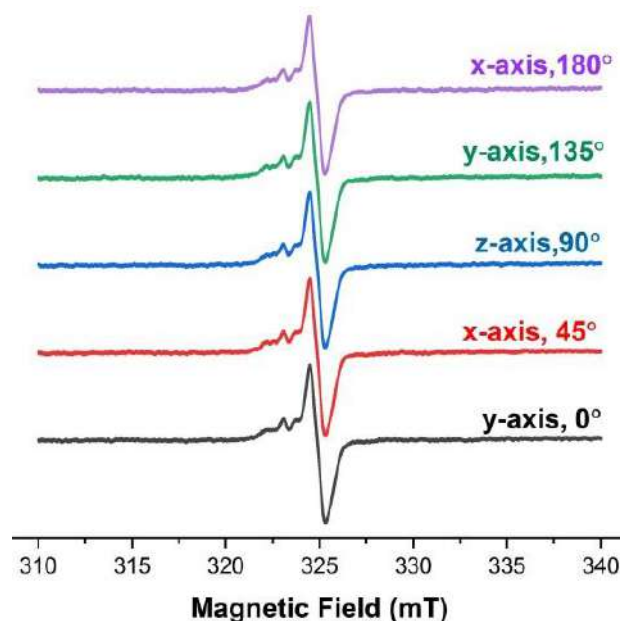


Figure 5 The EPR spectra of gamma-irradiated TRIPOD at different angles towards the x, y, z axes in magnetic field at room temperature

Figure 5 showed that one strong peak and one weak peak were obtained from the EPR measurements. Also, the shapes, intensities and distances between lines were not changed in the spectra along the three (x, y,

z) axes which are perpendicular to each other. So, the results mean that those isotropic behaviors were seen. Also, it was found that obtained spectra were not dependent on the magnetic field.

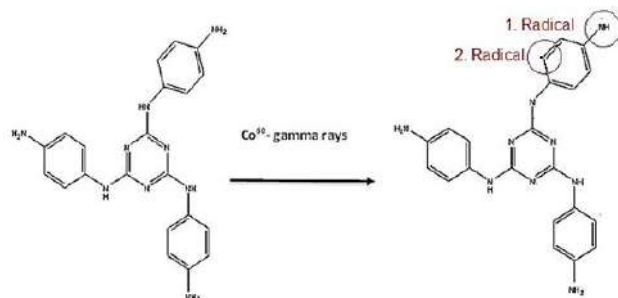


Figure 6 Radicalic molecular structures

When the recorded spectra were examined, it was defined unpaired electrons, which were produced by breaking of bonding of nitrogen and hydrogen atoms (NH<sub>2</sub>, NH). As a result of deep analyzed, it was determined that there were two radicals formed under the gamma-rays (its representation is marked as 1. radical and 2. radical in Figure.6). Taking account to recorded EPR spectra and molecular structure, the first radical was defined as NH, so the spectrum was split into 1:1 intensity ratio, firstly and then split into 1:1:1 intensity ratio, due to hydrogen and nitrogen atoms in the molecular structure, respectively. The second radical was localized on the carbon atom and interacted with hydrogen atom. But, it was found that, its hyperfine constant was small. So, it was observed that second radical has small effects on the spectrum. The hyperfine constants and spectroscopic splitting factors (g-values) were calculated for each radical as follow:  $a_H=1.475$  mT,  $a_N=0.985$ mT and  $g=1.9995$  for labeled 1. radical;  $a_H= 0.38$ mT and  $g=1.9957$  for labeled 2. radical. Also, these arguments were supported by a simulation, as shown in Figure 7.

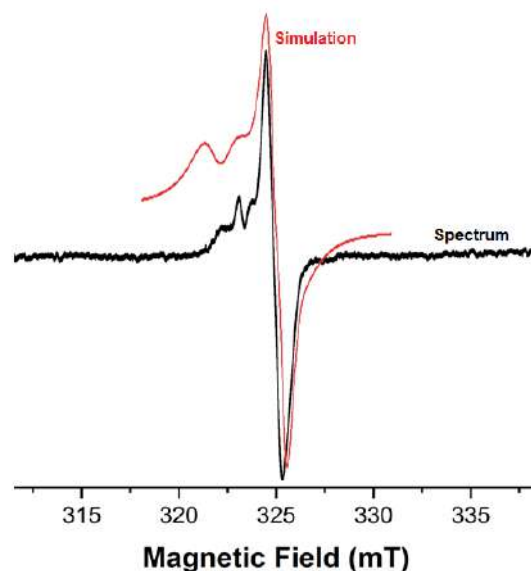


Figure 7 The EPR spectrum of gamma irradiated TRIPOD and its simulation

#### 4. CONCLUSION

In present work, multidirectional cyanuric chloride based was synthesized. The versatile molecule including 1, 3, 5-triazine derivative was prepared by the reaction of cyanuric chloride with p-phenylenediamine. The one step was consisted of preparing 2,4,6-tris(p-aminoanilino)-1,3,5-triazine by substitution of only chloride atoms of cyanuric chloride. It was characterized by the elemental analysis, <sup>1</sup>H - NMR, FT-IR measurements where exchange of the chloro by the amine group was seen. According to the EPR measurement, unirradiated polycrystalline sample did not give any signal. After irradiation, the stable free radical structure was determined. Hyperfine couplings and spectroscopic splitting factor of radical structure were formed under the gamma-rays and these values were calculated and verified by computer simulation.

### **Acknowledgments**

The authors would like to acknowledge the reviewers and editors of Sakarya University Journal of Science.

### **Funding**

This study was partially supported by the Scientific Research Projects coordination center of Selçuk University, Konya, Turkey (Project No: 20401116).

### **Authors' Contribution**

The authors contributed equally to the study.

### **The Declaration of Conflict of Interest/ Common Interest**

No conflict of interest or common interest has been declared by the authors.

### **The Declaration of Ethics Committee Approval**

This study does not require ethics committee permission or any special permission.

### **The Declaration of Research and Publication Ethics**

The authors of the paper declare that they comply with the scientific, ethical and quotation rules of SAUJS in all processes of the paper and that they do not make any falsification on the data collected. In addition, they declare that Sakarya University Journal of Science and its editorial board have no responsibility for any ethical violations that may be encountered, and that this study has not been evaluated in any academic publication environment other than Sakarya University Journal of Science.

## **REFERENCES**

[1] S. Singh, M. K. Mandal, A. Masih, A. Saha, S. K. Ghosh, H. R. Bhat, U. P. Singh, "1,3,5-Triazine: A versatile pharmacophore with diverse biological

activities", *Archiv der Pharmazie*, vol. 354, no. 6, pp. 1-23, 2021.

[2] D. Maliszewski, A. Wrobel, B. Kolensinska, J. Fraczyk, D. Drozdowska, "1,3,5-Triazine Nitrogen Mustards with Different Peptide Group as Innovative Candidates for AChE and BACE1 Inhibitors", *Molecules*, vol. 26, pp. 3942, 2021.

[3] F. Li, C. Wang, Y. Xu, Z. Zhao, J. Su, C. Luo, Y. Ning, Z. Li, C. Li, L. Wang, "Efficient synthesis of unsymmetrical trisubstituted 1,3,5-triazines catalyzed by hemoglobin", *Molecular Catalysis*, vol. 505, pp. 111519, 2021.

[4] K. Kaminska, J. Ziemb, J. Ner, J. S. Schwed, D. Łazewska, M. Wiecek, T. Karcz, A. Olejarz, G. Latacz, K. Kuder, T. Kottke, M. Zygmunt, J. Sapa, J. K. Wojciechowska, H. Stark, K. K.-Kononowicz, K., "(2-Arylethenyl)-1,3,5-triazin-2-amines as novel histamine H4 receptor ligands", *European Journal of Medicinal Chemistry*, vol. 103, pp. 238–251, 2015.

[5] W. Huang, W. Zheng, D. J. Urban, J. Inglese, E. Sidransky, C. P. Austin, C. J., Thomas, "N4-phenyl modifications of N2-(2-hydroxyl) ethyl-6-(pyrrolidin-1-yl)-1,3,5-triazine-2,4-diamines enhance glucocerebrosidase inhibition by small molecules with potential as chemical chaperones for Gaucher disease", *Bioorganic & Medicinal Chemistry Letters*, vol. 17, pp. 5783–5789, 2007.

[6] K. Iikubo, Y. Kondoh, I. Shimada, T. Matsuya, K. Mori, Y. Ueno, M. Okada, "2. Discovery of N-{2-Methoxy-4-[4-(4-methylpiperazin-1-

- yl) piperidin-1-yl] phenyl}-N'-[2-(propane-2-sulfonyl) phenyl]-1,3,5-triazine-2,4-diamine (ASP3026), a Potent and Selective Anaplastic Lymphoma Kinase (ALK) Inhibitor”, *Chemical and Pharmaceutical Bulletin*, vol. 66, pp. 251–262, 2018.
- [7] K. Kaitoh, A. Nakatsu, S. Mori, H. Kagechika, Y. Hashimoto, S. Fujii, “Design, Synthesis and Biological Evaluation of Novel Nonsteroidal Progesterone Receptor Antagonists Based on Phenylamino-1,3,5-triazine Scaffold”, *Chemical and Pharmaceutical Bulletin*, vol. 67, pp. 566–575, 2019.
- [8] N. Lolak, S. Akocak, S. Bua, R. K. K. Sanku, C. T. Supuran, “Discovery of New Ureido Benzenesulfonamides Incorporating 1,3,5-Triazine Moieties as Carbonic Anhydrase I, II, IX and XII Inhibitors”, *Bioorganic & Medicinal Chemistry*, vol. 27, no. 8, pp. 1588–1594, 2019.
- [9] Z. Tber, M. Wartenberg, J. E. Jacques, V. Roy, F. Lecaille, D. Warszycki, A. J. Bojarski, G. Lalmanach, L. A. Agrofoglio, “Selective inhibition of human cathepsin S by 2,4,6-trisubstituted 1,3,5-triazine analogs”, *Bioorganic & Medicinal Chemistry*, vol. 26, pp. 4310–4319, 2018.
- [10] P. Singh, S. Kaur, P. Kumari, B. Kaur, M. Kaur, G. Singh, R. Bhatti, M. Bhatti, “Ailoring the Substitution Pattern on 1,3,5-Triazine for Targeting Cyclooxygenase-2: Discovery and Structure–Activity Relationship of Triazine–4-Aminophenylmorpholin-3-one Hybrids that Reverse Algesia and Inflammation in Swiss Albino Mice”, *Journal of Medicinal Chemistry*, vol. 61, pp. 7929–7941, 2018.
- [11] A. V. Shastin, A. O. Petrov, G. V. Malkov, T. N. Gavrishova, “Synthesis of azidopropargylamino-substituted 1,3,5-triazines- novel monomers for the production of energetic polymers”, *Chemistry of Heterocyclic Compounds*, vol. 57, no. 7/8, pp. 866–870, 2021.
- [12] E. M. Smolin, “s-Triazine and Derivatives”, *Rapoport L.*, Interscience Publishers, New York, 1959.
- [13] Bartholomew, D., Pergamon, Oxford, 1996.
- [14] D. L. Comins, O. Connor, “Advances in Heterocyclic Chemistry”, A. R. Katritzky (Ed.), Academic, New York, 1988.
- [15] G. Giacomelli, A. Porcheddu, L. D. Luca, “[1,3,5]-Triazine: A Versatile Heterocycle in Current Applications of Organic Chemistry”, *Current Organic Chemistry*, vol. 8, pp. 1497–1519, 2004.
- [16] R. R. Gupta, M. Kumar, V. Gupta, vol. 2, SpringerVerlag, Berlin, Heidelberg, New York, 1998.
- [17] R. R. Gupta, M. Kumar, V. Gupta, Springer-Verlag, Berlin, Heidelberg, New York, 1999.
- [18] G. Blonty, *Tetrahedron*, “Recent applications of 2,4,6-trichloro-1,3,5-triazine and its derivatives in organic synthesis”, vol. 62, no. 41, pp. 9507–9522, 2006.
- [19] E. Hollink, E. E. Simanek, D. E. Bergbreiter, “Strategies for protecting and manipulating triazine derivatives”,

- Tetrahedron Letters, vol. 46, pp. 2005-2008, 2005.
- [20] T. Carofiglio, A. Varotto, U. Tonellato, "One-Pot synthesis of cyanuric acid-bridged porphyrin-porphyrin dyads", *The Journal of Organic Chemistry*, vol. 69, no. 23, pp. 8121-8124, 2004.
- [21] T. J. Mooibroek, P. Gamez, "The s-triazine ring, a remarkable unit to generate supramolecular interactions", *Inorganica Chimica Acta*, vol. 360, no.1, 381-404, 2007.
- [22] D. P. Hoog, P. Gamez, W. L. Dressen, J. Reedijk, "New polydentate and polynucleating N-donor ligands from amines and 2,4,6-trichloro-1,3,5-triazine", *Tetrahedron Letters*, vol. 43, pp. 6783-6786, 2002.
- [23] Z. E. Koc, "Complexes of iron (III) and chromium (III) salen and salophen Schiff bases with bridging 1, 3, 5 triazine derived multidirectional ligands", *Journal of Heterocyclic Chemistry*, vol. 48, no. 4, pp. 769-775, 2011.
- [24] A. Usta, H. C. Vural, B. Asik, K. Usta, "Screening of free radical formation in crystals of guanosine by ESR study", *Journal of Molecular Structure*, vol. 1004, no. 1-3, pp. 292-295, 2011.
- [25] D. Chatterjee, A. Mahata, "Evidence of superoxide radical formation in the photodegradation of pesticide on the dye modified TiO<sub>2</sub> surface using visible light", *Journal of Photochemistry and Photobiology A*, vol. 165, pp. 19-23, 2004.
- [26] A. Usta, H. C. Vural, K. Usta, E. Aras, Y. Ceylan, A. Ozmen, "An EPR study on cytosine irradiated", *Journal of Physical Organic Chemistry*, vol. 24, pp. 635-639, 2011.
- [27] N. D. Yordanov, K. Aleksieva, "EPR studies on gamma-irradiated snails hard tissues", *Radiation Physics and Chemistry*, vol. 78, pp. 213-216, 2019.
- [28] G. Onay, R. Sahin, "Optical properties of the electron and gamma-ray irradiated soda-lime glass samples", *Sakarya University Journal of Science*, 22(6), 1518-1523, 2018.
- [29] A. Kahraman, E. Yilmaz, "Evaluation of the pre-irradiation electrical characteristics of the RadFET dosimeters with diverse gate oxides by TCAD simulation program", *Sakarya University Journal of Science*, 21(6), 1258-1265, 2017.
- [30] K. Usta, O. O. Karakus., A. Usta, H. Deligoz, "Identification of radiation-induced radical structure in azocalix [4] arene: an EPR study", *Magnetic Resonance in Chemistry*, vol. 51, pp. 671-675, 2013.
- [31] Y. Ceylan, K. Usta, A. Kunduracioglu, A. Usta, B. Cetinkaya, "Identification of radical structures on 1-pentamethylbenzyl-3-ethylimidazoliumsilver(I)bromide and 1,3-bis(pentamethylbenzyl)-4,5-dimethylbenzimidazoliumsilver(I)bromide exposed to gamma rays: an EPR study", *Magnetic Resonance in Chemistry*, vol. 54, pp. 864-869, 2016.
- [32] K. Usta, Y. Ceylan, A. Usta, N. Ceylan, E. Aras, "An EPR Study on Radiation-Induced 2-(piperidin-1-ylmethyl) phenol Single Crystal", *Acta Physica Polonica A*, vol. 130, no. 1, pp. 178-180, 2016.

- [33] Y. Ceylan, K. Usta, N. Ceylan, A. Usta, Y. Koc, "Comparative Study of Influences of Gamma Rays on Calix [4] Arene and 25,27-di(4-Nitrobenzyl)-26,28-Dihydroxycalix [4] Arene: EPR Study", *Acta Physica Polonica A*, vol. 132, pp. 1211-1213, 2017.
- [34] Ö. Aybirdi, H. Necefoğlu, "Metal (II) p-dimetilaminobenzoatların izonikotinamid komplekslerinin sentezi, spektroskopik ve termal karakterizasyonu", *Sakarya University Journal of Science*, 20(2), 167-175, 2016.
- [35] O. Karatas, E. Aras, "Electron paramagnetic resonance of gamma-irradiated single crystals of ethan-1,2 disulfonic acid disodium", *Journal of Molecular Structure*, vol. 1027, pp. 49-52, 2012.
- [36] O. Karatas, E. Aras, A. H. Karadag, Y. Islek, "Electron paramagnetic resonance study of gamma ( $\gamma$ )-irradiated methyl 4-methyl benzoate (C<sub>9</sub>H<sub>10</sub>O<sub>2</sub>)", *Radiation Effects&Defects in Solids*, vol. 171, no. 7-8, pp. 651-657, 2016.
- [37] E. Aras, O. Karatas, Y. Meric, H. K. Abbass, M. Birey, A. Kılıc, "EPR study of  $\gamma$ -irradiated cholesteryl methyl carbonate", *Radiation Effects&Defects in Solids*, vol. 169, no. 9, pp. 754-758, 2014.
- [38] O. Karatas, Y. Ceylan, "X-band EPR studies of gamma irradiated a new isoquinoline sulfonamide: C<sub>17</sub>H<sub>20</sub>BrNO<sub>3</sub>S", *Konya Journal of Engineering Sciences*, vol. 8, pp. 46-52, 2020.
- [39] Y. Ceylan, K. Usta, A. Usta, E. Maltas, S. Yildiz, "Evaluation of Antioxidant Activity, Phytochemicals and ESR Analysis of Lavandula Stoechas", *Acta Physica Polonica A*, vol. 128, pp. B-483-B-488, 2015.
- [40] Y. Ceylan, A. Usta, K. Usta, F. Cobankara Kont, C. Yildirim, M. Birey, "In vitro analysis of AHPlus and MM-Seal by ESR and thermoanalytical methods", *Acta Physica Polonica A*, vol. 128, pp. B-479 -B-482, 2015.
- [41] Q. Fang, X. Ding, X. Wu, L. Jiang, "Synthesis and characterization of a novel functional monomer containing two allylphenoxy groups and one S-triazine ring and the properties of its copolymer with 4,4'-bismaleimidodiphenylmethane (BMDPM)", *Polymer*, vol. 42, pp. 7595-7602, 2001.
- [42] R. Ragno, S. Simeoni, S. Castellano, C. Vicidomini, A. Mai, A. Caroli, A. Tramontano, C. Bonaccini, P. Trojer, I. Bauer, G. Brosch, G. Sbardella, "Small molecule inhibitors of histone arginine methyltransferases: Homology modeling, molecular docking, binding mode analysis, and biological evaluations", *Journal of Medicinal Chemistry*, vol. 50, pp. 1241-1253, 2007.
- [43] S. F. Teng, K. Sproule, A. Husain, C. R. Lowe, "Affinity chromatography on immobilized biomimetic ligands synthesis, immobilization and chromatographic assessment of an immunoglobulin G-binding ligand", *Journal of Chromatography B*, vol. 740, pp. 1-15, 2000.

- [44] X. Wang, S. Ma, D. Sun, S. Parkin, H. Zhou, "A Mesoporous Metal–Organic Framework with Permanent Porosity", *Journal of the American Chemical Society*, vol. 128, pp. 16474-16475, 2006.
- [45] K. A. Kolmakov, "An efficient, "green" approach to aryl amination of cyanuric chloride using acetic acid as solvent", *Journal of Heterocyclic Chemistry*, vol. 45, no. 2, pp. 533-539, 2008.
- [46] L. Bruun, C. Koch, M. H. Jakopsen, B. Pedersen, M. Christiansen, Aamand, "Characterization of monoclonal antibodies raised against different structures belonging to the s-triazine group of herbicides", *Journal of Analytica Chimica Acta*, vol. 436, pp. 87-101, 2001.
- [47] Z. E. Koc, S. Uysal, "Synthesis and characterization of dendrimeric bridged salen/saloph complexes and investigation of their magnetic and thermal behaviors", *Helvetica Chimica Acta*, vol. 93, pp. 910-919, 2010.





SAKARYA ÜNİVERSİTESİ

# FEN BİLİMLERİ ENSTİTÜSÜ DERGİSİ

## Sakarya University Journal of Science SAUJS

ISSN 1301-4048 e-ISSN 2147-835X Period Bimonthly Founded 1997 Publisher Sakarya University  
<http://www.saujs.sakarya.edu.tr/>

Title: Structural Strength Properties of Waste Textile Fiber Reinforced Cementitious  
Lightweight Composite Mortars

Authors: Şevket Onur KALKAN, Lütfullah GÜNDÜZ

Received: 2022-04-22 00:00:00

Accepted: 2022-10-11 00:00:00

Article Type: Research Article

Volume: 26

Issue: 6

Month: December

Year: 2022

Pages: 1180-1195

How to cite

Şevket Onur KALKAN, Lütfullah GÜNDÜZ; (2022), Structural Strength Properties of  
Waste Textile Fiber Reinforced Cementitious Lightweight Composite Mortars.

Sakarya University Journal of Science, 26(6), 1180-1195, DOI:

10.16984/saufenbilder.1107127

Access link

<https://dergipark.org.tr/en/pub/saufenbilder/issue/74051/1107127>

New submission to SAUJS

<http://dergipark.gov.tr/journal/1115/submission/start>

## Structural Strength Properties of Waste Textile Fiber Reinforced Cementitious Lightweight Composite Mortars

Şevket Onur KALKAN\*<sup>1</sup>, Lütfullah GÜNDÜZ<sup>1</sup>

### Abstract

This study aims to investigate the utilization of recycled textile waste fiber (RTWF) as fiber reinforcement in cementitious lightweight composite mortars. The effect of RTWF percentage on cementitious lightweight composite mortar (CLCM) consistency, plastic and dry set density, splitting tensile and compressive strength was measured. In particular, the effect of RTWF percentage on the structural mechanical properties of hardened mortar was examined in detail. Mohr-Coulomb Failure Criterion was used to examine the structural strength properties of composite mortars. Failure angle, internal friction angle, normal and shear strength and cohesion of RTWF reinforced composite mortars were investigated. Three different types of fibers were used including cotton-polyester mixture (Type 1), only polyester (Type 2) and cotton-polyester-acrylic mixture (Type 3). Different percentages of fibers, i.e. 1%, 2%, 3%, 5% and 7%, were added to CLCM. Test results showed reduction in dry set densities compared with the control specimen. It has been determined that the use of 1 % fiber improves the mechanical properties of light mortars. On the other hand, decreasing trend was observed in compressive and splitting tensile strength of mortars with higher amount of fiber usage. When structural strength properties were considered, same trend was kept. However, this research work has unique value from an innovative perspective in terms of evaluation of structural strength parameters.

**Keywords:** Waste textile fiber, lightweight, mortar, composite, structural strength, fiber reinforcement

### 1. INTRODUCTION

Construction sector is one of the most widely resource of material user industry. Therefore, more effective raw materials should be used in producing construction materials. Recycling materials and/or reusable materials are effective materials in terms of sustainability. One of these materials is textile waste fiber. Textile production in worldwide scale is more than 88.5 million tons per year.

Large amount of waste from textile industry and discarded textile products after used are disposed worldwide. Textile industry produces around 12 million tons of waste in a year in Europa. Some of the wastes are turned into yarn at the recycling factory. However, fibers in very small sizes are created as waste products in this recycling process. Such textile waste fiber or textile waste cuttings are burned in various plants [1, 2]. Thus, they are damaging to the environment because they are

\* Corresponding author: onur\_kalkan@hotmail.com

<sup>1</sup> İzmir Katip Çelebi University

E-mail: lutfi.1966@hotmail.com

ORCID: <https://orcid.org/0000-0003-0250-8134>, <https://orcid.org/0000-0003-2487-467X>



non-biodegradable, or they are burned. In fact, this large amount of textile waste fiber accumulation creates an opportunity for the use of textile wastes in construction materials. Textile and garment industry is one of the main sectors that receiving driving force in the booming economy of Turkey. According to 2014 data, Turkey is the third country among European countries on textile export. Also, it is the world's sixth largest garment exporter. With such a large production capacity, waste and/or residual materials are composed depends on the production in Turkey's textile sector. It can be seen that some of these materials are used in the internal components of the sector as a recycling material again. However, also the accumulation of waste fiber amount leftover from the recycling process can not be underestimated. The use of waste materials in the construction industry is gaining increasing importance in recent years. These wastes are used in cementitious materials due to their various advantages such as thermal conductivity, sound insulation, structural reinforcement, to lighten composite, etc. One of these waste raw materials is the textile waste fiber. Nowadays, the use of these materials could be investigated more in the cementitious composites, in the economical and sustainable points of views.

The use of fiber in concrete in developed countries began in the early 1960s and the use of fiber-reinforced concrete applications has been increased [3]. It can be seen that in the literature, various types of fibers are used as reinforcement element in cementitious composites. Various studies about fiber reinforcement in cementitious composites according to different advantages of the fibers as follows; steel fibers [4, 5], polypropylene fibers [6, 7], glass fibers [8, 9] and organic fibers, such as sisal [10, 11], coconut and oil palm [12], banana [13], etc. Though textile reinforced cementitious composites are frequently studied in order to strengthening masonry walls and concrete sections [14-18], studies on the usage of waste textile fibers in cementitious composites have not been investigated enough. In the literature, waste

carpet fiber use as reinforcement material is seen more [19-21] than other types of waste textile fibers such as cotton [2, 22], polypropylene [23] and acrylic [24, 25].

Due to the increasing use of waste materials in the construction industry, it is predicted that advanced engineering properties should be examined in depth. For this purpose, the structural mechanical properties of the specimens carried out, i.e., the structural strength, are tested. Internal friction angle, failure angle, normal strength, shear strength and cohesion were predicted as structural strength parameters by the authors. Structural strength analysis of materials provides more comprehensive information about the material. Also, it can be obtained from structural strength parameters better understanding about what happens inside the material before it reaches fracture. For example, normal strength gives the strength value when the first crack occurs while loading the material. Mohr Coulomb Failure Criterion was tried to use to determine the structural strength properties of the specimens. Mohr Coulomb Failure Criterion could be estimated by some mechanical properties of concrete based on the tension and compression. Although a few Mohr Coulomb failure criterion practices related with concrete can be seen in the literature [26, 27], there are no such studies related to cementitious mortars.

Also, the usage of lightweight aggregates shows an increasing trend thanks to reduce dead load and provide insulation in the construction industry. Lightweight aggregates can be divided into two: organic cellular such as expanded polystyrene foam (EPS), extruded polystyrene foam (XPS) and polyurethane foam and inorganic cellular from natural and artificial sources such as expanded perlite, expanded clay, exfoliated vermiculite, etc. [28, 29]. Cementitious lightweight composite mortar normally created by these lightweight aggregates such as pumice, perlite, expanded clay, vermiculite, or air entraining agents [30].

Lightweight aggregates have a wide weight range distribution from 80 to 900 kg/m<sup>3</sup> [31]. According to TS EN 998-1 [32] a lightweight mortar is required to have a dry hardened density of less than 1300kg/m<sup>3</sup>.

In this study, the use of short-dimensional textile recycling waste materials as reinforcement in cementitious mortars was investigated. Effect of short-dimensional recycled textile fibers on CLCM is a developing subject and a few studies available about this topic in the literature. Furthermore, this investigation can be interesting from technical point of view because any study of the structural strength properties of cement mortar cannot be found in the literature.

The study presented in this paper reports a research on the behavior of cement-based lightweight composite mortar produced by mixing EN 197-1 CEM I 52.5R white cement with various ratios of RTWF. Compressive strength values of specimens were obtained from compressive strength tests on cubic specimens and splitting tensile strength values of the specimens were obtained from Brazilian Test on cylindrical specimens.

In this study, a total 16 mortar mixtures were casted, and it was aimed to have the internal strength values of the materials produced by combining these two parameters, compressive strength and splitting tensile strength, through the Mohr circles.

## 2. EXPERIMENTAL WORK

### 2.1. Materials Used in the Study

In this experimental work, White Ordinary Portland cement (PC) conforming to EN 197-1 CEM I 52.5R white was used as binder material. Since the fibers used in the study are textile waste fibers, they have different colors. The reason for using white cement in this study is to see the coloration of the final product due to the colors of the waste textile fibers (Fig.1). The chemical composition of the white Portland cement is shown in Table

1. The X-ray Fluorescence (XRF) analysis was used to determine mineralogical composition of the aggregates, lime, and cement. Also, physical and mechanical properties of white Portland cement are shown in Table 2.

In this study, pumice was evaluated as the main aggregate. Also, due to low unit volume weight of pumice, it was used as lightweight aggregate in this experimental work. Pumice is a geological material, and it has spongy and porous structure. Pumice contains numerous pores, because during the formation, gases in the structure in the pumice rapidly leave the body and then sudden cooling takes place. Thus, the porous structure occurs. Disconnected hollows generally form these pores. Therefore, pumice has low permeability, and it has very high thermal and sound insulation. Because of these characteristics, pumice is widely used as a lightweight aggregate in lightweight concrete designs. Besides, pumice is used in production of lightweight building elements such as bricks, masonry blocks, panels, and boards, etc. [33].

Table 1 Chemical composition of WPC, NPA, HPL and EP

Major element	PC (%)	NPA (%)	HPL (%)	EP (%)
SiO <sub>2</sub>	21.60	74.10	< 1.3	72.20
Al <sub>2</sub> O <sub>3</sub>	4.05	13.45	0.4 – 0.8	11.40
Fe <sub>2</sub> O <sub>3</sub>	0.26	1.40	< 0.3	0.53
CaO	65.70	1.17	80	0.63
MgO	1.30	0.35	< 2	0.33
SO <sub>3</sub>	3.30	-	< 2	1.87
Na <sub>2</sub> O	0.30	3.70	< 0.8	3.3
K <sub>2</sub> O	0.35	4.10	-	4.20

PC : White Portland Cement  
 NPA : Nevşehir Pumice Aggregate  
 HPL : Hydrated Powder Lime  
 EP : Expanded Perlite

Pumice aggregate used in this experimental work was supplied from a pumice mining quarry in Nevşehir-Turkey. Nevşehir pumice aggregate (NPA) was primarily crushed by a crusher and then screened into 0/0.5 mm as fine aggregate and 0.5/3 mm as coarse aggregate for this study.

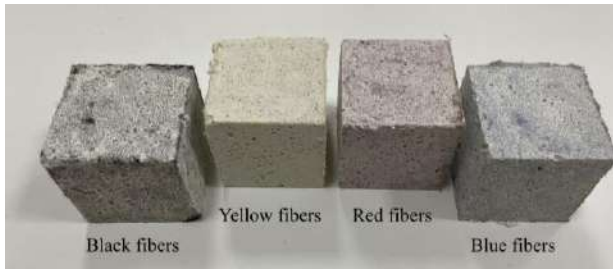


Figure 1 Mortar specimens produced using different colored fibers

Expanded perlite was used in this experimental work as lightweight aggregate. Expanded perlite as a commercial product used in this study was supplied from İzmir Region in a size of 0-2 mm. Any procedure was not applied to the material and was directly used in the CLCM combinations.

Table 2 Physical and mechanical features of PC

Specific gravity (g/cm <sup>3</sup> )	3.06
Blaine specific surface (cm <sup>2</sup> /g)	4600
Initial setting time (min)	100
Final setting time (min)	130
Volume expansion (mm/m)	1
Compressive strength (MPa)	
7 days	37.0
14 days	50.0
28 days	60.0

Perlite is a glassy and volcanic origin rock type. When perlite granules are heated in the temperature range between 900 °C and 1100 °C, its volume increases about 20 times and it becomes a porous structure. Resulting new material after heat-treating is called expanded perlite. This formal transformation or expansion makes expanded perlite a very lightweight material and very efficient thermal insulator. Expanded perlite aggregate is often used for these features when thermal insulation and lightness required cases are needed. In Table 1, the chemical component of the expanded perlite is also given.

Hydrated Powder Lime (HPL) was supplied as a commercial product in the sector. The HPL used in this study belongs to the CL80 category according to EN 459-1 standard. HPL additive was used in the mixture combinations in order to stabilize pH balance. The chemical content of HPL is given in Table 1.

The mixing water was regular tap water. Recycled textile fiber as a new type of reinforcement element is proposed in this study. Recycled textile fibers used in CLCM combinations were collected from denim factories in Uşak Region, textile recycling center of Turkey. In these factories, wastes are produced at three stages such as, production stage, ageing stage, and abrasion stages. Textile wastes produced after these stages are powder sized.

Three types of recycling waste are supplied from Uşak Region (Fig.2). First one is mixture of cotton waste fibers from recycling of cotton products and polyester waste fibers, the waste of plastic bottles during the conversion of PET bottles to textile fiber. Cotton fiber is a vegetable textile fiber. The main component of cotton fiber is cellulose with a ratio of 94%. The remaining of cotton fibers consists of hemicellulose, pectin and inorganic substances. While diluted bases minimal effect on cotton fiber, cotton fiber shows degradation with concentrated and strong acids. Cotton fibers do not exhibit degradation up to 150 °C [34, 35].



Figure 2 Fiber specimens

The second type of recycled textile waste fiber consists of fully polyester fibers. Polyesters

fibers are chemical fibers with synthetic raw materials [35]. Polyester fibers can be obtained by recycling of PET (Polyethylene terephthalate) bottles. PET has usage areas such as soft drink, food and beverage containers, and polyester fibers. Polyester fibers are resistant to weak acids even at the boiling point. They have good resistance to strong acids at room temperature while poor resistance to strong bases. Melting point of polyester fibers is 250 °C [34, 35].

The last type of RTWF is mixture of cotton waste fiber, polyester waste fiber and acrylic waste fiber, the remaining waste from the recycling stage of the acrylic products were made from synthetic fibers. Acrylic fibers are obtained by mixing ratio of 85 % acrylonitrile polymers and more than one monomer with a ratio of 15 %. Acrylic fibers are resistant to other acids except nitric acid. Especially dense and hot state alkali damages the fibers. There is not a certain melting point of the acrylic fibers. Melting point of them ranges from 215 to 255 ° C [35].

Recycled textile waste fiber (RTWF) was used in this research to improve mortar's physical and mechanical properties. Any pretreatment was not applied to the RTWFs used. Physical properties of RTWFs are given in Table 3.

Table 3 Physical properties of fibers

Color	Blue, white, black, pink
Fiber length (µm)	< 200
Fiber diameter (µm)	<20
Specific gravity of cotton (g/cm <sup>3</sup> )	1.50-1.55
Specific gravity of polyester (g/cm <sup>3</sup> )	1.38
Specific gravity of acrylic (g/cm <sup>3</sup> )	1.14-1.20
Water absorption capacity of cotton	25-27 %
Water absorption capacity of polyester	0.2-0.8 %
Water absorption capacity of acrylic	0.30-1.30 %

## 2.2. Mortar Mix Design

Mixture proportioning of the CLCM combinations for this experimental study is shown in Table 4. Sixteen different cementitious mortar combinations were prepared and analyzed in order to observe the

possible effect of utilizing very fine sized textile waste fibers on CLCMs. The amount of cement ratio was kept constant as 33 % by weight for all mixture combinations.

Table 4 Mortar combinations and mix design

	PC (wt.%)	NPA (wt.%)	EP (wt.%)	Fiber (wt.%)	HPL	w/s	w/c
LF-R	33.0	48.0	10.0	0.0	9.0	0.50	1.52
LF1-1	33.0	47.0	10.0	1.0	9.0	0.51	1.55
LF1-2	33.0	46.0	10.0	2.0	9.0	0.60	1.82
LF1-3	33.0	45.0	10.0	3.0	9.0	0.69	2.09
LF1-5	33.0	43.0	10.0	5.0	9.0	0.80	2.42
LF1-7	33.0	41.0	10.0	7.0	9.0	0.97	2.94
LF2-1	33.0	47.0	10.0	1.0	9.0	0.55	1.67
LF2-2	33.0	46.0	10.0	2.0	9.0	0.67	2.03
LF2-3	33.0	45.0	10.0	3.0	9.0	0.75	2.27
LF2-5	33.0	43.0	10.0	5.0	9.0	0.97	2.94
LF2-7	33.0	41.0	10.0	7.0	9.0	1.18	3.58
LF3-1	33.0	47.0	10.0	1.0	9.0	0.56	1.70
LF3-2	33.0	46.0	10.0	2.0	9.0	0.68	2.06
LF3-3	33.0	45.0	10.0	3.0	9.0	0.76	2.30
LF3-5	33.0	43.0	10.0	5.0	9.0	0.93	2.82
LF3-7	33.0	41.0	10.0	7.0	9.0	1.10	3.33

Again, the amount of the expanded perlite and hydrated powder lime ingredients in all mixes was kept constant as 10 and 9 % by weight, respectively. Within the scope of the study, the mixture design was evaluated by weight. In order to keep the total mixture amount constant as 100%, the amount of fiber added to the mixtures by weight was removed from the pumice aggregate in the same proportion.

First mortar mixture, which is named as LF-R, was analyzed as a reference mortar and this mixture does contain RTWF additive. This mix actually was considered to understand the impact of textile waste fiber to the mortar's properties.

In order to examine the physical and mechanical properties of CLCMs reinforced with different types of fibers, three different types of RTWF were studied in this research. First five mixtures (LF1-1, LF1-2, LF1-3, LF1-5, LF1-7) were mixed with combination of cotton and polyester fibers and this group is going to be named as Type 1 RTFW, second five mixtures (LF2-1, LF2-2, LF2-3, LF2-5, LF2-7) were mixed with only polyester fibers and this group is going to be named as Type 2 RTWF and the last five mixtures (LF3-1, LF3-2, LF3-3, LF3-5, LF3-7) were mixed with combination of cotton, polyester and acrylic



fibers and this group is going to be named as Type 3 RTWF, in this work.

In order to determine the water demand for each mixture separately and to provide the same workability for each mixture, flow table test was carried out by the requirements of the ASTM C 1437-13 standard. The water/solid ratios were changed from 0.50 to 1.18. The water-solids ratio investigated in this research can be defined as the ratio of total mass of water to the total mass of solids (cement, lime, aggregates, and fibers). Mixing was carried out by a mortar mixer. Then, the fresh cement mortar specimens were placed into the molds and left for 24 hours. Subsequently, specimens were removed from the molds and placed in wet surface curing condition ( $21 \pm 1$  °C and 95 % RH) for the first 3 days and after that the specimens were left to dry in a normal air condition ( $21 \pm 1$  °C and 40 % RH) to the testing time (7 and 28 days).

In this work, the influence of RTWF was investigated in the usage of simultaneously, 1, 2, 3, 5 and 7 %. The fresh mortar properties such as consistency and fresh density were studied. 7- and 28-days compressive strength of mortars were investigated. Also, splitting tensile strength of hardened mortars were tested on 28 days. Compressive and splitting tensile strength tests were conducted on 50x50x50 mm cubic test specimens and Ø50x100 mm cylindrical test specimens, respectively. Compressive and splitting tensile strength were determined as the average of 3 specimens test results. Structural strength values of the CLCMs have been achieved through splitting tensile and compressive strength tests by using Mohr Circles.

### 3. TEST RESULTS AND DISCUSSION

#### 3.1. Flow and Water Demand

The flow diameters and water demand of mortar mixtures were analyzed on fresh mortar specimens. The water to solid ratio (W/S) of all mixtures is shown in Table 4. The

W/S of the mixtures were changed from 0.50 to 1.18 based on the RTWF amounts. Flow diameters of mixtures were calculated according to ASTM C1437-13 standard with flow table test and were given in Figure 3. In the study, when the water/solid ratio is fixed, there are great problems in the mixing and molding stages of the mortars using high fiber ratios. For this reason, mortars with similar workability were produced by keeping the flow diameters constant in all mixtures. The flow diameters of all mixtures were fixed to be  $142 \pm 5$  mm. For all three types of fiber, the mixing water was increased depending on the fiber ratio in order to provide a similar workability in fresh mortars.



Figure 3 Flow diameter of CLCMs versus RTWF percentage of CLCM specimens

#### 3.2. Fresh and Hardened Densities

With the increase of the W/S ratio, in plastic unit weight changes were not observed too much. However, despite the increase in W/S ratio, gradually decreasing at dry set densities was recorded in all three types of RTWF mixtures (Table 5). This is because the fibers have fluffy structure and thus, bring more unit

volume to the mortar. The fresh density of cement mortar specimens was varied between  $1055 \text{ kg/m}^3$  and  $1184 \text{ kg/m}^3$  based on the percentage of RTWF ratio. Dry set density values were varied between  $611 \text{ kg/m}^3$  and  $959 \text{ kg/m}^3$ . Compared to the control specimen, Type 1, Type 2 and Type 3 mixtures containing 1.0 % fiber were found 1.04 %, 3.75 % and 5.94 % lighter, respectively. The same case was observed at 7 % RTWF containing mixtures. They were found 23.15 %, 36.29 and 32.74 % lighter than unit volume weight of control specimen. It is stated that in TS EN 998-1 standard [32], lightweight mortars should be lighter than  $1300 \text{ kg/m}^3$ . In this research, it was reached much better results than this value.

Table 5 Physical and mechanical properties of mortars

Mix	Flow (mm)	Fresh density ( $\text{kg/m}^3$ )	Hardened density ( $\text{kg/m}^3$ )	28-days compressive strength (MPa)	28-days splitting tensile strength (MPa)
LF-R	154	1159	959	4.89	0.83
LF1-1	142	1143	949	6.88	1.05
LF1-2	130	1164	902	5.64	0.96
LF1-3	120	1184	854	4.38	0.86
LF1-5	112	1393	816	4.06	0.68
LF1-7	110	1254	737	2.58	0.47
LF2-1	146	1124	923	5.77	0.68
LF2-2	138	1120	830	3.30	0.51
LF2-3	136	1142	794	2.53	0.44
LF2-5	131	1121	708	1.38	0.30
LF2-7	126	1055	611	0.82	0.25
LF3-1	141	1147	902	5.48	0.87
LF3-2	130	1138	850	3.77	0.55
LF3-3	128	1135	800	2.88	0.47
LF3-5	120	1123	730	1.98	0.36
LF3-7	112	1138	645	1.27	0.30

### 3.3. Compressive Strength

Compressive strength is the ability to resist the show to break the material under axial load impact. The compressive strength tests were conducted according to EN 1015-11 standard. In the compressive strength tests, cubic specimens were used for each batch. The specimens, after removal from the molds and cured in water for 3 days and then dried at room temperature until the testing time, were taken directly on the compressive strength test without any further action. The 7- and 28-days compressive strength values of all mortar mixtures are presented in Figure 4 and Figure

5 based on percentage of RTWF usage by weight, respectively.

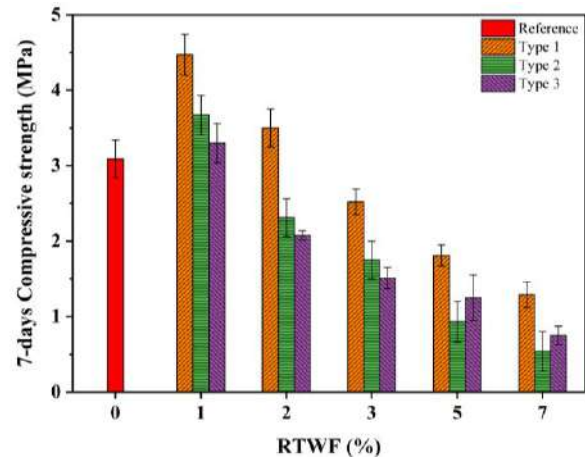


Figure 4 Compressive Strength versus RTWF percentage of CLCM specimens on 7 days curing time

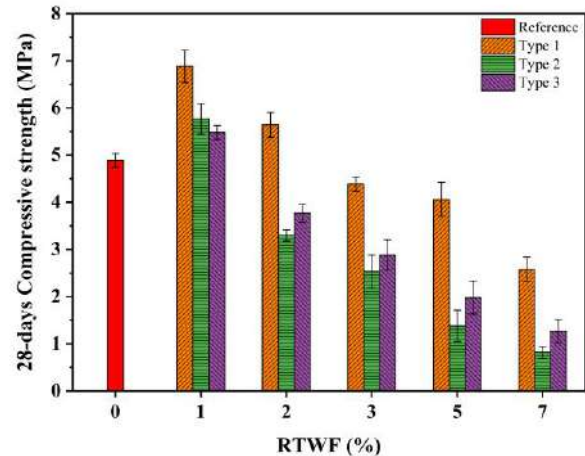


Figure 5 Compressive Strength versus RTWF percentage of CLCM specimens on 28 days curing time

The results showed that compressive strength of mixture combinations was decreased with increase in fiber content in both 7 days and 28 days curing time. One reason for this is that the fibers agglomerate with the increase in the fiber content, and another reason is that with the increase in the fiber content, the amount of mixing water increases and the water/cement ratio decreases. On the other hand, at 1 % fiber usage rate, all three types of fibers improved the compressive strength of lightweight mortars. In addition, Type 1 fibers with a fiber usage rate of 2 % are also effective in improving the compressive strength. With the addition of 1 % fiber to the lightweight



mortars, the compressive strengths of the mortars with the addition of Type 1, Type 2 and Type 3 fibers were improved by 40.70 %, 18.00 % and 12.07 %, respectively, compared to the reference mortar. However, above 1 % usage for Type 2 and Type 3 fibers, and above 2 % of Type 1 fiber, the compressive strength tends to decrease, and the compressive strengths remain below the compressive strength of the reference mortar with the increase in fiber usage ratio. The reason can be regarded as, because fiber usage causes an increase in volume of mortar, unit volume weight of mortar decreases, and this decrease creates lighter unit volume weight. This action causes a return of loss of compressive strength, as mentioned before. The other reason for these reductions is that the use of high fiber content reduces the workability of the mortar. To fix the workability of mortars, extra mixing water added to the fresh mortars, and extra water increased the w/c of the fresh mortar. Increasing w/c caused a decrease in compressive strength. Also, agglomeration occurs as a result of the effect of its distribution and orientation of fibers in the mortar. Studies have shown that the fiber fraction can affect the compressive strength of concrete by 25%, either positively or negatively [36, 37].

Analyzing Figure 5, compressive strength values of specimens with 28 days curing time were found higher than 7 days curing time specimens, as it should be. When examined according to fiber types, it is seen that the specimens mixed with Type 1 RTWF has the highest compressive strength. Comparing 1 % fiber usage specimens for 28 days compressive strengths, Type 1 RTWF content specimens can be described as the best and Type 2 and the last one is Type 3. However, above 1% of fiber usage, it was observed that Type 3 RTWF content mixtures have greater compressive strength values than Type 2 RTWF content mixtures. As previously mentioned, Type 1 contains cotton and synthetic fibers, Type 2 contains only synthetic fibers and Type 3 contains mostly synthetic and a small amount of cotton fibers.

Having studied the compressive strength values, specimens containing cotton fibers appear to be higher compressive strength values. This phenomenon can be explained as; cotton fiber makes better bonds with the mortar.

When viewed under a microscope, face of the synthetic fibers seems to be rounded shape and smooth surface. On the contrary, surface of cotton fibers is rough and they have volute structure (Fig. 6a and 6b). Therefore, it can be said that cotton fibers can hold the mortar better.

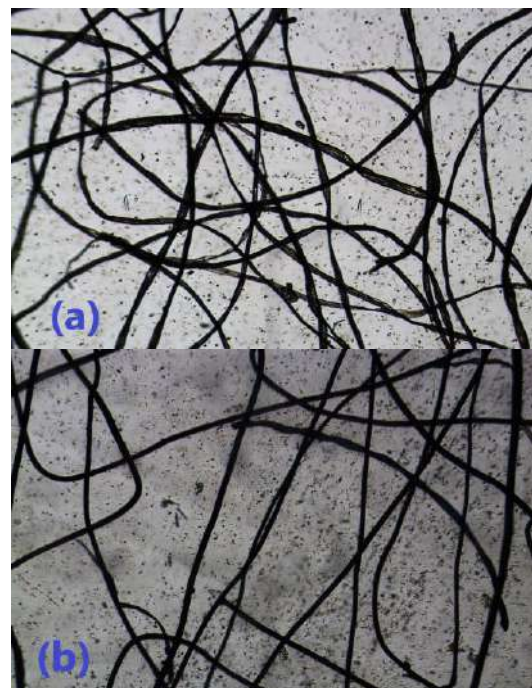


Figure 6 Microscope view of the cotton (a) and synthetic (b) fibers.

28 days compressive strength classification of cement mortars are grouped in 4 different classes in TS EN 998-1 standard. These compressive strength classes are;

- CS I (0.4 – 2.5 N/mm<sup>2</sup>),
- CS II (1.5 – 5.0 N/mm<sup>2</sup>),
- CS III (3.5 – 7.5 N/mm<sup>2</sup>)
- CS IV (≥6 N/mm<sup>2</sup>).

When compressive strength values of CLCM specimens is evaluated according to the prescribed categories in TS EN 998-1 standard, it was observed that the 28 days curing time compressive strength values for 1% and 2% fiber utilization in CLCM ensure

the compressive strength of 3.5 N/mm<sup>2</sup> for CS III class and the strength values drop to CS II class between 3 % and 5 % fiber utilization and 7 % fiber usage in CLCM drops the compressive strength class for CS II to CS I. In fact, even the lowest compressive strength value (0.54 N/mm<sup>2</sup>) at 7 days curing time ensures CS I class foreseen in TS EN 998-1 standard (Fig. 3).

### 3.4. Splitting Tensile Strength

The simplest and most frequently applied method used to determine the tensile strength of concrete is splitting tensile test also known as the Brazilian Test. This test provides a lower coefficient of variation. In splitting tensile test, same materials and equipment are used with compression test. This test is performed by applying a diametric compressive force along the length of a cylindrical specimen between two plates [38-40].

The splitting tensile strength,  $T$ , can be calculated by the following Equation (1):

$$T = \frac{2P}{\pi Ld} \quad (1)$$

Where,  $T$  is splitting tensile strength in N/mm<sup>2</sup>,  $P$  is peak load in N,  $d$  is diameter of specimen in mm and  $L$  is length of specimen in mm.

For the splitting tensile strength testing, cylindrical specimens, with dimensions of Ø50x100 mm, were used for each batch. The specimens, after removal from the molds, they cured at 3 days in a wet surface condition and then dried at room temperature until the testing time. They were taken directly on the test without any further action after 28 days curing time. 28 days splitting tensile strength results of all mortar mixtures are given in Figure 7 based on weight percentage of RTWF usage.

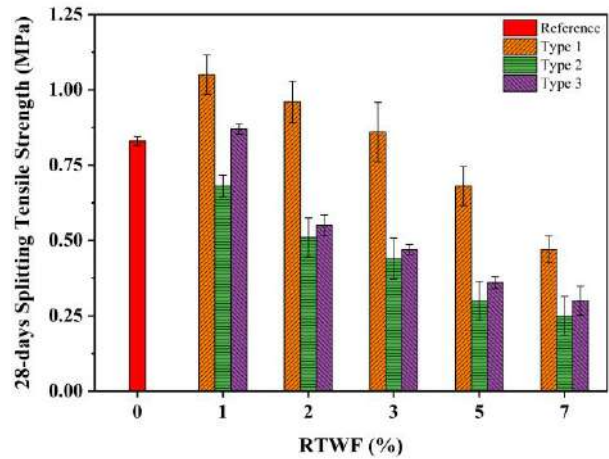


Figure 7 Splitting Tensile Strength versus RTWF percentage of CLCM specimens on 28 days curing time

As analyzing Figure 7, it can be easily seen that the owner of the better values is Type 1 RTWF. Type 2, which has only polyester fiber content in it, comes after Type 1 and Type 3 RTWF, exhibits the worst splitting tensile strength values. The mixture of different fibers provides more improvement effect on the tensile strength of hardened mortars. These fibers are the wastes that occur while producing yarn from textile wastes. Therefore, these fibers are woven fibers. However, only polyester fibers (Type 2) are obtained from pet bottles and are non-woven. Therefore, the strength of composite fibers is higher (Type 1 and Type 3). As a general acceptance, compressive strength and splitting tensile strength are proportional to each other. This phenomenon can be clearly observed from the results of compressive strength and splitting tensile strength experiments. Having 1 % fiber content specimens have the highest splitting tensile strength values as they have in the compressive strength. Likewise, having 7 % fiber content specimens have the lowest splitting tensile strength values as they have in the compressive strength.

In cementitious composites, there is a relation between strength values and unit volume weight of composites. This relationship is given in the Figure 8. In this figure, relation between compressive strength and unit

volume weight and relation between splitting tensile strength and unit volume weight are given.

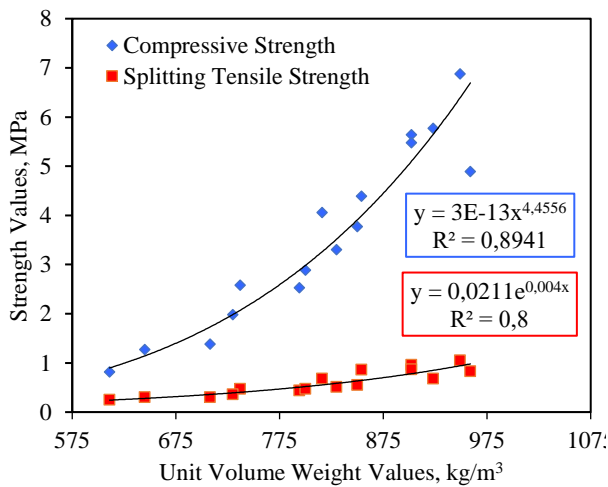


Figure 8 Strength versus Unit Volume Weight of CLCM specimens

According to Fig. 7, both compressive and splitting tensile strength and unit volume weight relations were obtained as increasing in a form of power function. According to this function, when the unit volume increases, both the compressive strength and the splitting tensile strength have been shown to increase.

### 3.5. Structural Strength Properties

Structural mechanical properties, which are internal friction angle, failure angle, normal strength, shear strength and cohesion parameters, of the specimens were carried out in this study. Structural strength analysis of materials provides more comprehensive information about internal actions of the material.

Mohr Coulomb Failure Criterion was used to determine the structural strength properties of specimens. Mohr Coulomb Failure Criterion can be estimated some mechanical properties of concrete based on the tension and compression stresses.

Mohr envelopes were drawn by the use of the compressive and splitting tensile stress data. One examples of drawn Mohr envelopes is given in Figure 9. These drawings have been

done separately for each mixture combination and structural mechanical properties of the materials have been found through the drawings.

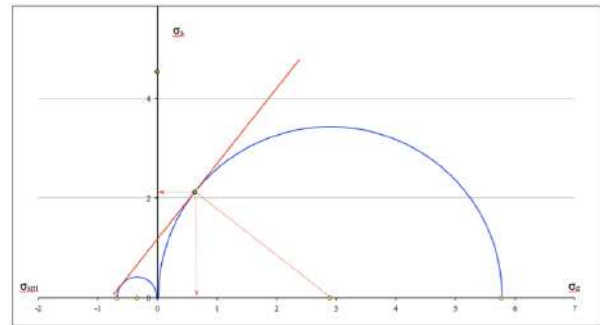


Figure 9 Mohr Circle drawing of LF6

Firstly, a coordinate system, which x plane represents normal strength and y plane represents shear strength, is drawn. Mohr circles were generated by plotting a half circle to the left of the x-axis of the coordinate system representing splitting tensile strength and another half circle to the right of the x-axis of the coordinate system representing compressive strength. Then, a tangent line is drawn to the two half circles. The slope of this line gives the internal friction angle of the material. The point where the tangent line cut the y plane gives cohesion. Center of the compressive strength and tangent line are joint by a straight line. Value of this point at x-axis gives normal strength and at y-axis shear strength. In this study, these values are discussed as structural strength values.

Structural strength parameters are chiefly used in rock mechanics and soil mechanics. Internal friction angle, failure angle and cohesion parameters are the main parameters in rock and in soil classification and load bearing calculations. Mohr coulomb criterion is used to obtain these parameters. With a similar approach, in order to find these parameters and to understand the inner structure of cementitious mortars, Mohr Coulomb criterion was used. Structural strength properties of CLCMs are given in Table 6.

Table 6 Structural mechanical properties of the CLCMs

Mix	$\alpha$ (°)	$\phi$ (°)	$\sigma_n$ (MPa)	C (MPa)	$\sigma_s$ (MPa)
<b>LF-R</b>	66.5	43.0	0.79	1.13	2.24
<b>LF1-1</b>	68.0	46.0	0.99	1.35	2.35
<b>LF1-2</b>	67.0	45.0	0.88	1.17	2.03
<b>LF1-3</b>	66.0	42.0	0.73	1.00	1.64
<b>LF1-5</b>	67.5	45.0	0.59	0.82	1.40
<b>LF1-7</b>	66.0	44.0	0.41	0.58	0.95
<b>LF2-1</b>	71.0	52.0	0.69	1.00	1.98
<b>LF2-2</b>	68.5	47.0	0.46	0.65	1.13
<b>LF2-3</b>	66.5	45.0	0.41	0.54	0.92
<b>LF2-5</b>	64.0	41.0	0.26	0.33	0.54
<b>LF2-7</b>	60.0	32.0	0.20	0.23	0.35
<b>LF3-1</b>	68.5	47.0	0.73	1.10	1.85
<b>LF3-2</b>	68.5	48.0	0.50	0.72	1.26
<b>LF3-3</b>	67.5	45.0	0.44	0.60	1.01
<b>LF3-5</b>	66.5	44.0	0.31	0.43	0.72
<b>LF3-7</b>	64.0	38.0	0.25	0.31	0.50

$\alpha$ : Failure Angle

$\phi$ : Internal Friction Angle

$\sigma_n$ : Normal Strength

C: Cohesion

$\sigma_s$ : Shear Strength

In rock mechanics, the value of failure angle mostly depends on formation type of the rock. Whereas failure angle is steeper in hard and brittle rock, it is less inclined in other words; value of failure angle is smaller, in the soft and ductile rock types. In particular, the value of the failure angle is very small in the formations that can be easily slide, such as sand. The same approach may be valid for cementitious compounds. When examining Table 6, decreasing trend was observed in failure angle of CLCMs with an increase in the amount of fiber content in the mixtures. In the fiber usage from 1 % to 7 %, failure angle of Type 1 fiber mixtures decreased 2 degrees, 11 degrees decrease was seen in Type 2 fiber mixtures and 4.5 degrees declining was observed in Type 3 fiber mixtures. Therefore, use of Type 2 fiber in mixtures could be said to make the mortar more ductile. When the fibers are included into the cement mortar, it loses its brittle property and it becomes more flexible structure. Therefore, as the acceptance of rock and soil mechanics, failure angle values of the CLCMs are decreased because of the increase of their flexibilities. It can be seen in the table that the most ductile

specimen was found as LF2-7 with a failure angle of 60 ° and the most brittle one was found as LF2-1 with a failure angle of 71 °.

Internal friction angle for a given material is the angle on the Mohr's Circle graph of the shear stress and normal stresses at which shear failure occurs. Researchers have used the internal friction angle in rock and soil classification. In soil classification, soils with less than 30° internal friction angle are considered as very loose and as the internal friction angle increases the classification continues as loose, compact, dense and very dense soil. Similar phenomenon can be seen in rock classification; rocks with internal friction angle less than 15° are called as very poor and as the internal friction angle increases the classification continues as poor, fair, good and very good rock. With this perspective, cementitious composites with higher value of internal friction angle could be evaluated as better-compacted materials. According to Table 6, internal friction angles of CLCMs decreases with increase in fiber content. CLCMs are becoming more loose structure with increase in RTWF content in the mortar combinations. Thus, it is thought that the loose mortar structure reduces the internal friction angle of the material.

The most compact specimen was found as LF2-1 with an internal friction angle of 52 ° and the loosest specimen was found as LF2-7 with an internal friction angle of 32 °.

The normal strength and shear strength is found, which cause the failure, by using the angle of slope of the plane of failure on Mohr Circle. Normal strength is the normal load to be carried by the material. Normal strength is the load that material could carry without deforming. Higher loading than normal strength of material causes deformation in the material. Up to normal strength that found by Mohr's Circle, deformation does not occur in the material. However, the material is permanently damaged between normal strength and compressive strength. In this case, it could be said that normal strength is

the moment that material take the first damage. According to Table 6, it is seen that normal strengths of CLCMs have a decreasing trend depending on the reduction in splitting tensile and compressive strength in each type of mixtures. As it can be seen from the Table 6, normal strength parameter of Type 1 mixtures with highest value of 0.99 MPa (LF1-1) and lowest value of 0.41 MPa (LF1-7) are greater than the others as in splitting tensile and compressive strengths. Which means that Type 1 mixtures could resist more load before first deformation inside. As previously mentioned, according to TS EN 998-1 standard, minimum compressive strength of cementitious mortars must be at least 0.4 MPa. It is seen from Table 6 that normal strength values of almost all mixtures are less than the value (0.4 MPa) specified in TS EN 998-1 standard. In other words, the produces mixtures can provide the compressive strength condition prescribed in the standard even without any deformation inside the material.

Cohesion is the force that holds the particles of concrete or mortar together. Cohesion indicates that what extent materials that forming the concrete or mortar are connected to each other. Additionally, the strength of the mortar or cement paste is dependent on the cohesion of the cement paste and adhesion of cement paste with aggregate particles [41]. If an assessment is done with this approach, it could be said that decrease in strength parameters of produced mortar specimens is caused by the decrease in the cohesion parameter (Table 6). According to the cohesion values given in Table 6, it is easily observed that Type 1 mixtures have the best cohesion values and Type 2 mixtures have the lowest cohesion values. This phenomenon could be explained by the inability of cement to adhesion on the polyester fiber as previously discussed.

According to Mohr-Coulomb Criterion, factors that affect the shear strength are normal strength, cohesion, and internal friction angle. Besides, shear strength can be obtained by the Mohr's Circle. Decrease in

internal friction angle and cohesion leads a reduction on shear strength parameter according to Mohr-Coulomb Criterion. This situation can be easily seen in Table 6. When the table is examined, Type 1 specimens exhibit the highest shear strength values. On the other hand, despite the reduction on shear strength parameters, specimens were gained flexibility characteristics against vertical and lateral loads by fiber content.

#### 4. CONCLUSIONS

In this paper, a unique experimental work on the influence of RTWF additive on CLCMs' mechanical and structural strength parameters is reviewed and mainly presented. The results obtained from the study are summarized as follows:

1. As the RTWF is an industrial solid waste of textile recycling sector, this paper can be evaluated as an important piece of work on behalf of utilization of the waste. The results analyzed in this work present that the effect of adding of RTWF in the behavior of composite lightweight cementitious mortar is promising. It could be concluded that the use of RTWF can improve the ductility and flexibility of composite mortar. Produced CLCMs provides the criterions foreseen in TS EN 998-1 standard in terms of unit volume weight and compressive strength.
2. Type 1 fiber, which is the mixture of cotton and polyesters waste fibers, was found as more suitable in order to use it in lightweight composite mortars. It provided higher compressive and splitting tensile strength through its cotton content during the tests. It is thought that cotton fibers can fit to the mortar by its rough surface. Besides, it was found that Type 1 mixtures had better characteristics on structural strength parameters than Type 2 and Type 3 mixtures.
3. It has been determined that the use of 1 % of the fibers used in the study in lightweight mortars strengthens the mortar in terms of compressive and splitting tensile strength.



4. In all mixture combinations, increase in fiber ratio is improved the lightweight characteristics of cementitious mortars. The lightest mortars were seen as 7 % fiber content mortars in all types. The lowest unit volume weighted type was found as Type 2 mortars with unit volume weight range of 923-611 kg/m<sup>3</sup>. If the specialties that lightness characteristics bring need to be examined in the future works, Type 2 fibers, which is a combination of cotton, polyester and acrylic fibers, could be examined.

5. Structural strength parameters, which are forming the main concept of this experimental research, were found by using Mohr's Circle. Mohr's Circles and Mohr-Coulomb Theory is widely used in soil and rock mechanics to understand the structural strength parameters of soils and rocks. Examples of this approach in concrete and/or mortar applications are not enough in the literature. Therefore, in this work, Mohr-Coulomb Criterion was tried to apply to lightweight composite mortars in order to understand the inner world of textile fiber reinforced cementitious mortars. Based on the results of the study, it was seen that Type 1 and 1% fiber usage gave better results in normal strength, cohesion, and shear strength parameters. The most ductile specimen was found as LF2-7 with a failure angle of 60 °. The most compact specimen was found as LF2-1 with an internal friction angle of 52 °.

This work could be evaluated as an important study to create a new research area as structural strength of cementitious composites.

#### ***Funding***

The author (s) has no received any financial support for the research, authorship or publication of this study.

#### ***The Declaration of Conflict of Interest/ Common Interest***

No conflict of interest or common interest has been declared by the authors.

#### ***Authors' Contribution***

The first author contributed 70%, the second author 30%.

#### ***The Declaration of Ethics Committee Approval***

This study does not require ethics committee permission or any special permission.

#### ***The Declaration of Research and Publication Ethics***

The authors of the paper declare that they comply with the scientific, ethical and quotation rules of SAUJS in all processes of the paper and that they do not make any falsification on the data collected. In addition, they declare that Sakarya University Journal of Science and its editorial board have no responsibility for any ethical violations that may be encountered, and that this study has not been evaluated in any academic publication environment other than Sakarya University Journal of Science.

## **REFERENCES**

- [1] C. Ryu, A. N. Phan, V. N. Sharifi, J. Swithenbank, "Co-combustion of textile residues with cardboard and waste wood in a packed bed," *Experimental Thermal and Fluid Science*, vol. 32, no. 2, pp. 450-458.
- [2] J. M. L. Reis, "Effect of textile waste on the mechanical properties of polymer concrete," *Materials Research*, vol. 12, no. 1, pp. 63-67, 2009.
- [3] K. Aghae, M. Foroughi, "Construction of lightweight concrete partitions using textile waste," *ICSDEC 2012: International Conference on Sustainable Design, Engineering, and Construction*, Texas, USA, 7-9 November 2012.
- [4] S. Pogorelov, G. Semenyak, "Frost resistance of the steel fiber reinforced concrete containing active mineral

- additives,” *Procedia Engineering*, vol. 150, pp. 1491-1495, 2016.
- [5] T. Grabois, G. Cordeiro, R. Toledo Filho, “Fresh and hardened-state properties of self-compacting lightweight concrete reinforced with steel fibers,” *Construction and Building Materials*, vol. 104, pp. 284-292, 2016.
- [6] H. Zhang, Y. Liu, H. Sun, S. Wu, “Transient dynamic behavior of polypropylene fiber reinforced mortar under compressive impact loading,” *Construction and Building Materials*, vol. 111, pp. 30-42, 2016.
- [7] S. Yin, R. Tuladhar, J. Riella, D. Chung, T. Collister, M. Combe, N. Sivakugan, “Comparative evaluation of virgin and recycled polypropylene fibre reinforced concrete,” *Construction and Building Materials*, vol. 114, pp. 134-141, 2016.
- [8] S. Marikunte, C. Aldea, S. Shah, “Durability of glass fiber reinforced cement composites: Effect of silica fume and metakaolin,” *Advanced Cement Based Materials*, vol. 5, no. 3-4, pp. 100-108, 1997.
- [9] S. P. Shah, D. Ludirdja, J. I. Daniel, B. Mobasher, “Toughness-durability of glass fiber reinforced concrete systems,” *ACI Materials journal*, vol. 85, no. 5, pp. 352-360, 1988.
- [10] H. Savastano, P. Warden, R. Coutts, “Mechanically pulped sisal as reinforcement in cementitious matrices,” *Cement and Concrete Composites*, vol. 25, no. 3, pp. 311-319, 2003.
- [11] H. Jr Savastano, A. Turner, C. Mercer, W. Soboyejo, “Mechanical behavior of cement-based materials reinforced with sisal fibers,” *Journal of Materials Science*, vol. 41, no. 21, pp. 6938-6948, 2006.
- [12] P. Lertwattanaruk, Suntijitto A, “Properties of natural fiber cement materials containing coconut coir and oil palm fibers for residential building applications,” *Construction and Building Materials*, vol. 94, pp. 664-669, 2015.
- [13] M. Mostafa, Uddin N, “Experimental analysis of compressed earth block (CEB) with banana fibers resisting flexural and compression forces,” *Case Studies in Construction Materials*, vol. 5, pp. 53-63, 2016.
- [14] C. Papanicolaou, T. Triantafillou, M. Papathanasiou, K. Karlos, “Textile reinforced mortar (TRM) versus FRP as strengthening material of URM walls: out-of-plane cyclic loading,” *Materials and Structures*, vol. 41, no. 1, pp. 143-157, 2008.
- [15] T. Triantafillou, C. Papanicolaou. “Shear strengthening of reinforced concrete members with textile reinforced mortar (TRM) jackets,” *Materials and Structures*, vol. 39, no. 1, 93-103, 2006.
- [16] H. Elsanadedy, T. Almusallam, S. Alsayed, Y. Al-Salloum, “Flexural strengthening of RC beams using textile reinforced mortar – Experimental and numerical study,” *Composite Structures*, vol. 97, pp. 40-55, 2013.
- [17] P. Larrinaga, C. Chastre, H. Biscaia, J. San-José, “Experimental and numerical modeling of basalt textile reinforced mortar behavior under uniaxial tensile stress,” *Materials & Design*, vol. 55, pp. 66-74, 2014.
- [18] L. Garmendia, P. Larrinaga, D. García, I. Marcos, “Textile-reinforced mortar as strengthening material for masonry arches,” *International Journal of Architectural Heritage*, vol. 8, no. 5, pp. 627-648, 2014.

- [19] Y. Wang, A. Zureick, B. Cho, D. Scott, "Properties of fibre reinforced concrete using recycled fibres from carpet industrial waste," *Journal of materials science*, vol. 29, no. 16, pp. 4191-4199, 1994.
- [20] F. Aspiras, J. Manalo "Utilization of textile waste cuttings as building material," *Journal of Materials Processing Technology*, vol. 48, no. 1-4, pp. 379-384, 1995.
- [21] M. Ucar, Y. Wang, "Utilization of recycled post consumer carpet waste fibers as reinforcement in lightweight cementitious composites," *International Journal of Clothing Science and Technology*, vol. 23, no. 4, pp. 242-248, 2011.
- [22] H. Binici, O. Aksogan, "Engineering properties of insulation material made with cotton waste and fly ash," *Journal of Material Cycles and Waste Management*, vol. 17, no. 1, pp. 157-162, 2014.
- [23] A. Murathan, A. Murathan, S. Karadavut, "Yüksek yoğunluklu polipropilen tekstil atıklarının kompozit malzeme üretiminde kullanılabilirliği (Usability of high density polypropylene textile waste in composite material production)," *Journal of the Faculty of Engineering and Architecture of Gazi Universtiy*, vol. 35, no. 1, pp. 9-14, 2014. (in Turkish)
- [24] J. Pinto, A. Peixoto, J. Vieira, L. Fernandes, J. Morais, V. Cunha, H. Varum, "Render reinforced with textile threads," *Construction and Building Materials*, vol. 40, pp. 26-32, 2013.
- [25] A. Briga-Sá, D. Nascimento, N. Teixeira, J. Pinto, F. Caldeira, H. Varum, A. Paiva, "Textile waste as an alternative thermal insulation building material solution," *Construction and Building Materials*, vol. 38, pp. 155-160, 2013.
- [26] A. Mahboubi, A. Ajorloo, "Experimental study of the mechanical behavior of plastic concrete in triaxial compression," *Cement and Concrete Research*, vol. 35, no. 2, pp. 412-419, 2005.
- [27] E. Öztekin, S. Pul, M. Hüsem, "Experimental determination of Drucker-Prager yield criterion parameters for normal and high strength concretes under triaxial compression," *Construction and Building Materials*, vol. 112, pp. 725-732, 2016.
- [28] H. Shoukry, M. F. Kotkata, S. A. Abo-EL-Enein, M. S. Morsy, S. S. Shebl, "Enhanced physical, mechanical and microstructural properties of lightweight vermiculite cement composites modified with nano metakaolin," *Construction and Building Materials*, vol. 112, pp. 276-283, 2016.
- [29] M. Shannag, "Characteristics of lightweight concrete containing mineral admixtures," *Construction and Building Materials*, vol. 25, no. 2, pp. 658-662, 2011.
- [30] G. M. Glenn, A. K. Klamczynski, B. S. Chiou, D. Wood, W. J. Orts, S. H. Imam, "Lightweight concrete containing an alkaline resistant starch-based aquagel," *Journal of Polymers and the Environment*, vol. 12, no. 3, pp. 189-196, 2004.
- [31] K. P. Metha, P. J. M. Monteiro, *Concrete Microstructure, Properties, and Materials*. 3rd ed. University of California at Berkeley, USA, McGraw-Hill; 2006.
- [32] TS EN 998-1. "Specification for mortar for masonry – part 1: rendering and plastering mortar". Turkish Standards Institution, Ankara, Turkey, 2006.
- [33] Gündüz L. *İnşaat Sektöründe Bimsblok*, Isparta, Turkey, Süleyman Demirel



- Üniversitesi Pomza Araştırma ve Uygulama Merkezi, 2005. (in Turkish).
- [34] Milli Eğitim Bakanlığı. “Giyim Üretim Teknolojisi Tekstil Lifleri 542TGD019”. [http://www.megep.meb.gov.tr/mte\\_program\\_modul/moduller\\_pdf/Tekstil%20Lifleri.pdf](http://www.megep.meb.gov.tr/mte_program_modul/moduller_pdf/Tekstil%20Lifleri.pdf) (21.04.2022) (in Turkish).
- [35] Saçak M. Lif Kimyası, Ankara, Turkey, A.O.F.F. Döner Sermaye işletmesi Yayınları No 18, 1994. (in Turkish).
- [36] D. A. Fanella, A. E. Naaman, “Stress-strain properties of fiber reinforced concrete in compression,” *ACI Journal*, vol. 82, no. 4, pp. 475 – 483, 1985.
- [37] H. Y. Ersoy, “Kompozit malzeme,” *Literatür Yayınları, Mimarlık Dizisi*, ISBN:975-8431-47-1, 2003.
- [38] N. Arioglu, Z. C. Girgin, E. Arioglu, “Evaluation of ratio between splitting tensile strength and compressive strength for concretes up to 120 mpa and its application in strength,” *ACI Materials Journal*, vol. 103, no. 1, 18-24, 2006.
- [39] D. Hannant, K. Buckley, J. Croft, “The effect of aggregate size on the use of the cylinder splitting test as a measure of tensile strength,” *Matériaux et Constructions*, vol. 6, no. 1, pp. 15-21, 1973.
- [40] V. Kadleček, S. Modrý, V. Kadleček, “Size effect of test specimens on tensile splitting strength of concrete: general relation,” *Materials and Structures*, vol. 35, no. 1, pp. 28-34, 2002.
- [41] A. M. Neville, *Properties of Concrete*. London, England, Pearson Education Ltd. 1999.



SAKARYA ÜNİVERSİTESİ

# FEN BİLİMLERİ ENSTİTÜSÜ DERGİSİ

Sakarya University Journal of Science  
SAUJS

ISSN 1301-4048 e-ISSN 2147-835X Period Bimonthly Founded 1997 Publisher Sakarya University  
<http://www.saujs.sakarya.edu.tr/>

Title: Effect of Different Solvents, Pore-Forming Agent and Solubility Parameter Differences on the Properties of PES Ultrafiltration Membrane

Authors: Seren ACARER

Received: 2022-06-24 00:00:00

Accepted: 2022-10-11 00:00:00

Article Type: Research Article

Volume: 26

Issue: 6

Month: December

Year: 2022

Pages: 1196-1208

How to cite

Seren ACARER; (2022), Effect of Different Solvents, Pore-Forming Agent and Solubility Parameter Differences on the Properties of PES Ultrafiltration Membrane. Sakarya University Journal of Science, 26(6), 1196-1208, DOI: 10.16984/saufenbilder.1135285

Access link

<https://dergipark.org.tr/en/pub/saufenbilder/issue/74051/1135285>

New submission to SAUJS

<http://dergipark.gov.tr/journal/1115/submission/start>

## Effect of Different Solvents, Pore-Forming Agent and Solubility Parameter Differences on the Properties of PES Ultrafiltration Membrane

Seren ACARER\*<sup>1</sup> 

### Abstract

In the production of polymeric membranes used in water treatment by the non-solvent-induced phase separation (NIPS) method, the materials used in the membrane casting solution and the interaction of these materials greatly affect the properties and performance of the obtained membranes. In this study, polyethersulfone (PES) membranes are produced by the NIPS method using two different solvents, dimethyl sulfoxide (DMSO) and N-methyl-2-pyrrolidone (NMP), and polyvinylpyrrolidone (PVP) as pore-forming agent. Chemical functional groups and morphologies of the produced membranes are investigated by Fourier transform infrared (FTIR) spectroscopy and scanning electron microscopy (SEM), respectively. The viscosity of the membrane casting solutions and the hydrophilicity, porosity, mean pore size, and mechanical properties of the membranes are characterized. The pure water flux (PWF) of the membranes is determined at 1 and 3 bar pressures. The Hansen solubility parameters (HSP) of the materials used in membrane production are calculated and the effect of the interactions of DMSO, NMP, and PVP with PES and/or non-solvent (water) on the membrane properties are investigated.

**Keywords:** Membrane characterization, phase separation, solvent, PVP, hansen solubility parameters

### 1. INTRODUCTION

Membrane processes are among the advanced treatment methods commonly used in the treatment of drinking water and wastewater [1, 2]. NIPS is a widely used method in the production of commercially available polymeric membranes used in water treatment [3]. The fact that the NIPS method is simpler than other methods used in the production of

polymeric membranes and that the porosity, pore size, and thickness of the membrane can be easily controlled by changing some conditions during production are among the main reasons for the widespread use of the NIPS method [4].

Polyethersulfone (PES) is widely preferred in the production of polymeric membranes due to its high chemical resistance, good chlorine resistance, good thermal and mechanical

\* Corresponding author: seren.acarer@ogr.iuc.edu.tr

<sup>1</sup> Istanbul University, Cerrahpaşa

ORCID: <https://orcid.org/0000-0001-6733-2067>



stability, low cost, and good miscibility with solvents [5, 6]. During the production of polymeric membranes, large amounts of conventional organic solvents such as NMP, DMSO, dimethylformamide (DMF), dimethylacetamide (DMAc), and tetrahydrofuran (THF) are used [7]. PES membranes are produced by many researchers using different solvents such as NMP [5, 8-9], DMSO [10], and DMF [8].

In membrane production with NIPS, the polymer-solvent relationship in the membrane casting solution and the solvent-non-solvent relationship when the membrane is immersed in the coagulation bath significantly affect the morphology of the membrane [11]. The thermodynamic stability of the casting solution, polymer-solvent affinity, and solvent-non-solvent affinity cause accelerated or delayed liquid-liquid demixing during phase separation, resulting in membranes with different structures, pore size, and porosity. For instance, Fahrina et al. reported that PES-NMP and PES-DMF membranes exhibit denser membrane surfaces and internal structure compared to PES-DMSO membranes, due to the lower affinity of NMP and DMF for water (non-solvent) than DMSO [12].

Pore-forming agents (such as PVP and PEG) added to the membrane casting solution cause the formation of membranes with different morphologies, properties, and performance due to their effects on the stability of the casting solution, their hydrophilicity, and solution viscosity [13-16]. In a recent study by Tofighy et al., it has been reported that 3% wt. PVP-doped PVDF membranes have higher hydrophilicity, porosity, and pore size compared to undoped PVDF, and the membrane's PWF is improved by incorporating PVP into PVDF membrane [17]. In the study of Kourde-Hanafı et al., it was found that PES-PVP membranes have a denser top layer than pure PES regarding casting solution viscosity,

but PES-PVP membrane has higher permeability than pure PES membrane due to the hydrophilic nature of PVP [18].

In this study, PES-DMSO, PES-NMP, and PES-PVP-NMP membranes are produced by the NIPS method to determine the effects of different solvents (DMSO and NMP) and pore-forming agent (PVP) on PES membrane properties and performance. The effects of DMSO, NMP, and PVP on the chemical groups, morphology, hydrophilicity, mechanical properties, and PWF of the membrane are revealed as a result of characterization studies.

## 2. MATERIAL AND METHOD

### 2.1. Materials

PES (VERADEL® 3000P) is obtained from Solvay Specialty Polymers. NMP and DMSO of  $\geq 99.5\%$  and  $\geq 99.9\%$  purity, respectively, are purchased from Merck. PVP with a molecular weight of 40,000 g/mol is purchased from Sigma-Aldrich.

### 2.2. Membrane Production

PES-DMSO, PES-NMP, and PES-PVP-NMP flat sheet membranes are produced by the NIPS method. Solutions containing 16% wt. PES and 84% wt. solvent (DMSO or NMP) are mixed in a heated magnetic stirrer (WiseStir, MSH-20A) for 24 hours at 60 °C. After obtaining a homogeneous solution, the solution is kept in an ultrasonic bath (Weightlab Instruments) at 25 °C for 30 minutes to remove air bubbles in the membrane casting solution. Membranes are cast on a glass plate to form polymeric films using a 200  $\mu\text{m}$  thick casting blade. After waiting for 10 seconds, the casting solution in the form of a film on the glass plate was immersed in a coagulation bath containing non-solvent (distilled water) and left for 15 minutes. Membranes are obtained as a result of the

change between solvent-non-solvent. After the obtained membranes are thoroughly washed with distilled water, they are kept in distilled water at 4 °C for 24 hours, and then the membranes are characterized. The production process of membranes produced with different solvents is shown schematically in Figure 1. The PES-PVP-NMP membrane is also produced using the same procedure using 8% wt. PVP and 76% wt. NMP. The composition of all produced membranes is given in Table 1.

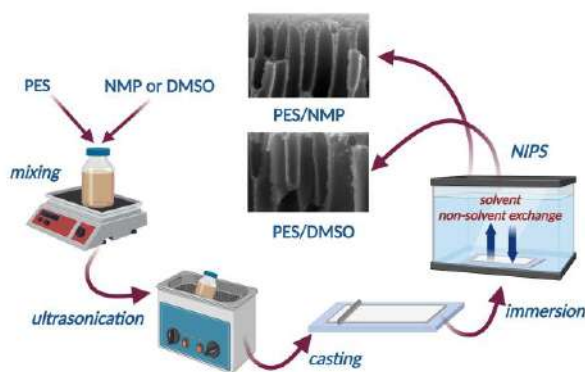


Figure 1 Schematic diagram of the membrane production process

Table 1 Composition of the produced membranes

Membrane Code	PES (wt.%)	DMSO (wt.%)	NMP (wt.%)	PVP (wt.%)
PES-DMSO	16	84	-	-
PES-NMP	16	-	84	-
PES-PVP-NMP	16	-	76	8

## 2.3. Membrane Characterization

### 2.3.1. Membrane casting solution viscosity

The viscosities of the casting solutions of the membranes are measured by a viscometer (AND, SV-10). Viscosity measurements are carried out at 25 °C.

### 2.3.2. FTIR

Chemical groups of the membranes are determined using the FTIR spectrometer

(Perkin Elmer, Spectrum 100). The FTIR spectra of the membranes are recorded in the wavenumber range of 4000-650 cm<sup>-1</sup>.

### 2.3.3. SEM

The surface and cross-sectional morphology of the produced membranes are investigated using SEM (FEG, FEI Quanta 250). To obtain SEM views, firstly, the insulating membrane surfaces are made conductive by coating them with gold. While the surface views of the membranes are examined at 20000x magnification, the cross-sectional views are examined at 10000x and 40000x magnifications.

### 2.3.4. Contact angle

The surface hydrophilicity of the membranes is determined by the sessile drop technique by contact angle meter (KSV Instruments, CAM 101). Contact angle measurements are carried out at 25 °C. The contact angle results are obtained by determining the angle between the distilled water and the membrane surface by dripping distilled water on the membrane surface. Distilled water is dropped at least three times in different locations of each membrane sample and contact angle results are given as the average of three measurements.

### 2.3.5. Water content

The produced membranes are left to dry in an oven at 60 °C (NUVE, EN 500) for 24 hours. The dry weights of the membranes are first determined using a precision balance (KERN, 573). Afterward, the membranes are immersed in a container filled with distilled water, and the excess water on them is quickly removed with a blotting paper, and the membranes are weighed again to determine their wet weight. The water content of the membranes is calculated using Equation 1.

$$\text{Water content (\%)} = \frac{W_w - W_d}{W_w} \times 100 \quad (1)$$

where  $W_w$  and  $W_d$  are wet and dry weights of membranes (g), respectively.

### 2.3.6. Porosity and mean pore size

The porosity ( $\varepsilon$ ) and mean pore size ( $r_m$ ) of the membranes are calculated using Equation 2 and Equation 3 (Guerout-Elford-Ferry Equation), respectively.

$$\varepsilon (\%) = \frac{W_w - W_d}{A l \rho} \times 100 \quad (2)$$

where  $W_w$  is the wet weight of the membrane (g),  $W_d$  is the dry weight of the membrane (g),  $A$  is the membrane area ( $\text{cm}^2$ ),  $l$  is the membrane thickness (cm), and  $\rho$  is the density of the water ( $0.998 \text{ g/cm}^3$ ).

$$r_m = \sqrt{\frac{(2.9 - 1.75\varepsilon) \times 8\eta l Q}{\varepsilon \times A \times \Delta P}} \quad (3)$$

where  $\varepsilon$  is membrane porosity,  $\eta$  is the viscosity of water ( $8.9 \times 10^{-4} \text{ Pa.s}$ ),  $l$  is membrane thickness (m),  $Q$  is the volume of permeate water per unit time ( $\text{m}^3/\text{s}$ ),  $A$  is effective membrane area ( $\text{m}^2$ ),  $\Delta P$  operating pressure (0.3 MPa).

### 2.3.7. Mechanical tests

Tensile tests of the membranes are carried out using a universal testing machine (Shimadzu, AG-IS (50kN)). The membranes are left to self-dry for 24 hours at room temperature at  $25^\circ\text{C}$ . The membranes are then adhered to the aluminum plates to prevent the slipping of the tips on the tester. The tensile strength and elongation at break of the produced membranes are determined.

### 2.3.8. PWF

A dead-end filtration system (Tin Mühendislik) is used in PWF tests of the membranes. The effective surface area of the membranes placed in the filtration system is  $19.6 \text{ cm}^2$ . In the pure

water tests, firstly, pure water is passed through the membranes at 5 bar pressure using nitrogen gas ( $\text{N}_2$ ) to obtain a stable flux and to open the pores of the membranes thoroughly. In other words, the membranes are first compressed at 5 bar. Then, distilled water is passed through each membrane at 1 bar and 3 bar, respectively. The permeate collected from the outlet of the filtration system is collected in a beaker on a precision scale and the time-weight graph is transferred to the computer and the PWF of the membranes is calculated in  $\text{L/m}^2.\text{h}$  unit. The PWF of the membranes is calculated using Equation 4.

$$J = \frac{V}{A \Delta t} \quad (4)$$

where  $J$  is the membrane flux ( $\text{L/m}^2.\text{h}$ ),  $V$  is the permeate volume (L),  $A$  is the effective membrane area ( $\text{m}^2$ ), and  $\Delta t$  is the time (h).

## 2.4. Calculation of HSP

The solubility parameter ( $\delta$ ) is useful in estimating the relative attraction force between solvents and solutes numerically [19]. Using the HSP, the total solubility parameter of the polymer or solvent is calculated using Equation 5.

$$\delta_t = \sqrt{\delta_d^2 + \delta_p^2 + \delta_h^2} \quad (5)$$

where  $\delta_t$  represents the total solubility parameter and  $\delta_d$ ,  $\delta_p$  and  $\delta_h$  are dispersion, polar, and hydrogen bonding parameters respectively.

The difference between the solubility parameter of the polymer and solvent can be calculated using Equation 6.

$$\Delta\delta_{p-s} = \sqrt{(\delta_{d,p} - \delta_{d,s})^2 + (\delta_{p,p} - \delta_{p,s})^2 + (\delta_{h,p} - \delta_{h,s})^2} \quad (6)$$

The difference between the solvent and non-solvent solubility parameters can be calculated using Equation 7.

$$\Delta\delta_{S-NS} = \sqrt{(\delta_{d,s} - \delta_{d,ns})^2 + (\delta_{p,s} - \delta_{p,ns})^2 + (\delta_{h,s} - \delta_{h,ns})^2} \quad (7)$$

where P, S, and NS represent polymer, solvent, and non-solvent (water), respectively.

Table 2 shows the solubility parameters of PES, DMSO, NMP, and water.

Table 2 Solubility parameters of PES, PVP, NMP, DMSO, and water

	$\delta_d$ (MPa) <sup>0.5</sup>	$\delta_p$ (MPa) <sup>0.5</sup>	$\delta_h$ (MPa) <sup>0.5</sup>	$\delta_t$ (MPa) <sup>0.5</sup>
PES	19.6	10.8	9.2	24.19
PVP	21.4	11.6	21.6	32.54
NMP	18	12.3	7.2	22.95
DMSO	18.4	16.4	10.2	26.67
Water	15.5	16	42.3	47.80

### 3. RESULTS

#### 3.1. Membrane Casting Solution Viscosity

The viscosity of the membrane casting solution plays an important role in the morphology of the membranes produced by NIPS. The viscosity results of membrane casting solutions at 25 °C are shown in Figure 2. The viscosity of the PES-DMSO casting solution (6.77 Pa.s) is found to be approximately 5 times higher than the viscosity of the PES-NMP solution (1.37 Pa.s). This result can be attributed to the fact that DMSO is more viscous than NMP [20]. With the inclusion of 8% wt. PVP in the casting solution of the PES-NMP membrane, the viscosity increased 6.7 times to 9.2 Pa.s. The higher polymer content of the PES-PVP-NMP solution (16% wt. PES and 8% wt. PVP) and lower solvent content (76% wt.) of the PES-NMP solution are increased viscosity. In this study, the increase in the membrane casting solution with the addition of PVP is consistent with the studies in the literature on the increase

in viscosity of polymeric solutions with the addition of PVP [21-23] and with the increase of PVP concentration [21, 24] in the solution.

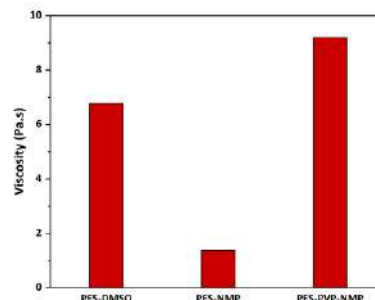


Figure 2 Viscosity of membrane casting solutions

#### 3.2. Confirmation of the Chemical Structure of Membranes

To confirm the chemical structure of PES and PES-PVP membranes, the chemical groups of the membranes are determined by FTIR analysis. FTIR spectra of PES-DMSO, PES-NMP, and PES-PVP-NMP membranes are shown in Figure 3. Similar peaks are obtained in PES-DMSO and PES-NMP membranes. In the NIPS method, an exchange occurs between the solvent in the casting solution and the non-solvent (water) in the coagulation bath, and the solvent moves away from the membrane structure. Therefore, similar bands are obtained as a result of the chemical characterization of PES-DMSO and PES-NMP membranes with FTIR, regardless of the solvent type used in the membrane production process. The C=C stretching vibration originating from the aromatic benzene rings of PES corresponded to the bands at 1485 and 1577 cm<sup>-1</sup>. The C-O-C stretching vibration of aromatic ether is confirmed by the band at 1237 cm<sup>-1</sup>. The peaks occurring at 1147 cm<sup>-1</sup> and 1103 cm<sup>-1</sup> are caused by the O=S=O vibration [25, 26]. In the FTIR spectrum of the PES-PVP-NMP membrane, unlike the PES-NMP and PES-DMSO membrane, a new peak occurred at 1675



$\text{cm}^{-1}$  corresponding to the stretching vibration of the carbonyl (C=O) group of PVP.

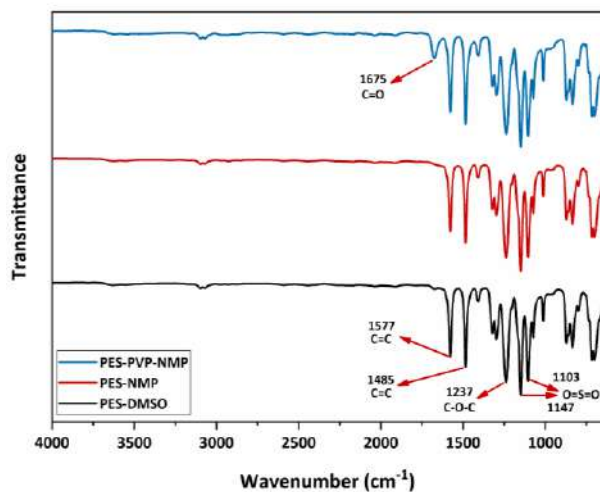


Figure 3 FTIR spectra of membranes

### 3.3. Membrane Morphology

#### 3.3.1. Effect of solvents on membrane morphology

SEM surface and cross-section views of the membranes are given in Figure 4. All membranes exhibited an asymmetrical structure consisting of a top layer responsible for selectivity and a porous sublayer. When DMSO was used as a solvent in the production of PES membrane, the surface porosity of the membrane increased significantly compared to the use of NMP. It is seen that both PES-DMSO and PES-NMP membranes exhibit finger-like pore structures. However, fewer but larger finger-like pores extending from the surface of the membrane to the sublayer occurred in PES-DMSO compared to PES-NMP. Another remarkable point is that the regions surrounding finger-like pores in the PES-NMP membrane are thicker and more pronounced sponge-like, while the thickness of these regions is less in the PES-DMSO membrane. In addition, a thin top layer responsible for selectivity is formed in the PES-DMSO membrane structure, while a thicker and sponge-like top layer is formed in the PES-NMP membrane. The membrane

structure is sponge-like and the thick top layer is the result of the delay of liquid-liquid demixing during phase separation [27]. SEM views revealed that the type of solvent used in membrane production affects membrane surface porosity, top layer thickness, top layer structure, and pore size.

The changes in membrane morphology depending on the solvent type can be explained by the solubility parameter ( $\delta$ ). Two factors, equilibrium thermodynamics and kinetics of the solution play an important role in the morphology of membranes produced with NIPS. High interaction between polymer and solvent, i.e. lower  $\delta_{P-S}$ , indicates high thermodynamic stability [28, 29]. On the other hand, the lower the  $\delta_{S-NS}$  value, the greater the interaction between the solvent and the non-solvent (water). Table 3 shows the polymer-solvent interaction (P-S) and solvent-non-solvent (water) interaction (S-NS) results calculated from the dispersion, polar, and hydrogen bonding parameters of PES, NMP, DMSO, and water. The fact that the interaction between PES-NMP ( $2.97 \text{ MPa}^{0.5}$ ) is stronger than the interaction between PES-DMSO ( $5.81 \text{ MPa}^{0.5}$ ) indicates that NMP is a better solvent for PES and its solution stability is higher. On the other hand, the fact that the DMSO-water interaction ( $32.23 \text{ MPa}^{0.5}$ ) is stronger than the NMP-water ( $35.38 \text{ MPa}^{0.5}$ ) interaction indicates that the affinity of DMSO to water is higher than that of NMP to water. The low affinity of DMSO for PES and high for water compared to NMP causes the acceleration of liquid-liquid demixing by increasing the interaction between non-solvent and solvent during the NIPS. If DMSO is preferred as the solvent in membrane production, the formation of a membrane with a less sponge-like structure and a thinner top layer is compatible with the affinity results calculated from Hansen solubility parameters.



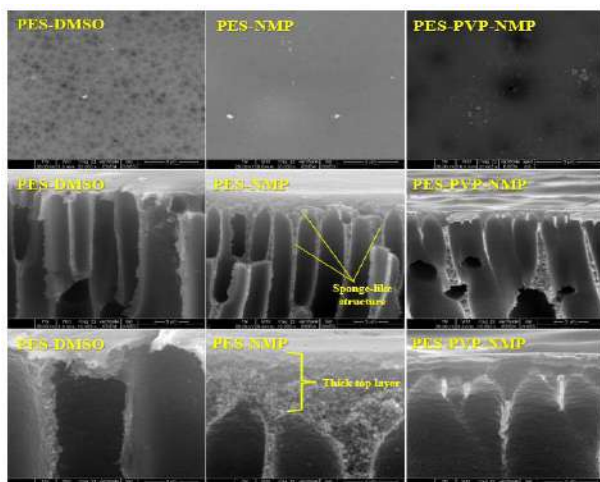


Figure 4 SEM surface and cross-section views of the membranes

Table 3 Hansen affinity parameter between PES-DMSO, PES-NMP, DMSO-water, and NMP-water

	PES-Solvent Interaction (P-S) (MPa) <sup>0.5</sup>	Solvent-Non-Solvent Interaction (S-NS) (MPa) <sup>0.5</sup>
NMP	2.97	35.38
DMSO	5.81	32.23

### 3.3.2. Effect of PVP on PES membrane morphology

As seen in Figure 4, the surface porosity of PES-NMP membranes increased with the addition of PVP. The increase in porosity can be attributed to the fact that the presence of a third component (PVP) other than polymer and solvent in the membrane casting solution causes an increase in the thermodynamic instability of the solution [30]. The fact that the  $\delta_t$  value of PVP is closer to the  $\delta_t$  value of water compared to the  $\delta_t$  value of PES indicates that PVP has a higher affinity for water (Table 2). Due to the high affinity of PVP for water and its solubility in water, large pores were formed on the membrane surface and the top layer of the membrane was thinned during the PVP washing from the near-surface parts of the membrane and passing from the casting solution to the water. On the other hand, the higher viscosity of the PES-PVP-NMP membrane resulted in a more sponge-like and tighter structure of the

membrane interior than the PES-NMP membrane. This result revealed that in addition to the kinetic factor, viscosity is also an important factor in membrane morphology.

### 3.4. Surface Hydrophilicity

Membrane surface hydrophilicity is characterized by the contact angle, and hydrophobic membrane surfaces are expressed with high contact angle while hydrophilic membrane surfaces are expressed with a low contact angle [31]. The contact angle and water content results of the membranes are shown in Figure 5. The fact that the contact angle of PES-DMSO ( $61.1^\circ$ ) is 28% lower than the contact angle of PES/NMP ( $78.4^\circ$ ), indicates that PES-DMSO has higher hydrophilicity. The significantly higher surface porosity of the PES-DMSO membrane (Figure 4) allowed increased diffusion of water and resulted in higher surface hydrophilicity. Similarly, PES-PVP-NMP membrane exhibited a more porous structure compared to PES-NMP and the hydrophilic carbonyl group (C=O) of PVP decreased the contact angle by 19.4% and increased the hydrophilicity of the membrane surface [32]. Since membranes with higher surface hydrophilicity exhibit higher antifouling properties, the order of membrane surfaces to exhibit higher fouling resistance under the same conditions are PES-DMSO > PES-PVP-NMP > PES-NMP.

Another parameter related to membrane hydrophilicity is the water content of the membranes. The water content of all membranes is above 70%. The water content of PES-DMSO is 5.5% higher compared to PES-NMP. The high surface porosity and the thinner top layer of PES-DMSO allowed water to pass into the membrane structure more easily and absorb more water in finger-like pores. The contact angle and water content results of the membranes produced with different solvents revealed that DMSO is a more suitable solvent

than NMP in the production of PES membrane to increase the hydrophilicity. On the other hand, the water content of PES-PVP-NMP was found to be 3% higher than that of PES-NMP, although the internal pores of PES-PVP-NMP were less than the internal pores of PES-NMP. This may be related to the fact that the large pores on the surface of the PVP-doped membrane and its thin top layer allow the water to pass through more and faster than PES-NMP, which has a denser surface and thicker top layer.

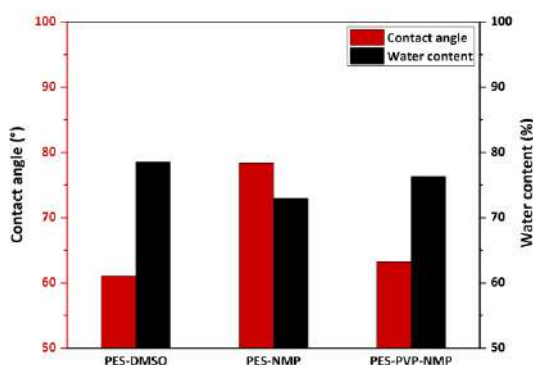


Figure 5 Contact angle and water content of membranes

### 3.5. Porosity and Mean Pore Size

The calculated porosity and mean pore size values of the membranes are given in Table 4. The highest porosity is obtained in the PES-DMSO membrane, and the lowest porosity is obtained in the PES-PVP-NMP membrane. The calculated porosity results are consistent with the SEM cross-sectional views. The mean pore sizes of the membranes varied in the range of 18.2-27.8 nm, and these mean pore sizes indicate that the produced membranes are ultrafiltration (UF) membranes [33].

Table 4 Porosity and mean pore size of the membranes

	Porosity (%)	Mean pore size (nm)
PES-DMSO	66.4	19.4
PES-NMP	60.1	18.2
PES-PVP-NMP	54.3	27.8

### 3.6. Mechanical Properties

To determine the mechanical properties of the membranes, tensile strength and elongation at break are investigated and the results are shown in Figure 6. The tensile strengths of PES-NMP and PES-DMSO membranes are found to be 15.1 MPa and 13.9 MPa, respectively. Since the high surface porosity of PES-DMSO causes a decrease in the membrane surface area, it has a negative effect on the mechanical strength of the membrane, causing it to exhibit lower tensile strength [34, 35]. Also, the elongation at break of PES-NMP membrane is higher than that of PES-DMSO. Also, the elongation at break of PES-NMP membrane is higher than that of PES-DMSO.

When the effect of PVP on the mechanical properties of the PES-NMP membrane is investigated, it was observed that the tensile strength and elongation at break decreased. The large diameter surface pores, high mean pore size, and thin top layer of PES-PVP-NMP resulted in a decrease in the maximum stress that the membrane can withstand before rupture. In addition, the elongation at break of the membrane is reduced by the incorporation of PVP into the PES matrix. In other words, PVP reduced the flexibility and ductility of the membrane [36].

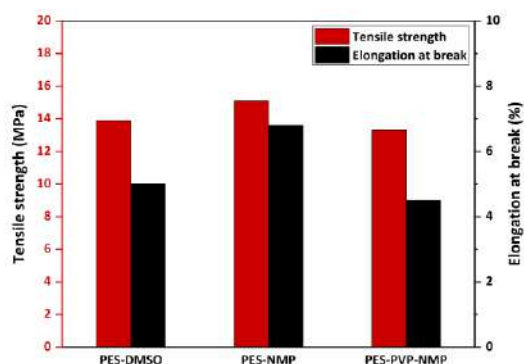


Figure 6 Mechanical properties of membranes

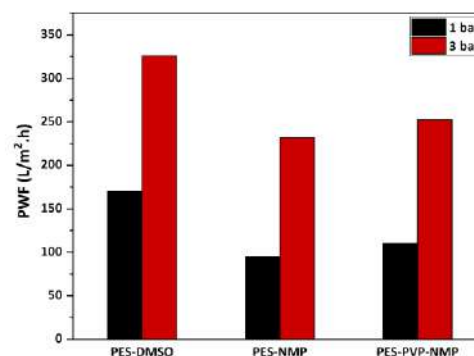


Figure 7 PWF performance of membranes

### 3.7. PWF Performance of Membranes

The PWF performance of the membranes at 1 bar and 3 bar pressure is presented in Figure 7. With the increase in pressure, the PWF performance of the membranes also increased. PWF of PES-DMSO is found to be 44.2% and 33% higher than PES-NMP at 1 bar and 3 bar, respectively. In addition, the results of the contact angle and water content of the membranes are compatible with the PWF performance results. The relatively high surface hydrophilicity of PES-DMSO increased the interaction between water and the membrane surface. In addition, the high porosity, larger pore sizes, and thinner skin layer of the PES-DMSO membrane reduced the hydraulic resistance of the membrane and increased the passage of water through the membrane.

Although the inclusion of PVP in PES-NMP increased the surface porosity and hydrophilicity, increasing the PWF, the PWF of PES-PVP-NMP is found to be lower than that of PES-DMSO. Since the addition of 8% wt. of PVP to the casting solution increased the viscosity, the formation of finger-like voids was suppressed, and this may have prevented much higher flux values from being reached in the PVP-doped membrane.

## 4. CONCLUSION

Determination of the most suitable membrane casting solution composition in terms of desired membrane properties and performance contributes to the production of water treatment membranes more economically and with the use of chemicals that are more harmless to the environment. In this study, PES-DMSO, PES-NMP, and PES-PVP-NMP membranes are produced by NIPS method and the characterization of the produced membranes was performed. In addition, the effect of different solvents (DMSO and NMP) on the membrane, especially their morphology, is explained by Hansen solubility parameters. As a result of the study, the following results were obtained:

- 1) According to Hansen solubility parameters calculations, the relatively stronger and weaker affinity of NMP to PES and water (non-solvent), respectively, caused a delay in demixing during the formation of the PES-NMP membrane. As a result of the demixing delay, the PES-NMP membrane with less porosity and a thicker internal structure is obtained. On the contrary, relatively weaker, and stronger interactions of DMSO with PES and water, respectively, resulted in a more porous and less dense membrane.

2) PES-DMSO membrane produced with DMSO, which is a more “green” solvent compared to NMP, has a more porous surface, thinner top layer, higher hydrophilicity, higher porosity and mean pore size compared to PES-NMP. PWF of PES-DMSO is found 44.2% higher than PES-NMP at 1 bar. However, PES-DMSO exhibited lower tensile strength and elongation at break compared to PES-NMP.

This study revealed that the use of different solvents in membranes produced by the NIPS and the inclusion of a pore-forming agent in the membrane casting solution led to different membrane properties and performance, provided that the polymer (PES) ratio in the membrane casting solution is the same.

#### ***Funding***

This research is funded by Istanbul University-Cerrahpasa Scientific Research Projects Coordination Unit, grant number: FYL-2020-34069

#### ***Authors' Contribution***

The first author S.A. contributed 100%.

#### ***The Declaration of Conflict of Interest/ Common Interest***

No conflict of interest or common interest has been declared by the authors.

#### ***The Declaration of Ethics Committee Approval***

This study does not require ethics committee permission or any special permission.

#### ***The Declaration of Research and Publication Ethics***

The authors of the paper declare that they comply with the scientific, ethical and quotation rules of SAUJS in all processes of the paper and that they do not make any falsification on the data collected. In addition, they declare that Sakarya University Journal of

3) With the inclusion of PVP, a pore-forming agent, in the PES-NMP membrane, the pore size, hydrophilicity, and PWF of the membrane increased, but the tensile strength and elongation at break decreased. Since the inclusion of 8% wt. PVP in the membrane casting solution provides a significant increase in the viscosity of the casting solution, a denser membrane interior structure was obtained.

Science and its editorial board have no responsibility for any ethical violations that may be encountered, and that this study has not been evaluated in any academic publication environment other than Sakarya University Journal of Science.

### **REFERENCES**

- [1] C. Aydiner, E. C. Doğan, B. K. Mert, A. O. Narci, E. Durna, and A. Akbacak, “Water recovery from pulp and paper mill wastewater with integrated membrane system and minimization of concentrated waste,” Sakarya University Journal of Science, vol. 21, no. 2, pp. 252–260, 2017.
- [2] F. İlhan, “Investigation of minimization and reusability of the reject from electro dialysis processes: an example textile wastewater,” Sakarya University Journal of Science, vol. 21, no. 5, pp. 943–950, 2017.
- [3] A. Kausar, “Phase Inversion Technique-Based Polyamide Films and Their Applications: A Comprehensive Review,” Polymer-Plastics Technology and Engineering, vol. 56, no. 13, pp. 1421–1437, Sep. 2017.
- [4] C. Algieri, S. Chakraborty, and U. Pal, “Efficacy of Phase Inversion Technique for Polymeric Membrane Fabrication,” Journal of Phase Change Materials, vol.

- 1, no. 1, p. 1, 2021, [Online]. Available: <https://j-pcm.org/index.php/jpcm/article/view/10>
- [5] K. P. Wai, C. H. Koo, W. C. Chong, S. O. Lai, Y. L. Pang, "Improving hydrophilicity of polyethersulfone membrane using silver nanoparticles for humic substances removal," *International Journal of Engineering, Transactions B: Applications*, vol. 31, no. 8, pp. 1364–1372, 2018.
- [6] W. Wang, L. Zhu, B. Shan, C. Xie, C. Liu, F. Cui, G. Li, "Preparation and characterization of SLS-CNT/PES ultrafiltration membrane with antifouling and antibacterial properties," *Journal of Membrane Science*, vol. 548, no. December, pp. 459–469, 2018.
- [7] X. Dong, A. Al-Jumaily, I. C. Escobar, "Investigation of the use of a bio-derived solvent for non-solvent-induced phase separation (NIPS) fabrication of polysulfone membranes," *Membranes*, vol. 8, no. 2, 2018.
- [8] M. Amirilargani, T. Mohammadi, "Effects of PEG on morphology and permeation properties of polyethersulfone membranes," *Separation Science and Technology*, vol. 44, no. 16, pp. 3854–3875, 2009.
- [9] A. Marjani, A. T. Nakhjiri, M. Adimi, H. F. Jirandehi, S. Shirazian, "Effect of graphene oxide on modifying polyethersulfone membrane performance and its application in wastewater treatment," *Scientific Reports*, vol. 10, no. 1, pp. 1–11, 2020.
- [10] P. H. Krishnamurthy, L. T. Yogarathinam, A. Gangasalam, A. F. Ismail, "Influence of copper oxide nanomaterials in a poly(ether sulfone) membrane for improved humic acid and oil–water separation," *Journal of Applied Polymer Science*, vol. 133, no. 36, pp. 1–10, 2016.
- [11] S. L. Duraikkannu, R. Castro-Muñoz, A. Figoli, "A review on phase-inversion technique-based polymer microsphere fabrication," *Colloids and Interface Science Communications*, vol. 40, no. December 2020, 2021.
- [12] A. Fahrina, T. Maimun, S. Humaira, C.M. Rosnelly, M.R. Lubis, I. B. R. Sunarya, A. Ghufan, N. Arahman, "The morphology and filtration performances of poly (ether sulfone) membrane fabricated from different polymer solution," *MATEC Web of Conferences*, vol. 197, pp. 1–4, 2018.
- [13] P. D. Amin, V. Bhanushali, S. Joshi, "Role of Polyvinylpyrrolidone in Membrane Technologies," *International Journal of ChemTech Research*, vol. 11, no. 9, pp. 247–259, 2018.
- [14] Y. W. Guo, W. Cui, W. Xu, Y. Jiang, H. Liu, J. Xu, Z. Gao, L. Liu, "Effect of PVP hydrophilic additive on the morphology and properties of PVDF porous membranes," *Advanced Materials Research*, vol. 981, pp. 891–894, 2014.
- [15] S. Mansur, M. H. D. Othman, A. F. Ismail, M. N. Z. Abidin, N. Said, P. S. Goh, H. Hasbullah, S. H. S. A. Kadir, F. Kamal, "Study on the effect of PVP additive on the performance of PSf/PVP ultrafiltration hollow fiber membrane," *Malaysian Journal of Fundamental and Applied Sciences*, vol. 14, no. 3, pp. 343–347, 2018.

- [16] H. Mekarizadeh, A. Raisi, "Industrial wastewater treatment using PES UF membranes containing hydrophilic additives: Experimental and modeling of fouling mechanism," *Environmental Technology and Innovation*, vol. 23, p. 101701, 2021.
- [17] M. A. Tofighy, T. Mohammadi, M. H. Sadeghi, "High-flux PVDF/PVP nanocomposite ultrafiltration membrane incorporated with graphene oxide nanoribbons with improved antifouling properties," *Journal of Applied Polymer Science*, vol. 138, no. 4, pp. 1–15, 2021.
- [18] Y. Kourde - Hanafi, P. Loulergue, A. Szymczyk, B. Van der Bruggen, M. Nachtnebel, M. Rabiller-Baudry, J. L. Audic, P. Pölt, K. Baddari, "Influence of PVP content on degradation of PES/PVP membranes: Insights from characterization of membranes with controlled composition," *Journal of Membrane Science*, vol. 533, no. October 2016, pp. 261–269, 2017.
- [19] S. Arefi-Oskoui, A. Khataee, V. Vatanpour, "Effect of solvent type on the physicochemical properties and performance of NLDH/PVDF nanocomposite ultrafiltration membranes," *Separation and Purification Technology*, vol. 184, pp. 97–118, 2017.
- [20] N. Ucar, N. Kizildag, A. Onen, I. Karacan, O. Eren, "Polyacrylonitrile-polyaniline composite nanofiber webs: Effects of solvents, redoping process and dispersion technique," *Fibers and Polymers*, vol. 16, no. 10, pp. 2223–2236, 2015.
- [21] B. Eren, E. Eren, M. Guney, Y. C. Jean, J. D. Van Horn, "Positron annihilation lifetime spectroscopy study of polyvinylpyrrolidone-added polyvinylidene fluoride membranes: Investigation of free volume and permeation relationships," *Journal of Polymer Science*, vol. 58, no. 4, pp. 589–598, 2020.
- [22] L. F. Greenlee, N. S. Rentz, "Influence of nanoparticle processing and additives on PES casting solution viscosity and cast membrane characteristics," *Polymer*, vol. 103, pp. 498–508, 2016.
- [23] T. Anokhina, A. Raeva, S. Makaev, I. Borisov, V. Vasilevsky, and A. Volkov, "Express method of preparation of hollow fiber membrane samples for spinning solution optimization: Polysulfone as example," *Membranes*, vol. 11, no. 6, 2021.
- [24] D. S. Lakshmi, T. Cundari, E. Furia, A. Tagarelli, G. Fiorani, M. Carraro, A. Figoli, "Preparation of polymeric membranes and microcapsules using an ionic liquid as morphology control additive," *Macromolecular Symposia*, vol. 357, no. 1, pp. 159–167, 2015.
- [25] F. Russo, M. Bulzomi, E. Di Nicolò, C. Ursino, A. Figoli, "Enhanced anti-fouling behavior and performance of pes membrane by uv treatment," *Processes*, vol. 9, no. 2, pp. 1–17, 2021.
- [26] A. L. Ahmad, N. F. Shoparwe, N. H. E. Hanifa, "Equilibrium and kinetic study of bovine serum albumin (BSA) adsorption onto fabricated polyethersulfone (PES)/hydroxyapatite (HAP) adsorptive mixed matrix membrane (MMM)," *Journal of Physical Science*, vol. 30, no. Mmm, pp. 43–63, 2019.

- [27] K. A. Gebru, C. Das, "Effects of solubility parameter differences among PEG, PVP and CA on the preparation of ultrafiltration membranes: Impacts of solvents and additives on morphology, permeability and fouling performances," *Chinese Journal of Chemical Engineering*, vol. 25, no. 7, pp. 911–923, 2017.
- [28] A. K. Hołda, I. F. J. Vankelecom, "Understanding and guiding the phase inversion process for synthesis of solvent resistant nanofiltration membranes," *Journal of Applied Polymer Science*, vol. 132, no. 27, pp. 1–17, 2015.
- [29] A. Karimi, A. Khataee, V. Vatanpour, M. Safarpour, "The effect of different solvents on the morphology and performance of the ZIF-8 modified PVDF ultrafiltration membranes," *Separation and Purification Technology*, vol. 253, no. August, p. 117548, 2020.
- [30] Z. Sun, F. Chen, "Hydrophilicity and antifouling property of membrane materials from cellulose acetate/polyethersulfone in DMAc," *International Journal of Biological Macromolecules*, vol. 91, pp. 143–150, 2016.
- [31] S. Acarer, İ. Pir, M. Tüfekci, G. Türkoğlu Demirkol, N. Tüfekci, "Manufacturing and characterisation of polymeric membranes for water treatment and numerical investigation of mechanics of nanocomposite membranes," *Polymers*, vol. 13, no. 10, 2021.
- [32] H. Rafiei, M. Abbasian, R. Yegani, "Polyvinylidene fluoride as a neat and the synthesized novel membranes based on PVDF/polyvinyl pyrrolidone polymer grafted with TiO<sub>2</sub> nanoparticles through RAFT method for water purification," *Iranian Polymer Journal (English Edition)*, vol. 30, no. 8, pp. 769–780, 2021.
- [33] D. C. Hung, N. C. Nguyen, "Membrane processes and their potential applications for fresh water provision in Vietnam.," *Vietnam Journal of Chemistry*, vol. 55, no. 5, p. 533, 2017.
- [34] R. Kotsilkova, I. Borovanska, P. Todorov, E. Ivanov, D. Menseidov, S. Chakraborty, C. Bhattacharjee "Tensile and Surface Mechanical Properties of Polyethersulphone (PES) and Polyvinylidene Fluoride (PVDF) Membranes," *Journal of Theoretical and Applied Mechanics (Bulgaria)*, vol. 48, no. 3, pp. 85–99, 2018.
- [35] N. Arahman, S. Mulyati, M. R. Lubis, F. Razi, R. Takagi, H. Matsuyama, "Modification of polyethersulfone hollow fiber membrane with different polymeric additives," *Membrane Water Treatment*, vol. 7, no. 4, pp. 355–365, 2016.
- [36] T. T. Van Tran, S. R. Kumar, C. H. Nguyen, J. W. Lee, H. A. Tsai, C. H. Hsieh, S. J. Lue, "High-permeability graphene oxide and poly(vinyl pyrrolidone) blended poly(vinylidene fluoride) membranes: Roles of additives and their cumulative effects," *Journal of Membrane Science*, vol. 619, p. 118773, 2021.





SAKARYA ÜNİVERSİTESİ

# FEN BİLİMLERİ ENSTİTÜSÜ DERGİSİ

Sakarya University Journal of Science  
SAUJS

ISSN 1301-4048 e-ISSN 2147-835X Period Bimonthly Founded 1997 Publisher Sakarya University  
<http://www.saujs.sakarya.edu.tr/>

Title: Investigation of Pharmaceuticals in Sakarya Sewage Wastewater

Authors: Berna KIRIL MERT, Cemil YILMAZ, Nihan ÖZENGİN

Received: 2022-01-19 00:00:00

Accepted: 2022-10-17 00:00:00

Article Type: Research Article

Volume: 26

Issue: 6

Month: December

Year: 2022

Pages: 1209-1223

How to cite

Berna KIRIL MERT, Cemil YILMAZ, Nihan ÖZENGİN; (2022), Investigation of Pharmaceuticals in Sakarya Sewage Wastewater. Sakarya University Journal of Science, 26(6), 1209-1223, DOI: 10.16984/saufenbilder.1060212

Access link

<https://dergipark.org.tr/en/pub/saufenbilder/issue/74051/1060212>

New submission to SAUJS

<http://dergipark.gov.tr/journal/1115/submission/start>



## Investigation of Pharmaceuticals in Sakarya Sewage Wastewater

Berna KIRIL MERT<sup>\*1</sup> , Cemil YILMAZ<sup>1</sup> , Nihan ÖZENGİN<sup>2</sup> 

### Abstract

Active substances of drugs can cause various adverse effects by accumulating in the ecosystem. Many medications are resistant to biodegradation, given the recipient media in conventional wastewater treatment plants, and are thus released into the environment after only partial purification or no purification at all. The study focuses on 13 different pharmaceutical compounds belonging to drug classes of anti-depressants, antiepileptic's, anti-inflammatories, beta-blockers, lidocaine, and stimulants. These compounds were selected with reference to the literature as the ones most commonly encountered in domestic wastewater, surface, and groundwater. The presence of these compounds in the wastewater samples from Sakarya sewage and wastewater treatment plant was investigated. For this purpose, composite samples were taken at various sampling points, and duly analyzed. The analysis revealed the presence of the pharmaceutical residues in the sewage waters from Sakarya Municipality. Some of them were still present in the effluent of the treatment plant. On the other hand, fluoxetine, propranolol, and metoprolol drug active ingredients were not detected at any sampling point. Among all the compounds examined, the highest percentage of residues were observed in the case of active caffeine and paracetamol. In the light of these findings, advanced treatment units such as high-pressure membrane systems (including ozonizing, ultrafiltration, and reverse osmosis) can help adsorption rates at the treatment plant, increasing removal efficiency regarding drug compounds.

**Keywords:** Pharmaceutical compounds, sewage wastewater, treatment, removal

### 1. INTRODUCTION

Given the widespread use of personal care products and pharmaceuticals, their ingredients have been seeping into aquatic environments in ever-increasing rates. The most critical factors leading to increased drug consumption include socioeconomic factors such as developments in science and

technology as well as economic and cultural development, population growth, increased average life expectancy, urbanization, changes in income distribution, and the development of healthcare systems, not to mention the increase in the number of individuals who can benefit from these services [1].

\* Corresponding author: bkiril@sakarya.edu.tr

<sup>1</sup> Sakarya University

E-mail: cemil\_yilmaz@yahoo.com

ORCID: <https://orcid.org/0000-0001-6993-7916>, <https://orcid.org/0000-0002-0283-6296>

<sup>2</sup> Uludağ University

E-mail: nozengin@uludag.edu.tr

ORCID: <https://orcid.org/0000-0002-7647-921X>,



Water contamination may entail toxic effects on aquatic organisms, with consequences on the food chain, and cause direct effects on humans through consuming contaminated groundwater [2]. Usually, not all medication intake is retained by the human body; most is excreted in the form of urine and feces either in their original form or as active metabolites thereof [3]. The release of pharmaceuticals into the environment is quantified based on the dosage and the amount of drugs used, the frequency and intensity of excretion from the body, the tendency of the drug to be absorbed into solids, and the metabolic transformation capabilities of microorganisms in the wastewater treatment plant/storage area [4]. The amount of medical drugs used reach thousands of tons annually, and they eventually find their way into the sewage and treatment facilities. Although typical concentration levels detected are in the ng/L to low µg/L range, such micro-pollutants have still been observed to have toxic effects on aquatic organisms [5, 6].

These pollutants cannot be removed entirely during wastewater treatment. In addition, some pharmaceutical active substances are discharged from wastewater treatment plants to receiving environments almost unchanged. If they are not biodegradable or cannot be eliminated in treatment facilities, they can reach drinking water supply [7-9]. In this context, the problem is not limited to the drugs used in hospitals and homes. Drugs that are disposed of directly into the sewage system and garbage also contribute to the issue as primary sources of pollution [10]. Disposed drugs can mix with leachate water from landfills and cause pollution in aquatic systems [11]. Against this background, medicine ingredients that cannot be handily removed by wastewater treatment plants (WWTPs) cause pollution of groundwater and drinking water by being discharged into rivers, lakes, and estuaries [12, 13].

The conventional WWTPs' shortcomings in successfully removing PPCPs from wastewater pose major threats to aquatic

ecosystems and local water supply systems. There is growing concern over the detection of PPCPs in freshwater resources, and increasing amounts of evidence indicate the potential adverse effects their presence could have on aquatic life and the quality of resources future generations of humans will need. Most of these pollutants are persistent, ecotoxic, and bio-accumulative by nature, thereby posing severe threats to the aquatic food chain and biological resources [14].

Monitoring studies have been gaining importance in recent years due to the increase in the production and use of chemicals in the form of pharmaceuticals and personal care products. These substances' resistance to biological treatment, the lack of strict regulations on discharges to surface water bodies, and the potential health risks of such compounds in aquatic environments make the matter even more urgent. Monitoring data on various pharmaceutical residues in wastewater treatment plants and treated wastewater has been documented over the past two decades. Most of these data have been compiled from Europe and North America, along with some countries in Northeast Asia, such as Japan, South Korea, and China. In recent years, some but comparatively sparse data pertaining to Southeast Asian countries have also found their ways into the literature [15, 16]. However, a growing amount of research has been taking place in recent years, studying these substances' potential effects on the health of the ecosystem [17-19]. Various studies found medicinal drugs and their metabolites at high rates in wastewater treatment plant effluents, surface waters, underground, and drinking water. Their ranges and concentration levels in aquatic environments vary depending on many factors such as location, the composition of sewage, design and operation of wastewater treatment facilities, proximity to wastewater facilities, and weather conditions (especially floods) [20,21]. The observation of micro-contaminants arising from the use of medicinal drugs, in aquatic environments, and

their potential effects on living creatures in this environment cause ever-increasing concerns.

Until recently, regulations did not mandate monitoring the presence of pharmaceuticals in freshwaters or wastewaters. However, changes were slowly breeding in the regulatory scene. For instance, 2013 saw the issuance of Directive 2013/39/EU in the EU, to expand on existing directives 2000/60/EC and 2008/105/EC. The new regulations especially focused on pharmaceuticals in the wider field of water policy, in a bid to control and reduce the contamination of aquatic environments by these compounds [22]. In response to the changes in the regulatory framework, new high-quality monitoring and prioritization measures were taken to meet the requirements as per article 16 of Directive 2000/60/EC. As part of the efforts, a watch list covering a number of contaminants was created. The list provided the basis of the requirements to monitor the presence of the contaminants named, to record data, and to assess the risk they may pose on the environment. The initial watch list introduced in the decision 2015/495/EU was subsequently revised in 2018/840/EU. Two years later, a further revision followed as the Decision 2020/1161/EU. The latest decision names the pharmaceuticals to be monitored so as to collect data for detailed assessment. Some of these compounds such as the antibiotics amoxicillin, ciprofloxacin, erythromycin, clarithromycin, azithromycin, sulfamethoxazole, and trimethoprim; the hormones 17-Alpha-ethinylestradiol, 17-Beta-estradiol, and estrone; the synthetic hormone norethisterone; the antidepressant venlafaxine; and three antifungal pharmaceuticals, clotrimazole, fluconazole, miconazole were already included in earlier versions of the watch list [23].

Pharmaceutical products monitored in this study were selected among the products with the highest sales in Turkey according to IMS Turkey Pharmaceutical Index and IMS Turkey Hospital Index. The compounds

included in the study are Atenolol, Paracetamol, Caffeine, Lidocaine, Citalopram, Carbamazepine, Sertraline, Naproxen, Diclofenac, Etodolac, Metoprolol, and Propranolol. The presence of these compounds was investigated in samples taken from sewage and sewage treatment plants at certain points. Measures to be taken in the light of the data include curbing pharmaceutical use, prohibition or restriction of non-degradable substances. In parallel to these efforts waste control and reduction of discharge amounts, and appropriate storage will gain importance. The data will certainly inform efforts to make assessments regarding enhancing water treatment, and working with more advanced treatment systems.

## 2. MATERIAL AND METHOD

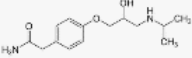
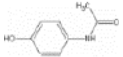
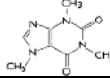
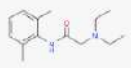
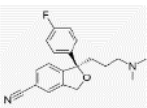
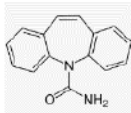
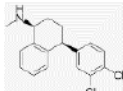
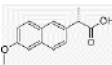
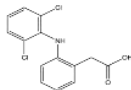
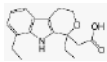
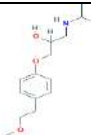

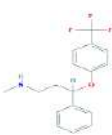
### 2.1. Monitored Pharmaceuticals

The pharmaceuticals monitored within the scope of the study are presented in Table 1.

### 2.2. Wastewater Sampling Points and Features

To determine the pharmaceutical concentrations in wastewater (both domestic and industrial) discharged into the sewage in Sakarya, sampling points were utilized in hospitals located on the sewerage network connecting to the Karaman Wastewater Treatment Facility serving the Sakarya region. In addition, samples were taken from the wastewater treatment plant influent and effluent. Located in the north of Sakarya Province, the Central Wastewater Treatment Facility affiliated with SASKI (Sakarya Water and Sewage Administration) treats wastewater from residences and industrial establishments. Wastewater from industrial establishments is pre-treated before being fed into the wastewater treatment facility. The facility is capable of treating 198,800 m<sup>3</sup>/day in dry weather and 271,941 m<sup>3</sup>/day in rainy weather. The facility's operations are based on two basic treatment methods: physical and biological.

Table 1 Properties of the pharmaceuticals analyzed [24].

Pharmaceutical products	Chemical Formula	CAS No	Molecular weight (g/mol)	Explanation
<b>Atenolol</b>		29122-68-7	266.3	Atenolol is a beta1-selective adrenergic antagonist.
<b>Paracetamol</b>		103-90-2	151.163	Paracetamol is an antipyretic and analgesic drug substance.
<b>Caffeine</b>		58-08-2	194.19	It is an alkaloid, also called guaranine or matein.
<b>Lidocaine</b>		137-58-6	234.34	Lidocaine is a medicine used to numb the tissue in a certain area.
<b>Citalopram</b>		59729-33-8	324.392	It is a selective serotonin reuptake inhibitor. Serotonin is the most selective molecule with the highest specificity.
<b>Carbamazepine</b>		298-46-4	236.269	Its primary use is in neuropathic pain relief and epilepsy medicine. It is not effective in absence seizures and myoclonus.
<b>Sertraline</b>		79617-96-2	306.229	Sertraline is an antidepressant that is a selective serotonin reuptake inhibitor.
<b>Naproxen</b>		22204-53-1	230.259	Naproxen is a non-steroidal anti-inflammatory drug.
<b>Diclofenac</b>		15307-86-5	296.14	Diclofenac is an effective medicine for pain relief on inflammatory conditions. It is a non-steroidal anti-inflammatory (NSAII) group drug.
<b>Etodolac</b>		41340-25-4	287.35	Etodolac is a non-steroidal and anti-inflammatory medicine derived from indole.
<b>Metoprolol</b>		51384-51-1	267.369	Metoprolol is a cardioselective beta-blocker commonly used in the treatment of hypertension and angina pectoris.
<b>Propranolol</b>		525-66-6	259.349	Propranolol is a non-selective beta-adrenergic receptor blocker (beta-blocker) widely used for the treatment of hypertension, heart rhythm, angina pectoris, and hyperthyroidism.
<b>Fluoxetine</b>		54910-89-3	309.332	Fluoxetine is a selective serotonin reuptake inhibitor (SSRI) commonly used as an antidepressant.

With the support of SASKI, the current situation in Sakarya Province was assessed by taking samples from specific points for a period of six months. The sampling points are as follows:

- Four different hospital outlets (Adatip Hospital, Altnova Hospital, Korucuk Training and Research Hospital, Sakarya Training and Research Hospital)
- Treatment plant intake and treatment plant outlet (at Karaman Wastewater Treatment Plant)
- One sewerage network

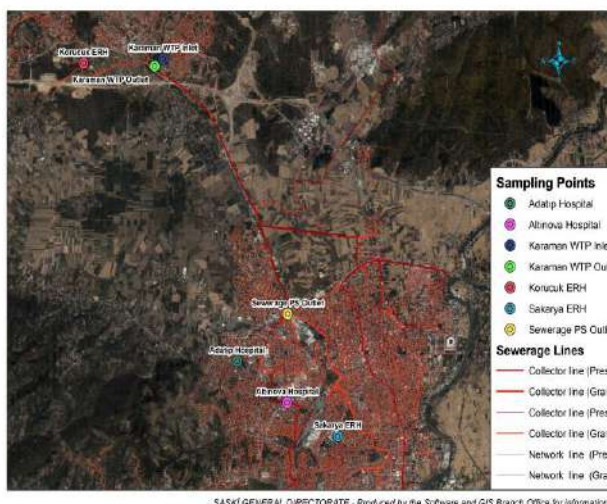


Figure 1 Map of sampling points

### 2.3. Pollutant Analysis Method

Prior to each round of analysis, mixed standard solution was prepared. The process involved diluting the stock solutions with ultrapure water produced by a Milli-Q unit. LC-MS-MS instrument was used for the analysis of microfoulers. The process took place on a liquid chromatography system (Agilent 6460 QQQ). An Agilent Poroshell C-18 (3x100mm, 2.7 $\mu$ m) column served as the medium of chromatographic separation, with 5  $\mu$ l injection volume. A gradient elution program was used at 0.5 ml min<sup>-1</sup> flow rate for both reservoirs with 5 mM ammonium formate + 0.1% formic acid in (A) water and (B) methanol. All samples were stored at 4°C in dark. Standards used are Sigma-Aldrich

(Steinheim, Germany) and Dr., which were purchased from Ehrenstorfer (Augsburg, Germany).

MS/MS experiments were carried out on an ion mass spectrometer running in positive ion mode with multiple reaction monitoring (MRM). Instrument control and data collection functions were managed on MassHunter analyst software. The nebulizer was set to 35 psi, whereas the flow rate was 11 L/min. The temperature of the nebulizer was set to 300°C. The capillary voltage setting was 3,500 V while the source temperature was set to 400°C. The recoveries of samples extracted for quality assurance/quality control were calculated by comparing wastewater samples. With the calibration curve of 13 pharmaceuticals and good linearity, the R<sup>2</sup> value for each micro-contaminant was found to be higher than 0.999.

TOC, COD, SS, and Ammonia parameters were set as per standard methods [25]. Analyses of pH, TDS, and conductivity parameters were performed with a multi-parameter measuring device (Hach HQ440d-Hach-Lange GmbH). The analyses for COD and TOC parameters, in turn, were based on 5310-B high-temperature catalytic oxidation method, using the 5220-D closed colorimetric reflux method for COD, and Teledyne Tekmar analyzer for TOC. The suspended solid (SSM) content of the samples was analyzed by drying at 103-105°C temperature range as stipulated by the 2540-D gravimetric method. Ammonia was produced through 4500 NH<sub>3</sub> B: Pre-Distillation Method.

## 3. RESULTS AND DISCUSSION

### 3.1. Sewage water characterization

The wastewater characteristics of the samples taken at the sampling points shown in Figure 1 are presented in Table 2.

Table 2 Sewage water samples analysis results.

Sampling Points	pH	Tds (mg/L)	EC ( $\mu\text{S}/\text{cm}$ )	TOC (mg/L)	COD (mg/L)	NH <sub>3</sub> (mg/L)	SS (mg/L)
Altınova Hospital	9.34	1601	827	98.60	508	24	115
Adatıp Hospital	8.02	674	327	23.64	180	4.3	25
Karaman WTP Inlet	8,15	953	476	21.27	256	4.2	220
Karaman WTP Outlet	8.08	791	382	10.03	22	2.3	20
Korucuk ERH	10.15	855	422	29.64	194	1.8	80
Sewage PS Outlet	8.13	753	368	18.79	96	4.2	35
Sakarya ERH	7.78	454	218,1	68.57	332	3.1	35

### 3.2. Pharmaceutical Values

Thirteen different pharmaceutical compounds including Paracetamol, Caffeine, Lidocaine, Citalopram, Carbamazepine, Sertraline, Naproxen, Diclofenac, Etodolac, Metoprolol, Propranolol, Fluoxetine (anti-depressants, antiepileptic's, anti-inflammatories, beta-blockers, lidocaine, and stimulant) were found in varying concentration levels. The results are presented below.

#### 3.2.1. Anti-depressants

Anti-depressants find their way into M-WWTs either in their original form, or in the form of their metabolized products present in human urine. For example, around 20 to 30 percent of fluoxetine taken is metabolized in human body, to form the active metabolites of the compound –i.e. fluoxetine glucuronide and norfluoxetine–, while the rest remains unprocessed, and eventually reaches sewage plants [26].

Golovko et al. (2014) kept track of citalopram and sertraline compounds in the inlet and outlet waters of a treatment plant for one year. At the inlet of the treatment plant, the concentration levels of these compounds were found to vary in the 0.027-0.18  $\mu\text{g}/\text{L}$  and 0.007-0.027  $\mu\text{g}/\text{L}$  ranges, respectively. At the outlet, the measured ranges for the two compounds were 0.03-0.12  $\mu\text{g}/\text{L}$  and 0.003-0.006  $\mu\text{g}/\text{L}$ , respectively [27]. The treatment

plant removal efficiencies for these compounds were found to be 18% and 81%, respectively. Another important study observed fluoxetine and sertraline compounds in fish [20].

As seen in Figure 2, in this study, fluoxetine was not observed in any sample taken from various points of the sewage system and at the wastewater treatment plant's inlet and outlet. Sertraline, in turn, was found only at the Korucuk Hospital sampling point, and at 0.2163  $\mu\text{g}/\text{L}$  concentration level, while Citalopram was found only in the samples taken at Altınova Hospital (0.9399  $\mu\text{g}/\text{L}$  concentration level) and at Korucuk Hospital (0.2312  $\mu\text{g}/\text{L}$  concentration level).

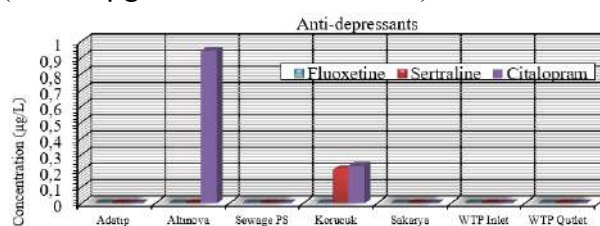


Figure 2 Antidepressant concentration levels at sampling points

#### 3.2.2. Antiepileptics

Carbamazepine is a widely prescribed antiepileptic that is included in the EU's watch list of substances under the Water Framework Directive. The compound is observed often in groundwater, and at relatively high concentrations then. In the literature, the



maximum concentration levels noted for carbamazepine was 0.39  $\mu\text{g/L}$  in 42% of samples collected from 164 locations in 23 European countries [28]. Nam et al. (2014), in turn, measured carbamazepine concentrations at wastewater treatment plants in the summer and winter months, to find 0.0031-0.0307  $\mu\text{g/L}$  and 0.0052-0.0464  $\mu\text{g/L}$  ranges, respectively [29]. In the present study, no carbamazepine was detected in the samples taken at the Altınova hospital (Figure 3). However, that observation proved to be an outlier, and concentrations in the 0.1462-0.4651  $\mu\text{g/L}$  range were observed at other sampling locations. The concentration level at the wastewater treatment plant's intake was 0.2508  $\mu\text{g/L}$ , compared to the 0.2438  $\mu\text{g/L}$  figure measured at the plant's outlet. In a similar study, carbamazepine concentration levels in inlets and outlets of wastewater treatment plants in different countries were found to be in <0.04-3.78  $\mu\text{g/L}$  and <0.005-4.60  $\mu\text{g/L}$  ranges, respectively. Moreover, lifting efficiency was reported to be in the 0–62.3% range [30]. The results of the present study are consistent with these ranges noted in the literature.

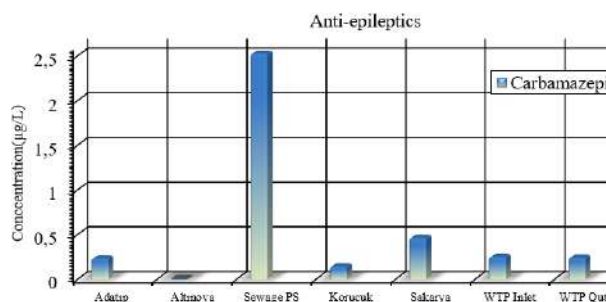


Figure 3 Antiepileptic concentration levels at sampling points

Previous studies show that some pharmaceutical compounds can be removed from the wastewater through adsorption taking place in physical purification processes. Other compounds, such as ibuprofen, naproxen, sulfamethoxazole, and iopromide compounds, in turn, can be eliminated through subsequent biological treatment stages, which achieve 30 to 75% removal rates for most anti-inflammatories

and antibiotics. Carbamazepine is not one of them, however. Several reports show that wastewater treatment facilities are not effective in removing significant amounts of carbamazepine from wastewater [31-33].

### 3.2.3. Anti-inflammatories

Like antibiotics, NSAIDs such as naproxen and diclofenac can potentially be extremely toxic for various bacteria. Aquatic environments as well as human life are also subject to significant risks these substances may pose. In response, the European Union included diclofenac in the first version of the watch list (WL) issued under the Water Framework Directive (WFD) in 2015 (Decision 2915/495). More recently, however, the substance was removed from the WL under Decision 2020/1161, given the availability of adequate levels of high quality data produced through monitoring efforts [26].

Ibuprofen, diclofenac and paracetamol are the anti-inflammatories and analgesics which are most commonly detected in groundwater. The reason is their extensive consumption in response to the symptoms of a number of conditions. Mutiyar et al. (2018) noted that diclofenac is used commonly to treat pain and other symptoms suffered by human patients. However, a rather less expected use case of the substance is prevalent in livestock farming. Nonetheless, it is observed that the use of diclofenac on animal populations has been decreasing due to rapid urbanization [3]. In Delhi, India, the Yamuna River into which sewage waters are also discharged, ibuprofen and paracetamol compounds are detected, with average concentrations of 1.49 and 1.08  $\mu\text{g/L}$ , respectively. Vystavna et al. (2017) detected 12 compounds in samples taken in 2012 and 2015 from the influent and effluent of the treatment plant [34]. It was also noteworthy that the measured concentrations of naproxen, triclosan, paracetamol, ibuprofen and carbamazepine detected in the influent of the plant had increased in that time frame. The most significant increases were observed in

the case of carbamazepine and naproxen, the concentration levels of which increased by 50 and 10 times, respectively. In contrast, the input concentrations of diclofenac and caffeine were reduced significantly.

The analysis of samples from Udy River exhibited decreasing concentration levels for diclofenac (-97%), triclosan (-88%), caffeine (-80%), and paracetamol (-5%), and increasing concentration levels for ibuprofen (+80%) and carbamazepine (+96%). Removal efficiencies observed in both years covered in the study were greater than 80% (high) for propranolol and naproxen, and between 50 and 80% (moderate) for other compounds included in the analysis.

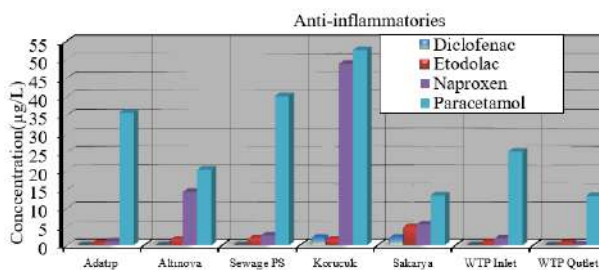


Figure 4 Anti-inflammatory concentration levels at sampling points

In this study, as seen in Figure 4, diclofenac was detected only in the samples taken at Korucuk and Sakarya Hospitals, with 2.3469 µg/L and 2.3234 µg/L concentration levels, respectively. Etodolac, Naproxen and Paracetamol compounds were detected in the 0.8683-5.2467 µg/L, 0.2362-48.8507 µg/L, and 13.3412-52.5798 µg/L ranges for all sampling locations, respectively. The results presented in another study for wastewater analyses conducted in different countries are close to the results reached here. The concentration level of diclofenac in wastewater was 3 µg/L, with a corresponding removal efficiency level of 17%. The comparable figures for naproxen were 1.8-40.7 µg/L and 40-100%, while the figures for paracetamol were 6.9 µg/L and 100% [35].

Paracetamol was detected in various European sewage wastewater treatment plants, with concentration levels ranging

around 6 mg/L. Higher concentration figures were found elsewhere though, with values up to 10 mg/L being observed in some surface waters in the US, and up to 65 mg/L in the Tyne River in England. In addition, a study on organic wastewater pollutants in US waters found paracetamol in surface waters, at a maximum concentration of 10 µg/L with a frequency of 23.8 % [36].

Paracetamol is the most widely used analgesic/antipyretic globally and is a very common occurrence in hospital wastewaters (HWW), with concentration levels in  $10^1$  to  $10^3$  µg/L range. Paracetamol was also found in hospital sewage samples (at 7.5 µg/L concentration levels). Diclofenac is another typical analgesic, with concentrations in HWW ranging between  $10^{-1}$  and  $10^2$  µg/L. Diclofenac concentrations in 0.83 to 3.59 µg/L range were detected in another set of HWW samples [37].

### 3.2.4. Beta Blockers

In a study on beta blocker concentrations in the city of Barcelona, Spain, Lopez-Serna et al. (2013) found various concentrations of propranolol ( $< 0.00938$  µg/L) and metoprolol (at most 0.355 µg/L) in groundwater samples. In the case of wastewater, the picture varied from site to site, with the concentrations of atenolol observed in Cuernavaca, Mexico were around half of those detected in India [38].

The average concentration of atenolol reported in wastewater worldwide is 4.5 µg/L. At the inlet of the Acapantzingo treatment plant in Mexico, very high concentration levels were recorded for atenolol (0.2-3.1 µg/L) [39]. In another study, the atenolol compound was observed in relatively substantial concentrations as high as 21,610 µg/L in wastewater samples taken from municipal wastewater treatment plants after the final settling [40].

In this study, propranolol and metoprolol compounds were not detected at any point.



Atenolol concentration levels, in turn, were found to be 0-0.8949  $\mu\text{g/L}$ . No atenolol was detected in the treatment plant's inlet and outlet (Figure 5).

In a similar study, Tran et al. (2018) found the following concentration levels at the influent and effluents of wastewater treatment plants for atenolol: 0-0.294.7  $\mu\text{g/L}$  in Asia, 0.5-2.642  $\mu\text{g/L}$  in North America, and 0-0.0331  $\mu\text{g/L}$  in Europe. In the case of metoprolol, the concentration levels Tran et al. found were 0-0.0795  $\mu\text{g/L}$  in Asia, 0.016-0.154  $\mu\text{g/L}$  in North America, and 0-4.148  $\mu\text{g/L}$  in Europe. Finally, their results for propranolol were 0-0.00956  $\mu\text{g/L}$  in Asia, and 0-1.962  $\mu\text{g/L}$  in Europe, which is quite low [16].

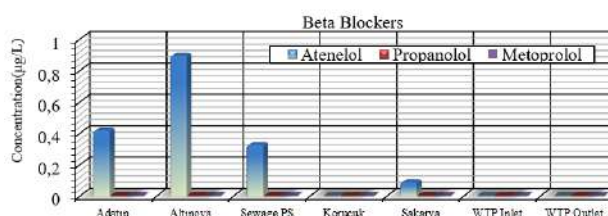


Figure 5 Beta Blockers' concentration levels at sampling points

### 3.2.5. Lidocaine

Local anaesthetic Lidocaine (LDC), also used as an antiarrhythmic agent, is another widely prescribed drug. Recent studies found LDC in wastewater samples from wastewater treatment plants, as well as samples taken from some rivers and lakes in Europe and North America. However, the data available on the removal rates achieved at wastewater treatment plants with respect to these compounds and their metabolites is limited.

While the amount of LDC at various points in Lake Constance, Switzerland was measured as 0.001  $\mu\text{g/L}$  [41], levels as high as 0.01  $\mu\text{g/L}$  were observed in surface waters in the Netherlands [42]. Oftentimes, studies on LDC presence in wastewater and its behavior in treatment plants found concentration levels in excess of 1  $\mu\text{g/L}$  in untreated wastewater.

Rarely can wastewater treatment plants achieve complete removal of these compounds, often resulting in their discharge to receiving waters. The presence of these drugs –either in their original form or in the form of their metabolites– in surface waters is important because their infiltration into groundwater can pose a problem in terms of water quality. The average LDC concentration level noted in the literature is 0.107  $\mu\text{g/L}$ , as observed in samples from wastewater treatment plants that only treat wastewater from homes and hospitals [42]. In this study, however, the Lidocaine levels in the samples ranged from 0.2207  $\mu\text{g/L}$  to 4.8735  $\mu\text{g/L}$ , with those taken at the intake of the treatment plant being on the lower end of the range (Figure 6). Furthermore, LDC was found to be completely removed at the outlet of the plant.

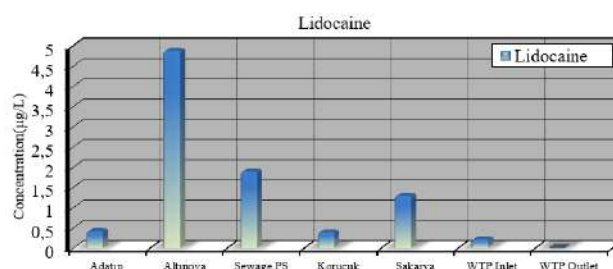


Figure 6 Lidocaine concentration levels at sampling points

### 3.2.6. Stimulant

Humans consume substantial amounts of coffee, tea and soft drinks containing caffeine, which is a most common stimulant. The average concentration of caffeine in these popular drinks is 360  $\text{mg/L}$ . Upon discharge from human body in the form of urine, the substance reaches the sewage system. Studies have proven that caffeine can contaminate sewage wastewater, septic tanks, wastewater leachate and surface waters to which wastewater is discharged. Eventually, the substance finds its way to ground water.

Various studies have shown the presence of caffeine in sewage effluent, septic tanks, not to mention landfill leachates. Eventually, these sources lead to the contamination of surface water. From that point on, it is only a

matter of time for the substance to reach groundwater sources through contamination during the natural process of water recycling [28].

The substance is so widely consumed, and thus extremely high concentrations are not surprising to find in the environment. For instance, concentration levels reaching 146  $\mu\text{g/L}$  have been reported in wastewater samples. Average caffeine concentrations measured at the inlets and outlets of various wastewater treatment plants in Seville, Spain, varied between 0.22–11.40  $\mu\text{g/L}$  and 0.15–3.20  $\mu\text{g/L}$ , respectively [43]. Yet another study reported caffeine concentration levels in the 12–499  $\mu\text{g/L}$  range in a number of samples taken from wastewaters [44].

In the present study, the highest concentration of caffeine was detected in the samples taken at Korucuk Hospital, reaching 120  $\mu\text{g/L}$ . The levels for the samples taken at other sites were also substantial. The intake of the treatment plant contained 33.8718  $\mu\text{g/L}$  caffeine. However, it is noteworthy that the plant's removal rate for the substance was 100%. In Figure 7, the caffeine concentration values at the sampling points are given. Similar findings are reported in the literature, with removal efficiencies in the 49.9–99.6% range published for conventional wastewater treatment plants in China, Europe, Greece, Korea, Spain, and England [30].

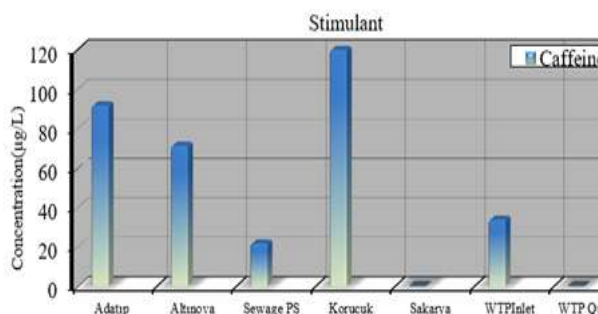


Figure 7 Stimulant concentration levels at sampling points

It is also noteworthy that Caffeine was also detected in Costa Rica's WWTPs with mean concentration in the influent being 69.9  $\mu\text{g/L}$  [45].

#### 4. CONCLUSIONS

In the study, 13 different pharmaceutical compounds were investigated in sewage samples taken from 7 different measurement points, which are mainly from Sakarya sewerage and Karaman Wastewater Treatment Plant. The highest measured values are as follows: at Altinova sampling point, antidepressant citalopram with a concentration level of 0.9399  $\mu\text{g/L}$ , beta blocker atenolol with a concentration level of 0.8949  $\mu\text{g/L}$  and LDC with a concentration level of 4.8735  $\mu\text{g/L}$ , at the Sewage PS sampling point, antiepileptic carbamazepine with a concentration level of 2.5281  $\mu\text{g/L}$ , and at the Korucuk sampling point, anti-inflammatory paracetamol with a concentration level of 52.5798  $\mu\text{g/L}$ , and stimulant caffeine with a concentration level of 120  $\mu\text{g/L}$ . Fluoxetine, propranolol and metoprolol pharmaceutical compounds could not be detected at any sampling point.

The conventional treatment plant covered in the study was found to have efficiency levels in excess of 85% for caffeine, lidocaine and naproxen, whereas the plant's efficiency level was as low as 3% for carbamazepine. For pharmaceuticals that are difficult to remove, it is possible to achieve better removal efficiencies reaching 99.7% through advanced treatment. In this context, it is advisable to implement advanced treatment methods for conventional treatment units as well. These results highlight the alarming level of contamination of surface waters, and put the issue to the forefront of environment debate. On the other hand, the findings of this study show that, at current levels, there is no risk of acute toxicity of drug active ingredients. However, the threat of chronic effects cannot be ignored, given the fact that of multiple drugs find their way into water sources. Further monitoring of aquatic environments in

this area will make it easier to assess and evaluate aquatic organisms' and the environment's chronic or long-term exposure to these new types pollutants. Understanding the problem will be the first step for the efforts to improve water quality through better wastewater management.

#### ***Acknowledgments***

We would like to thank Sakarya Water and Sewerage Administration for their support in sampling and contributing to our work.

#### ***Funding***

This study was supported by the Science Master's Thesis Project named "Investigation of Drug Compounds in Sewage Water in Sakarya Province" within the scope of Sakarya University Scientific Research Projects numbered "2013-50-01-010".

#### ***The Declaration of Conflict of Interest/ Common Interest***

No conflict of interest or common interest has been declared by the author.

#### ***Authors' Contribution***

The authors contributed equally to the study.

#### ***The Declaration of Ethics Committee Approval***

This study does not require ethics committee permission or any special permission.

#### ***The Declaration of Research and Publication Ethics***

The authors of the paper declare that he complies with the scientific, ethical, and quotation rules of SAUJS in all processes of the paper and that he does not make any falsification on the data collected. In addition, he declares that Sakarya University Journal of Science and its editorial board have no responsibility for any ethical violations that may be encountered and that this study has not been evaluated in any academic publication environment other than Sakarya University Journal of Science.

## **REFERENCES**

- [1] R. R. Z. Tarpani, A. Azapagic "Life cycle environmental impacts of advanced wastewater treatment techniques for removal of pharmaceuticals and personal care products (PPCPs)," *Journal of Environmental Management*, vol. 215, pp. 258-272, June 2018.
- [2] C. Morosini, E. Postè, M. Mostachetti, Vincenzo Torretta, "Pharmaceuticals in water cycle: a review on risk assessment and wastewater and sludge treatment," *Environmental Engineering and Management Journal*, Vol.19, No. 8, 1339-1378, August 2020.
- [3] P. K. Mutiyar, S. K. Gupta, A. K. Mittal, "Fate of pharmaceutical active compounds (PhACs) from River Yamuna, India: An ecotoxicological risk assessment approach," *Ecotoxicology and Environmental Safety*, vol. 150, pp. 297-304, 15 April 2018.
- [4] C. G. Daughton, T. A. Ternes, "Pharmaceuticals and personal care products in the environment: agents of subtle change," *Environmental Health Perspectives*, vol. 107, pp 907-938, 6 December 1999.
- [5] G. Knopp, C. Prasse, T. A. Ternes, P. Corne, "Elimination of micropollutants and transformation products from wastewater treatment plant effluent through pilot scale ozonation followed by various activated carbon and biological filters," *Water Research*, vol. 100, pp. 580-592, 1 September 2016.
- [6] C. Dai, S. Li, Y. Duan, K. H. Leong, Y. Tu, L. Zhou, "Human health risk assessment of selected pharmaceuticals in the five major river basins, China," *Science of The Total Environment*, 801, 149730, 2021.

- [7] Q. Sui, J. Huang, S. Deng, G. Yu, Q. Fan, "Occurrence and removal of pharmaceuticals, caffeine and DEET in wastewater treatment plants of Beijing, China," *Water Research*, vol. 44, pp. 417–426, 2010.
- [8] B. Subedi, N. Codru, D. M. Dziewulski, L. R. Wilson, J. Xue, S. Yun, K. Kannan, "A pilot study on the assessment of trace organic contaminants including pharmaceuticals and personal care products from on-site wastewater treatment systems along Skaneateles Lake in New York State, USA," *Water Research*, vol.72, pp.28-39, 2015.
- [9] B. Subedi, K. Balakrishna, D. I. Joshua, K. Kannan, "Mass loading and removal of pharmaceuticals and personal care products including psychoactives, antihypertensives, and antibiotics in two sewage treatment plants in southern India," *Chemosphere*, vol. 167, pp. 429-437, January 2017.
- [10] A. J. Ebele, M. A. E. Abdallah, S. Harrad, "Pharmaceuticals and personal care products (PPCPs) in the freshwater aquatic environment," *Emerging Contaminants*, vol 3(1), p.p1-16., 2017.
- [11] Holm, M. Bakken, O. Vangen, R. Rekaya, "Genetic analysis of age at first service, return rate, litter size, and weaning-to-first service interval of gilts and sows," *Journal Animal Science* vol. Pp. 83:41-48, 2005.
- [12] K. Fent, A. A. Weston, D. Caminada, "Ecotoxicology of human pharmaceuticals," *Aquatic Toxicology*, vol.76 (2), p.p 122-159, 2006.
- [13] A, Kurt, B. K. Mert, N. Özengin, Ö. Sivrioğlu, T. Yonar, "Treatment of antibiotics in wastewater using advanced oxidation processes (AOPs)," *Physico-Chemical Wastewater Treatment and Resource Recovery*, Intech Open Science, Londrina, pp. 175-211, 2017.
- [14] V. Singh, S. Suthar, "Occurrence, seasonal variations, and ecological risk of pharmaceuticals and personal care products in River Ganges at two holy cities of India," *Chemosphere*, 268, 129331, 2021.
- [15] N. Han Tran, K. Y. Hoong Gin, "Occurrence and removal of pharmaceuticals, hormones, personal careproducts, and endocrine disrupters in a full-scale water reclamation plant," *Science of the Total Environment*, pp.1503–1516, 2017.
- [16] N. Han Tran, M. Reinhard, K. Y. Hoong Gin, "Occurrence and fate of emerging contaminants in municipal wastewater treatment plants from different geographical regions-a review," *Water Research*, vol. 133, pp. 182-207, 2018.
- [17] S. Gaw, K. V. Thomas, T. H. Hutchinson, "Sources, impacts and trends of pharmaceuticals in the marine and coastal environment," *Philos Trans R Soc. Lond. B Biol Sci.*, 369(1656), Nov 19 2014.
- [18] P. K. Jjemba, "Excretion and ecotoxicity of pharmaceutical and personal care products in the environment," *Ecotoxicology and Environmental Safety*, vol. 63, no. 1, 2006, pp. 113-130, January 2006.
- [19] D. W. Kolpin, E. T. Furlong, M. T. Meyer, E. M. Thurman, S. D. Zaugg, L. B. Barber, H. T. Buxton, "Pharmaceuticals, Hormones, and Other Organic Wastewater Contaminants in U.S. Streams, 1999–200: A National Reconnaissance," *Environmental Science Technology*, vol.36, no.6, pp. 1202–1211, 2002.

- [20] Nikolaou, S. Meric, D. Fatta, "Occurrence patterns of pharmaceuticals in water and wastewater environments. *Analytical and Bioanalytical Chemistry*," vol. 387, no.4, pp. 1225-1234, 2007.
- [21] J. Sui, H. Afzalimehr, A. K. Samani, M. Maherani, "Clear-water scour around semi-elliptical abutments with armored beds," *International Journal of Sediment Research*, vol.25, no.3, pp. 233-245, 2010.
- [22] A. S. Ajibola, S. T. Fawole, F. O. Ajibola, G. O. Adewuyi, "Diclofenac and ibuprofen determination in sewage sludge using a QuEChERS approach: Occurrence and ecological risk assessment in three Nigerian wastewater treatment plants," *Bulletin of Environmental Contamination and Toxicology*, 106(4), 690-699, 2021.
- [23] J. P. Fernandes, C. M. R. Almeida, M. A. Salgado, M. F. Carvalho, A. P. Mucha, "Pharmaceutical compounds in aquatic environments—Occurrence, fate and bioremediation prospective," *Toxics*, 9(10), 257, 2021.
- [24] PubChem, National Institutes of Health. (2022). National Library of Medicine [Online] Available: <https://pubchem.ncbi.nlm.nih.gov>
- [25] E. W. Rice, R. B. Baird, A. D. Eaton, L. S. Clesceri, APHA, Standard methods for the examination of water and wastewater, 21th Ed. American Public Health Association Publication, Washington, USA, 2012.
- [26] O. F. S. Khasawneh, P. Palaniandy, "Occurrence and removal of pharmaceuticals in wastewater treatment plants," *Process Safety and Environmental Protection*, 150, 532-556, 2021.
- [27] O. Golovko, V. Kumar, G. Fedorova, T. Randak, R. Grabic, "Seasonal changes in antibiotics, antidepressants/psychiatric drugs, antihistamines and lipid regulators in a wastewater treatment plant," *Chemosphere*, vol. 111, pp. 418–426, 2014.
- [28] Q. Sui, X. Cao, S. Lu, W. Zhao, Z. Qiu, G. Yu, "Occurrence, sources and fate of pharmaceuticals and personal care products in the groundwater: A review" *Emerging Contaminants*, pp.14-24, 2015.
- [29] S. W. Nam, B.-Il Jo, Y. Yoon, K. D. Zoh, "Occurrence and removal of selected micropollutants in a water treatment plant," *Chemosphere*, vol.95, pp.156–165, 2014.
- [30] Y. Luo, W. Guo, H. H. Ngo, L. D. Nghiem, F. I. Hai, J. Zhang, S. Liang, X C. Wang, "A review on the occurrence of micropollutants in the aquatic environment and their fate and removal during wastewater treatment," *Science of the Total Environment*, vol. 473–474, pp. 619–641, 2014.
- [31] Strenn, M. Clara, O. Gans, N. Kreuzinger, "Carbamazepine, diclofenac, ibuprofen and bezafibrate-investigations on the behaviour of selected pharmaceuticals during wastewater treatment," *Water Science Technology*., vol.50 (5), pp. 269–276, 2004.
- [32] M. Clara, B. Strenn, O. Gans, E. Martinez, N. Kreuzinger, H. Kroiss, "Removal of selected pharmaceuticals, fragrances and endocrine disrupting compounds in a membrane bioreactor and conventional wastewater treatment plants," *Water Research*. Vol.39 (19), pp. 4797-4807, 2005.

- [33] J. Rivera-Utrilla, M. Sánchez-Polo, M. Á. Ferro-García, G. Prados-Joya, R. Ocampo-Pérez, “Pharmaceuticals as emerging contaminants and their removal from water. A review,” *Chemosphere*, vol. 93(7), pp. 1268-1287, 2013.
- [34] Y. Vystavnaa, Z. Frkova, L. Marchan, Y. Vergeles, F. Stolberg, “Removal efficiency of pharmaceuticals in a full scale constructed wetland in East Ukraine”, *Ecological Engineering*, vol.108, , pp.50-58, November 2017.
- [35] Ş. Saygı, D. Battal, N. Ö. Şahin, “Çevre ve insan sağlığı yönünden ilaç atıklarının önemi,” *Marmara Pharmaceutical Journal*, vol. 16, pp. 82-90, 2012.
- [36] M. Khamis, R. Karaman, F. Ayyash, A. Qtait, O. Deeb, A. Manssra, “Efficiency of Advanced Membrane Wastewater Treatment Plant towards Removal of Aspirin, Salicylic Acid, Paracetamol and p-Aminophenol,” *Journal of Environmental Science and Engineering*, vol. 5, pp. 121-137, 2011.
- [37] E. A. Serna-Galvis, A. M. Botero-Coy, M. Rosero-Moreano, J. Lee, F. Hernández, R. A. Torres-Palma, “An initial approach to the presence of pharmaceuticals in wastewater from hospitals in Colombia and their environmental risk,” *Water*, 14(6), 950, 2022.
- [38] R. Lopez-Serna, A. Jurado, E. Vazquez-Sune, J. Carrera, M. Petrovic, D. Barcelo, “Occurrence of 95 pharmaceuticals and transformation products in urban groundwaters underlying the metropolis of Barcelona, Spain,” *Environmental Pollution*, vol.174, pp.305-315, 2013.
- [39] J. A. Rivera-Jaimes, C. Postigo, R. M. Melgoza-Alemán, J. Aceña, D. Barceló, M. López de Alda “Study of pharmaceuticals in surface and wastewater from Cuernavaca, Morelos, Mexico: Occurrence and environmental risk assessment,” *Science of the Total Environment*, vol.613-614, pp.1263-1274, 2018.
- [40] R. Salgado, V. J. Pereira, G. Carvalho, R. Soeiro, V. Gaffney, C. Almeida, V. Vale Cardoso, E. Ferreira, M.J. Benoliel, T.A. Ternes, A. Oehmen, M.A.M. Reis, J. P. Noronha, “Photodegradation kinetics and transformation products of ketoprofen, diclofenac and atenolol in pure water and treated wastewater,” *Journal of Hazardous Materials*, vol. 244- 245, pp. 516- 527, 2013.
- [41] P. C., Rua-Gomez, W. Püttmann, “Occurrence and removal of lidocaine, tramadol, venlafaxine, and their metabolites in German wastewater treatment plants,” *Environmental Science and Pollution Research*, vol.19(3), pp.689-699, 2012a.
- [42] P. C., Rua-Gomez, W. Püttmann, “Impact of wastewater treatment plant discharge of lidocaine, tramadol, venlafaxine and their metabolites on the quality of surface waters and groundwater,” *Journal of Environmental Monitoring*, vol. 12, pp. 3047- 3310, 22 November 2012b.
- [43] J. L. Santos, I. Aparicio, E. Alonso, “Occurrence and risk assessment of pharmaceutically active compounds in wastewater treatment plants. A case study: Seville city (Spain),” *Environment International*, vol. 33, pp. 596-601, 2007.
- [44] J. M. Philip, U.K. Aravind, C. T. Aravindakumar, “Emerging contaminants in Indian environmental matrices - A review,” *Chemosphere*, vol. 190, pp.307-326, 2018.

- [45] D. Ramírez-Morales, M. Masís-Mora, J.R. Montiel-Mora, J. C. Cambronero-Heinrichs, S. Briceño-Guevara, C. E. Rojas-Sánchez, M. Méndez-Rivera, V. Arias-Mora, R. Tormo-Budowski, L. Brenes-Alfaro, C. E. Rodríguez-Rodríguez, “Occurrence of pharmaceuticals, hazard assessment and ecotoxicological evaluation of wastewater treatment plants in Costa Rica,” *Science Total Environment*, 746, 141200, 2020.



SAKARYA ÜNİVERSİTESİ

# FEN BİLİMLERİ ENSTİTÜSÜ DERGİSİ

Sakarya University Journal of Science  
SAUJS

ISSN 1301-4048 e-ISSN 2147-835X Period Bimonthly Founded 1997 Publisher Sakarya University  
<http://www.saujs.sakarya.edu.tr/>

Title: Synthesis, DPPH and ABTS Activity of Novel Furfuryl-Chalcone Derivatives

Authors: Fatih SÖNMEZ, Enes AKGÜN, Zuhul ŞAHİN

Received: 2022-05-23 00:00:00

Accepted: 2022-10-17 00:00:00

Article Type: Research Article

Volume: 26

Issue: 6

Month: December

Year: 2022

Pages: 1224-1232

How to cite

Fatih SÖNMEZ, Enes AKGÜN, Zuhul ŞAHİN; (2022), Synthesis, DPPH and ABTS Activity of Novel Furfuryl-Chalcone Derivatives. Sakarya University Journal of Science, 26(6), 1224-1232, DOI: 10.16984/saufenbilder.1119766

Access link

<https://dergipark.org.tr/en/pub/saufenbilder/issue/74051/1119766>

New submission to SAUJS

<http://dergipark.gov.tr/journal/1115/submission/start>



## Synthesis, DPPH and ABTS Activity of Novel Furfuryl-Chalcone Derivatives

Fatih SÖNMEZ<sup>\*1</sup> , Enes AKGÜN<sup>2</sup> , Zuhâl ŞAHİN<sup>1</sup> 

### Abstract

In this study, novel furfuryl-chalcone derivatives substituted sulfonyl chloride or sulphonamide were synthesized. Their antioxidant properties were investigated via DPPH and ABTS assays. All furfuryl-chalcones had high antioxidant properties. Among them, (E)-5-(3-(4-(chlorosulfonyl)-3-hydroxyphenyl)-3-oxoprop-1-en-1-yl)furan-2-sulfonyl chloride (4e) and (E)-5-(3-(3-(chlorosulfonyl)-4-hydroxyphenyl)-3-oxoprop-1-en-1-yl)furan-2-sulfonyl chloride (4d) exhibited the highest DPPH activity with the IC<sub>50</sub> values of 4.23 μM and 6.68 μM, respectively, which are almost 2- and 1.5-fold more than quercetin activity (IC<sub>50</sub> = 8.69 μM), well-known as antioxidant agent and used as a standard. Also, 4e and 4d had the highest ABTS activity with the IC<sub>50</sub> value of 5.55 μM and 7.84 μM, respectively, which are almost 2.8- and 2-fold higher than that of quercetin (IC<sub>50</sub> = 15.49 μM). The structure-activity relationship results revealed that most of synthesized sulfonyl chloride derivatives (4a-e) have higher antioxidant activity than the sulphonamide derivatives (5a-c) and also 4d and 4e, including hydroxyl group, exhibited the strongest antioxidant activity as expected.

**Keywords:** Antioxidant activity, chalcone, furan

### 1. INTRODUCTION

Oxidative stress, which is one of the factors that cause many common diseases such as diabetes, cancer and aging, arises from the imbalance between the antioxidant defence system of the cell and reactive oxygen species (ROS) [1, 2]. While low levels of ROS show biological

effects such as a defence mechanism against pathogenic microorganisms and intercellular communication, high concentrations of ROS cause damage to DNA, lipids and proteins, and even cell death [3, 4]. Therefore, the ROS level in the body should be kept at the right rate. To maintain this ratio, the antioxidant system is activated to reduce free radical toxicity [5].

\* Corresponding author: fsonmez@subu.edu.tr

<sup>1</sup> Sakarya Applied Sciences University

E-mail: zuhalsahin@subu.edu.tr

ORCID: <https://orcid.org/0000-0001-7486-6374>, <https://orcid.org/0000-0001-9856-8064>

<sup>2</sup> Sakarya University

E-mail: enes.akgun@akcoat.com

ORCID: <https://orcid.org/0000-0002-2293-925X>



However, exceeding the antioxidant defence system capacity and excessive presence of superoxide radical result in the formation of ROS [6]. In these cases, the use of natural or synthetic antioxidants may be necessary. Antioxidants act an active role in the prevention of many diseases by catching free radicals in the living body [7, 8]. Therefore, the design and synthesis of effective new antioxidants continue to be the focus of interest for scientists.

It is known that chalcones (1,3-diphenyl-2-propen-1-one) have two aromatic rings linked by  $\alpha,\beta$  unsaturated carbonyl system [9]. Natural and synthetic chalcones have widespread biological activity [10-12]. In particular, they have the potential to be developed as pioneer molecules for the discovery of antioxidant and anti-cancer agents [13]. In the researches, it has been determined that the  $\alpha,\beta$  unsaturated carbonyl system acts a key role in the versatile biological activities of chalcones, and the elimination or deterioration of this structural feature causes loss of their bioactivities [14, 15]. Without disturbing this  $\alpha,\beta$  unsaturated carbonyl system, new bioactive chalcone analogues can be synthesized by modifications to both phenyl rings [16]. Heteroaryl chalcones are obtained by modifications of phenyl rings [17]. Several studies have shown that heteroaryl chalcones have widespread biological potential such as anti-fungal, antibacterial, antimalarial, anticancer, anti-inflammatory, anti-angiogenic and anti-HIV activities [18-20].

In this study, eight novel furfuryl-chalcones were synthesized as heteroarylchalcone derivatives and their heterocyclic and/or phenyl rings were modified by attaching of sulfonylchloride and sulfonamide moiety. Their DPPH and ABTS activities were evaluated as antioxidant property.

## 2. MATERIALS AND METHODS

The used solvents and chemicals were bought from Sigma-Aldrich. Varian Infinity Plus spectrometer were used for  $^1\text{H}$  NMR (300 MHz) and  $^{13}\text{C}$  NMR (75 MHz) analysis. Leco CHNS-932 instrument and BioTek Power Wave XS were used for the elemental analyses and antioxidant assay, respectively.

### 2.1. Synthetic Procedures and Spectral Data

Synthesis of furfuryl-chalcone derivatives (3a-e): 1.5 mmol of 2-furfuraldehyde (1) and 1 mmol of acetophenone derivatives (2a-e) were dissolved in 30 mL of ethanol. 5 mL of 10% aqueous NaOH was added. The mixture was stirred for 5 hours at 25 °C and the mixture was poured onto 100 mL of ice water acidified with 5 mL of 2 M HCl. The obtained precipitates were filtered and washed with cold water. The solids were dried in vacuum oven.

(E)-3-(furan-2-yl)-1-(p-tolyl)prop-2-en-1-one (3a): Yellow powder, 92% yield.  $^1\text{H}$  NMR ( $\text{CDCl}_3$ , 300 MHz)  $\delta$ /ppm: 2.43 (3H, s), 6.50 (1H, s), 6.70 (1H, s), 7.28 (2H, d,  $J=7.6$  Hz), 7.41-7.61 (3H, m), 7.94 (2H, d,  $J=7.6$  Hz);  $^{13}\text{C}$  NMR ( $\text{CDCl}_3$ , 75 MHz)  $\delta$ /ppm: 21.9, 112.9, 116.3, 119.5, 128.8, 129.5, 130.6, 135.7, 143.9, 145.0, 151.9, 189.6.

(E)-3-(furan-2-yl)-1-(4-methoxyphenyl)prop-2-en-1-one (3b): Cream powder, 96% yield.  $^1\text{H}$  NMR ( $\text{CDCl}_3$ , 300 MHz)  $\delta$ /ppm: 3.87 (3H, s), 6.50 (1H, s), 6.68 (1H, s), 6.96 (2H, d,  $J=8.2$  Hz), 7.43-7.60 (3H, m), 8.04 (2H, d,  $J=8.2$  Hz);  $^{13}\text{C}$  NMR ( $\text{CDCl}_3$ , 75 MHz)  $\delta$ /ppm: 55.7, 112.9, 114.0, 116.2, 119.3, 130.2, 131.0, 131.2, 145.0, 152.0, 163.6, 188.3.

(E)-1-(4-chlorophenyl)-3-(furan-2-yl)prop-2-en-1-one (3c): Yellow powder, 95% yield.  $^1\text{H}$  NMR ( $\text{CDCl}_3$ , 300 MHz)  $\delta$ /ppm: 6.50-6.52 (1H, dd,  $J_1=2.0$  Hz,  $J_2=3.2$  Hz), 6.73 (1H, d,  $J=3.2$  Hz), 7.40 (1H, d,  $J=15.2$  Hz), 7.45 (2H, d,

J= 8.5 Hz), 7.53 (1H, s), 7.59 (1H, d, J= 15.2 Hz), 7.97 (2H, d, J= 8.5 Hz);  $^{13}\text{C}$  NMR ( $\text{CDCl}_3$ , 75 MHz)  $\delta/\text{ppm}$ : 113.0, 117.0, 118.8, 129.1, 130.0, 131.3, 136.6, 139.4, 145.4, 151.7, 188.7.

(E)-3-(furan-2-yl)-1-(4-hydroxyphenyl)prop-2-en-1-one (3d): Cream powder, 88% yield.  $^1\text{H}$  NMR ( $\text{CDCl}_3+\text{DMSO}-d_6$ , 300 MHz)  $\delta/\text{ppm}$ : 6.28 (1H, t, J= 1.7 Hz), 6.47 (1H, d, J= 3.2 Hz), 6.67 (2H, d, J= 7.9 Hz), 7.20 (1H, d, J= 15.5 Hz), 7.25-7.31 (2H, m), 7.70 (2H, d, J= 8.2 Hz);  $^{13}\text{C}$  NMR ( $\text{CDCl}_3+\text{DMSO}-d_6$ , 75 MHz)  $\delta/\text{ppm}$ : 112.7, 115.6, 115.7, 119.3, 129.6, 129.7, 130.9, 144.8, 151.7, 162.3, 187.9.

(E)-3-(furan-2-yl)-1-(3-hydroxyphenyl)prop-2-en-1-one (3e): Cream powder, 90% yield.  $^1\text{H}$  NMR ( $\text{CDCl}_3$ , 300 MHz)  $\delta/\text{ppm}$ : 6.50-6.52 (1H, dd,  $J_1=2.6$  Hz,  $J_2=7.9$  Hz), 7.36 (1H, t, J= 7.6 Hz), 7.46 (1H, d, J= 15.5 Hz), 7.50-7.60 (3H, m), 7.72 (1H, t, J= 2.3 Hz);  $^{13}\text{C}$  NMR ( $\text{CDCl}_3$ , 75 MHz)  $\delta/\text{ppm}$ : 113.0, 115.3, 117.1, 119.3, 120.7, 121.2, 130.1, 131.4, 139.6, 145.4, 151.8, 156.7, 190.4.

Synthesis of furfurylchalcone-sulfonylchloride derivatives (4a-e): 1 mmol of furfuryl-chalcone derivatives (3a-e) was placed in the reaction flask in an ice bath and 5 mL of chlorosulfonic acid was added and stirred at 25 °C for 15 hours. Then, the mixture was poured dropwise onto 100 g of ice and stirred until the ice melted. The precipitates were filtered and washed with cold water. The solids were dried in vacuum oven.

(E)-5-(3-oxo-3-(p-tolyl)prop-1-en-1-yl)furan-2-sulfonyl chloride (4a): Brown powder, 77% yield,  $^1\text{H}$  NMR ( $\text{CDCl}_3$ , 300 MHz)  $\delta/\text{ppm}$ : 2.39 (3H, s), 6.75 (1H, d, J= 3.5 Hz), 7.19-7.29 (3H, m), 7.50 (1H, d, J= 15.5 Hz), 7.68 (1H, d, J= 15.5 Hz), 7.91 (2H, d, J= 8.2 Hz);  $^{13}\text{C}$  NMR ( $\text{CDCl}_3$ , 75 MHz)  $\delta/\text{ppm}$ : 22.0, 115.3, 120.8, 125.6, 127.9, 129.1, 129.8, 134.8, 145.0, 150.1, 156.7, 188.3. Anal. Calcd. for  $\text{C}_{14}\text{H}_{11}\text{ClO}_4\text{S}$ : C, 54.11; H, 3.57; found: C, 54.18; H, 3.52.

(E)-5-(3-(3-(chlorosulfonyl)-4-methoxyphenyl)-3-oxoprop-1-en-1-yl)furan-2-sulfonyl chloride (4b): Brown powder, 82% yield,  $^1\text{H}$  NMR ( $\text{CDCl}_3+\text{DMSO}-d_6$ , 300 MHz)  $\delta/\text{ppm}$ : 3.86 (3H, s), 6.75 (1H, d, J= 3.8 Hz), 7.05 (1H, d, J= 8.8 Hz), 7.14 (1H, d, J= 3.8 Hz), 7.33 (1H, d, J= 15.5 Hz), 7.42 (1H, d, J= 15.5 Hz), 8.14-8.17 (1H, dd,  $J_1=2.4$  Hz,  $J_2=8.8$  Hz), 8.29 (1H, d, J= 2.0 Hz);  $^{13}\text{C}$  NMR ( $\text{CDCl}_3$ , 75 MHz)  $\delta/\text{ppm}$ : 57.6, 113.6, 116.1, 120.6, 123.8, 129.4, 129.8, 131.0, 132.3, 137.7, 150.6, 156.0, 161.0, 185.4. Anal. Calcd. for  $\text{C}_{14}\text{H}_{10}\text{Cl}_2\text{O}_7\text{S}_2$ : C, 39.54; H, 2.37; found: C, 39.12; H, 2.22.

(E)-5-(3-(4-chlorophenyl)-3-oxoprop-1-en-1-yl)furan-2-sulfonyl chloride (4c): Brown powder, 95% yield,  $^1\text{H}$  NMR ( $\text{CDCl}_3$ , 300 MHz)  $\delta/\text{ppm}$ : 6.83 (1H, d, J= 3.2 Hz), 7.36 (1H, d, J= 3.0 Hz), 7.51 (2H, d, J= 7.6 Hz), 7.59 (1H, d, J= 15.6 Hz), 7.70 (1H, d, J= 7.6 Hz), 8.01 (2H, d, J= 7.9 Hz);  $^{13}\text{C}$  NMR ( $\text{CDCl}_3$ , 75 MHz)  $\delta/\text{ppm}$ : 115.7, 120.7, 124.8, 128.7, 129.5, 130.3, 135.6, 140.4, 150.4, 156.3, 187.6. Anal. Calcd. for  $\text{C}_{13}\text{H}_8\text{Cl}_2\text{O}_4\text{S}$ : C, 47.15; H, 2.44; found: C, 46.98; H, 2.47.

(E)-5-(3-(3-(chlorosulfonyl)-4-hydroxyphenyl)-3-oxoprop-1-en-1-yl)furan-2-sulfonyl chloride (4d): Black powder, 62% yield,  $^1\text{H}$  NMR ( $\text{CDCl}_3$ , 300 MHz)  $\delta/\text{ppm}$ : 6.90 (1H, d, J= 3.8 Hz), 7.29 (1H, d, J= 8.8 Hz), 7.37 (1H, d, J= 3.8 Hz), 7.66 (2H, s), 8.33-8.36 (1H, dd,  $J_1=2.0$  Hz,  $J_2=7.0$  Hz), 8.57 (1H, d, J= 2.3 Hz);  $^{13}\text{C}$  NMR ( $\text{CDCl}_3$ , 75 MHz)  $\delta/\text{ppm}$ : 116.3, 119.9, 120.7, 123.6, 128.9, 129.6, 129.7, 130.1, 138.0, 150.6, 155.9, 158.5, 185.3. Anal. Calcd. for  $\text{C}_{13}\text{H}_8\text{Cl}_2\text{O}_7\text{S}_2$ : C, 37.97; H, 1.96; found: C, 37.91; H, 2.02.

(E)-5-(3-(4-(chlorosulfonyl)-3-hydroxyphenyl)-3-oxoprop-1-en-1-yl)furan-2-sulfonyl chloride (4e): Black powder, 62% yield,  $^1\text{H}$  NMR ( $\text{CDCl}_3$ , 300 MHz)  $\delta/\text{ppm}$ : 4.22 (1H, br, OH), 6.85 (1H, d, J= 3.8 Hz), 7.13-7.17 (1H, m), 7.36 (1H, d, J= 3.8 Hz), 7.42 (1H, t, J= 7.6 Hz), 7.54-7.68 (2H, m), 7.71 (1H, d, J= 15.5

Hz);  $^{13}\text{C}$  NMR ( $\text{CDCl}_3$ , 75 MHz)  $\delta$ /ppm: 115.3, 115.7, 120.7, 121.5 (x2), 125.3, 128.6, 130.5, 138.6, 150.3, 156.3, 156.7, 189.1. Anal. Calcd. for  $\text{C}_{13}\text{H}_8\text{Cl}_2\text{O}_7\text{S}_2$ : C, 37.97; H, 1.96; found: C, 38.02; H, 1.92.

Synthesis of furfurylchalcone-sulfonamide derivatives (5a-e): 1 mmol of furfurylchalcone-sulfonylchloride derivatives (4a-e) were dissolved in 20 mL of ethanol and 15 mL ethanolic solution of methylamine was added dropwise to it in ice bath and was stirred at 25 °C for 2 hours. The mixture was evaporated under vacuum. The solid products were washed with chloroform (15 mL), filtered and dried in vacuum oven.

(E)-N-methyl-5-(3-oxo-3-(p-tolyl)prop-1-en-1-yl)furan-2-sulfonamide (5a): Brown powder, 90% yield,  $^1\text{H}$  NMR ( $\text{CDCl}_3$ , 300 MHz)  $\delta$ /ppm: 2.38 (3H, s), 2.74 (3H, s), 6.71 (1H, d,  $J=3.3$  Hz), 7.07 (1H, d,  $J=3.3$  Hz), 7.26 (2H, d,  $J=7.9$  Hz), 7.50 (1H, d,  $J=15.5$  Hz), 7.56 (2H, d,  $J=15.5$  Hz), 7.90 (2H, d,  $J=8.2$  Hz);  $^{13}\text{C}$  NMR ( $\text{CDCl}_3$ , 75 MHz)  $\delta$ /ppm: 21.9, 29.5, 115.6, 118.6, 123.1, 129.0, 129.1, 129.7, 135.0, 144.6, 148.8, 154.8, 189.0. Anal. Calcd. for  $\text{C}_{15}\text{H}_{15}\text{NO}_4\text{S}$ : C, 59.00; H, 4.95; N, 4.59; found: C, 59.42; H, 4.75; N, 4.81.

(E)-5-(3-(4-methoxy-3-(N-methylsulfamoyl)phenyl)-3-oxoprop-1-en-1-yl)-N-methylfuran-2-sulfonamide (5b): Dark brown powder, 84% yield,  $^1\text{H}$  NMR ( $\text{CDCl}_3$ , 300 MHz)  $\delta$ /ppm: 2.58 (3H, d,  $J=5.2$  Hz), 2.72 (3H, s), 4.00 (3H, s), 5.07 (1H, q,  $J=5.2$  Hz, NH), 5.35 (1H, br, NH), 6.72 (1H, d,  $J=3.5$  Hz), 7.07 (1H, d,  $J=3.5$  Hz), 7.10 (1H, d,  $J=8.8$  Hz), 7.53 (2H, s), 8.22-8.24 (1H, dd,  $J_1=2.3$  Hz,  $J_2=8.8$  Hz), 8.50 (1H, d,  $J=2.0$  Hz);  $^{13}\text{C}$  NMR ( $\text{CDCl}_3$ , 75 MHz)  $\delta$ /ppm: 29.5, 29.8, 57.2, 112.6, 116.3, 118.9, 122.0, 126.4, 129.9, 130.6, 131.7, 135.8, 149.0, 154.6, 160.0, 186.6. Anal. Calcd. for  $\text{C}_{16}\text{H}_{18}\text{N}_2\text{O}_7\text{S}_2$ : C, 46.37; H, 4.38; N, 6.76; found: C, 46.58; H, 4.14; N, 6.52.

(E)-5-(3-(4-chlorophenyl)-3-oxoprop-1-en-1-yl)-N-methylfuran-2-sulfonamide (5c): Brown powder, 73% yield,  $^1\text{H}$  NMR ( $\text{CDCl}_3$ , 300 MHz)  $\delta$ /ppm: 2.80 (3H, d,  $J=5.0$  Hz), 4.89 (1H, q,  $J=5.2$  Hz, NH), 6.77 (1H, d,  $J=3.5$  Hz), 7.12 (1H, d,  $J=3.5$  Hz), 7.48 (2H, d,  $J=8.5$  Hz), 7.55 (2H, s), 7.98 (2H, d,  $J=8.8$  Hz);  $^{13}\text{C}$  NMR ( $\text{CDCl}_3$ , 75 MHz)  $\delta$ /ppm: 29.6, 116.0, 118.8, 122.5, 129.3, 129.7, 130.2, 135.9, 140.1, 148.9, 154.6, 188.0. Anal. Calcd. for  $\text{C}_{14}\text{H}_{12}\text{ClNO}_4\text{S}$ : C, 51.62; H, 3.71; N, 4.30; found: C, 51.12; H, 3.97; N, 4.72.

(E)-5-(3-(4-hydroxy-3-(N-methylsulfamoyl)phenyl)-3-oxoprop-1-en-1-yl)-N-methylfuran-2-sulfonamide (5d) and (E)-5-(3-(3-hydroxy-4-(N-methylsulfamoyl)phenyl)-3-oxoprop-1-en-1-yl)-N-methylfuran-2-sulfonamide (5e): Black crude products could not be purified.

## 2.2. Antioxidant Activity

1,1-diphenyl-2-picrylhydrazyl free radical was used for DPPH assay according to literature [21]. 2, 5, 10 and 20  $\mu\text{L}$  from 1000  $\mu\text{M}$  stock solutions of the compounds were taken. Their volumes were completed to 40  $\mu\text{L}$  with ethanol and then 160  $\mu\text{L}$  of 0.1 mM 1,1-diphenyl-2-picrylhydrazyl solution was added. The absorbance values of the prepared solutions were measured at 517 nm after 30 minutes of incubation in the dark at room temperature. Inhibition values (%) of the compounds were calculated from the obtained absorbance values.

2,2'-azino-bis(3-ethylbenzothiazoline-6-sulphonic acid diammonium salt) solution was used for ABTS assay according to the literature [22]. This solution was kept in the dark for 24 hours at room temperature and used for the experiment after the absorbance of the solution was fixed to  $\sim 0.70$  at 734 nm by dilution. The solutions of the compounds were prepared in 4 different concentrations (10, 50, 100 and 250  $\mu\text{M}$ ) of DMSO and added to a flat-bottomed 96-

well plate. The ABTS solution was added and incubated for 15 min at room temperature in the dark, and the absorbance was measured at 734 nm. Inhibition values (%) of the compounds were calculated from the obtained absorbance values.

### 3. RESULTS AND DISCUSSIONS

The synthesis route is shown in Figure 1. The furfuryl-chalcones were obtained by reacting 2-furfuraldehyde (1) with various acetophenones (2a-e) in alcoholic bases known as Claisen-Smith condensation. The furfuryl-chalcones (3a-e) were treated with excess chlorosulfonic acid to obtain sulfonyl chloride derivatives (4a and 4c, Figure 2). In this step for compounds 4b, 4d, and 4e ( $R_1$  was methoxy or hydroxyl, which are strong electron donating groups), two sulfonyl chlorides were attached both heteroaryl ring and phenyl ring.

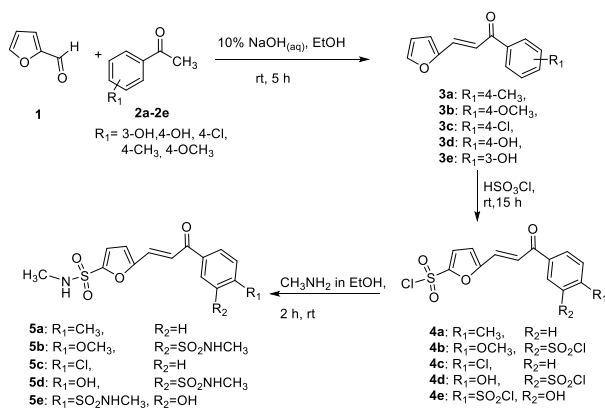


Figure 1 Synthesis of furfuryl-chalcone derivatives

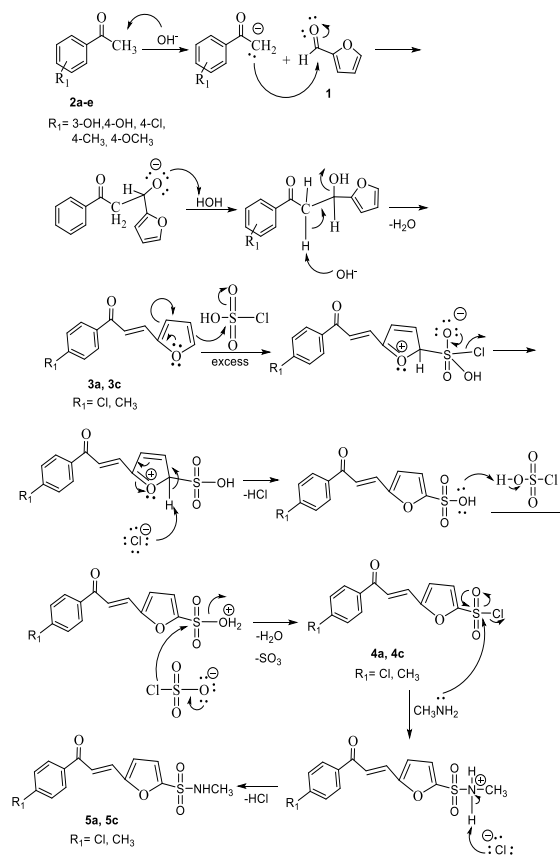


Figure 2 Mechanism of compounds 5a and 5c having one sulphonamide moiety

These compounds were treated with small amount of chlorosulfonic acid for binding sulfonyl chloride to only heteroaryl ring; however, compounds 4b, 4d, and 4e, (having two sulfonyl chloride groups) were obtained again. These results indicated that the reaction mechanism occurred through simultaneous sulfonation of both rings. The estimated mechanism is depicted in Figure 3. 4a-e was reacted with the methylamine in EtOH solution at 25 °C for 2h to give sulphonamide derivatives. In this step, compounds 5d and 5e were obtained as black sticky gel-like crude products in low yields and they could not be purified.

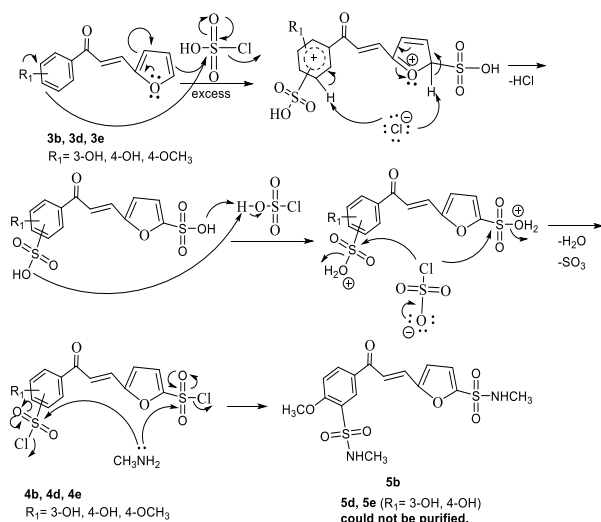


Figure 3 Mechanism of compounds 5b having two sulphonamide moieties

All synthesized compounds had the antioxidant futures. The  $IC_{50}$  values of them were between  $4.23 \mu\text{M}$  and  $106.51 \mu\text{M}$  in DPPH assay, while they were between  $5.55 \mu\text{M}$  and  $111.44 \mu\text{M}$  in ABTS assay.

Among them, 4e and 4d exhibited the strongest DPPH activity with the  $IC_{50}$  value of  $4.23 \mu\text{M}$  and  $6.68 \mu\text{M}$ , respectively, which are almost 2- and 1.5-fold stronger than quercetin activity ( $IC_{50} = 8.69 \mu\text{M}$ ) used as a standard. Furthermore, 4e and 4d had the highest ABTS activity with the  $IC_{50}$  value of  $5.55 \mu\text{M}$  and  $7.84 \mu\text{M}$ , respectively, which are almost 2.8- and 2-fold higher than that of quercetin ( $IC_{50} = 15.49 \mu\text{M}$ ).

It was reported that the many synthetic and natural antioxidants. Most of synthesized chalcones, in this study, exhibited stronger DPPH activity than bis-carbohydrazones ( $IC_{50}$  values of them ranging from  $51.82 \mu\text{M}$  to not active) [23] and isatin derivatives ( $IC_{50} = 64.03\text{--}204.90 \mu\text{M}$ ) [21], whereas they showed lower ABTS activity than bis-thiocarbohydrazones ( $IC_{50} = 2.69\text{--}5.32 \mu\text{M}$ ) [23] and isatin derivatives ( $IC_{50} = 0.39\text{--}6.83 \mu\text{M}$ ) [21]. On the other hand, the synthesized chalcones have higher ABTS activity than some reported natural extracts ( $IC_{50} = 40.22\text{--}106.01 \mu\text{M}$ ) [24].

From Table 1, the structure–activity relationship (SAR) can be observed as follows:

Generally, most of synthesized sulfonyl chloride derivatives (4a-e) exhibited stronger both DPPH and ABTS activity than the sulphonamide derivatives (5a-c). Additionally, most of them showed better DPPH activity than ABTS. As expected, compounds 4d and 4e, containing hydroxyl group, have the highest antioxidant activity among the synthesized compounds. Changing the position of hydroxyl with sulfonyl chloride moiety did not significantly alter antioxidant activity.

Table 1 The results of DPPH and ABTS assays

Compound	DPPH ( $IC_{50}$ , $\mu\text{M}$ ) <sup>a</sup>	ABTS <sup>•+</sup> ( $IC_{50}$ , $\mu\text{M}$ ) <sup>a</sup>
4a	$48.27 \pm 0.04$	$64.06 \pm 0.53$
4b	$33.59 \pm 0.12$	$52.20 \pm 0.40$
4c	$56.42 \pm 0.14$	$58.32 \pm 0.51$
4d	$6.68 \pm 0.06$	$7.84 \pm 0.02$
4e	$4.23 \pm 0.02$	$5.55 \pm 0.04$
5a	$62.54 \pm 0.24$	$70.78 \pm 0.44$
5b	$50.31 \pm 0.30$	$68.25 \pm 0.77$
5c	$106.51 \pm 1.18$	$111.44 \pm 0.98$
Quercetin	$8.69 \pm 0.04$	$15.49 \pm 2.33$

<sup>a</sup> $IC_{50}$  values are given according to three parallel measurement results.

Compounds 4b and 5b, having  $-\text{OCH}_3$  as  $R_1$  substituent, showed the second most effective antioxidant activity after those containing hydroxyl group.

It is well-known that the DPPH and ABTS mechanisms involve an electron transfer process [25-28]. It is considered that 4e can oxidize to quinone product, known as one of the anticancer agents. Quinones act antitumor activity via reversible enzymatic reduction and oxidation [28, 29]. Therefore, the conversion of compound 4e to quinone may provide a distinct advantage in terms of its use in the treatment of some diseases.

#### 4. CONCLUSION

The furfuryl-chalcone derivatives substituted sulfonyl chloride or sulphonamide were synthesized and their DPPH and ABTS activities were investigated as antioxidant features. All furfuryl-chalcones showed good antioxidant activities. Compound 4e and 4d exhibited the strongest antioxidant activities with the IC<sub>50</sub> values of 4.23 µM and 6.68 µM for DPPH and 5.55 µM and 7.84 µM for ABTS activity, respectively. These values are better than that of quercetin (IC<sub>50</sub> = 8.69 µM and 15.49 µM for DPPH and ABTS, respectively), used as a standard. Generally, all synthesized sulfonyl chloride derivatives (4a-e) have higher antioxidant activity than the sulphonamide derivatives (5a-c). As expected, among the synthesized compounds, 4d and 4e, including hydroxyl group, exhibited the strongest antioxidant activity. These results indicated that the hydroxyl groups linked to the phenyl ring can act a critical role for antioxidant agents.

#### *Funding*

The author (s) has no received any financial support for the research, authorship or publication of this study.

#### *Authors' Contribution*

The authors contributed equally to the study. F.S: Literature research, writing, editing, method, consultancy. E.A: Synthesis of compounds. Z.S: Antioxidant activity assay.

#### *The Declaration of Conflict of Interest/ Common Interest*

This study was produced from the MSc thesis entitled "Sülfonamit Grubu İçeren Furfurilşalkon Türevlerinin Sentezi" by Sakarya University, which was accepted in 2019.

#### *The Declaration of Ethics Committee Approval*

This study does not require ethics committee permission or any special permission.

#### *The Declaration of Research and Publication Ethics*

The authors of the paper declare that they comply with the scientific, ethical and quotation rules of SAUJS in all processes of the paper and that they do not make any falsification on the data collected. In addition, they declare that Sakarya University Journal of Science and its editorial board have no responsibility for any ethical violations that may be encountered, and that this study has not been evaluated in any academic publication environment other than Sakarya University Journal of Science.

#### REFERENCES

- [1] J. D. Hayes, A.T. Dinkova-Kostova, K. D. Tew, "Oxidative stress in cancer", *Cancer Cells*, vol. 38, pp. 167-197, 2020.
- [2] A. M. Pisoschi, A. Pop, F. Iordache, L. Stanca, G. Predoi, A. I. Serban, "Oxidative stress mitigation by antioxidants-an overview on their chemistry and influences on health status", *European Journal of Medicinal Chemistry*, vol. 209, 112891, 2021.
- [3] H. Sies, D. P. Jones, "Reactive oxygen species (ROS) as pleiotropic physiological signalling agents", *Nature Reviews Molecular Cell Biology*, vol. 21, pp. 363-383, 2020.
- [4] N. Zhang, P. Hu, Y. Wang, Q. Tang, Q. Zheng, Z. Wang, Y. He, "A reactive oxygen species (ROS) activated hydrogen sulfide (H<sub>2</sub>S) donor with self-reporting fluorescence", *ACS Sensors*, vol. 5, pp. 319-326, 2020.
- [5] M. V. Irazabal, V. E. Torres, "Reactive oxygen species and redox signaling in chronic kidney disease", *Cells*, vol. 9, 1342, 2020.

- [6] A. Kirtonia, G. Sethi, M. Garg, "The multifaceted role of reactive oxygen species in tumorigenesis", *Cellular and Molecular Life Sciences*, vol. 77, pp. 4459–4483, 2020.
- [7] B. Z. Kurt, I. Gazioglu, N. O. Kandas, F. Sonmez, "Synthesis, anticholinesterase, antioxidant, and anti-aflatoxic activity of novel coumarin carbamate derivatives", *ChemistrySelect*, vol. 3, pp. 3978–3983, 2018.
- [8] B. Z. Kurt, I. Gazioglu, F. Sonmez, M. Kucukislamoglu, "Synthesis, antioxidant and anticholinesterase activities of novel coumarylthiazole derivatives", *Bioorganic and Medicinal Chemistry*, vol. 59, pp. 80–90, 2015.
- [9] N. Sahu, S. Balbhadra, J. Choudhary, D. Kohli, "Exploring pharmacological significance of chalcone scaffold: a review", *Current Medicinal Chemistry*, vol. 19, pp. 209-225, 2012.
- [10] P. Singh, A. Anand, V. Kumar, "Recent developments in biological activities of chalcones: A mini review", *European Journal of Medicinal Chemistry*, vol. 85, pp. 758-777, 2014.
- [11] A. Atahan, "Synthesis and characterisation of polyaromatic chalcones with electron donation", *Sakarya University Journal of Science*, vol. 24, no. 2, pp. 347-356, 2020.
- [12] W. Dan, J. Dai, "Recent developments of chalcones as potential antibacterial agents in medicinal chemistry", *European Journal of Medicinal Chemistry*, vol. 187, 111980, 2020.
- [13] F. Gao, G. Huang, J. Xiao, "Chalcone hybrids as potential anticancer agents: Current development, mechanism of action, and structure-activity relationship", *Medical Research Reviews*, vol. 40, pp. 2049-2084, 2020.
- [14] S. Verma, A. K. Srivastava, O. P. Pandey, "A review on chalcones synthesis and their biological activity", *PharmaTutor*, vol. 6, pp. 22-39, 2018.
- [15] D. W. Elias, M. A. Beazely, N. M. Kandepu, "Bioactivities of chalcones", *Current Medicinal Chemistry*, vol. 6, pp. 1125-1149, 1999.
- [16] L. Ni, C.Q. Meng, J.A. Sikorski, "Recent advances in therapeutic chalcones", *Expert Opinion on Therapeutic Patents*, vol. 14, pp. 1669-1691, 2004.
- [17] H. Karaca, "Catalytic oxidation of 2-mercaptoethanol by cobalt (II) phthalocyanines bearing chalcone with furan and thiophene", *Sakarya University Journal of Science*, vol. 22, no. 6, pp. 1699-1703, 2018.
- [18] P. Dandawate, K. Ahmed, S. Padhye, A. Ahmad, B. Biersack, "Anticancer active heterocyclic chalcones: recent developments", *Anti-Cancer Agents in Medicinal Chemistry*, vol. 21, pp. 558-566, 2021.
- [19] R. Salotra, D. Utreja, "A comprehensive appraisal of chalcones and their heterocyclic analogs as antimicrobial agents", *Current Organic Chemistry*, vol. 24, pp. 2755-2781, 2020.
- [20] C. Kesari, K. R. Rama, K. Sedighi, J. Stenvang, F. Björkling, S. Kankala, N. Thota, "Synthesis of thiazole linked chalcones and their pyrimidine analogues as anticancer agents", *Synthetic Communications*, vol. 51, pp. 1406-1416, 2021.
- [21] F. Sonmez, Z. Gunesli, B. Z. Kurt, I. Gazioglu, D. Avcı, M. Kucukislamoglu, "Synthesis, antioxidant activity and SAR study of novel spiro-isatin-based Schiff bases", *Molecular Diversity*, vol. 23, pp. 829–844, 2019.



- [22] B. Zengin Kurt, "Sinnamaldehytin yeni schiff bazlarının sentezi ve antioksidan özelliklerinin incelenmesi", *Sakarya University Journal of Science*, vol. 22, no. 3, pp. 1024-1032, 2018.
- [23] H. Muğlu, B. Zengin Kurt, F. Sönmez, E. Güzel, M. S. Çavuş, H. Yakan, "Preparation, antioxidant activity, and theoretical studies on the relationship between antioxidant and electronic properties of bis(thio/carbohydrazone) derivatives", *Journal of Physics and Chemistry of Solids*, vol.164, 110618, 2022.
- [24] I. Gazioglu, B. Zengin Kurt, E. Sevgi, F. Sonmez, "Anticholinesterase, antioxidant, antiaflatoxic activities of ten edible wild plants from Ordu area, Turkey", *Iranian Journal of Pharmaceutical Research*, vol. 17, pp. 1047-1056, 2018.
- [25] N. Belkheiri, B. Bouguerne, F. Bedos-Belval, H. Duran, C. Bernis, R. Salvayre, A. Negre-Salvayre, M. Baltas, "Synthesis and antioxidant activity evaluation of a syringic hydrazones family", *European Journal of Medicinal Chemistry*, vol. 45, 3019-3026, 2010.
- [26] B. D. Kumar, D. S. Rawat, "Synthesis and antioxidant activity of thymol and carvacrol based Schiff bases", *Bioorganic and Medicinal Chemistry Letters*, vol. 23, pp. 641-645, 2013.
- [27] A. M. Campos, E. A. Lissi, "Kinetics of the reaction between 2,2'-azinobis (3-ethylbenzothiazoline-6-sulfonic acid (ABTS) derived radical cations and phenols", *International Journal of Chemical Kinetics*, vol. 29, pp. 219-224, 1997.
- [28] T. Herraiz, J. Galisteo, "Endogenous and dietary indoles: A class of antioxidants and radical scavengers in the ABTS assay", *Free Radical Research*, vol. 38, pp. 323-331, 2004.
- [29] A. Atahan, N. Gencer, C. Bilen, E. Yavuz, H. Genc, F. Sonmez, M. Zengin, M. Ceyhan, M. Kucukislamoglu, "Synthesis, biological activity and structure-activity relationship of novel diphenylurea derivatives containing tetrahydroquinoline as carbonic anhydrase I and II inhibitors", *ChemistrySelect*, vol. 3, pp. 529-534, 2018.



SAKARYA ÜNİVERSİTESİ

# FEN BİLİMLERİ ENSTİTÜSÜ DERGİSİ

Sakarya University Journal of Science  
SAUJS

ISSN 1301-4048 e-ISSN 2147-835X Period Bimonthly Founded 1997 Publisher Sakarya University  
<http://www.saujs.sakarya.edu.tr/>

Title: Perturbation Solution for a Cracked Euler-Bernoulli Beam

Authors: Lütü Emir SAKMAN

Received: 2022-09-03 00:00:00

Accepted: 2022-10-17 00:00:00

Article Type: Research Article

Volume: 26

Issue: 6

Month: December

Year: 2022

Pages: 1233-1243

How to cite

Lütü Emir SAKMAN; (2022), Perturbation Solution for a Cracked Euler-Bernoulli Beam. Sakarya University Journal of Science, 26(6), 1233-1243, DOI: 10.16984/saufenbilder.1170458

Access link

<https://dergipark.org.tr/en/pub/saufenbilder/issue/74051/1170458>

New submission to SAUJS

<http://dergipark.gov.tr/journal/1115/submission/start>



## Perturbation Solution for a Cracked Euler-Bernoulli Beam

Lütfi Emir SAKMAN\*<sup>1</sup>

### Abstract

The natural frequencies and mode shapes of an Euler-Bernoulli beam with a rectangular cross-section, which has a surface crack, is investigated. The crack is modeled as a change (sudden or gradual) in the cross-section of the beam, and a modified perturbation approach is used assuming that the crack geometry is much smaller than the beam cross section. Computations of natural frequencies and mode shapes were carried out for various crack shapes and compared with a range of experiments and finite element analyses. It is concluded that the suggested modified perturbation approach gives reliable results with minimal effort for eigenfrequencies of cracked beams. Furthermore, as a new feature, the present perturbation method includes the shape of the crack in eigenfrequency computations and in principle, can work for any type of disturbance on the surface including a small bump for example.

**Keywords:** Perturbation, surface crack, Euler-Bernoulli beam

### 1. INTRODUCTION

Identification and characterization of cracks in engineering structures is an important problem from both theoretical and technical point of view. One type of problem deals with determination of vibration characteristics of the structure with a crack. Another problem might be the characterization of the crack from measured vibration characteristics of the structure; this is usually called an inverse problem. The practical solution of the inverse problem normally involves solving the forward problem for a wide range of crack types. Therefore, the ability to solve the vibration

characteristics of a cracked structure is an important step in diagnosing structures by means of eigenfrequency measurements.

Most studies dealing with cracked structures models the crack as a change in the elastic characteristics of the structure, and utilize some type of numerical method. The present study aims to model the detailed geometry of the crack therefore shedding light on the solution of the inverse problem. Furthermore, the perturbation theory approach will be used making the solution analytical. However, since the Euler-Bernoulli beam theory depends little on the actual shape of the cross-section (i.e., it

\* Corresponding author: sakman@istanbul.edu.tr

<sup>1</sup> İstanbul University, Cerrahpaşa, Faculty of Engineering

ORCID: <https://orcid.org/0000-0002-9599-8875>



only comes into consideration in the form of cross-sectional second area moment), the straightforward perturbation theory does not yield satisfactory results. In the present study, a scale factor depending on computed base and perturbation eigenvalues is introduced in front of the perturbed solution. The reasoning for such an approach will be discussed in the next section, nevertheless this method gave good agreement with a wide range of experiments.

One of the earlier studies, Adams et al., demonstrated a vibration method for non-destructive testing of structures [1]. Rubio treats the crack by means of a torsional spring and solves the inverse problem [2] while Morassi treats the crack as a point discontinuity and derives general results about the sensitivity of eigenfrequencies [3]. Shen and Pier studied the convergence of Galerkin approach for beams with symmetric cracks [4]. Papaconomou and Dimarogonas describe a transfer matrix model for a cracked prismatic bar [5]. Chondros and Dimarogonas used a variational formulation to analyze lumped and continuous cracks [6]. Khiem and Toan used a modification of the Rayleigh quotient method for detection of an unknown number of multiple cracks on beams [7]. Saez et al. performed damage detection by solving the inverse problem [8]. Chaudhari and Maiti used a rotational spring to represent the crack and worked on solving the inverse problem based on the measurement of natural frequencies [9]. He and Lin use an acoustic system for contact-type cracks [10]. Nejad et al. worked on analytical estimation of natural frequencies and mode shapes of a beam having two cracks [11]. Mazanoglu et al. modified the energy-based method [12] presented by Yang et al to solve the vibration of non-uniform Euler–Bernoulli beams with multiple cracks by defining the crack as a spring [13]. Open edge cracks were investigated by Aydin again modeling the crack as a spring [14]. Caddemi and Morassi proposed a justification of the rotational elastic

spring model of an open crack in a beam [15]. Finite element method is very popular for investigation of free vibration analysis of cracked beams [16-19]. Cracks in reinforced concrete structures is another popular research topic using Euler-Bernoulli Beam theory [20, 21]. Timoshenko Beam model was also used [22, 23]. Beams with cracks on elastic foundations were considered by Hasan [24]. Gudmundson gives general results using more general elasticity approaches and derives frequency in terms of strain energies of cracked and uncracked structures [25].

Shen and Pier assumes a stress distribution around the crack and derives equations of motion in a detailed study [26]. Cooley et al. again models the crack as a torsional spring with an extra factor in the spring constant derived from linear fracture mechanics [27]. Chu and Shen uses a piece-wise linear spring model [28]. A study on cracked thin-walled beam under torsion is Dang et al. using stress concentration factor; this can be easily extended to eigenfrequency analysis [29].

The studies mentioned above mostly do not consider the shape of the crack, but model it as a spring or a change in the local elastic properties. In this study the crack is expressed as a change in the beam cross-section as explained in Section 2. This allows the determination of vibration characteristics depending on the shape of the crack. For the present, our interest is the validation of the modified perturbation computations by a wide range of experiments.

## 2. BASIC DEFINITIONS AND THEOREMS

Considering an Euler-Bernoulli beam of length  $L$  and cross-sectional area  $A(x)$ , the governing equation for the vibrations is

$$-\frac{\partial^2}{\partial x^2} \left( E I(x) \frac{\partial^2 y}{\partial x^2} \right) = m(x) \frac{\partial^2 y}{\partial t^2} \quad (1)$$

$$A(x) = b(x) h(x) \quad (2a)$$

$$I(x) = \frac{1}{12} b(x) h(x)^3 \quad (2b)$$

$$m(x) = \rho b(x) h(x) \quad (2c)$$

where  $\rho$  is the density of the beam material. Both ends of the beam are assumed to be fixed for demonstrating the solution procedure,

$$y = \frac{\partial y}{\partial x} = 0 \text{ at } x = 0, L \quad (3)$$

But solutions for other boundary conditions will also be given including

Fixed – fixed

Free – free

Simply supported – simply supported

Cantilever

The non-damaged beam has uniform cross section with constant width and height  $b_0$  and  $h_0$  respectively. The crack is modeled as a change in the beam cross-sectional dimensions in the form

$$b(x) = b_0 + \varepsilon f(x) \quad (4a)$$

$$h(x) = h_0 + \varepsilon g(x) \quad (4b)$$

where  $\varepsilon$  is a small non-dimensional perturbation parameter and the functions  $f(x)$  and  $g(x)$  determine the shape of the crack; these are completely general at this point. Substituting Eq. (4) into (2) and (1), the vibration equation becomes, ignoring higher order terms,

$$-\frac{\partial^2}{\partial x^2} \left( \frac{E}{12} (b_0 h_0^3 + \varepsilon (3 b_0 h_0^2 g(x) + h_0^3 f(x))) \frac{\partial^2 y}{\partial x^2} \right) = \rho (b_0 h_0 + \varepsilon (b_0 g(x) + h_0 f(x))) \frac{\partial^2 y}{\partial t^2} \quad (5)$$

The governing equation is nondimensionalized with the following definitions, starred symbols showing non-dimensional variables,

$$x^* = \frac{x}{L} \quad (6a)$$

$$t^* = \frac{t}{\sqrt{\frac{\rho}{E} \frac{12 L^4}{h_0^2}}} \quad (6b)$$

$$y^* = \frac{y}{h_0} \quad (6c)$$

$$G^*(x^*) = \frac{g(x)}{h_0} \quad (6d)$$

$$F^*(x^*) = \frac{f(x)}{b_0} \quad (6e)$$

The non-dimensional vibration equation becomes, omitting stars after this point,

$$\frac{\partial^4 y}{\partial x^4} + \frac{\partial^2 y}{\partial t^2} = -\varepsilon \left[ \frac{\partial^2}{\partial x^2} \left( (3 G(x) + F(x)) \frac{\partial^2 y}{\partial x^2} \right) + (G(x) + F(x)) \frac{\partial^2 y}{\partial t^2} \right] \quad (7)$$

and the boundary conditions

$$y = \frac{\partial y}{\partial x} = 0 \text{ at } x = 0, 1 \quad (8)$$

Assuming a separated solution of the form

$$y(x, t) = u(x) p(t) \quad (9)$$

leads to

$$\ddot{p} + \lambda^4 p = 0 \quad (10a)$$

$$u'''' - \lambda^4 u + \varepsilon \psi(u, \lambda) = 0 \quad (10b)$$

Prime and dot denote differentiation with respect to  $x$  and  $t$ , respectively, and we defined

$$\psi(u, \lambda) = \left( (3 G(x) + F(x)) u'' \right)'' - \lambda^4 u (G(x) + F(x)) \quad (11)$$

Solution of Eq. (10b) is assumed to be in the form of a perturbation series for both the mode shape and the eigenvalue

$$u(x) = u_0(x) + \varepsilon u_1(x) + \dots \quad (12a)$$

$$\lambda = \lambda_0 + \varepsilon \lambda_1 + \dots \quad (12b)$$

Substituting, the zero and first order problems become

$$u_0'''' - \lambda_0^4 u_0 = 0 \quad (13a)$$

$$u_0(0) = u_0'(0) = u_0(1) = u_0'(1) = 0 \quad (13b)$$

and

$$u_1'''' - \lambda_0^4 u_1 = 4 \lambda_0^3 \lambda_1 u_0 - \psi(u_0, \lambda_0) \quad (14a)$$

$$u_1(0) = u_1'(0) = u_1(1) = u_1'(1) = 0 \quad (14b)$$

The solution of the zeroth order problem is

$$\cosh \lambda_0^{(n)} \cos \lambda_0^{(n)} = 1, \quad n = 1, 2, 3, \dots \quad (15a)$$

$$u_0^{(n)} = \frac{\cos \lambda_0^{(n)} - \cosh \lambda_0^{(n)}}{\sin \lambda_0^{(n)} - \sinh \lambda_0^{(n)}} (\cos \lambda_0^{(n)} x - \cosh \lambda_0^{(n)} x) + \sin \lambda_0^{(n)} x - \sinh \lambda_0^{(n)} x \quad (15b)$$

The solution of the first order problem, (14a) can be written by variation of constants as

$$u_1 = C_1(x) e^{\lambda_0 x} + C_2(x) e^{-\lambda_0 x} + C_3(x) \cos \lambda_0 x + C_4(x) \sin \lambda_0 x \quad (16)$$

Where

$$C_1'(x) = \frac{e^{-\lambda_0 x} [4 \lambda_0^3 \lambda_1 u_0 - \psi(u_0, \lambda_0)]}{4 \lambda_0^3} \quad (17a)$$

$$C_2'(x) = -\frac{e^{\lambda_0 x} [4 \lambda_0^3 \lambda_1 u_0 - \psi(u_0, \lambda_0)]}{4 \lambda_0^3} \quad (17b)$$

$$C_3'(x) = \frac{\sin \lambda_0 x [4 \lambda_0^3 \lambda_1 u_0 - \psi(u_0, \lambda_0)]}{2 \lambda_0^3} \quad (17c)$$

$$C_4'(x) = -\frac{\cos \lambda_0 x [4 \lambda_0^3 \lambda_1 u_0 - \psi(u_0, \lambda_0)]}{2 \lambda_0^3} \quad (17d)$$

Integrating Eqs. (17) and substituting in (16) gives the general solution in the form

$$u_1 = K_1 e^{\lambda_0 x} + K_2 e^{-\lambda_0 x} + K_3 \cos \lambda_0 x + K_4 \sin \lambda_0 x + \int_0^x [\sinh \lambda_0(x - \xi) - \sin \lambda_0(x - \xi)] \varphi(\xi) d\xi \quad (18)$$

where we defined

$$\varphi(x) = \frac{4 \lambda_0^3 \lambda_1 u_0 - \psi(u_0, \lambda_0)}{2 \lambda_0^3} \quad (19)$$

for brevity. K's are arbitrary constants found by applying the boundary conditions Eq. (14b); the result is the system of equations

$$K_1 + K_2 + K_3 = 0 \quad (20a)$$

$$K_1 - K_2 - K_4 = 0 \quad (20b)$$

$$K_1 e^{\lambda_0} + K_2 e^{-\lambda_0} + K_3 \cos \lambda_0 + K_4 \sin \lambda_0 = A \quad (20c)$$

$$K_1 e^{\lambda_0} - K_2 e^{-\lambda_0} - K_3 \sin \lambda_0 + K_4 \cos \lambda_0 = B \quad (20d)$$

where

$$A = -\int_0^1 [\sinh \lambda_0(1 - \xi) - \sin \lambda_0(1 - \xi)] \varphi(\xi) d\xi \quad (21a)$$

$$B = -\int_0^1 [\cosh \lambda_0(1 - \xi) - \cos \lambda_0(1 - \xi)] \varphi(\xi) d\xi \quad (21b)$$

The homogeneous part of the linear system Eqs. (20) is the same as the eigenvalue equation for the zeroth order problem. Therefore, for the system Eqs. (20) to have a solution, the consistency condition.

$$(e^{\lambda_0} + \sin \lambda_0 - \cos \lambda_0)A = (e^{\lambda_0} - \sin \lambda_0 - \cos \lambda_0)B \quad (22)$$

should be satisfied. Eq. (22) is the eigenvalue equation for  $\lambda_1$  (which is inside, Eq. (19), through A and B). Once  $\lambda_1$  is solved, the constants are found from Eqs. (20).

The eigenfrequencies of the cracked beam is computed from Eq. (12b),

$$\lambda = \lambda_0 + \varepsilon \lambda_1 + \dots \quad (23a)$$

When computations were carried out, the change in eigenfrequency between cracked and uncracked beams, i.e.,  $\varepsilon \lambda_1$ , was found to be consistently too small compared to experimental values. This is to be expected since beam theory basically averages the elasticity problem over the cross-section of the beam and the details of the cross section does

not matter as long as second area moment remains the same. However, there was a structure to the difference in frequency between computed and experimental and/or finite element values which suggested that the change could be fixed once and for all cracked beams by introducing a factor in the perturbation term.

To this end, it is proposed that the perturbation in the eigenvalue is to be enlarged by a factor depending on base and perturbed eigenvalues in the form

$$C \left( \frac{\lambda_0}{\lambda_1} \right)^p$$

i.e. instead of Eq. (23a) we assume

$$\lambda = \lambda_0 + \varepsilon C \left( \frac{\lambda_0}{\lambda_1} \right)^p \lambda_1 + \dots \quad (23b)$$

where C and p are constants to be determined by matching (23b) to two experimental measurements. Afterwards, if the method is successful, Eq.(23b) should give good results for other experiments.

The logic of this procedure might be questioned; however, it should be noted that virtually all studies on cracked beams still use beam theory away from the crack, and model the crack by modifying the cracked element either as a different spring constant or some factor depending on well-known fracture theory concepts as alluded to in the introduction. This can be considered as an application of the Saint Venant principle that the local changes in geometry should not affect the global results too much. Therefore, what is done here should be seen in the same light, i.e., it lacks mathematical rigor since beam theory cannot really treat cracks; nevertheless, its value should be evaluated by its possible success. Another advantage of the present method is that it naturally involves the shape of the crack in the computations.

As will be seen in the next section, the proposed method indeed gives good results compared to roughly about 100 experiments (counting higher modes, other boundary conditions and other material constant) once the constants in Eq. (23b) are fixed by comparing to only two experimental results. These were chosen since they gave the closest results to the straightforward perturbation expansion before introducing the factor in Eq. (23b). The result is

$$\lambda = \lambda_0 + \varepsilon \sqrt{\frac{2 \lambda_0}{\lambda_1}} \lambda_1 + \dots \quad (23c)$$

The solution procedure is the same for the other types of boundary conditions. We present the results.

Free – Free:

$$A = - \int_0^1 [\sinh \lambda_0(1 - \xi) + \sin \lambda_0(1 - \xi)] \varphi(\xi) d\xi \quad (24a)$$

$$B = - \int_0^1 [\cosh \lambda_0(1 - \xi) + \cos \lambda_0(1 - \xi)] \varphi(\xi) d\xi \quad (24b)$$

$$(e^{\lambda_0} + \sin \lambda_0 - \cos \lambda_0)A = (e^{\lambda_0} - \sin \lambda_0 - \cos \lambda_0)B \quad (25)$$

Cantilever:

$$A = - \int_0^1 [\sinh \lambda_0(1 - \xi) + \sin \lambda_0(1 - \xi)] \varphi(\xi) d\xi \quad (26a)$$

$$B = - \int_0^1 [\cosh \lambda_0(1 - \xi) + \cos \lambda_0(1 - \xi)] \varphi(\xi) d\xi \quad (26b)$$

$$(e^{\lambda_0} + \sin \lambda_0 - \cos \lambda_0)A = (e^{\lambda_0} + \sin \lambda_0 + \cos \lambda_0)B \quad (27)$$

Simply supported – Simply supported:

$$A = - \int_0^1 [\sinh \lambda_0(1 - \xi) - \sin \lambda_0(1 - \xi)] \varphi(\xi) d\xi \quad (28a)$$

$$B = - \int_0^1 [\cosh \lambda_0(1 - \xi) + \cos \lambda_0(1 - \xi)] \varphi(\xi) d\xi \quad (28b)$$

$$(e^{\lambda_0} + \sin \lambda_0 - \cos \lambda_0)A = (e^{\lambda_0} - \sin \lambda_0 - \cos \lambda_0)B \quad (29)$$

### 3. RESULTS

The eigenfrequencies for cantilever, fixed – fixed, free – free, and simply supported –

simply supported boundary conditions will be presented and compared with computed or measured values in Ref. [30-36].

Cantilever beam:

Tables 1 – 3 shows comparisons with Refs. [30-32]

Table 1 Comparison with experiment (Ref. [30]) for cantilever boundary conditions.

Crack (mm)		Method	Natural Frequency				
Pos	Depth		Mode 1	Mode 2	Mode 3		
10	2	Experiment	182.7	1149.4	3242.9		
		F.E.M	182.7	1149.2	3234.1		
		Lee and Chung	182.6	1148.0	3222.1		
	6	Analytic	Experiment	163.9	1073.4	3097.3	
			F.E.M	166.9	1083.9	3108.0	
			Lee and Chung	161.9	1048.7	3010.3	
		Analytic	Experiment	176.9	1114.9	3138.1	
			F.E.M	129.8	980.6	2954.2	
			Lee and Chung	136.9	996.1	3970.8	
		10	Analytic	Experiment	109.0	814.5	3533.9
				F.E.M	171.6	1085.5	3066.2
				Experiment	184.0	1160.0	3245.0
80	2	F.E.M	184.0	1159.8	3244.9		
		Lee and Chung	184	1159.2	3229.7		
		Analytic	183.2	1156.7	3225.3		
	6	Analytic	Experiment	174.7	1155.3	3134.8	
			F.E.M	181.8	1102.9	3250.7	
			Lee and Chung	175.2	1153.9	3082.5	
		Analytic	Experiment	179.6	1150.6	3180.9	
			F.E.M	153.5	1145.1	2934.3	
			Lee and Chung	158.4	1147.6	2974.5	
		10	Analytic	Experiment	156.0	1143.3	2764.7
				F.E.M	176.1	1144.4	3136.8
				Experiment	184.7	1153.1	3258.1
2	Analytic	F.E.M	184.7	1153.2	3257.2		
		Lee and Chung	184.7	1151.9	3246.4		
		Analytic	184.1	1150.0	3242.3		
	Experiment	Experiment	181.2	1092.9	3250.1		
		F.E.M	181.8	1102.9	3250.7		
		Lee and Chung	181.6	1086.3	3236.6		
	140	6	Analytic	182.1	1130.3	3231.4	
			Experiment	171.5	971.5	3233.6	
			F.E.M	174.0	997.7	3238.0	
10		Analytic	Experiment	175.3	941.3	3216.8	
			F.E.M	180.2	1110.9	3220.5	
			Experiment	185.0	1155.0	3238.6	
2		Analytic	F.E.M	185.0	1155.0	3238.4	
			Lee and Chung	185.0	1154.1	3223.2	
			Analytic	184.3	1150.2	3216.6	
200		6	Experiment	184.3	1106.3	3082.9	
			F.E.M	184.4	1114.8	3107.3	
			Lee and Chung	184.4	1106.5	3020.5	
	Analytic	Experiment	182.7	1131.1	3154.9		
		F.E.M	182.2	1025.0	2819.6		
		Experiment	182.7	1016.5	2871.0		
	10	Analytic	Lee and Chung	183.2	1004.8	2567.6	
			Experiment	181.2	1112.1	3093.8	
			Analytic	181.2	1112.1	3093.8	

The comparisons are shown in Tables 1 through 7; analytic column denotes the results found in the present study. All the dimensions in the tables are millimeters.

In this case, analytic solution gives good results for different crack depths and positions, compared to the experimental results.

Table 2 Comparison with experiment (Ref. [31]) for cantilever boundary conditions.

Crack		Method	Natural Frequencies (Hz)		
Location (mm)	Depth (mm)		Mode 1	Mode 2	Mode 3
133	No Crack		68.00	432.75	1195.00
	1	Exp	68.00	432.50	1193.50
		Anal	67.68	425.54	1188.33
	2	Exp	67.75	431.50	1190.00
		Anal	67.27	424.37	1181.86
	3	Exp	67.50	430.50	1185.50
		Anal	66.87	423.21	1175.41
	4	Exp	67.25	429.00	1169.50
		Anal	66.47	422.05	1168.98
	5	Exp	66.00	427.25	1156.25
		Anal	66.07	420.88	1162.57
	No Crack		67.25	427.25	1184.00
240	1	Exp	67.25	426.50	1183.00
		Anal	67.98	423.91	1188.88
	2	Exp	67.25	424.50	1180.00
		Anal	67.88	421.13	1182.96
	3	Exp	67.25	422.00	1175.25
		Anal	67.78	418.35	1177.06
	4	Exp	67.25	418.25	1169.25
		Anal	67.68	415.59	1171.17
	5	Exp	67.00	411.25	1161.00
		Anal	67.58	412.83	1165.30

Table 2 and Table 3 presents comparisons of experimental and analytic results for different crack depths and locations. Again, analytic results are close to experimental results.



Table 3 Comparison with experiment (Ref. [32]) for cantilever boundary conditions.

Normalized crack location	Crack Depth Ratio	Method	Natural Frequency Mode 1 (Hz)	Natural Frequency Mode 2 (Hz)
No Crack	No Crack	Exp	13.45	84.30
0.1	0.5	Exp	12.80	82.89
		Analytic	12.82	82.57
0.2	0.5	Exp	13.02	84.30
		Analytic	12.96	84.95
0.3	0.5	Exp	13.15	83.30
		Analytic	13.10	85.40
0.4	0.5	Exp	13.28	82.87
		Analytic	13.26	83.11
.5	0.5	Exp	13.37	81.82
		Analytic	13.43	82.17
0.6	0.5	Exp	13.40	81.93
		Analytic	13.58	82.10
0.7	0.5	Exp	13.43	82.50
		Analytic	13.39	82.75

Both ends fixed:

Tables 4 and 5 presents comparisons with Refs. [33, 34]. In this tables, results shows that, analytic solutions are suitable for different boundary conditions. Here, analytic solution have effective results against FEM results.

Table 4 Comparison with experiment (Ref. [33]) for both ends fixed boundary conditions.

Crack (mm)		Method	Natural Frequency		
Position	Depth		Mode 1	Mode 2	Mode3
255	3	Exp	83.984	235.792	462.712
		F.E.M	74.710	223.760	426.146
		Analytic	84.897	234.894	456.869

Table 5 Comparison with experiment (Ref. [34]) for both ends fixed boundary conditions.

Crack Loc. (mm)	Crack Depth Ratio (%)	Method	Mode 1	Mode 2	Mode 3
45	10	No Crack	431.7	1190.0	2333.0
		Exp	431.4	1189.9	2331.6
		Analytic	429.2	1184.7	2316.6
		Mode 4	Mode 5	Mode 6	
		Exp	3856.0	5761.0	8046.0
		Analytic	3855.2	5759.1	8041.7

Both ends free:

Table 6 Comparison with experiment (Ref. [35]) for both ends free boundary conditions.

Crack (mm)		Method	Natural Frequency			
Pos	Depth		Mode1	Mode 2	Mode3	Mode4
430	4	Exp	74.688	205.625	405.62	666.250
		Reduced EI	74.670	205.190	405.64	669.335
		Lee and Chung Sinha et al.	74.938	206.262	405.97	670.550
		Exp	74.406	204.183	405.36	668.429
		Analytic	74.136	204.043	403.88	665.973
		Exp	74.063	202.500	404.68	662.813
430	8	Reduced EI	74.004	202.630	404.90	666.527
		Lee and Chung Sinha et al.	74.224	203.458	405.23	667.615
		Exp	73.628	201.283	404.55	665.356
		Analytic	73.108	200.899	401.56	660.479
		Exp	72.813	197.188	403.12	655.938
		Reduced EI	72.284	198.278	403.67	661.720
430	12	Lee and Chung Sinha et al.	72.634	197.764	403.77	661.635
		Exp	72.958	198.928	403.91	662.874
		Analytic	72.088	197.780	399.25	650.123

Table 6 presents comparisons with Ref [35]. Analytic solution compares with different solution procedures and experimental results.

Table 7 presents comparisons with Ref [36]. Also to fix the constants in Eq. (23b), two cases from Ref. [36], crack position 200 mm, and

depths of cracks 1 and 3 mm in Table 7, were chosen to be matched to the computed eigenfrequencies.

In all cases the perturbation solution (the present study) obtains good results compared with experiment, in some cases even surpassing the FEM computations (Ref. [30], [33]). It is also interesting to note that the perturbation solution seems to remain valid for quite deep cracks.

Both ends simply supported:

Table 7 Comparison with experiment (Ref. [36]) for both ends simply supported boundary conditions.

Crack (mm)		Method	Natural Frequency	
Position	Depth		Mode 1	Mode 2
		Experiment	151.20	599.80
	1	Yoon et al.	150.48	601.18
		Analytic	149.80	597.26
		Experiment	151.00	588.20
80	3	Yoon et al.	149.61	590.21
		Analytic	148.22	587.10
		Experiment	147.80	568.50
	5	Yoon et al.	145.95	556.08
		Analytic	146.66	577.02
		Experiment	150.50	604.20
	1	Yoon et al.	150.38	601.16
		Analytic	149.50	597.26
		Experiment	149.80	594.20
120	3	Yoon et al.	148.75	588.50
		Analytic	147.34	587.10
		Experiment	143.80	564.50
	5	Yoon et al.	142.16	543.42
		Analytic	145.19	577.02
		Experiment	149.20	599.80
	1	Yoon et al.	150.27	602.37
		Analytic	149.25	602.36
		Experiment	146.80	597.80
200	3	Yoon et al.	147.81	602.37
		Analytic	146.58	602.34
		Experiment	139.20	593.00
	5	Yoon et al.	138.32	602.37
		Analytic	143.93	602.32

Normally, the perturbation solution is expected to be more accurate for very small crack depths compared to beam cross-section; but as mentioned, after “fixing” the theoretical results by the factor introduced in Eq. (23c), good agreement with the experimental values is obtained for crack depths from very small cracks up to cracks with a depth of half of the beam height. Another point to note is, the cracks in experiments were produced by cutting the beam to a certain depth, thus resulting in a crack of rectangular shape. The depth and width of these rectangles were input in to the function  $g(x)$ , Eq.(4b). The present method should be able to handle other crack shapes, e.g., triangular, circular, etc., by modifying the function  $g(x)$ . But no such experiments were available for us to compare.

#### 4. CONCLUSION

A modified perturbation solution was presented to compute the mode shapes and eigenvalues of cracked Euler-Bernoulli beams. The method is general enough and allows computation of mode shapes and eigenvalues for specific crack geometries. In conclusion, the idea that the results of perturbation computations in the nondimensionalised (thus, universal), cracked beam vibration equation can be modified to agree with a wide set of experimental results has been verified [10]

#### Nomenclature

$A(x)$	area of cross section
$b(x), h(x)$	width and height of beam cross section
$b_0, h_0$	width and height of non-cracked beam cross section
$I(x)$	second area moment
$m(x)$	mass per unit length
$E$	modulus of elasticity
$\rho$	density
$L$	length of the beam
$\varepsilon$	perturbation parameter
$f(x), g(x)$	crack shape functions
$y(x, t)$	vertical displacement
$u(x)$	mode shape
$p(t)$	separated time function
$\lambda$	eigenvalue

[ ]\* non-dimensional [ ]  
C, p Parameters in modification factor

### **Funding**

The authors have not received any financial support for the research, authorship or publication of this study.

### **The Declaration of Conflict of Interest/Common Interest**

No conflict of interest or common interest has been declared by the authors.

### **The Declaration of Ethics Committee Approval**

This study does not require ethics committee permission or any special permission.

### **The Declaration of Research and Publication Ethics**

During the writing process of our study, the information of which is given above, international scientific, ethical and citation rules have been followed, no falsification has been made on the data collected, and Sakarya University Journal of Science and its editorial board have no responsibility for any ethical violations that may be encountered. I undertake that I have full responsibility that this study has not been evaluated in any academic environment other than Sakarya University Journal of Science.

## **REFERENCES**

- [1] R. D. Adams, P. Cawley, C. J. Pye, B. J. Stone, "A vibration technique for non-destructively assessing the integrity of structures," *Journal of Mechanical Engineering Science*, vol. 20, no. 2, pp. 93–100, 1978.
- [2] L. Rubio, "An efficient method for crack identification in simply supported Euler – Bernoulli Beams," *Journal of Vibration and Acoustics*, vol. 131, no. 5, pp. 1-6, 2009.
- [3] A. Morassi, "Crack-induced changes in eigenparameters of beam structures," *Asce - Journal Engineering Mechanics*, vol. 119, no. 9, pp. 1798–1803, 1993.
- [4] M. H. H. Shen, C. Pierre, "Natural modes of Bernoulli-Euler Beams with symmetric cracks," *Journal of Sound and Vibration*, vol. 138, no. 1, pp. 115–134, 1990.
- [5] N. Papaeconomou, A. Dimarogonas, "Vibration of cracked beams," *Computational Mechanics*, vol. 5, no. 2, pp. 88–94, 1989.
- [6] T. G. Chondros, A. D. Dimarogonas, "Vibration of a cracked cantilever beam," *Journal of Vibration and Acoustics*, vol. 120, no. 3, pp. 742–746, 1998.
- [7] N. T. Khiem, L. K. Toan, "A novel method for crack detection in beam-like structures by measurements of natural frequencies," *Journal of Sound and Vibration*, vol. 333, no. 18, pp. 4084–4103, 2014.
- [8] J. F. Sáez, A. Morassi, M. Pressacco, L. Rubio, "Unique determination of a single crack in a uniform simply supported beam in bending vibration," *Journal of Sound and Vibration*, vol. 371, no. 9, pp. 94–109, 2016.
- [9] T. D. Chaudhari, S. K. Maiti, "Modelling of transverse vibration of beam of linearly variable depth with edge crack," *Engineering Fracture Mechanics*, vol. 63, no. 4, pp. 425–445, 1999.
- [10] Q. He, Y. Lin, "Assessing the severity of fatigue crack using acoustics modulated

by hysteretic vibration for a cantilever beam,” *Journal of Sound and Vibration*, vol. 370, no. 26, pp. 306–318, 2016.

- [11] F. B. Nejad, A. Khorram, M. Rezaeian, “Analytical estimation of natural frequencies and mode shapes of a beam having two cracks,” *International Journal of Mechanical Sciences*, vol. 78, no. 1, pp. 193–202, 2014.
- [12] K. Mazanoglu, I. Yesilyurt, M. Sabuncu, “Vibration analysis of multiple-cracked non-uniform beams,” *Journal of Sound and Vibration*, vol. 320, no. 4-5, pp. 977–989, 2009.
- [13] X. F. Yang, A. S. J. Swamidas, R. Seshadri, “Crack identification in vibrating beams using the energy method,” *Journal of Sound and Vibration*, vol. 244, no. 2, pp. 339–357, 2001.
- [14] K. Aydin. “Free vibration of functionally graded beams with arbitrary number of surface cracks,” *European Journal of Mechanics - A/Solids*, vol. 42, no. 11-12, pp. 112–124, 2013.
- [15] S. Caddemi, A. Morassi, “Multi-cracked Euler–Bernoulli Beams: Mathematical modeling and exact solutions,” *International Journal of Solids and Structures*, vol. 50, no. 6, pp. 944–956, 2013.
- [16] M. Kisa, J. Brandon, M. Topcu, “Free vibration analysis of cracked beams by a combination of finite elements and component mode synthesis methods,” *Computers and Structures*, vol. 67, no. 4, pp. 215–223, 1998.
- [17] D. Y. Zheng, N. J. Kessissoglou, “Free vibration analysis of a cracked beam by finite element method,” *Journal of Sound and Vibration*, vol. 273, no. 3, pp. 457–475, 2004.
- [18] M. Kisa, M. A. Gurel, “Free vibration analysis of uniform and stepped cracked beams with circular cross sections,” *International Journal of Engineering Science*, vol. 45, no. 2-8, pp. 364–380, 2007.
- [19] J. P. Blasques, R. D. Bitsche, “An efficient and accurate method for computation of energy release rates in beam structures with longitudinal cracks,” *Engineering Fracture Mechanics*, vol. 133, no. 1, pp. 56–69, 2015.
- [20] C. Dundar, I. F. Kara, “Three dimensional analysis of reinforced concrete frames with cracked beam and column elements,” *Engineering Structures*, vol. 29, no. 9, pp. 2262–2273, 2007.
- [21] T. Xu, A. Castel, “Modeling the dynamic stiffness of cracked reinforced concrete beams under low-amplitude vibration loads,” *Journal of Sound and Vibration*, vol. 368, no. 4, pp. 135–147, 2016.
- [22] M. Heydari, A. Ebrahimi, M. Behzad, “Forced vibration analysis of a Timoshenko cracked beam using a continuous model for the crack,” *Engineering Science and Technology, an International Journal*, vol. 17, no. 4, pp. 194–204, 2014.
- [23] B. Panigrahi, G. Pohit, “Nonlinear modelling and dynamic analysis of cracked Timoshenko functionally graded beams based on neutral surface approach,” *Journal of Mechanical Engineering Science*, 230, vol. 9, pp. 1486–1497, 2016.

- [24] P. Gudmundson, "Eigenfrequency changes of structures due to cracks, notches or other geometrical changes," *Journal of the Mechanics and Physics of Solids*, vol. 30, no. 5, pp. 339–353, 1982.
- [25] W. M. Hasan, "Crack detection from the variation of the eigenfrequencies of a beam on elastic foundation," *Engineering Fracture Mechanics*, vol. 52, no. 3, pp. 409–421, 1995.
- [26] P. E. Cooley, J.C. Slater, O.V. Shiryayev, "Fatigue crack modeling and analysis in beams," 53rd IAA/ASME/ASCE/AHS/ASC Structures, Structural Dynamics and Materials Conference AIAA Paper, pp. 2012-1874, 2012.
- [27] M. H. H. Shen, C. Pierre, "Natural modes of Bernoulli-Euler Beams with a single-edge crack," 31st ASME/ASCE/AHS/ASC Structures, Structural Dynamics and Materials Conference AIAA Paper, pp. 1990-1124, 1990.
- [28] Y. C. Chu, M. H. H. Shen, "Analysis of forced bilinear oscillators and the application to cracked beam dynamics," *AIAA Journal*, vol. 30, no. 10, pp. 2512–2519, 1992.
- [29] T. D. Dang, R. K. Kapania, M. J. Patil, "Analytical modeling of cracked thin-walled beams under torsion," *AIAA Journal*, vol. 48, no. 3, pp. 664–675, 2010.
- [30] Y. S. Lee, M. J. Chung, "A study on crack detection using eigenfrequency test data," *Computers and Structures*, vol. 77, no. 3, pp. 327–342, 2000.
- [31] S. Moradi, P. Razi, L. Fatahi, "On the application of bees algorithm to the problem of crack detection," *Computers and Structures*, vol. 89, no. 23-24, pp. 2169–2175, 2011.
- [32] K. H. Barad, D. S. Sharma, V. Vyas, "Crack detection in cantilever beam by frequency based method," *Procedia Engineering*, vol. 51, pp. 770–775, 2013.
- [33] N. Hu, X. Wang, H. Fukunaga, Z. H. Yao, H. X. Zhang, Z. S. Wu, "Damage assessment of structures using modal test data," *International Journal of Solids and Structures*, vol. 38, no. 18, pp. 3111–3126, 2001.
- [34] N. T. Khiem, L. K. Toan, "A novel method for crack detection in beam-like structures by measurements of natural frequencies," *Journal of Sound and Vibration*, vol. 333, no. 18, pp. 4084–4103, 2014.
- [35] J. K. Sinha, M. I. Friswell, S. Edwards, "Simplified models for the location of cracks in beam structures using measured vibration data," *Journal of Sound and Vibration*, vol. 251, no. 1, pp. 13–38, 2002.
- [36] H. I. Yoon, I. S. Son, S. J. Ahn, "Free vibration analysis of Euler-Bernoulli Beam with double cracks," *Journal of Mechanical Science and Technology*, vol. 21, no. 3, pp. 476–485, 2007.



SAKARYA ÜNİVERSİTESİ

# FEN BİLİMLERİ ENSTİTÜSÜ DERGİSİ

## Sakarya University Journal of Science SAUJS

ISSN 1301-4048 e-ISSN 2147-835X Period Bimonthly Founded 1997 Publisher Sakarya University  
<http://www.saujs.sakarya.edu.tr/>

Title: Frequency Analysis of Rounded Shaped Inductive Metallic Objects in Waveguides  
via some PEC Approximations and GSM Method

Authors: Ahmet AYDOĞAN

Received: 2022-06-28 00:00:00

Accepted: 2022-10-18 00:00:00

Article Type: Research Article

Volume: 26

Issue: 6

Month: December

Year: 2022

Pages: 1244-1252

How to cite

Ahmet AYDOĞAN; (2022), Frequency Analysis of Rounded Shaped Inductive Metallic  
Objects in Waveguides via some PEC Approximations and GSM Method. Sakarya  
University Journal of Science, 26(6), 1244-1252, DOI:  
10.16984/saufenbilder.1136854

Access link

<https://dergipark.org.tr/en/pub/saufenbilder/issue/74051/1136854>

New submission to SAUJS

<http://dergipark.gov.tr/journal/1115/submission/start>

## Frequency Analysis of Rounded Shaped Inductive Metallic Objects in Waveguides via some PEC Approximations and GSM Method

Ahmet AYDOĞAN\*<sup>1</sup> 

### Abstract

A hybrid method is proposed for the frequency analysis of rounded metallic objects inductively loaded in rectangular waveguides. The proposed method combines the efficiency of the generalized scattering matrix method (*GSM*) and the flexibility of the method of moments (*MoM*) and the fact that fields cannot exist inside perfect electric conductors. Metallic discontinuities are modelled as a dielectric medium with extreme conductivity and the volume is emptied except the surrounding area. The proposed method is tested against several structures including a band-pass filter composed of metallic rods and an arbitrarily shaped discontinuity. The accuracy of the method is compared to commercial software based on the finite element method. The proposed method is exclusively competent for the frequency analysis of rounded or arbitrarily shaped metallic discontinuities.

**Keywords:** Arbitrarily shaped discontinuities, computational efficiency, generalized scattering matrix method, microwave devices, waveguide discontinuities.

### 1. INTRODUCTION

Due to their high-power handling, high-quality factor, and low insertion loss, waveguides are essential for military, space, and terrestrial communication systems [1]. Scattering analysis of the modes supported by rectangular waveguides loaded with inductive discontinuities is simpler than that of waveguides loaded with capacitive or inductive and capacitive discontinuities. Furthermore, due to their ease of fabrication, inductive waveguides are popular microwave

device elements. As a result, there is a large body of literature devoted to the fast and reliable analysis of inductively loaded waveguide structures.

A variational method was proposed for inductive metallic and low-valued dielectric posts with a small radius positioned in a waveguide [2]. In the following decades, physical property limitations are eliminated by analyzing higher-order modes and employing computational methods such as the method of moments (*MoM*) for the analysis of various

\* Corresponding author: ahmet.aydogan@marmara.edu.tr

<sup>1</sup> İzmir Bakırçay University,

ORCID: <https://orcid.org/0000-0002-6037-0578>



and arbitrarily cross-sectioned dielectric posts [3], or the numerically cost-effective mode-matching (*MM*) method for the analysis of inductive parts [4]. The demand for high numerical flexibility and efficiency on problem configuration resulted in the development of hybrid methods that integrate the effectiveness of *MM* method with the flexibility of spatial techniques such as the finite element method (*FEM*), *MoM*, or finite difference (*FD*), for which an extensive study was published [5]. To investigate the scattering of dielectric posts, a circular boundary technique is utilized [6], however, this approach becomes inefficient once the discontinuities are close to the step discontinuities since the method regards only the dominant mode and higher-order mode interaction should be regarded in mentioned cases. Higher-order modes overcome this barrier [7], allowing inductive step frequency responses to be analyzed independently using the well-known mode matching method [8]. A more generic solution in terms of the shape and type of discontinuities (metallic and/or homogeneous dielectric bodies) for inductively loaded waveguides was introduced by solving the surface integral equation with *MoM* [9] and the same procedure is applied to a similar waveguide problem with a step offset combining two waveguides [10]. Although having no capability for metallic discontinuities, a hybrid technique for an effective analysis of dielectric discontinuities using a volumetric *MoM* procedure removes the restrictions on the homogeneity of dielectric discontinuities [11]. A method for the efficient analysis of metallic discontinuities is proposed in [12] where the basic strategy is inspired by [11]. In [12] the metallic discontinuities are modeled with extremely lossy dielectric values [13] and the analyzed shapes are competitive with cuboid shapes since the analysis of non-cuboid obstacles has a high computational cost due to the volumetric analysis of discretized cells in *MoM* procedure. The recent interest in the fast and efficient analysis of waveguide

structures is not limited to only inductive structures but also directed to those of capacitive structures and axially symmetric waveguides or discontinuities. In [14], the integral equation method introduced in [9] is adapted for capacitive obstacles, and in [15] capacitive obstacles in waveguides with step offsets are analyzed. The fast analysis of discontinuities in axially symmetric waveguides [16] and axially symmetric discontinuities in waveguides [17] via hybrid techniques are introduced to the community. Besides, the *GSM* method is still a powerful, efficient, and reliable tool for actual guided wave problems [18, 19].

In this study, the high computational cost is reduced for non-cuboid shapes by utilizing the boundary conditions of electric fields for *PEC* objects. Therefore, the electric fields inside the objects are null and no computational analysis is needed inside the objects. This new efficient analysis tool also has the potential to propose new design possibilities for microwave devices built by waveguides loaded with inductively and arbitrarily shaped *PEC* obstacles. The time dependency is chosen as  $e^{-i\omega t}$  during numerical analysis.

## 2. PROBLEM DESCRIPTION

Fig. 1 depicts the problem to be considered. Arbitrarily shaped metallic discontinuities are located in a rectangular waveguide. Obstacles fill the waveguide in the height (i.e.,  $y$  direction) so only  $TE^{m0}$  type modes can exist in the waveguide in the dominant mode region and the case of dominant mode excitation.

Note that several metallic discontinuities aligned horizontally (by discretizing the whole system in the widthwise direction) and/or longitudinally (by cascading the *GSMs* of longitudinal elements) can be analyzed with the proposed method in the most general sense. The scattering parameters for the two-port network



are aimed to be calculated at *Port 1* and *Port 2*.

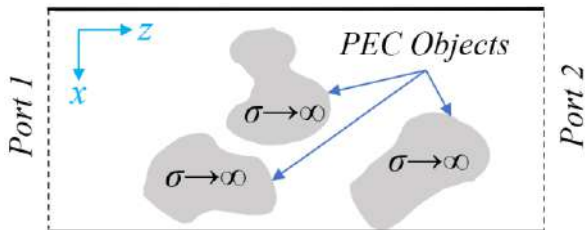


Figure 1 Problem description – longitudinal and top view of the waveguide loaded with arbitrarily shaped and oriented PEC objects ( $\sigma$  is the electrical conductivity)

### 3. METHOD

The cascading capabilities of the GSM approach are used to perform the scattering analysis of the discontinuities, while the elements of *GSM* for the cascaded structures are built using an *MoM*-based procedure [12]. The obstacles are divided into individual blocks in the longitudinal direction ( $z$ -direction in Fig. 1) and the GSM of each individual block is constructed separately. Finally, the GSM of the obstacles and the whole system is obtained by cascading the GSMs of individual blocks and GSMs of longitudinally separated obstacles, respectively. In terms of electrical response, all metallic discontinuities are considered to have an extremely high loss dielectric characteristic model as applied in [12] by a complex relative permittivity of  $\epsilon_r = 1 + j\sigma/\omega\mu_0$ , where  $\omega$ ,  $\mu_0$ , and  $\sigma$  are the angular frequency, magnetic constant of free space, and the conductivity of the dielectric model under investigation, respectively. Modal interactions are examined utilizing the orthogonality of the modes and some powerful acceleration steps are applied. To avoid repetition, the interested readers are referred to [11], [12]. Due to the high change in the value of the Dyadic Green's Function (*DGF*) as the kernel in the integral equation of the interested scattering problem for an extremely lossy model (e.g., extremely high conductivity), one should discretize the obstacles with tiny cells. Hence, the number of

cells increases tremendously and the proposed method in [12] becomes competitive for repeating individual blocks such as longitudinally oriented cubes, and inductive discontinuities but not for rounded or arbitrary shapes due to a high amount of individual blocks with too many cells to be examined. In this study, this challenge is tackled, and to reduce the numerical cost, the number of cells to be analyzed is decreased by utilizing the fact that the electric fields are null inside the PEC. A narrative illustration of the mentioned steps is given in Fig. 2. In Fig. 2a, two representative PEC obstacles are separated by a distance  $d$  in the longitudinal direction as the original problem. The GSM of separated parts, if exist, can be obtained by using the transmission line approach. In Fig. 2, the GSM of the gap with the length of  $d$  for an  $M \times M$  modal analysis is a diagonal matrix for which the diagonal elements  $D_{mm} = e^{j\beta_m d}$ ,  $m = 1, 2, \dots, M$  and  $\beta_m$  is the propagation constant for related  $TE^{m0}$  mode. Note that since the obstacles are invariant in  $y$  direction, only  $TE^{m0}$  type modes can be excited. Then, obstacles are discretized with tiny cells as in Fig. 2b where cells are not scaled as in the practical case but depicted comparatively large for the sake of narration. Also, discretized cells are modeled with extremely high lossy dielectric material instead of PEC behavior. The considered problem can be solved with such discretization (as in Fig. 2b) at the cost of immensely high computational effort with the method given in [12]. In this study, Fig. 2c and Fig. 2d strategies are proposed to solve the original problem. In Fig. 2c, it is illustrated that the discretized cells are removed except those at the boundary applying the theoretical fact that fields are null inside. Then the computation domain is reduced by removing the repeating individual blocks as in Fig. 2d if any exist. The reduced discretized cells are arranged as individual blocks containing lateral cells and the GSMs of individual blocks are calculated via the proposed method in [11] and the calculations

are also accelerated by applying the proposed strategies in [12]. A considerable amount of the computational cost for each individual block arises due to the number of cells in the width-wise direction (i.e.,  $x$  direction).

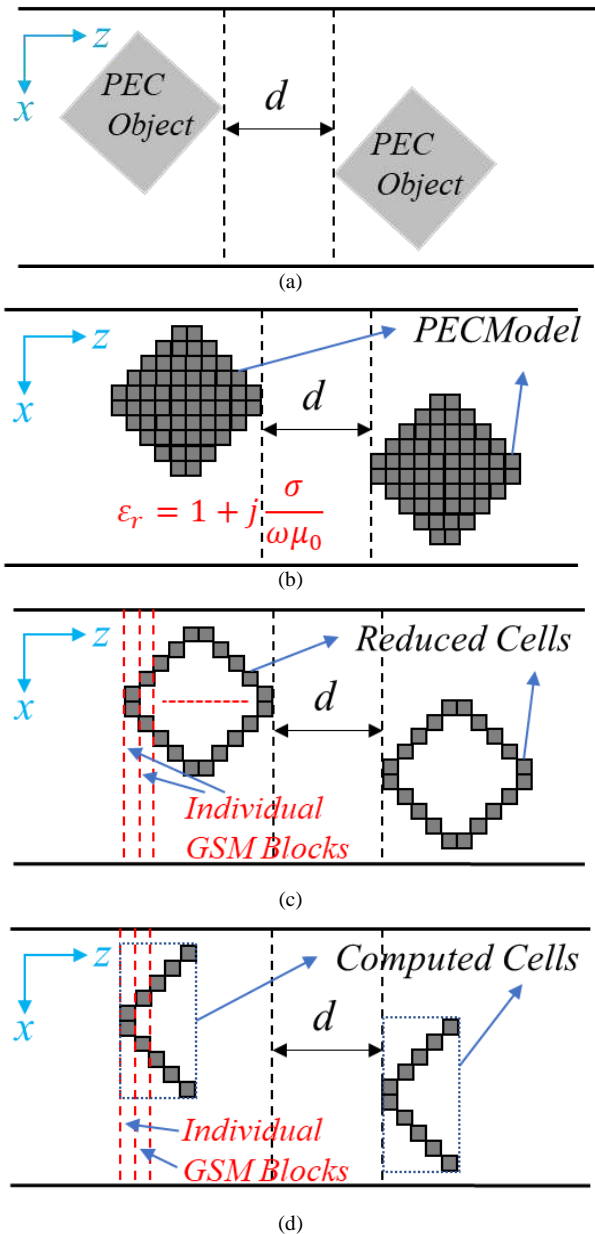


Figure 2 Example problem (a) original case (b) discretized PEC model (c) proposed approach with reduced cells (d) final computation case

A new computational strategy is also applied in this study alongside the previous strategies mentioned. One should discretize the cells so

that the integral of the DGF becomes stable as much as possible for the applied point-matching *MoM*. The DGF to be integrated inside each cell varies as a function of the medium parameters only in the  $z$  direction ( $e^{j\beta_m|z-z'|}$  term in (Equation (1), [11])). On the other hand, the roundedness of an arbitrarily shaped object decreases as the cubicity of the discretized cells increases. Regarding these points, the cells are discretized tinier in the direction of the propagation (i.e.,  $z$  direction in the given geometry) and larger in the height ( $y$  direction) and width ( $x$  direction). Finally, all GSMs (those of the PEC bodies, the gap between bodies, etc.) are cascaded to obtain the general scattering matrix of the whole system [20].

#### 4. NUMERICAL CONSIDERATIONS & EXAMPLES

A band-stop filter [13] and an arbitrarily shaped PEC obstacle are analyzed to test the proposed method and obtained results are compared with FEM-based commercially available software high-frequency structure simulator (*HFSS*). PEC obstacles are modeled with a relative complex permittivity of  $\epsilon_r = 1 + j \sigma / \omega \mu_0$  where conductivity value is assigned as  $\sigma = 10^{30} S/m$ . The analyses are carried out on a standard PC. The heights of the waveguides are reduced to that of the cell size in the vertical direction (i.e.,  $y$  direction in the given problem geometry) which gives one discretized cell in the height as proposed in [11], [12]. Besides, each individual block has one discretized cell in the direction of propagation (i.e., in the  $z$  direction). The obstacles are discretized with  $(3\Delta, 3\Delta, \Delta)$  in  $(x, y, z)$  directions, respectively to reduce the computational cost and provide computational stability where  $\Delta = \lambda_{min}/600$  is the cell dimension and  $\lambda_{min}$  is the smallest wavelength in the analyzed frequency band. The frequency band is divided into  $S$  equispaced points for both examples.

In the first example, the analysis of a band-pass filter composed of constant diameter and off-centered circular metallic cylinders is performed [7]. The analysis is conducted for  $S=91$  equispaced frequency points in the given band. The geometry and dimensions of the system and the discretized mesh distribution are given in Fig. 3. As mentioned previously, the inner cells are removed and the GSMs of each separate cylinder and those of the empty parts between cylinders are calculated. Then, the GSMs of the cylinders and the empty regions are cascaded to obtain the GSM of the whole structure. The desired S- parameters are extracted from the GSM of the whole structure, and these are the dominant mode ( $TE^{10}$ ) to dominant mode ( $TE^{10}$ ) interaction between ports. The frequency response of the metallic-cylinder filter is compared in Fig. 4 between the proposed method and HFSS both for phase and magnitude. A close agreement can be observed and the average computation times per frequency are recorded as 1.31 s and 4.46 s for the proposed method and HFSS, respectively. The comparison of computational time for the commercial software and this method is given in Table 1.

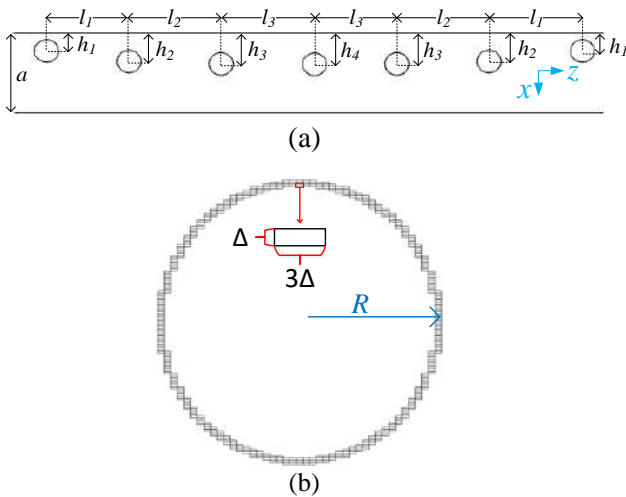


Figure 3 (a) Geometry of the metallic post filter with  $a = 22.86 \text{ mm}$ ,  $r = 3.21 \text{ mm}$ ,  $h_1 = 5.215 \text{ mm}$ ,  $h_2 = 8.172 \text{ mm}$ ,  $h_3 = 8.863 \text{ mm}$ ,  $h_4 = 8.971 \text{ mm}$ ,  $l_1 = 21.895 \text{ mm}$ ,  $l_2 = 24.461 \text{ mm}$ ,  $l_4 = 24.797 \text{ mm}$ , (b) mesh distribution of an equal cylinder in the system

Table 1 Comparison of computational times

Time per frequency	Method	HFSS
Example 1	1.31 s/f	4.46 s/f
Example 2	0.82 s/f	2.27 s/f

In the second example, an arbitrarily shaped PEC obstacle is investigated in the 8 – 12 GHz band which is depicted with geometrical properties in Fig. 5a. The commercial software model of the object is also shown as an inset in Fig. 6. Also, the discretized cell distribution analyzed via proposed method is given in Fig. 5b. As in the previous example, the inner cells are removed and the object is divided into individual blocks in the direction of propagation (i.e., z direction).

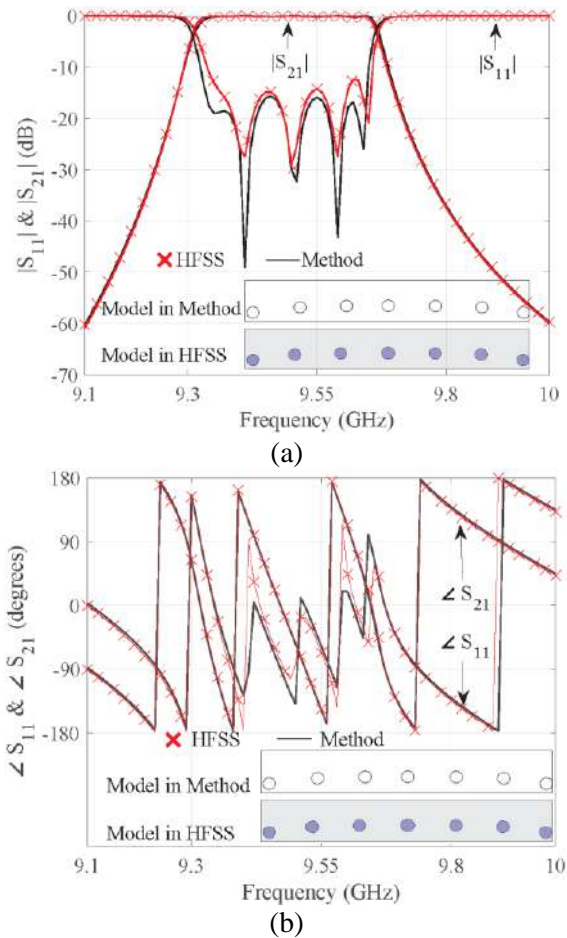


Figure 4 Comparison between the proposed method and HFSS for the frequency response of the band-pass filter (a) magnitude (b) phase

Following the calculation of the GSM of each individual block, these GSMs are cascaded to obtain the GSM of the whole structure (the arbitrarily shaped PEC object). Then, the desired modal interaction is obtained from the whole GSM. In this problem, it is the dominant mode ( $TE^{10}$ ) to dominant mode ( $TE^{10}$ ) interaction between ports. The frequency band is divided into  $S = 41$  equispaced frequency points in the given band. An excellent agreement can be observed both for magnitude and phase of the scattering parameters observed at *Port 1* and *Port 2* as shown in Fig. 6. The average computation times per frequency is recorded as  $0.82\text{ s/f}$  and  $2.27\text{ s/f}$  for the proposed method and *HFSS*, respectively. The comparison of computational time for the commercial software and this method is listed in the second row of Table 1.

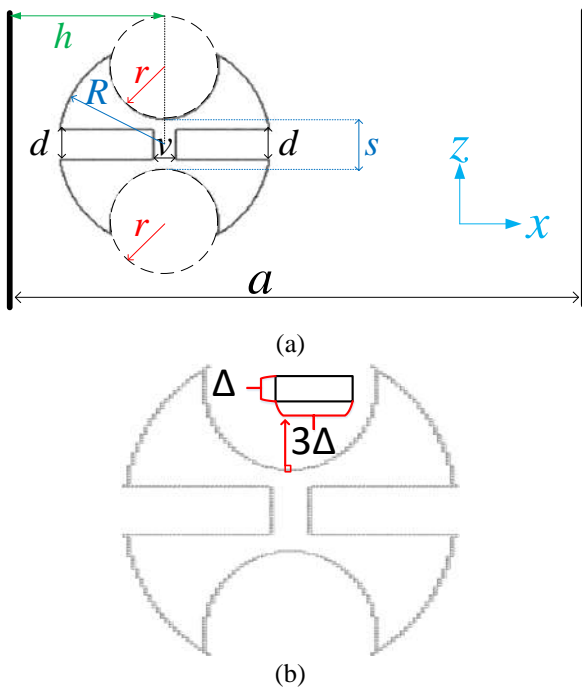


Figure 5 Arbitrarily shaped rounded PEC object  
 a) the geometry with  $R = 2\text{ mm}$ ,  $h = 3.715\text{ mm}$ ,  $r = 1\text{ mm}$ ,  $v = 0.8\text{ mm}$ ,  $s = 0.6$ ,  $d = 0.6\text{ mm}$  b) constructed model in the method

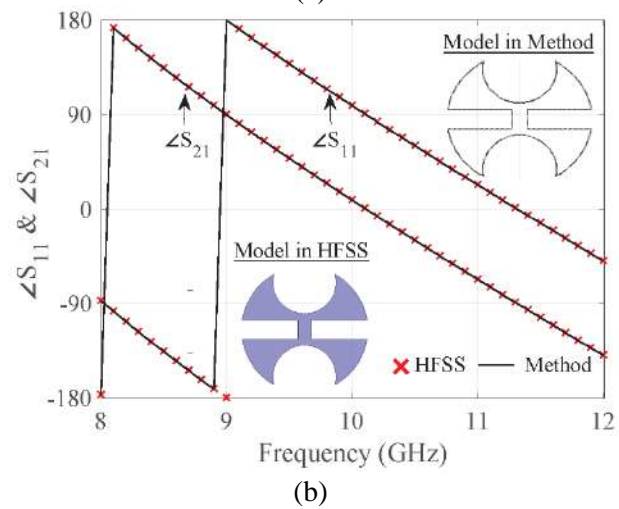
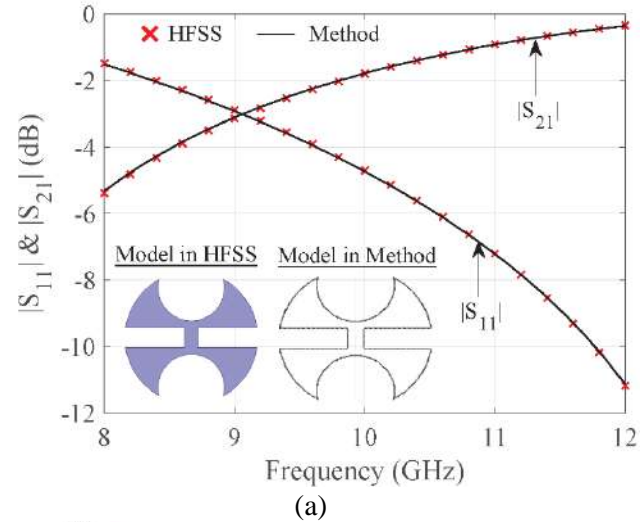


Figure 6 Comparison between the proposed method and *HFSS* for the frequency response of the arbitrarily shaped PEC object (a) magnitude (b) phase

### 5. CONCLUSIONS

The previous inefficiency in the computational competency of volumetric analysis for metallic obstacles inductively located in a rectangular waveguide is addressed. The metallic obstacle is modeled by an extremely lossy dielectric material and discretized for an *MoM* procedure. PEC boundary conditions are utilized and the inner cells are removed which immensely reduces the computational cost. The scattering analysis of the whole structure is carried out via the *GSM* method. The proposed method is tested with numerical examples involving

rounded or arbitrarily shaped metallic obstacles and compared with *HFSS*. The results show that the proposed method provides a fast and reliable analysis tool for the frequency analysis of arbitrarily shaped metallic objects inductively loaded in rectangular waveguides. This method may provide new possibilities with analysis capabilities for the design of microwave devices via iterative optimization techniques where a fast and reliable analysis of the system is vital. Besides, the considered problem can be extended to the analysis of systems composed of both dielectric and rounded metallic obstacles.

#### ***The Declaration of Conflict of Interest/ Common Interest***

No conflict of interest or common interest has been declared by the author.

#### ***The Declaration of Ethics Committee Approval***

This study does not require ethics committee permission or any special permission.

#### ***The Declaration of Research and Publication Ethics***

The author of the paper declares that they comply with the scientific, ethical, and quotation rules of SAUJS in all processes of the paper and that they do not make any falsification on the data collected. In addition, they declare that Sakarya University Journal of Science and its editorial board have no responsibility for any ethical violations that may be encountered and that this study has not been evaluated in any academic publication environment other than Sakarya University Journal of Science.

### **REFERENCES**

- [1] R. J. Cameron, C. M. Kudsia, R. R. Mansour, *Microwave Filters for Communication Systems*, Hoboken, NJ, USA: John Wiley & Sons, Inc., 2018.
- [2] J. Schwinger, D. Saxon, *Discontinuities in Waveguides: notes on Lectures by Julian Schwinger*. CRC Press, 1968.
- [3] Chung-I G. Hsu, H. A. Auda, "Multiple Dielectric Posts in a Rectangular Waveguide," *IEEE Transactions on Microwave Theory and Techniques*, vol. 34, no. 8, pp. 883–891, Aug. 1986.
- [4] M. Guglielmi, G. Gheri, M. Calamia, G. Pelosi, "Rigorous multimode network numerical representation of inductive step," *IEEE Transactions on Microwave Theory and Techniques*, vol. 42, no. 2, pp. 317–326, 1994.
- [5] F. Arndt; J. Brandt; V. Catina; J. Ritter; I. Rullhusen; J. Dauelsberg; U. Hilgefort; W. Wessel, "Fast CAD and Optimization of Waveguide Components and Aperture Antennas by Hybrid MM/FE/MoM/FD Methods—State-of-the-Art and Recent Advances," *IEEE Transactions on Microwave Theory and Techniques*, vol. 52, no. 1, pp. 292–305, Jan. 2004.
- [6] H. Esteban, S. Cogollos, V. E. Boria, A. S. Blas, M. Ferrando, "A new hybrid mode-matching/numerical method for the analysis of arbitrarily shaped inductive obstacles and discontinuities in rectangular waveguides," *IEEE Transactions on Microwave Theory and Techniques*, vol. 50, no. 4, pp. 1219–1224, Apr. 2002.
- [7] C. Bachiller, H. Esteban, H. Mata, M. Á. Valdes, V. E. Boria, Á. Belenguer, J. V. Morra, "Hybrid mode matching method for the efficient analysis of metal and dielectric rods in H plane rectangular waveguide devices," *IEEE Transactions on Microwave Theory and Techniques*, vol. 58, no. 12, pp. 3634–3644, 2010.



- [8] J. M. Reiter, F. Arndt, "Rigorous Analysis of Arbitrarily Shaped H- and E-Plane Discontinuities in Rectangular Waveguides by a Full-Wave Boundary Contour Mode-Matching Method" *IEEE Transactions on Microwave Theory and Techniques*, vol. 43, no. 4, 1995.
- [9] F. D. Pereira; V. E. Boria, J. P. Garcia, A. V. Pantaleoni; A. A. Melcon, J. L. Tornero, B. Gimeno "Efficient analysis of arbitrarily shaped inductive obstacles in rectangular waveguides using a surface integral-equation formulation," *IEEE Transactions on Microwave Theory and Techniques*, vol. 55, no. 4, pp. 715–721, 2007.
- [10] F. D. Pereira, C. Gómez Molina, A. Alvarez Melcon, V. E. Boria, M. Guglielmi, "Novel Spatial Domain Integral Equation Formulation for the Analysis of Rectangular Waveguide Steps Close to Arbitrarily Shaped Dielectric and/or Conducting Posts," *Radio Science*, vol. 53, no. 4, pp. 406–419, 2018.
- [11] A. Aydoğan, "A hybrid MoM/MM method for fast analysis of E-plane dielectric loaded waveguides," *AEU - International Journal of Electronics and Communications*, vol. 100, pp. 9–15, 2019.
- [12] A. Aydoğan, "An inclusive analysis of inductive dielectric and/or metallic discontinuities in a rectangular waveguide," *Microwave and Optical Technology Letters*, vol. 63, no. 2, 2021.
- [13] A. Sihvola, I. V. Lindell, H. Wallén, P. Ylä-Oijala, "Material realizations of perfect electric conductor objects," *Applied Computational Electromagnetic Society Journal*, vol. 25, no. 12, pp. 1007–1016, 2010.
- [14] F. D. Pereira, A. Romera Perez, P. Vera Castejon, A. Alvarez Melcon, "Integral-Equation Formulation for the Analysis of Capacitive Waveguide Filters Containing Dielectric and Metallic Arbitrarily Shaped Objects and Novel Applications," *IEEE Transactions on Microwave Theory and Techniques*, vol. 63, no. 12, pp. 3862–3873, Dec. 2015.
- [15] F. D. Pereira, C. Gomez Molina, A. Alvarez Melcon, V. E. Boria Esbert, M. Guglielmi, "On the analysis of capacitive rectangular waveguide discontinuities close to arbitrarily shaped conducting and dielectric posts," *AEU - International Journal of Electronics and Communications*, vol. 113, 2020
- [16] M. Warecka, R. Lech, P. Kowalczyk, "Efficient Finite Element Analysis of Axially Symmetrical Waveguides and Waveguide Discontinuities," *IEEE Transactions on Microwave Theory and Techniques*, vol. 67, no. 11, 2019.
- [17] M. Warecka, R. Lech, P. Kowalczyk, "Hybrid analysis of structures composed of axially symmetric objects," *IEEE Transactions on Microwave Theory and Techniques*, vol. 68, no. 11, 2020.
- [18] C. Kohlberger, A. Stelzer, "Multi-Modal Scattering and Propagation Through Several Close Periodic Grids," *IEEE Transactions on Antennas and Propagation*, vol. 70, no. 7, pp. 5758-5769, July 2022.
- [19] C. Stoumpos, J. P. Fraysse, G. Goussetis, C. G. Gonzalez, R. Sauleau, H. Legay, "Highly Efficient Broadband Pyramidal Horn Antenna with Integrated H-Plane Power Division," *IEEE Transactions on Antennas and Propagation*, vol. 70, no. 2, pp. 1499-1504, Feb. 2022.

- [20] T. S. Chu, T. Itoh, "Generalized Scattering Matrix Method For Analysis Of Cascaded And Offset Microstrip Step Discontinuities.," IEEE Transactions on Microwave Theory and Techniques, vol. 34, no. 2, Feb. 1986.



SAKARYA ÜNİVERSİTESİ

# FEN BİLİMLERİ ENSTİTÜSÜ DERGİSİ

Sakarya University Journal of Science  
SAUJS

ISSN 1301-4048 e-ISSN 2147-835X Period Bimonthly Founded 1997 Publisher Sakarya University  
<http://www.saujs.sakarya.edu.tr/>

Title: A Phased Array Antenna System of a Millimeter-wave FMCW Radar for Blind Spot  
Detection of Mobile Robots

Authors: Hüseyin Şerif SAVCI

Received: 2022-06-15 00:00:00

Accepted: 2022-10-20 00:00:00

Article Type: Research Article

Volume: 26

Issue: 6

Month: December

Year: 2022

Pages: 1253-1261

How to cite

Hüseyin Şerif SAVCI; (2022), A Phased Array Antenna System of a Millimeter-wave  
FMCW Radar for Blind Spot Detection of Mobile Robots. Sakarya University Journal  
of Science, 26(6), 1253-1261, DOI: 10.16984/saufenbilder.1131504

Access link

<https://dergipark.org.tr/en/pub/saufenbilder/issue/74051/1131504>

New submission to SAUJS

<http://dergipark.gov.tr/journal/1115/submission/start>



## A Phased Array Antenna System of a Millimeter-wave FMCW Radar for Blind Spot Detection of Mobile Robots

Hüseyin Şerif SAVCI\*<sup>1</sup> 

### Abstract

Mobile robots have been extensively used in manufacturing plants for inter-logistic transportation in recent years. This paper covers a phased array antenna design for a millimeter wave radar system to improve lidar-based navigation systems' safety and environmental consciousness. The K-band phased array antenna, when integrated with 24 GHz Frequency-Modulated-Continuous-Wave (FMCW) radar, not only enhances the accuracy of the 2-D Area Scanning lidar system but also helps with the safe operation of the vehicle. The safety improvement is made by covering blind spots to mitigate collision risks during the rotations. The paper first reviews the system-level details of the 2D lidar sensor and shows the blind spots when integrated into a Mobile Robot prototype. Then continues with the inclusion of an FMCW Low-Speed Ramp radar system and discusses the design details of the proposed K-band antenna array, which will be integrated with a radar sensor.

**Keywords:** Mobile robots, lidar, FMCW radar, blind-spot detection, natural navigation, planar antenna array

### 1. INTRODUCTION

With the advancement of sensory devices, autonomous aerial, water, and ground vehicles are found in many usages, from surveillance to transportation. Autonomous Mobile Robots (MoRo) are becoming an essential part of heavy industry production plants to improve safety and reduce the risk of material and human loss and damage. Mobile Robots have been performing indoor transportation tasks in many plants without an operator. They transfer inter-

logistic production parts in factories, carry luggage in airports, and offer hotel room service. The system specs, physical constraints, and shapes may vary considerably depending

on the use case. However, they all used similar sensors and had to tackle similar problems [1].

The emergence of Industry 4.0 and intelligent plants put autonomous vehicles on the front lines of manufacturing operations to reduce the risk of operator failure and equipment loss and

\* Corresponding author: [hsavci@medipol.edu.tr](mailto:hsavci@medipol.edu.tr)

<sup>1</sup> İstanbul Medipol University, Department of Electrical and Electronics Engineering

ORCID: <https://orcid.org/0000-0002-5881-1557>



to increase overall efficiency and throughput. As the product variety has increased in the factories, more parts must be moved to the edge of the production line with highly accurate timing. Such a time-sensitive operation requires complex logistic management in an extremely dynamic environment. That is the main reason behind deploying mobile robots with self-navigating capability. For example, in a typical modern automotive assembly line, roughly 25 manual forklifts work around the clock with 80 operators [2]. However, the same assembly line can function with only eight autonomous mobile robots, resulting in the same productivity and increased safety. These numbers show that a mobile robot can amortize itself in 1.5 years. For these reasons, autonomous mobile robots will be one of the significant inter-logistic equipment in heavy-duty assembly lines of factories very soon [3].

There are several different navigation and guidance systems for mobile vehicles. The natural navigation system is the most suitable for manufacturing plants with dynamically changing environments due to its manageable implementations and fast adaptations. Also, facilities with highly hazardous environments, such as nuclear fusion reactors, benefit from autonomous mobile vehicles with navigation technologies [4]. Other systems require structural changes in plants, such as installing RF beacons and magnetic stripes as guiding tracks on the floor. These are more expensive and less flexible than natural navigation systems [5, 6].

MoRos, with natural navigation guidance systems, employ a laser-based scanning technology called Laser Detection and Ranging (lidar) [7]. These scanners are placed on the body of the vehicle. The MoRo continuously uses the lidar sensor in map generation, navigation, and environment detection for safe operation. In natural navigation systems, reference images of the vehicle's operating area are stored in the vehicle's memory. Navigation

uses data reflected from the objects around the vehicle, such as walls, columns, machines, and barriers. Positioning is found by comparing the incoming point clouds with the ones stored in the memory [8].

For the autonomous navigation of mobile robots, various sensor technologies such as ultrasonic sensors, magnetic tapes, low energy Bluetooth, UHF RFID, mono/stereo cameras, lidar, and radar-based systems are being used [9, 10]. As part of safe navigation, the precision of obstacle detection and avoidance would determine the level of safety for mobile robots. Several obstacle detection and avoidance techniques use different sensors, such as ultrasound-based, camera-based, radar-based, and lidar-based. These sensors are not only used for natural navigation and the primary localization system but also a safety alarm by constantly surveilling the surrounding against safety hazard issues [8, 11]. Each sensor has its unique strength and weakness. The camera-based systems do real-time image-capturing of the environment and perform image processing techniques on the live images [8]. In addition, several studies, such as deep learning-based intelligent surveillance, utilize only cameras [12]. However, this solution requires extensive processing power and raises some privacy concerns. For example, radar sensors lack the ability of object classification and the level of accuracy compared to other systems. Lidar is the leading technology for mobile vehicle navigation and obstacle avoidance systems. Although the costs are too high for consumer use, the lidar is still superior to the alternatives from an accuracy and safety point of view [13].

Moreover, with the lidar wavelengths around 700nm-1500nm, the system sensitivity is in the order of centimeters which meets the safety demands of inter-logistic transportation in manufacturing plants. However, lidar is not the ultimate standalone solution. The high cost of lidar units limits the number of such sensors installed on a vehicle. This limitation results in

significant safety flaws, such as blind spots. Therefore, other technologies, such as radar and camera sensors, are also being considered to complete autonomous operations [8, 11, 13, 14]. However, in the current commercial developments, neither of these sensors (lidar, radar, camera) can alone be used in mobile robots. However, each may have some advantages over others in some specific cases.

Figure 1 shows a performance comparison among three major sensor types: radar, lidar, and camera. The plot evaluates them on nine different conditions. Here 0 is the worst, and ten is the best in the corresponding category. We can see that some have superior performance for different conditions while inferior for others. None is sufficient in all situations and cases, especially detecting obstacles and blind spots. However, combining different technologies reduces the risk of failure to sufficiently cover all possible scenarios. However, the optimum combination is solely dependent on the use case. As complementary to lidar-based systems, radar comes as one of the best solutions for its high-speed operation, safe usage, privacy concerns, ruggedness against environmental factors such as smoke, dust, and dirt, and less demand for processing power. It is seen from Figure 1 that the limited horizontal resolution of the lidar would risk the mobile robot's safe operation. This limitation is addressed by integrating a radar sensor into a mobile robot's lidar-based sensing system. Finally, they together can satisfy a 360° continuous environment detection for mobile robots [8, 11].

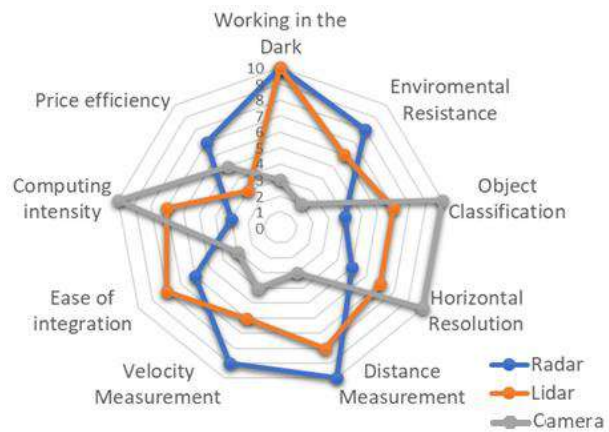


Figure 1 The capability of different sensors

## 2. SYSTEM CONSIDERATIONS

Figure 2 shows a 3D system sketch of an autonomous mobile robot. The system's power train consists of an industrial PLC, a safety PLC, two front and rear caster wheels, two DC-motor-powered driver wheels in the middle, and two lidars in the front and rear.

This study is carried out in two phases. First, in the prototype, the mobile robot prototype includes only a lidar sensor. The lidar data are obtained in a natural working environment.

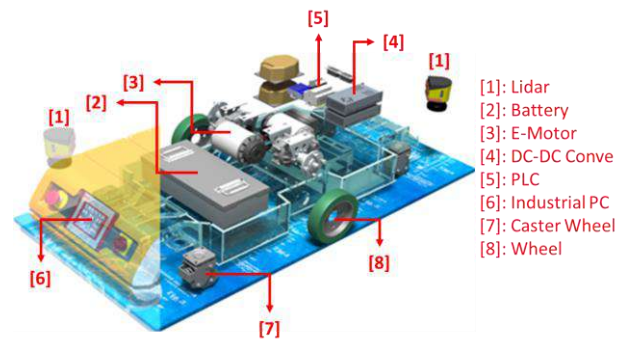


Figure 2 System Blocks of Mobile Robots

The shortcomings of lidar-only detection are found. In the second phase, commercially available millimeter wave ISM (Industrial, Scientific, and Medical) radar systems are investigated to be used as a complementary system to lidar-only detection. Analog Devices

Eval-Radar-MMIC2 24GHz FMCW, radar development kit, is selected. This radar measures the range, velocity, and angle of arrival of the objects in its range. The equipment needs a phased array antenna system. The design and measurement of the antenna system are explained in detail.

## 2.1. Lidar, Point Clouds, and Blind Spots

A lidar system detects the objects in front and behind the mobile vehicles as point clouds which are the positive pixels detected as bouncing-back laser beams from a nearby object. The 2D lidar system continuously scans the laser beam in azimuth angles and generates such time and space-variant point clouds.

Figure 3 shows the measurement data taken by the actual lidar system mounted in the front and rear bumper of a Mobile Robot. In this picture, the orange square represents the vehicle itself. The red arrow points to the direction of movement and the front side of the vehicle. Blue dots in the point cloud indicates objects around. The point cloud distributions change as time and vehicle progress. Data shown here is from the same instance of time and state of the vehicle. A dynamic map is generated by combining the front and rear lidar raw data when data is processed on the static map. It is seen from this figure that lidar helps the navigation of the vehicle by constantly detecting the objects around it. Each lidar scans an area with an angle of  $210^\circ$ . However, it is also seen that there are regions marked with yellow question marks that are unreachable by any of the lidar laser beams. Each of these regions corresponds to an angle of roughly 30 degrees midway on both sides of the vehicle. These unlit regions are called blind spots, which cause significant safety risks. Therefore, it is crucial to detect any static or moving object in these areas to be able to make a sudden left or right turn safely.

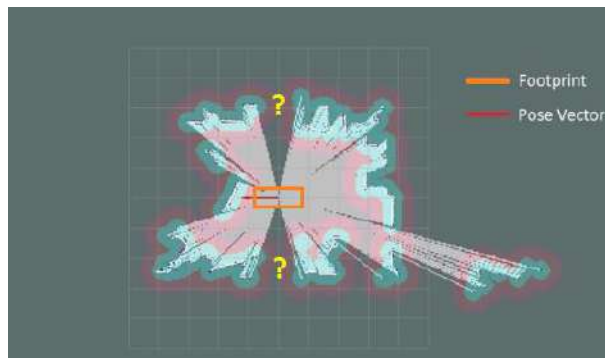


Figure 3 lidar beams coverage and blind spots

The lidar technology's cost and size limit the number of sensors to be used in a mobile robot. Thus, a radar sensor is adopted to improve the coverage and detection of objects in the blind spot, which ultimately increases the vehicle's safety and enhances the accuracy of navigation maps.

## 2.2. Radar and Antenna Arrays

Radar technology only found its usage in the aviation and defense industry (ADEF) for many decades due to its high cost and bulky size up until the 2000s. Over the last two decades, integrating RF and digital parts of entire transceiver circuits in Silicon-based semiconductor technologies such as SOI-CMOS and SiGe BiCMOS enabled its wide usage in many commercial applications and reduced overall cost tremendously [15]. In recent years, radar is becoming a standard part of Advanced Driver Assistance Systems (ADAS) in many automobiles. Including radar for blind spot detection, short-range and long-range collision avoidance, parking assistance, lane tracking/changing assistance, vital function monitor, gesture recognition, and contactless infotainment has dramatically improved the safety, security, and comfort of the vehicles.

A Frequency Modulated Continuous Wave (FMCW) radar can obtain various information concerning the detected objects using a chirp signal with a linearly increasing frequency over

a specific period. The received signal bounced from an object is mixed with a signal the same as the transmitted one, generating a down-converted intermediate frequency signal, IF. The information related to the object is determined by analyzing this IF signal. Like the wavelength of the lidar laser beams, the frequency, and bandwidth of the transmitted radar signal limit detection resolution. The more the time duration of linear-frequency-increasing chirp (namely, the larger its bandwidth), the finer the resolution for the detection of radar. So, the range resolution depends on the bandwidth swept by the chirp. However, since Analog-to Digital Converter would digitize the IF signal, its sampling rate also limits the radar's maximum range. Thus, the larger the chirp bandwidth, the better the range resolution. Also, the larger the IF bandwidth, the faster the chirps, and the better the maximum distance.

The radar makes it possible to detect the moving object's distance, arrival time, movement direction, and speed. There are two different architectures for radar systems used in the current automotive applications: the Frequency-Modulated Continuous Wave (FMCW) radar and the Pulse-Doppler radar. FMCW is used in %90 of the existing applications. The FMCW radar has two types related to the RF signal it sends for detection. LSR- Low-Speed Ramp and HSR- High-Speed Ramp according to the speed of the sent ramp sign. The most common one is LSR, with %60 usage in today's market. It does the detection by sending a triangle ramp sign with a rise time of 3ms. HSR, which utilizes the trapezoidal wave changing between the range of 20s and 100s for the measurements, is used in %30 of the market. Pulse-Doppler radars are used in the remaining %10 of the automotive market radar applications. It is possible to immediately measure an object's speed and distance by sending many sequential pulse trains. In this work, Analog Devices' EVAL-RADAR-MMIC2 radar kit is adopted. EVAL-RADAR-

MMIC2 is an Evaluation Board for a 24 GHz LSR FMCW-based radar system. Various frequencies were investigated for the radar system to improve the resolution. However, due to the limitation of measurement equipment and availability of the design kits 24GHz ISM band is preferred.

Figure 4 shows the block diagram of the 24GHz LSR-based FMCW radar system. The signal chain chipsets are ADF5901, a 24 GHz VCO and PGA with 2-Channel PA Output; ADF5904, a 4-Channel, 24 GHz receiver Downconverter; and ADF4159 which is a Direct Modulation/Fast Waveform Generating, 13 GHz, Fractional-N Frequency Synthesizer. They are all developed for commercial use in ADAS and industrial applications.

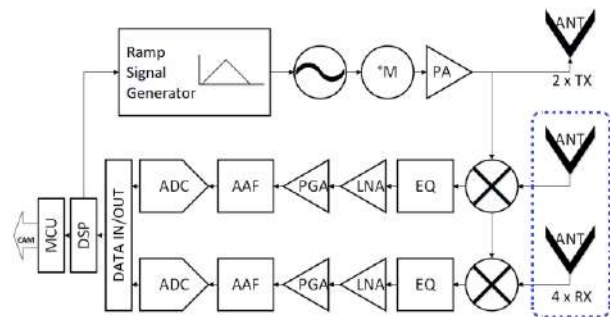


Figure 4 ISM Radar Phased Array Antennas

The system has a transmitter and receiver antenna system. The transmit antenna is like the receive antenna but only has two independent radiating elements instead of 4. The system operates in full duplex mode to support both transmit and receive. For phased array antenna, different topologies and technologies got studied. Although the end-fired antennas, such as the Vivaldi type, have superior performance in gain and directivity, their radiation pattern is perpendicular to the PCB's normal vector, which has a problematic installation on the flat body of the MoRo. Due to the production cost and ease of implementation, the microstrip patch antenna in series and the parallel combination is preferred for the arrays. Initially, a patch antenna at 24.35 GHz with



linear polarization is designed on a 6-mil Rogers substrate with a dielectric constant of 3.48. The antenna sizes (Width  $W$  and Length  $L$ ) were obtained using the following design formula [16]. The inset opening was used to allow the feed line to connect to the low-impedance point of the antenna. The length of this inset,  $x_p$ , was calculated according to equation 3. The spacing of the inset was chosen as 200 $\mu$ m, dictated by the PCB vendor as the minimum manufacturable spacing with reasonable precision.

$$W = \frac{c}{2f_m \sqrt{\epsilon_{reff}}} \quad (1)$$

$$L = \frac{c}{2f_m \sqrt{\epsilon_{reff}}} - L_{fringe} \quad (2)$$

$$x_p = \frac{\cos^{-1}\left(\sqrt{\frac{R_i}{R_e}}\right)}{\pi} L \quad (3)$$

$$\epsilon_{reff} = \frac{\epsilon_r + 1}{2} + \frac{\epsilon_r - 1}{2} \left[1 + 12 \frac{h}{W}\right]^{-1/2} \quad (4)$$

Here,  $W$  is the patch width,  $L$  is the patch length,  $c$  is the speed of light,  $h$  is substrate height,  $f_m$  is the working frequency of the antenna,  $\epsilon_{reff}$  is the effective dielectric constant,  $L_{fringe}$  is the patch length due to the fringing electric field,  $x_p$  is the inset length,  $R_i$  is the feeding line impedance, and  $R_e$  is the patch edge impedance.

The sizes of antenna design were further optimized using a Method-of-Moments-based EM simulator for an operation at 24.35GHz. The final dimensions were obtained for patch width and length as 3220 $\mu$ m x 4120 $\mu$ m. A 5.1dBi maximum gain was obtained from this patch antenna according to the simulation results.

However, higher gain performance is targeted for the system requirements. Based on the designed single patch, a 4-element parallel antenna array is developed to enhance the gain. Additionally, 4-patch antennas were placed at

$\lambda/2$  distance from each other. Each antenna was designed according to 50 $\Omega$  impedance, and  $\lambda/4$  impedance converter lines were used to adapt 25 $\Omega$  impedance, which occurs when two antennas are connected parallel, to the system impedance of 50 $\Omega$ . Each patch's theoretical extra 3dBi gain contribution is limited due to the feedline losses. Figure 5 shows the simulation results for the four-element-patch array. The antenna system has a resonance of about 24.35 GHz with 10.3dBi gain.

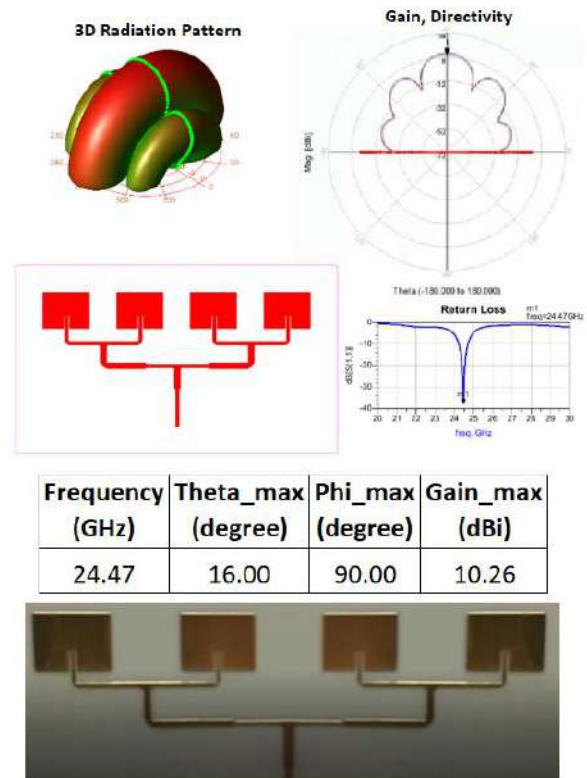


Figure 5 The antenna system with four parallel inset elements: Layout, simulated 3D radiation pattern, 2D polar pattern, return loss, gain, directivity, and tabulated summary

A 4-port 4x4 microstrip antenna array is designed to increase the antenna's gain further. The antenna is changed from an inset-fed structure to a probe-fed form using a multi-layer PCB for properly routing the feeding networks. The design is carried out using the equations in [17].

As shown 6-a, the design has 16 elements, each of which has dual-probe-fed ports and a stripline feeding network. The vertical antenna on a single column is parallel connected and fed from a single input. The design has 4 of these placed half-wavelengths. The antenna array is mounted on a Perfect Electric Conductor (a copper plate) to replicate the mobile robot body, as shown in Figure 6-b. Here port#2 is measured on the VNA while all other ports are terminated.

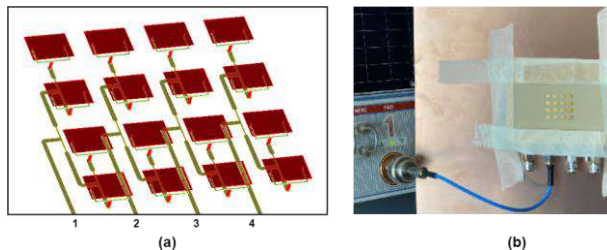


Figure 6 (a) Antenna array and feed network (b) measurement setup

Figure 7 shows the reflection coefficient in decibels, dB(S22). It is seen from the graph that the antenna system has broadband response starting from 24.45GHz and going beyond 30.65GHz with a 15dB reflection coefficient.

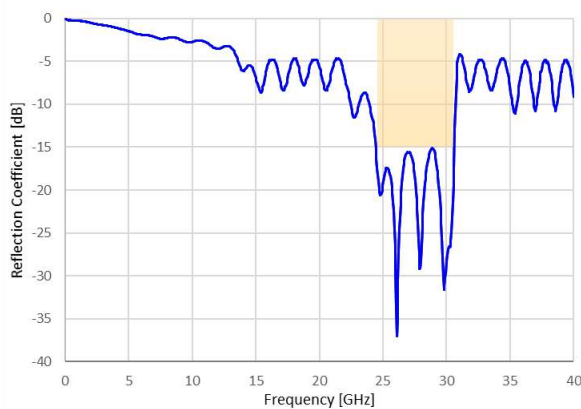


Figure 7 Single Port reflection coefficient in dB

The 2D pattern is measured using a reference antenna and RMS power detector. Figure 8 shows the antenna's radiation pattern when all ports are excited with equal phase and magnitude. The array shows a 20-degree

beamwidth and 16.2 dBi gain in its maximum direction.

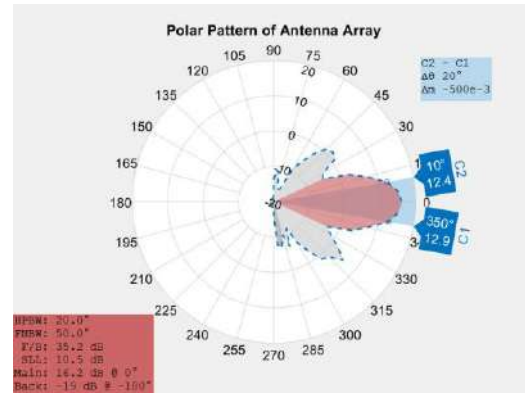


Figure 8 Radiation pattern under all ports equal-excitation

### 3. CONCLUSION

This study analyses the safety and accuracy of lidar-based navigation of industrial mobile robots. Data obtained from lidar for natural navigation reveals that due to the position of lidar sensors, there are unavoidable blind regions on the sides of vehicles that pose a high risk of collision during sudden and abrupt turns. For example, a millimeter wave ISM band FMCW automotive radar sensor with Low-Speed Ramp is used along with the proposed antenna system. The design steps, working principals, and simulated and measured results of the proposed 4-channel receiving antenna system are explained in detail. Finally, integrating lidar and radar sensors would give the mobile robots a continuous 360-degree peripheral consciousness.

#### Funding

The author has not received any financial support for this study's research, authorship, or publication.

#### The Declaration of Conflict of Interest/ Common Interest

No conflict of interest or common interest has been declared by the authors.

### ***The Declaration of Ethics Committee Approval***

This study does not require ethics committee permission or any special permission.

### ***The Declaration of Research and Publication Ethics***

The authors of the paper declare that they comply with the scientific, ethical, and quotation rules of SAUJS in all processes of the paper and that they do not make any falsification on the data collected. In addition, they declare that Sakarya University Journal of Science and its editorial board have no responsibility for any ethical violations that may be encountered, and that this study has not been evaluated in any academic publication environment other than Sakarya University Journal of Science.

### **REFERENCES**

- [1] M. Karamuk, I. H. Savci, H. Ocaklı, "A Survey on Traction System Development of Automated Guided Vehicles," *European Journal of Technique*, vol. 12, no. 1, pp. 1-12, Jun. 2022.
- [2] I. H. Savci, A. Yilmaz, S. Karaman, H. Ocaklı, H. Temeltas, "Improving Navigation Stack of a ROS-Enabled Industrial Autonomous Mobile Robot (AMR) to be Incorporated in a Large-Scale Automotive Production," *The International Journal of Advanced Manufacturing Technology*, vol. 120, pp. 3647–3668, Mar. 2022.
- [3] M. Qi, X. Li, X. Yan, C. Zhang, "On the evaluation of AGVS-based warehouse operation performance," *Simulation Modelling Practice and Theory*, vol. 87, pp. 379-394, Sep. 2018.
- [4] A. Vale, R. Ventura, R. Lopes, I. Ribeiro, "Assessment of navigation technologies for automated guided vehicle in nuclear fusion facilities," *Robotics and Autonomous Systems*, vol. 97, pp. 153-170, 2017.
- [5] G. Bocewicz, Z. Banaszak, I. Nielsen, W. Muszynski, "Re-scheduling of AGVs steady-state flow," *IFAC-Papers On-Line*, vol. 50 no. 1, pp. 3493-3498, Jul. 2017.
- [6] H. Balaji, S. Shaikh, A. Phalke S. Jadhav, "Design and methodology of automated guided vehicle - a review," *IOSR Journal of Mechanical and Civil Engineering*, vol. 1, pp. 29-35, May 2022.
- [7] S. Quan, J. Chen, "AGV Localization Based on Odometry and LiDAR," *2nd World Conference on Mechanical Engineering and Intelligent Manufacturing*, pp. 483-486, Nov. 2019.
- [8] A. Rangesh, M. M. Trivedi, "No blind spots: full-surround multi-object tracking for autonomous vehicles using cameras and lidars," *IEEE Transactions on Intelligent Vehicles*, vol. 4, no.4, pp. 588-599, Dec. 2019.
- [9] R. P. Mahapatra, S. V. Kumar, G. Khurana, R. Mahajan, "Ultrasonic sensor-based blind spot accident prevention system," *International Conference on Advanced Computer Theory and Engineering*, pp. 992-995, Dec. 2008.
- [10] S. Lee, H. Wang, "Navigation of automated guided vehicles using magnet spot guidance method," *Robotics and Computer Integrated Manufacturing*, vol. 28, no. 3, pp. 425-436, Jun. 2012.
- [11] G. Liu, L. Wang, S. Zou, "Radar-based blind spot detection and warning system for driver assistance," *IEEE 2nd Advanced Information Technology*,



Electronic and Automation Control Conference, pp. 2204-2208, Mar. 2017.

- [12] Y. Shen, W. Q. Yan, "Blind spot monitoring using deep learning," International Conference on Image and Vision Computing New Zealand, Auckland, pp. 1-5, Nov. 2018.
- [13] A. Hiçdurmaz, A. Tuncer, "Real-Time Obstacle Avoidance Based on Floor Detection for Mobile Robots," Sakarya University Journal of Science, vol. 24, no. 5, pp. 845-853, Oct. 2020.
- [14] J. Verhaever, "Detection of vulnerable road users in blind spots through Bluetooth low energy," Progress in Electromagnetics Research Symposium - Spring (PIERS), pp. 227-231, May. 2017.
- [15] D. Saunders, S. Bingham, G. Menon, D. Crockett, J. Tor, R. Mende, M. Behrens, N. Jain, A. Alexanian, Rajanish, "A single-chip 24 GHz SiGe BiCMOS transceiver for low cost FMCW airborne radars," Proceedings of the IEEE 2009 National Aerospace & Electronics Conference, pp. 244-247, Jul. 2009.
- [16] T. Milligan, Modern Antenna Design, Wiley-IEEE Press, New Jersey, 2005.
- [17] A. Elsherbeni, P. Nayari, C.J. Reddy, Antenna Analysis and Design Using FEKO Electromagnetic Simulation Software, SciTech Publishing, New Jersey, 2014.



SAKARYA ÜNİVERSİTESİ

# FEN BİLİMLERİ ENSTİTÜSÜ DERGİSİ

Sakarya University Journal of Science  
SAUJS

ISSN 1301-4048 e-ISSN 2147-835X Period Bimonthly Founded 1997 Publisher Sakarya University  
<http://www.saujs.sakarya.edu.tr/>

Title: A Note On E-Injective Modules

Authors: Abuzer GÜNDÜZ, Osama NAJİ

Received: 2022-03-28 00:00:00

Accepted: 2022-10-22 00:00:00

Article Type: Research Article

Volume: 26

Issue: 6

Month: December

Year: 2022

Pages: 1262-1266

How to cite

Abuzer GÜNDÜZ, Osama NAJİ; (2022), A Note On E-Injective Modules. Sakarya University Journal of Science, 26(6), 1262-1266, DOI:

10.16984/saufenbilder.1094262

Access link

<https://dergipark.org.tr/en/pub/saufenbilder/issue/74051/1094262>

New submission to SAUJS

<http://dergipark.gov.tr/journal/1115/submission/start>

## A Note On E-Injective Modules

Abuzer GÜNDÜZ<sup>\*1</sup>, Osama NAJİ<sup>1</sup>

### Abstract

Let  $R$  be a commutative ring with identity,  $M$  an  $R$ -module and  $E$  a torsion-free  $R$ -module. A submodule  $N$  of  $M$  is said to be essential (large) in  $M$  if the intersection of  $N$  with each nonzero submodule of  $M$  is nonzero, that is,  $N \cap Rm \neq 0$  for any nonzero element  $m \in M$  and we write  $N \leq_e M$ . It is clear that the class of  $e$ -exact sequences is larger than the class of exact sequences. In this study we present the concept of  $e$ -injective modules as a generalization of injective modules. The main goal is to give a characterization of  $e$ -injective modules in terms of contravariant functor  $Hom(-, E)$ .

**Keywords:**  $E$ -injective modules,  $e$ -exact sequences, contravariant functor

### 1. INTRODUCTION

Let  $R$  be a commutative ring with identity and  $M$  an  $R$ -module. A submodule  $N$  of  $M$  is said to be essential (large) in  $M$  if the intersection of  $N$  with each nonzero submodule of  $M$  is nonzero, that is,  $N \cap Rm \neq 0$  for any nonzero element  $m \in M$  and we write  $N \leq_e M$ . A sequence of  $R$ -modules and  $R$ -module homomorphisms  $f_i$

$$\dots \rightarrow M_{i-1} \xrightarrow{f_{i-1}} M_i \xrightarrow{f_i} M_{i+1} \xrightarrow{f_{i+1}} \dots$$

is called *exact* at  $M_i$  if  $Im(f_{i-1}) = Ker(f_i)$ . Akray and Zebari in [1] introduced the  $e$ -exact sequences as a generalization of exact sequences. The above sequence is called  $e$ -exact at  $M_i$  if  $Im(f_{i-1}) \leq_e Ker(f_i)$  and it is called  $e$ -

*exact* if it is  $e$ -exact at each  $M_i$ . Expectedly, they defined the sequence

$$0 \rightarrow A_1 \xrightarrow{f_1} A_2 \xrightarrow{f_2} A_3 \rightarrow 0$$

to be short  $e$ -exact if  $Ker(f_1) = 0$ ,  $Im(f_1) \leq_e Ker(f_2)$  and  $Im(f_2) \leq_e A_3$ , where  $f_i: A_i \rightarrow A_{i+1}$  is an  $R$ -module homomorphism for  $i = 1, 2$ . Recall from [1] that an  $R$ -morphism  $f: A_1 \rightarrow A_2$  is called *epic* if  $Im(f_1) \leq_e A_2$  and *essential monic* if  $Ker f_1 = 0$ . It is clear that the class of  $e$ -exact sequences is larger than the class of exact sequences. For example consider the short  $e$ -exact sequence

$$0 \rightarrow 8\mathbb{Z} \xrightarrow{f_1} \mathbb{Z} \xrightarrow{f_2} \mathbb{Z}/8\mathbb{Z} \rightarrow 0$$

\* Corresponding author: abuzergunduz@sakarya.edu.tr

<sup>1</sup> Sakarya University

E-mail: onaji14@gmail.com

ORCID: <https://orcid.org/0000-0003-3351-2443>, <https://orcid.org/0000-0002-6498-7620>



where  $f_1(8n) = 4n$  and  $f_2(n) = 2n + 8\mathbb{Z}$ . Since  $f_1$  and  $f_2$  are epic, the sequence is *e* – exact. Note that  $f_2$  is not an *epimorphism*, so the sequence is not *exact*.

In the sake of completeness, we recall from [2] some basic definitions. An element  $m$  of  $M$  is said to be torsion of  $M$  if there exists a regular element  $r \in R$  such that  $rm = 0$ . The set of all torsion elements  $T(M)$  is a submodule of  $M$ . Also, an  $R$ -module  $M$  is called *torsion* if  $T(M) = M$ , and called *torsion – free* when  $T(M) = \{0\}$ .

Let  $E$  be an  $R$  – module.  $E$  is said to be injective module if the following condition is satisfied: For any monic map  $f_1: A_1 \rightarrow A_2$  and any map  $f_2: A_1 \rightarrow E$ , there exist  $f_3: A_2 \rightarrow E$  such that  $f_3f_1 = f_2$ .

$$\begin{array}{ccccc}
 0 & \longrightarrow & A_1 & \xrightarrow{f_1} & A_2 \\
 & & \downarrow f_2 & \nearrow f_3 & \\
 & & E & & 
 \end{array}$$

Moreover, if  $E$  is injective module, then the contravariant functor  $\text{Hom}(-, E)$  is an exact sequence [3].

A group  $D$  is called *divisible* if for every positive integer  $n$  and every  $d \in D$ , there exists  $0 \neq x \in D$  such that  $nx = d$ . It is known that a group  $D$  is *divisible* if and only if it is *injective* [3].

Throughout this note, all modules are assumed to be torsion-free. In section 2, we introduce the definition of *e* – injective  $E$ . It is shown that a module  $E$  is *e* – injective if and only if the contravariant functor  $\text{Hom}(-, E)$  is an *e* – exact sequence.

## 2. CHARACTERIZATION OF E-INJECTIVE MODULE

In this part, we investigate some results about *e* – injective modules such as when the contravariant functor  $\text{Hom}(-, M)$  is an *e* – exact sequence,  $E = \prod_{i \in \Delta} E_i$  is *e* –

injective for each  $E_i$  be an  $R_i$ -module for every  $i \in \Delta$  and short *e* – exact sequence is *e* – split.

The following theorem shows that the contravariant functor  $\text{Hom}(-, M)$  is a left *e* – exact functor when  $M$  is a *torsion – free*  $R$ -module.

**Theorem 1** [1] Suppose that the following sequence of  $R$ -modules and  $R$ -morphism

$$M_1 \xrightarrow{f_1} M_2 \xrightarrow{f_2} M_3 \rightarrow 0$$

is *e* – exact. Then for all *torsion – free*  $R$ -module  $M$ , the sequence

$$\begin{array}{ccc}
 0 \rightarrow \text{Hom}(M_3, M) & \xrightarrow{f_2^*} & \text{Hom}(M_2, M) \\
 & & \xrightarrow{f_1^*} & \text{Hom}(M_1, M)
 \end{array}$$

is *e* – exact. The converse is true if  $M_3/\text{Im}(f_2)$  and  $M_2/\text{Im}(f_1)$  are *torsion – free*  $R$ -modules.

**Definition 1** Let  $R$  be a ring and  $E$  an  $R$  – module.  $E$  is said to be *e* – injective if the following condition is satisfied: For any monic map  $f_1: A_1 \rightarrow A_2$  and any map  $f_2: A_1 \rightarrow E$ , there exist  $0 \neq r \in R$  and  $f_3: A_2 \rightarrow E$  such that  $f_3f_1 = r \cdot f_2$ .

$$\begin{array}{ccccc}
 0 & \longrightarrow & A_1 & \xrightarrow{f_1} & A_2 \\
 & & \downarrow f_2 & \nearrow f_3 & \\
 & & E & & 
 \end{array}$$

**Theorem 2** Let  $R$  be a ring and  $E$  an  $R$ -module. Then the following statements are equivalent:

- (i)  $E$  is an *e* – injective  $R$ -module.
- (ii)  $\text{Hom}(-, E)$  is an *e* – exact sequence.

**Proof.** (i) $\Rightarrow$ (ii): Suppose that  $E$  is an *e* – injective  $R$ -module. Then by Theorem 1,  $\text{Hom}(-, E)$  is left *e* – exact functor. It

remains to show that  $Hom(-, E)$  is right  $e$ -exact functor. Assume that

$$0 \rightarrow A_1 \xrightarrow{f_1} A_2$$

is an  $e$ -exact sequence and we want to show that

$$Hom(A_2, E) \xrightarrow{f_1^*} Hom(A_1, E) \rightarrow 0$$

is  $e$ -exact. Since the contravariant functor  $Hom(-, E)$  is left  $e$ -exact, it is enough to prove that  $Im(f_1^*) \leq_e Hom(A_1, E)$ . Since we have that  $f_1$  is monic and let pick  $f_2 \in Hom(A_1, E)$ , by the definition of  $e$ -injective, we have  $f_3 f_1 = r \cdot f_2$  for some  $0 \neq r \in R$  and  $f_3: A_2 \rightarrow E$ . This implies that  $f_1^*(f_3) = r \cdot f_2$ . Thus,  $Im(f_1^*) \cap Rf_2 \neq 0$  and we obtain that  $Im(f_1^*) \leq_e Hom(A_1, E)$ .

(ii) $\Rightarrow$ (i): Assume that  $Hom(-, E)$  is an  $e$ -exact functor. Let  $f_1: A_1 \rightarrow A_2$  be a monic map and  $f_2: A_1 \rightarrow E$  any map. Since the sequence

$$0 \rightarrow A_1 \xrightarrow{f_1} A_2$$

is  $e$ -exact, then by assumption, the sequence

$$Hom(A_2, E) \xrightarrow{f_1^*} Hom(A_1, E) \rightarrow 0$$

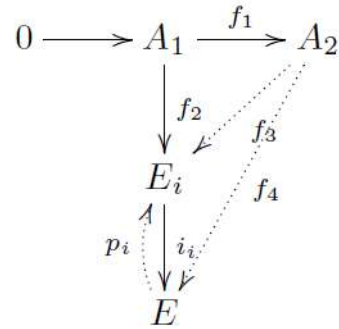
is also  $e$ -exact. Then we have  $Im(f_1^*) \leq_e Hom(A_1, E)$ . As  $f_2 \in Hom(A_1, E)$ , there exist  $0 \neq r \in R$  and  $f_3 \in Hom(A_2, E)$  such that  $f_1^*(f_3) = r \cdot f_2$ . This implies that  $f_3 f_1 = r f_2$ . Hence  $E$  is  $e$ -injective.

**Theorem 3** Let  $E_i$  be an  $R_i$ -module for each  $i \in \Delta$ , where  $\Delta$  is an index set. Assume that  $R = \prod_{i \in \Delta} R_i$  and  $E = \prod_{i \in \Delta} E_i$ . Then the following statements hold:

(i) If  $E$  is an  $e$ -injective  $R$ -module, then  $E_i$  is an  $e$ -injective  $R_i$ -module for some  $i \in \Delta$ .

(ii) If  $E_i$  is an  $e$ -injective  $R_i$ -module for each  $i \in \Delta$ , then  $E$  is an  $e$ -injective  $R$ -module.

**Proof.** (i): Suppose that  $f_1: A_1 \rightarrow A_2$  is a monic map and  $f_2: A_1 \rightarrow E_i$ . Consider the following diagram

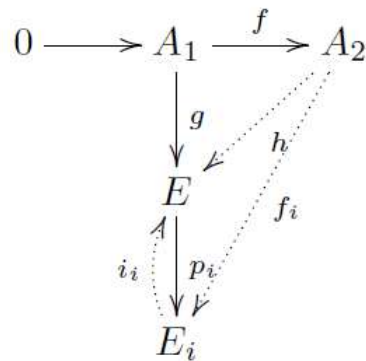


where  $i_i: E_i \rightarrow E$  is the injective map and  $p_i: E \rightarrow E_i$  is the projective map. Since  $i_i f_2: A_1 \rightarrow E$  and  $E$  is an  $e$ -injective  $R$ -module, there exist  $0 \neq r = (r_i)_{i \in \Delta} \in R$  and  $f_4: A_2 \rightarrow E$  such that  $f_4 f_1 = r \cdot (i_i f_2)$ . Assume that  $r_k \neq 0$  for some  $k \in \Delta$  and define  $f_3: A_2 \rightarrow E_k$  by  $f_3 = p_k f_4$ . Since  $p_k \circ i_k = 1_{E_k}$ , we obtain

$$f_3 f_1 = p_k f_4 f_1 = p_k (r \cdot i_k f_2) = r_k p_k i_k f_2 = r_k f_2$$

Therefore,  $E_k$  is an  $e$ -injective  $R_k$ -module.

(ii): Assume that  $f: A_1 \rightarrow A_2$  is a monic map and  $g: A_1 \rightarrow E$ . Consider the following diagram



Since  $E_i$  is  $e$ -injective and  $p_i g: A_1 \rightarrow E_i$  for each  $i \in \Delta$ , there exist  $0 \neq r_i \in R_i$  and  $f_i: A_2 \rightarrow E_i$  such that  $f_i f = r_i (p_i g)$ . Then

there exists  $h: A_2 \rightarrow E$  such that  $f_i = p_i h$ . Let  $0 \neq r = (r_i) \in R$  and note that  $p_i h f = f_i f = r_i p_i g = p_i (r g)$ . Hence, we get  $h f = r g$ . Therefore,  $E$  is an  $e$ -injective  $R$ -module.

**Theorem 4** *Let  $R$  be a ring and  $E$  be an  $e$ -injective  $R$ -module. For any monic map*

$$0 \rightarrow E \xrightarrow{f} L$$

there exists an  $R$ -homomorphism  $\alpha: L \rightarrow E$  such that  $\alpha f = r \cdot 1_E$  for some  $0 \neq r \in R$ .

*Proof.* It is clear.

**Definition 2** [1] *Let*

$$0 \rightarrow E \xrightarrow{f_1} A_1 \xrightarrow{f_2} A_2 \rightarrow 0$$

be a short  $e$ -exact sequence. If for any map  $f_1: E \rightarrow A_1$  there exist  $g: A_1 \rightarrow E$  and  $r \in R$  such that  $g f_1 = r \cdot 1_E$ . Then the above short  $e$ -exact sequence is called  $e$ -split.

**Theorem 5** *An  $e$ -exact sequence*

$$0 \rightarrow E \xrightarrow{f_1} A_1 \xrightarrow{f_2} A_2 \rightarrow 0$$

is  $e$ -split if  $E$  is an  $e$ -injective module.

*Proof.* Suppose that

$$0 \rightarrow E \xrightarrow{f_1} A_1 \xrightarrow{f_2} A_2 \rightarrow 0$$

is an  $e$ -exact sequence and  $E$  is an  $e$ -injective  $R$ -module. Then by Theorem 2, the sequence

$$\begin{aligned} &0 \\ &\rightarrow \text{Hom}(A_2, E) \\ &\xrightarrow{f_2^*} \text{Hom}(A_1, E) \xrightarrow{f_1^*} \text{Hom}(E, E) \rightarrow 0 \end{aligned}$$

is  $e$ -exact. Since  $f_1^*$  is epic,  $\text{Im}(f_1^*) \leq_e \text{Hom}(E, E)$ . Note that  $1_E \in \text{Hom}(E, E)$ , so there exist a map  $g: A_1 \rightarrow E$  and  $r \in R$  such that  $f_1^*(g) = r \cdot 1_E$  and

hence  $g f_1 = r \cdot 1_E$ . Therefore the sequence is  $e$ -split.

### 3. CONCLUSION

As a result, we get the definition of the  $e$ -injective  $R$ -module and some results. We hope that the results give rise to new results in Homological Algebra with regard to  $e$ -exact theory such as  $e$ -flat module and  $e$ -homology,  $e$ -functor.

#### Acknowledgement

The authors would like to thank the referees for their valuable suggestions that improved this paper.

#### Funding

The authors received no financial support for the research, authorship and publication of this study.

#### Authors' Contribution

The authors contributed equally to the study.

#### The Declaration of Ethics Committee Approval

The study does not require ethics committee permission or any special permission.

#### The Declaration of Research and Publication Ethics

The authors of the paper declare that they comply with the scientific, ethical, and quotation rules of SAUJS in all processes of the paper and that they do not make any falsification of the data collected. In addition, they declare that Sakarya University Journal of Science and its editorial the board has no responsibility for any ethical violations that may be encountered, and that this the study has not been evaluated in any academic publication environment other than Sakarya University Journal of Science.

## REFERENCES

- [1] I. Akray, A. Zebari, “Essential exact sequences,” *Communications of the Korean Mathematical Society*, 2020; 35(2):469-480.
- [2] A. Tercan, C. C. Yücel, “Module Theory, Extending Modules and Generalizations,” *Bassel: Birkhäuser, Springer*, 2016.
- [3] J. J. Rotman, J. J. Rotman, “An introduction to homological algebra,” *New York: Springer*, 2009.



SAKARYA ÜNİVERSİTESİ

# FEN BİLİMLERİ ENSTİTÜSÜ DERGİSİ

Sakarya University Journal of Science  
SAUJS

ISSN 1301-4048 e-ISSN 2147-835X Period Bimonthly Founded 1997 Publisher Sakarya University  
<http://www.saujs.sakarya.edu.tr/>

Title: Stability of Partial Differential Equations by Mahgoub Transform Method

Authors: Harun BİÇER

Received: 2022-07-07 00:00:00

Accepted: 2022-10-23 00:00:00

Article Type: Research Article

Volume: 26

Issue: 6

Month: December

Year: 2022

Pages: 1267-1273

How to cite

Harun BİÇER; (2022), Stability of Partial Differential Equations by Mahgoub Transform Method. Sakarya University Journal of Science, 26(6), 1267-1273, DOI: 10.16984/saufenbilder.1142084

Access link

<https://dergipark.org.tr/en/pub/saufenbilder/issue/74051/1142084>

New submission to SAUJS

<http://dergipark.gov.tr/journal/1115/submission/start>



## Stability of Partial Differential Equations by Mahgoub Transform Method

Harun BİÇER\*<sup>1</sup> 

### Abstract

The stability theory is an important research area in the qualitative analysis of partial differential equations. The Hyers-Ulam stability for a partial differential equation has a very close exact solution to the approximate solution of the differential equation and the error is very small which can be estimated. This study examines Hyers-Ulam and Hyers-Ulam Rassias stability of second order partial differential equations. We present a new method for research of the Hyers-Ulam stability of partial differential equations with the help of the Mahgoub transform. The Mahgoub transform method is practical as a fundamental tool to demonstrate the original result on this study. Finally, we give an example to illustrate main results. Our findings make a contribution to the topic and complete those in the relevant literature.

**Keywords:** Hyers-Ulam stability, Mahgoub transform, partial differential equation

### 1. INTRODUCTION

In the domains of chemistry, biology, engineering, physics, economics etc., partial differential equations can be used as very effective tools for mathematical modeling of systems and processes. Therefore, several real-world events related to the sciences and engineering method disciplines depend greatly on the qualitative characteristics of partial differential equation solutions. However, we do not want to go into the specifics of the partial differential equation applications here. This material highlights the significance of

researching qualitative characteristics, Hyers-Ulam stability (HUS) and Hyers-Ulam Rassias stability (HURS) of partial differential equations.

The classic Fourier integral is where the Mahgoub transform gets its name. Mahgoub improved the Mahgoub transform to make it easier to solve ordinary and partial differential equations in the time domain. The most practical mathematical methods for solving differential equations are often Fourier, Laplace, Elzaki, Aboodh, Sumudu and Mahgoub transforms. In order to solve

\* Corresponding author: hbicer@bingol.edu.tr

<sup>1</sup> Bingöl University

ORCID: <https://orcid.org/0000-0002-9854-0595>



differential equations, the Mahgoub transform and some of its essential features are also used.

Ulam discussed the stability of homomorphism in 1940 (see [1]). Hyers [2] in the Banach spaces provided a partial solution to this puzzle. Numerous academics have since studied the stability problems of functional differential equations ( see [1-18]).

In 2009, Jung [7] studied the (HUS) of first-order linear partial differential equations

$$au_x(x, y) + bu_y(x, y) + g(y)u(x, y) + h(y) = 0$$

and

$$au_x(x, y) + bu_y(x, y) + g(x)u(x, y) + h(x) = 0$$

in the cases of  $a \leq 0, b > 0$  and  $a > 0, b \leq 0, (a, b \in \mathbb{R})$  respectively.

Thereafter, Lungu and Popa [9] proved the (HUS) of first order partial differential equation of the form

$$p(x, t)u_x + q(x, t)u_t = p(x, t)r(x)u + f(x, t).$$

Huang and Li [10] proved the (HUS) of the first order linear partial differential equations in n-dimensional space.

See, in particular, the publications of Biçer and Tunç [3-4], Jung and Brzdek [8], Huang and Li [10], Otrocal and Ilea [12], and Tunç and Biçer [16] and the references therein for additional results on the (HUS) of ordinary or partial differential equations.

In this study, using Mahgoub transform method, we investigate the (HUS) of the homogeneous and nonhomogeneous second order partial differential equations

$$u_{\gamma\kappa}(\gamma, \kappa) - \lambda^2 u(\gamma, \kappa) = 0, \quad (1)$$

$$u_{\gamma\kappa}(\gamma, \kappa) - \lambda^2 u(\gamma, \kappa) = g(\gamma, \kappa) \quad (2)$$

for  $(\gamma, \kappa) \in D, D = I \times I, I = [a, b], f \in C(I \times I) = \{g: I \times I \rightarrow \mathbb{R}: g \text{ is continuous}\}, -\infty < a < b < \infty.$

## 2. PRELIMINARIES

This section introduces several common terminologies and notations that will help to support our primary findings.

If there exist constants  $X, Y \in \mathbb{R}$  such that

$$|h_1(z)| \leq X e^{Yt}$$

for all  $z \geq 0$ , then the function  $h_1: [0, \infty) \rightarrow \mathbb{R}$  is of exponential order.

Similarly, if there exist constants  $X, Y \in \mathbb{R}$  such that

$$|h_2(z)| \leq X e^{Yt}$$

for all  $z \geq 0$ , then the function  $h_2: (-\infty, 0] \rightarrow \mathbb{R}$  is of exponential order.

**Definition 2.1. ([1])** The definition of Mahgoub integral transform for the function  $u: [0, \infty) \rightarrow \mathbb{R}$  is

$$\mathcal{M}\{u(\kappa)\} = v \int_0^{\infty} u(s) e^{-vs} ds = U(v),$$

in which  $\mathcal{M}$  is the Mahgoub integral transform operator.

If  $u(\kappa)$  is piecewise continuous and of exponential order, the Mahgoub integral transform for the function  $u: [0, \infty) \rightarrow \mathbb{R}$  exists. These are the only prerequisites that are sufficient conditions for the existence the Mahgoub transform of the function  $u(\kappa)$ .

For partial differential equation, the Mahgoub transform of the function  $u(\gamma, \kappa)$  is

$$\mathcal{M}\{u(\gamma, \kappa)\} = v \int_0^{\infty} u(\gamma, s) e^{-vs} ds = U(\gamma, v).$$

Using integration by parts we obtain the Mahgoub transform for partial derivatives as follows:

$$\mathcal{M}\{u_\gamma(\gamma, \kappa)\} = v \int_0^\infty u_\gamma(\gamma, s)e^{-vs} ds = \frac{d}{d\gamma} U(\gamma, v),$$

$$\begin{aligned} \mathcal{M}\{u_{\gamma\gamma}(\gamma, \kappa)\} &= v \int_0^\infty u_{\gamma\gamma}(\gamma, s)e^{-vs} ds \\ &= \frac{d^2}{d\gamma^2} U(\gamma, v), \end{aligned}$$

$$\begin{aligned} \mathcal{M}\{u_\kappa(\gamma, \kappa)\} &= v \int_0^\infty u_\kappa(\gamma, s)e^{-vs} ds \\ &= vU(\gamma, v) - vu(\gamma, 0), \end{aligned}$$

$$\begin{aligned} \mathcal{M}\{u_{\kappa\kappa}(\gamma, \kappa)\} &= v \int_0^\infty u_{\kappa\kappa}(\gamma, s)e^{-vs} ds \\ &= v^2 U(\gamma, v) - v^2 u(\gamma, 0) \\ &\quad - vu_\kappa(\gamma, 0). \end{aligned}$$

**Definition 2.2 ([1])** Let  $u$  and  $w$  be Lebesgue-integrable functions on  $(-\infty, \infty)$ . The convolution of the functions  $u(\kappa)$  and  $w(\kappa)$  is denoted by  $u(\kappa) * w(\kappa)$  and is defined by

$$\begin{aligned} u(\kappa) * w(\kappa) &= (u * w)(\kappa) \\ &= \int_{-\infty}^\infty u(s)w(\kappa - s)ds. \end{aligned}$$

**Theorem 2.3. (Convolution theorem for Mahgoub transform) ([1]).** Suppose that  $u(\kappa)$  and  $w(\kappa)$  are given functions defined for  $\kappa \geq 0$ . If  $\mathcal{M}\{u(\kappa)\} = U(v)$  and  $\mathcal{M}\{w(\kappa)\} = W(v)$ , then

$$\mathcal{M}\{u(\kappa) * w(\kappa)\} = \frac{1}{v} U(v)W(v).$$

**Definition 2.4.** If there is a constant  $K > 0$  such that if for  $\varepsilon > 0$ , there exists  $u: I \times I \rightarrow \mathbb{R}$ , fulfilling the inequality

$$|u_{\kappa\kappa}(\gamma, \kappa) - \lambda^2 u(\gamma, \kappa)| \leq \varepsilon$$

for all  $(\gamma, \kappa) \in D$ , then there exists a solution  $w: I \times I \rightarrow \mathbb{R}$  satisfying the differential equation

$$w_{\kappa\kappa}(\gamma, \kappa) = \lambda^2 w(\gamma, \kappa)$$

such that

$$|u(\gamma, \kappa) - w(\gamma, \kappa)| \leq K\varepsilon$$

for all  $(\gamma, \kappa) \in D$ , where  $K$  is the (HUS) constant for (1). In this case, we say that the differential equation (1) has the (HUS).

**Definition 2.5.** If there is a constant  $K_\varphi > 0$  such that if for every  $\varepsilon > 0$ , there exists  $u: I \times I \rightarrow \mathbb{R}$ , fulfilling the inequality

$$|u_{\kappa\kappa}(\gamma, \kappa) - \lambda^2 u(\gamma, \kappa) - g(\gamma, \kappa)| \leq \varepsilon\varphi(\gamma, \kappa)$$

for all  $(\gamma, \kappa) \in D$ , then there exists a solution  $w: I \times I \rightarrow \mathbb{R}$  satisfying the differential equation

$$w_{\kappa\kappa}(\gamma, \kappa) = \lambda^2 w(\gamma, \kappa) + g(\gamma, \kappa)$$

such that

$$|u(\gamma, \kappa) - w(\gamma, \kappa)| \leq K_\varphi \varepsilon \varphi(\gamma, \kappa)$$

for all  $(\gamma, \kappa) \in D$ . We call such  $K_\varphi$  the (HURS) constant for (2). In this case, we say that the differential equation (1) has the (HURS).

### 3. MAIN RESULTS

**Theorem 3.1.** The differential equation (1) has the (HUS).

**Proof.** Let  $\varepsilon > 0$ . Assume that  $u: I \times I \rightarrow \mathbb{R}$  satisfies

$$|u_{\kappa\kappa}(\gamma, \kappa) - \lambda^2 u(\gamma, \kappa)| \leq \varepsilon \tag{3}$$

for all  $(\gamma, \kappa) \in D$ . We will show that there exists a  $K > 0$  such that

$$|u(\gamma, \kappa) - w(\gamma, \kappa)| \leq K\varepsilon$$

for some  $w: I \times I \rightarrow \mathbb{R}$  satisfying

$$w_{\kappa\kappa}(\gamma, \kappa) - \lambda^2 w(\gamma, \kappa) = 0$$

for all  $(\gamma, \kappa) \in D$ . Define the function  $p: I \times I \rightarrow \mathbb{R}$

by

$$p(\gamma, \kappa) =: u_{\kappa\kappa}(\gamma, \kappa) - \lambda^2 u(\gamma, \kappa)$$

for all  $(\gamma, \kappa) \in D$ . By (3), we have

$$|p(\gamma, \kappa)| \leq \varepsilon.$$

Applying the Mahgoub transform to  $p$ , we obtain

$$\mathcal{M}\{p(\gamma, \kappa)\} = \frac{(v^2 - \lambda^2)\mathcal{M}\{u(\gamma, \kappa)\} - v^2 u(\gamma, 0) - v u_{\kappa}(\gamma, 0)}{v^2 - \lambda^2}, \quad (4)$$

and so

$$\mathcal{M}\{u(\gamma, \kappa)\} = \frac{\mathcal{M}\{p(\gamma, \kappa)\} + v^2 u(\gamma, 0) + v u_{\kappa}(\gamma, 0)}{v^2 - \lambda^2}. \quad (5)$$

From (4), a function  $u_0: I \times I \rightarrow \mathbb{R}$  is a solution of (1) if and only if

$$(v^2 - \lambda^2)\mathcal{M}\{u_0\} - v^2 u_0(\gamma, 0) - v(u_0)_{\kappa}(\gamma, 0) = 0.$$

Set

$$w(\gamma, \kappa) = u(\gamma, 0) \left( \frac{e^{\lambda\kappa} + e^{-\lambda\kappa}}{2} \right) + u_{\kappa}(\gamma, 0) \left( \frac{e^{\lambda\kappa} - e^{-\lambda\kappa}}{2\lambda} \right).$$

Then, we obtain  $w(\gamma, 0) = u(\gamma, 0)$  and  $w_{\kappa}(\gamma, 0) = u_{\kappa}(\gamma, 0)$ . Applying the Mahgoub transform of  $w$ , we get

$$\mathcal{M}\{w(\gamma, \kappa)\} = \frac{v^2 u(\gamma, 0) + v u_{\kappa}(\gamma, 0)}{v^2 - \lambda^2}, \quad (6)$$

for  $0 < \lambda < v$ . Moreover,

$$\begin{aligned} & \mathcal{M}\{w_{\kappa\kappa}(\gamma, \kappa) - \lambda^2 w(\gamma, \kappa)\} \\ &= (v^2 - \lambda^2)\mathcal{M}\{w(\gamma, \kappa)\} \\ & \quad - v^2 w(\gamma, 0) - v w_{\kappa}(\gamma, 0). \end{aligned}$$

Using (6), we get

$$\mathcal{M}\{w_{\kappa\kappa}(\gamma, \kappa) - \lambda^2 w(\gamma, \kappa)\} = 0.$$

Since  $\mathcal{M}$  is a one-to-one linear operator, we have

$$w_{\kappa\kappa}(\gamma, \kappa) - \lambda^2 w(\gamma, \kappa) = 0.$$

As a result of above equality, we say that  $w$  is a solution of (1). It follows from (5) and (6) that

$$\begin{aligned} & \mathcal{M}\{u(\gamma, \kappa)\} - \mathcal{M}\{w(\gamma, \kappa)\} \\ &= \frac{\mathcal{M}\{p(\gamma, \kappa)\} + v^2 u(\gamma, 0) + v u_{\kappa}(\gamma, 0)}{v^2 - \lambda^2} \\ & \quad - \frac{v^2 u(\gamma, 0) + v u_{\kappa}(\gamma, 0)}{v^2 - \lambda^2} \\ &= \frac{\mathcal{M}\{p(\gamma, \kappa)\}}{v^2 - \lambda^2}, \end{aligned}$$

$$\begin{aligned} & \mathcal{M}\{u(\gamma, \kappa)\} - \mathcal{M}\{w(\gamma, \kappa)\} \\ &= \mathcal{M}\left\{p(\gamma, \kappa) * \left( \frac{e^{\lambda\kappa} - e^{-\lambda\kappa}}{2\lambda} \right)\right\}. \end{aligned}$$

From this equalities, we conclude that

$$u(\gamma, \kappa) - w(\gamma, \kappa) = p(\gamma, \kappa) * \left( \frac{e^{\lambda\kappa} - e^{-\lambda\kappa}}{2\lambda} \right).$$

Using  $|p(\gamma, \kappa)| \leq \varepsilon$  and taking the modulus on both sides of above equality, we obtain

$$\begin{aligned} & |u(\gamma, \kappa) - w(\gamma, \kappa)| \\ &= \left| p(\gamma, \kappa) * \left( \frac{e^{\lambda\kappa} - e^{-\lambda\kappa}}{2\lambda} \right) \right| \\ &\leq \left| \int_{-\infty}^{\infty} p(\gamma, s) \left( \frac{e^{\lambda(\kappa-s)} - e^{-\lambda(\kappa-s)}}{2\lambda} \right) ds \right| \\ &\leq \varepsilon \left| \int_{-\infty}^{\infty} \left( \frac{e^{\lambda(\kappa-s)} - e^{-\lambda(\kappa-s)}}{2\lambda} \right) ds \right| \end{aligned}$$

for all  $(\gamma, \kappa) \in D$ , where

$$K = \left| \int_{-\infty}^{\infty} \left( \frac{e^{\lambda(\kappa-s)} - e^{-\lambda(\kappa-s)}}{2\lambda} \right) ds \right|.$$

Hence  $|u(\gamma, \kappa) - w(\gamma, \kappa)| \leq K\varepsilon$ .

**Theorem 3.2.** The differential equation (2) has the (HURS).

**Proof.** Let  $\varepsilon > 0$  and  $\varphi \in C(I \times I)$ . Assume that  $u: I \times I \rightarrow \mathbb{R}$  satisfies

$$|u_{\kappa\kappa}(\gamma, \kappa) - \lambda^2 u(\gamma, \kappa) - g(\gamma, \kappa)| \leq \varepsilon\varphi(\gamma, \kappa) \quad (7)$$

for all  $(\gamma, \kappa) \in D$ . We will show that there exists a  $K_\varphi > 0$  such that

$$|u(\gamma, \kappa) - w(\gamma, \kappa)| \leq K_\varphi \varepsilon\varphi(\gamma, \kappa)$$

for some  $w: I \times I \rightarrow \mathbb{R}$  satisfying

$$w_{\kappa\kappa}(\gamma, \kappa) - \lambda^2 w(\gamma, \kappa) = g(\gamma, \kappa)$$

for all  $(\gamma, \kappa) \in D$ . Define the function  $p: I \times I \rightarrow \mathbb{R}$  by

$$p(\gamma, \kappa) =: u_{\kappa\kappa}(\gamma, \kappa) - \lambda^2 u(\gamma, \kappa) - g(\gamma, \kappa)$$

for all  $(\gamma, \kappa) \in D$ . By (7), we have

$$|p(\gamma, \kappa)| \leq \varepsilon\varphi(\gamma, \kappa).$$

Applying the Mahgoub transform to  $p$ , we obtain

$$\mathcal{M}\{p(\gamma, \kappa)\} = (v^2 - \lambda^2)\mathcal{M}\{u(\gamma, \kappa)\} - v^2 u(\gamma, 0) - v u_\kappa(\gamma, 0) - \mathcal{M}\{g(\gamma, \kappa)\},$$

and so

$$\mathcal{M}\{u(\gamma, \kappa)\} = \frac{\mathcal{M}\{p(\gamma, \kappa)\} + v^2 u(\gamma, 0) + v u_\kappa(\gamma, 0) + \mathcal{M}\{g(\gamma, \kappa)\}}{v^2 - \lambda^2}. \quad (8)$$

From (8), a function  $u_0: I \times I \rightarrow \mathbb{R}$  is a solution of (2) if and only if

$$\mathcal{M}\{g(\gamma, \kappa)\} = (v^2 - \lambda^2)\mathcal{M}\{u_0\} - v^2 u_0 - v(u_0)_\kappa(\gamma, 0).$$

Putting  $r(\kappa) = \frac{e^{\lambda\kappa} - e^{-\lambda\kappa}}{2\lambda}$ , we obtain

$$w(\gamma, \kappa) = u(\gamma, 0) \left( \frac{e^{\lambda\kappa} + e^{-\lambda\kappa}}{2} \right) + u_\kappa(\gamma, 0)r(\kappa) + [r(\kappa) * g(\gamma, \kappa)].$$

Then, we have  $w(\gamma, 0) = u(\gamma, 0)$  and  $w_\kappa(\gamma, 0) = u_\kappa(\gamma, 0)$ . Applying the Mahgoub transform of  $w$ , we get

$$\mathcal{M}\{w(\gamma, \kappa)\} = \frac{v^2 u(\gamma, 0) + v u_\kappa(\gamma, 0) + \mathcal{M}\{g(\gamma, \kappa)\}}{v^2 - \lambda^2} \quad (9)$$

for  $0 < \lambda < v$ . As opposed to that,

$$\begin{aligned} \mathcal{M}\{w_{\kappa\kappa}(\gamma, \kappa) - \lambda^2 w(\gamma, \kappa)\} &= (v^2 - \lambda^2)\mathcal{M}\{w(\gamma, \kappa)\} \\ &\quad - v^2 w(\gamma, 0) - v w_\kappa(\gamma, 0). \end{aligned}$$

Using (9), we have

$$\mathcal{M}\{w_{\kappa\kappa}(\gamma, \kappa) - \lambda^2 w(\gamma, \kappa)\} = \mathcal{M}\{g(\gamma, \kappa)\}.$$

The last equality implies that

$$w_{\kappa\kappa}(\gamma, \kappa) - \lambda^2 w(\gamma, \kappa) = g(\gamma, \kappa).$$

This means that  $w$  is a solution of (2). It follows from (8) and (9) that

$$\begin{aligned} \mathcal{M}\{u(\gamma, \kappa)\} - \mathcal{M}\{w(\gamma, \kappa)\} &= \frac{\mathcal{M}\{p(\gamma, \kappa)\}}{v^2 - \lambda^2} \\ &= \mathcal{M}\{p(\gamma, \kappa) * r(\kappa)\}. \end{aligned}$$

Thus  $u - w = p * r$ . Using  $|p(\gamma, \kappa)| \leq \varepsilon\varphi(\gamma, \kappa)$  and taking the modulus on both sides of above equality, we obtain

$$\begin{aligned} |u(\gamma, \kappa) - w(\gamma, \kappa)| &= \left| p(\gamma, \kappa) * \left( \frac{e^{\lambda\kappa} - e^{-\lambda\kappa}}{2\lambda} \right) \right| \\ &\leq \left| \int_{-\infty}^{\infty} p(\gamma, s)r(\kappa - s)ds \right| \\ &\leq \varepsilon\varphi(\gamma, \kappa) \left| \int_{-\infty}^{\infty} \left( \frac{e^{\lambda(\kappa-s)} - e^{-\lambda(\kappa-s)}}{2\lambda} \right) ds \right| \\ &\leq K_\varphi \varepsilon\varphi(\gamma, \kappa) \end{aligned}$$

where

$$K_\varphi = \left| \int_{-\infty}^{\infty} \left( \frac{e^{\lambda(\kappa-s)} - e^{-\lambda(\kappa-s)}}{2\lambda} \right) ds \right|.$$

The proof is now complete.

**Example 3.3.** Consider

$$u_{\kappa\kappa}(\gamma, \kappa) - 4u(\gamma, \kappa) = 2\sin\kappa, \quad (10)$$

in which  $g(\gamma, \kappa) = 2\sin\kappa$  is a function of exponential order and  $\lambda = 2$ .

If a continuously differentiable function  $y: I \times I \rightarrow \mathbb{R}$  satisfies

$$|y_{\kappa\kappa}(\gamma, \kappa) - 4y(\gamma, \kappa) - 2\sin\kappa| \leq \varepsilon$$

for some  $\varepsilon > 0$  and all  $\kappa \geq 0$ , then there exists a solution  $w: I \times I \rightarrow \mathbb{R}$  of differential equation (10) such that

$$|y(\gamma, \kappa) - w(\gamma, \kappa)| \leq K_\varphi \varepsilon,$$

for all  $x \geq 0$ . Here

$$K_\varphi = \left| \int_{-\infty}^{\infty} \left( \frac{e^{2(\kappa-s)} - e^{-2(\kappa-s)}}{4} \right) ds \right|.$$

#### 4. CONCLUSION

In this study, we used the Mahgoub transform to examine the (HUS) of second order homogeneous partial differential equation and (HURS) of second order nonhomogeneous partial differential equation. This study also demonstrates that the Mahgoub transform method is more practical for looking at stability issues with partial differential equations.

#### **Funding**

The author (s) has no received any financial support for the research, authorship or publication of this study.

#### **The Declaration of Conflict of Interest/ Common Interest**

No conflict of interest or common interest has been declared by the authors.

#### **The Declaration of Ethics Committee Approval**

This study does not require ethics committee permission or any special permission.

#### **The Declaration of Research and Publication Ethics**

The authors of the paper declare that they comply with the scientific, ethical and quotation rules of SAUJS in all processes of the paper and that they do not make any falsification on the data collected. In addition, they declare that Sakarya University Journal of Science and its editorial board have no responsibility for any ethical violations that may be encountered, and that this study has not been evaluated in any academic publication environment other than Sakarya University Journal of Science.

#### REFERENCES

- [1] S. M. Ulam, "Problems in Modern Mathematics," Science Editions, John Wiley & Sons, Inc., New York, 1964.
- [2] D. H. Hyers, "On the stability of the linear Functional equation," Proceedings of the National Academy of Sciences, U.S.A., vol. 27, pp. 222-224, 1941.
- [3] E. Biçer, C. Tunç, "New Theorems for Hyers-Ulam stability of Lienard equation with variable time lags," International Journal of Mathematics and Computer Science, vol. 3, no. 2, pp. 231-242, 2018.
- [4] E. Biçer, C. Tunç, "On the Hyers-Ulam stability of certain partial differential equations of second order," Nonlinear Dynamics and Systems Theory, vol. 17, no.2, pp. 150-157, 2017.
- [5] D. H. Hyers, T. M. Rassias, "Approximate homomorphisms," Aequationes Mathematicae, vol. 44, pp. 125-153, 1992.
- [6] D. H. Hyers, G. Isac, TM. Rassias, "Stability of Functional Equations in Several Variables," Progress in

Nonlinear Differential Equations and their Applications, vol. 34, Boston, 1998.

- [7] S. M. Jung, "Hyers–Ulam stability of linear partial differential equations of first order," *Applied Mathematics Letters*, vol. 22, no.1, pp. 70-74, 2009.
- [8] S. M. Jung, J. Brzdek, "Hyers-Ulam stability of the delay equation  $y'(t)=\lambda y(t-\tau)$ ," *Abstract and Applied Analysis*, vol. 2010, pp. 1-10, 2010.
- [9] N. Lungu, D. Popa, "Hyers-Ulam stability of a first order partial differential equation," *Journal of Mathematical Analysis and Applications*, vol. 385, pp. 86-91, 2012.
- [10] J. Huang, Y. Li, "Hyers-Ulam Stability of Linear Functional Differential Equation," *Journal of Mathematical Analysis and Applications*, pp. 1192-1200, 2015.
- [11] M. Obłozza, "Connections between Hyers and Lyapunov stability of the ordinary differential equations," *Rocznik Naukowo Dydaktyczny Wsp W Krakowie*, vol. 14, pp. 141-146, 1997.
- [12] D. Otrocol, V. Ilea, "Ulam stability for a delay differential equation," *Central European Journal of Mathematics*, vol. 11, no. 7, pp. 1296-1303, 2013.
- [13] T.M. Rassias, "On the stability of the linear mapping in Banach spaces," *Proceedings of the American Mathematical Society*, vol. 72, no. 2, pp. 297-300, 1978.
- [14] T. M. Rassias, "On the Stability of Functional Equations and a Problem of Ulam," *Acta Applicandae Mathematicae*, vol. 62, pp. 23-130, 2000.
- [15] S. E. Takahasi, T. Miura, S. Miyajima, "On the Hyers-Ulam stability of the Banach space-valued differential equation  $y'=\lambda y$ ," *Bulletin of the Korean Mathematical Society*, vol. 39, pp. 309-315, 2002.
- [16] C. Tunç, E. Biçer, "Hyers-Ulam-Rassias stability for a first order functional differential equation," *Journal of Mathematical and Fundamental Sciences*, vol. 47, no. 2, pp. 143-153, 2015.
- [17] S. M. Jung, P. S. Arumugam, R. Murali, "Mahgoub Transform and Hyers Ulam stability of first order linear differential equations," *Journal of Mathematical Inequalities*, vol.15, no. 3, pp. 1201-1218, 2021.
- [18] S. Aggarwal, N. Sarma, N. Chauhan, "Solution of linear Volterra integro-differential equations of second kind using Mahgoub transform," *International Journal of Latest Technology in Engineering Management and Applied Science*, vol. 7, no. 5, pp. 173-176, 2018.



SAKARYA ÜNİVERSİTESİ

# FEN BİLİMLERİ ENSTİTÜSÜ DERGİSİ

Sakarya University Journal of Science  
SAUJS

ISSN 1301-4048 e-ISSN 2147-835X Period Bimonthly Founded 1997 Publisher Sakarya University  
<http://www.saujs.sakarya.edu.tr/>

Title: The Fatty Acid Compositions and Textural Properties of Dry Clotted Creams  
Produced in Different Drying Systems

Authors: Esmâ ÇAPA, Bedia ŞİMŞEK

Received: 2022-06-07 00:00:00

Accepted: 2022-10-26 00:00:00

Article Type: Research Article

Volume: 26

Issue: 6

Month: December

Year: 2022

Pages: 1274-1287

How to cite

Esmâ ÇAPA, Bedia ŞİMŞEK; (2022), The Fatty Acid Compositions and Textural  
Properties of Dry Clotted Creams Produced in Different Drying Systems. Sakarya  
University Journal of Science, 26(6), 1274-1287, DOI:  
10.16984/saufenbilder.1127548

Access link

<https://dergipark.org.tr/en/pub/saufenbilder/issue/74051/1127548>

New submission to SAUJS

<http://dergipark.gov.tr/journal/1115/submission/start>



## The Fatty Acid Compositions and Textural Properties of Dry Clotted Creams Produced in Different Drying Systems

Esma ÇAPA<sup>1</sup> , Bedia ŞİMŞEK\*<sup>1</sup> 

### Abstract

In this study, the properties of dry clotted creams produced in different drying systems (vacuum and tray drying systems) and traditional methods have been determined. Physico-chemical, color, textural, microbiological, and sensory analysis as well as fatty acid composition analysis and appearance analysis of dry clotted creams were carried out during storage. During the storage, it was observed that pH and titration acidity values of samples increased. The hardness levels of the clotted cream produced with the tray dryer were found to be higher than the vacuum and traditional methods. The highest ratio of saturated fatty acids was observed in the samples produced with a vacuum dryer. As a result, it was found that a product similar to traditional dry cream could be produced in industrial tray drying systems. When vacuum drying was applied, more successful results were obtained against oxidation than other drying techniques. However, it was determined that some of its features were also lost. It was also determined that in this system, the dry cream production time may be shortened by at least 50 % compared to the traditional production.

**Keywords:** Dry clotted cream, tray dryer, vacuum drying

### 1.INTRODUCTION

A drying process is applied to the food in order to extend the shelf life [1]. The most common drying methods for this product are air drying and shade drying. This process can result in negative effects such as taking a long time, low productivity, unhygienic conditions, and detrimental quality features such as loss of product flavor, color, texture and nutrients [2,

3]. For this reason, industrial drying systems have been developed for the dry food industry. The tray dryer system consists of a motor, fan and tray with an adjustable temperature and air-flow rate [4]. In vacuum drying systems, natural liquids and gases in the food system are removed through partial vacuum pressure, and low temperatures are produced in an oxygen-free environment [5]. It is seen that drying studies are mostly on fruits and vegetables. However, tray dryers can be used for drying dairy products such as Keş [6], Cokelek [7],

\* Corresponding author: bediasimsek@sdu.edu.tr

<sup>1</sup> Süleyman Demirel University, Faculty of Engineering

E-mail: capaesma07@gmail.com

ORCID: <https://orcid.org/0000-0002-7497-1542>, <https://orcid.org/0000-0002-9608-9710>



İzmir Tulum Cheese [8], etc. It is seen that vacuum dryers are also involved in the production of Lor cheese [9] and dried cheese puffs [10]. When dairy products with high fat content are dried at high temperatures, the fat in the dairy product would leak. Therefore, it has been reported that dairy products with high fat content should be dried at low temperatures [11].

Milk fat is a food that does not last very long even in refrigerator conditions. The freezing process, on the other hand, brings a huge cost. Therefore, drying milk fat is seen as a good alternative to extend the shelf life [12]. Among the dried products with high milk fat content, the most widely known are cream powders and whole milk powders [13]. Among the dried products with high milk fat content, the most commonly known ones are cream powders and whole milk powders. Among the traditional products, dry clotted cream is one of the dried products containing high milk fat [14].

Clotted cream is a slightly acidic dairy product rich in milk fat. It is made from buffalo milk in Western and Central Anatolia, and from cow's milk in the Eastern regions [15, 16]. Dry clotted cream is a traditional product that has different properties from clotted cream. The texture of traditional dry clotted cream is hard and crunchy. It is also defined as a natural wafer in the Central Anatolia region [17]. Dry clotted cream is a homemade product produced by small-scale producers; the milk is frothed from height onto aluminum trays and then cooked slowly. It is kept in a cool environment for about 12 to 14 hours and the fat layer is waiting for the fat layer to gather and harden on the surface. Afterwards, the clotted cream layer formed is cut with a knife and folded into half with the lower layers in the middle and then left to dry in a cool environment on a perforated container (sieve). It has been noted that 500 grams of dry clotted cream at a diameter of 60 to 70 cm is produced from approximately 6 liters of milk. The product obtained is used as a

breakfast or a snack in the form of a wafer-like structure. In a study conducted on dry clotted cream, it was found that the fat content ranged from 55.5 % to 70 % and the protein content ranged from 14.3 % to 20.3 % [16].

Dry clotted cream production is a process that requires traditional conditions and takes a long time. For this reason, its industrial production is limited. In order to expand the production of this product in the industry, the ability to be produced with different dryers has been evaluated in this study. The study aims are to dry the clotted cream using various food drying systems (tray dryer, vacuum dryer) and to compare the product properties with the traditional drying method.

## 2. MATERIALS AND METHOD

In this study on dry clotted cream production, raw cow's milk was provided from the Isparta Unsut facility in Turkey and cow milk cream (60 %) was used for fat standardization.

Dry clotted creams were produced using a Mikrotest MSD2.50 D8 (Turkey) tray dryer (at 25 °C and an air velocity of 1.3 m/s), and a Korean- branded Wiseven Fuzzy Control System vacuum (under an 0.8 MPa vacuum at 25°C).

### 2.1. Dry Clotted Cream Production and Experimental Design

In order to standardize the thickness of the clotted cream, the raw milk fat was standardized at 60 % by adding cream. The first heat treatment was applied to raw milk at 95±2°C for 20 minutes. Pasteurized milk, with a thickness of 12±3 mm, was transferred to the trays from a height of about one meter to foam it (to form a porous structure). The amount of height (approximately 1m) was determined by considering traditional production techniques. The milk in the trays has been left to cool to approximately 42±2 °C. Then, a secondary heat

treatment was applied at  $72\pm 2$  °C. The clotted cream was then left to cool at  $+4$ °C for about 12 hours to form a layer. The finally formed product layer was cut and placed on the perforated grids and separated from the milk at the bottom [18]. The resulting product was divided into three parts. The clotted creams were dried using a traditional drying method (natural drying with air at a room temperature of 25 °C) for the control group (A), with the tray drying system for group B, and the vacuum drying system for group C. The drying process was terminated when at least 75 % dry matter had been produced. The samples were dried at 25 °C for  $46\pm 2$  hours, in the traditional drying method,  $14\pm 2$  hours in tray drying system and 24 hours in the vacuum drying system. The products obtained were vacuum packed and stored at  $+4$  °C for 20 days.

## 2.2. Physicochemical Analysis

The thickness of the dry clotted cream samples was measured using digital calipers to a tolerance of 0.001 mm (Mitutoyo, Tokyo, Japan) [19]. Dry matter ratios (%) of clotted cream and dry clotted cream samples were determined using the gravimetric method. The fat (%) and total nitrogen were analyzed by the Gerber method [20] and micro-Kjeldahl method, respectively. The protein ratio was determined by multiplying the total nitrogen by the coefficient of 6.38 [19]. The pH values were determined with the help of a digital pH meter (WTW pH 315-Weilhelm, Germany), and titratable acidity (LA %) was determined with titration [15]. For the determination of acidity values, 5 g of filtered pure milk fat was weighed. Then 50 ml of an alcohol-ether mixture (1:1) was added into the weighed milk fat to dissolve it. The acid value was then determined with the use of the formula by titrating with phenolphthalein indicator and 0.1 N NaOH [20].

### 2.2.1. Peroxide value

The peroxide values of clotted cream and dry clotted cream samples were found by weighing out 2 g fat extract, then, adding 25 ml of chloroform-acetic solution (2: 3) to dissolve the milk fat. Then, 0.5 ml of saturated potassium iodide was added. The samples were kept in the dark for 1 minute, before adding 75 ml of purified water. The value was then calculated with the help of the formula after titrating with 0.002 N sodium thiosulphate and 0.5 ml 1% starch solution indicator [19].

### 2.2.2. Thiobarbituric acid value

The 2-thiobarbituric acid (TBA) value was determined by a spectrophotometric method with a BOECO S20 (Hamburg, Germany) branded device. A 50 ml amount of 20 % cold trichloroacetic acid solution (TCA) was added to 5 g of each sample and homogenized. After adding 50 ml of cold distilled water, the extract was filtered through Whatman No: 1 filter paper. A 5 ml amount of the extract was poured into a tube and 5 ml of 2-TBA solution was added. An absorbance reading was then performed at wavelength of 532 nm [21].

### 2.2.3 Free fatty acids and the fatty acid composition

Fatty acid analysis of clotted cream and dry clotted cream samples were quantitatively determined on the 1<sup>st</sup> and 20<sup>th</sup> days of storage using Perkin Elmer Auto System XL branded gas chromatography (GC) device and the analysis of fatty acid methyl esters was performed according to the AOAC [22] 996.06 method. The flame ionization detector method used a mobile helium phase at 15 PSI, an injection volume of 1  $\mu$ L, VARIAN CP sil 88 column (50 mx 0.25 mm) for FAME compounds and a film thickness of 0.2 microns. The sample injection rate (split) was 1/200. The injector and detector temperatures were 240°C. The column temperature was programmed to

be 80°C for 4 minutes, then maintained at 175°C for 25 minutes. The column was later maintained at 215°C for 2 minutes and operated at 240°C for 10 minutes. The total analysis time was approximately 40 minutes. The standard mix of FAMES (Supelco® 37 Component FAME Mix, Cat. No. 47885 U) was obtained from Sigma-Aldrich (St. Louis, MO, ABD).

### **2.3. Textural Analysis**

Dry clotted cream samples were kept at +4°C for at least 24 hours and measured by a TA XT 2i (Stable Micro Systems, UK) branded texture analyzer with the help of a ball-type probe P/0.75S number ¾ over 15 minutes [20]. The measurements were immersed in 3 different parts of the product at a speed of 1 mm/s to a depth of 10 mm and performed under a force of 1 N [15, 23].

### **2.4. Color Analysis**

Color values (L\*, a\* and b\*) of the samples were determined using a Chroma Meter CR 400. An AC Adapter 5V AC-A17 (Minolta Co. Ltd, Osaka, Japan) branded automatic color determination device was used to determine the L\* value range from bright to dark (0 black, 100 white), the green/red a\* value (-60 green, 60 red) and blue/yellow b\* value (-60 blue, 60 yellow) [23].

### **2.5. Appearance Analysis**

The surface photos of the dry clotted cream samples were obtained using a digital camera (Nikon D7100 DSLR, Japan), and then the images were analyzed with the help of a Windows 8.1 PC containing an Intel I5 CPU, using the OpenCV image processing library and the C++ language. The program examined the contrast between the two phases in the image, the pores, and the surface. The color images were first converted to a grayscale where the pixel values were converted to units of length with the help of bars of known length.

Porosity was expressed as the ratio of the area of pores in the cross section examined in the analysis of the total area [24].

### **2.6. Sensory Analysis**

Sensory analysis of dry clotted cream samples were conducted according to a scoring method by 7 educated panelists (5 women and 2 men) aged 20-50 years on the 1<sup>st</sup>, 10<sup>th</sup>, and 20<sup>th</sup> days of storage. Two different methods, the Descriptive Analysis Method and the Hedonic Test, were used in the sensory analyses of the samples. Whereas the hedonic scale of 1 to 9 points was used in the sensory evaluation panel, the dry clotted cream samples were also evaluated in terms of color, appearance, texture, odor and general acceptability. Examples representing very good and very bad in terms of sensory characteristics were introduced to the panelists and necessary training was given on this subject. For the evaluation of the original samples, the panelists were asked to use these samples as references. The methods given by Lawless and Heymann, [25] were used in the application of sensory analysis.

### **2.7. Microbiological Analysis**

Yeast-mold counts in cream and dried cream samples were counted on Potato Dextrose Agar (PDA) and E.coli, and coliform microorganisms were counted on Eosin Methylene Blue (EMB) agar media [26].

### **2.8. Statistical Analysis**

The statistical evaluation of the study was performed by using the SPSS 17.0 program and by determining the significance of the differences between groups with the help of the Duncan multiple comparison test. The study was carried out with three replications. In this study, Principal Component Analysis method was applied to provide a visual representation of the similarity or distance model between a

set of objects and to reduce the size of the data. Analyzes were performed at 95% confidence intervals. Sensory analysis data (color, appearance, texture, odor) was evaluated in all samples (A, B, C, A10, B10, C10, A20, B20 and C20) using the principal component analysis (PCA) Xlstat trial version-2020.

### 3. RESULTS AND DISCUSSION

#### 3.1. Clotted Cream Analysis Results

The dry matter (%), fat (%) and protein (%) percentages of the clotted cream used in the production of dry clotted cream were  $65.89 \pm 2.61$  %,  $64.66 \pm 0.47$  % and  $2.22 \pm 0.04$  %, respectively. These results showed similarity to the research findings of Tosun [15]. The titration acidity of the clotted cream samples was  $0.22 \pm 0.03$  % and pH  $6.23 \pm 0.04$ . The research results of Albay and Şimşek [27] showed similarity in terms of titration acidity and pH values. The peroxide, acid degree and TBA values of the samples were  $0.44 \pm 0.04$  meq O<sub>2</sub>/ kg fat,  $1.25 \pm 0.03$  KOH/g fat and  $0.04 \pm 0.008$  malonaldehyde/kg fat respectively. In the study by Kocaturk et al. [28], the total free fatty acidity values are 0.40 to 0.51 meq O<sub>2</sub>/ 100 g oil, ranging from 0.40 to 0.51 meq O<sub>2</sub>/ 100 g oil, and Kahyaoglu [29] reported that the TBA value of butter varied between 0.01 and 0.03 mg malonaldehyde/kg fat at the beginning of storage. It was observed that the data of clotted cream in this study was close to the results of Tosun [15], Albay and Şimşek [24], Kocaturk et al. [28] and Kahyaoglu [29]. The L\*, a\*, and b\* color values of samples were  $88.87 \pm 1.26$ ,  $-2.99 \pm 0.16$  and  $13.40 \pm 0.26$ , respectively. L\* a\* and b\* color values in the study given by Albay and Şimşek [27] were similar to the values in this study.

#### 3.2. Results of Dry Clotted Cream Analysis

##### 3.2.1. Results of physicochemical analysis

In the thickness measurements of the dry clotted cream, B was reported to be the thickest sample ( $15.04 \pm 0.68$  mm), while C was reported to be the thinnest ( $10.60 \pm 0.70$  mm). Sample A was detected with a thickness of  $12.23 \pm 0.13$  mm. The statistical difference between the samples was found to be significant ( $p < 0.05$ ). Since the vacuum effect reduces fat globules and surface tension, it was thought that a thin structure might have been formed in the C sample.

The data, including the chemical properties of the dry clotted cream samples produced in different drying systems, have been presented in Table 1. In this study, the dry matter values of the dry clotted cream samples varied from  $78.15 \pm 0.25$  % to  $79.59 \pm 0.88$  % and similar to the dry matter values of 70.8 % to 91.3 % determined in the dry clotted cream study by Cakmakcı and Hayaloglu [16]. The fat content of the dry clotted cream samples was found to be adequate according to the Turkish Food Codex Custard and Cream Communique [30]. When the dry clotted cream samples were examined in terms of the amount of protein, it was observed that samples A and C were statistically close to each other, and sample B had a higher amount. Depending on the composition of the milk used in the raw material, the protein values found in this study were lower than those reported by Cakmakci and Hayaloglu [16] for dry clotted cream. At the beginning of storage, the dry clotted cream sample B had the lowest pH ( $6.03 \pm 0.04$ ), while at the end of storage, a decrease was observed in all three samples and the highest pH was observed in the dry clotted cream sample C ( $5.34 \pm 0.05$ ). It was observed that titratable acidity similarly increased in dry clotted cream samples due to a pH decrease. It was noted that the dry clotted cream B sample had the lowest titratable acidity while the dry clotted cream

samples had the highest titratable acidity. This change between the groups was attributed to the longer production process of the tray drying system compared to the vacuum drying system.

storage, the highest value at the end of storage was determined to be  $1.41 \pm 0.34$  meq O<sub>2</sub>/ kg fat for the sample A. The peroxide value, which is one of the oxidation indicators related to fat

Table 1 Physicochemical properties of Dry Clotted Cream

Samples (**)	Dry Matter (%)	Fat (%)	Protein (%)	Titratable Acidity (%)	pH	Peroxide Value (meq O <sub>2</sub> /kg fat)	Acid Value (mg KOH/g fat)	TBA Value (mg malonaldehyde /kg fat)
<b>1<sup>st</sup> day (*) (M±SD)**</b>								
A	78.31±0.49	69.33±1.69	2.42±0.08 <sup>b</sup>	0.37±0.04 <sup>b</sup>	5.91±0.05 <sup>abc</sup>	0.44±0.19 <sup>bc</sup>	1.34±0.09 <sup>bc</sup>	0.08±0.02 <sup>bc</sup>
B	79.57±0.76	70.33±1.24	2.58±0.09 <sup>a</sup>	0.35±0.03 <sup>b</sup>	6.03±0.04 <sup>a</sup>	0.42±0.31 <sup>bc</sup>	1.17±0.13 <sup>c</sup>	0.07±0.03 <sup>bc</sup>
C	78.15±0.25	71.33±0.94	2.38±0.05 <sup>b</sup>	0.37±0.05 <sup>b</sup>	5.98±0.02 <sup>ab</sup>	0.49±0.28 <sup>bc</sup>	1.14±0.07 <sup>c</sup>	0.09±0.05 <sup>bc</sup>
<b>10<sup>th</sup> day (*)</b>								
A	78.10±0.69	70.00±2.16	2.43±0.01 <sup>b</sup>	0.52±0.11 <sup>ab</sup>	5.79±0.01 <sup>cd</sup>	0.74±0.32 <sup>abc</sup>	1.83±0.06 <sup>ab</sup>	0.25±0.01 <sup>a</sup>
B	79.58±0.80	70.33±1.24	2.60±0.02 <sup>a</sup>	0.47±0.07 <sup>ab</sup>	5.93±0.04 <sup>abc</sup>	0.92±0.22 <sup>ab</sup>	1.21±0.02 <sup>c</sup>	0.11±0.04 <sup>abc</sup>
C	77.91±2.92	71.33±0.94	2.42±0.01 <sup>b</sup>	0.47±0.10 <sup>ab</sup>	5.79±0.17 <sup>bcd</sup>	0.59±0.37 <sup>bc</sup>	1.38±0.03 <sup>bc</sup>	0.14±0.02 <sup>ab</sup>
<b>20<sup>th</sup> day (*)</b>								
A	78.27±0.97	69.33±1.33	2.43±0.04 <sup>b</sup>	0.57±0.09 <sup>ab</sup>	5.69±0.05 <sup>d</sup>	1.41±0.34 <sup>a</sup>	2.16±0.15 <sup>a</sup>	0.28±0.02 <sup>a</sup>
B	79.59±0.88	70.33±1.24	2.63±0.05 <sup>a</sup>	0.50±0.12 <sup>ab</sup>	5.77±0.11 <sup>cd</sup>	1.31±0.39 <sup>a</sup>	1.66±0.26 <sup>b</sup>	0.16±0.01 <sup>ab</sup>
C	77.88±0.99	71.33±0.94	2.46±0.02 <sup>b</sup>	0.62±0.16 <sup>a</sup>	5.34±0.05 <sup>e</sup>	1.24±0.40 <sup>a</sup>	1.90±0.17 <sup>ab</sup>	0.15±0.05 <sup>ab</sup>

\* a, b, c: Lower case letters indicate statistically significant differences (p < 0.05).

\*\* A: Traditionally dried Clotted Cream; B: Tray dried Clotted Cream; C: Vacuum dried, M: Mean, SD: Standart deviation

Acid values of dry clotted cream samples produced by different drying techniques have increased in particular because of lipolysis during storage, and the highest acid value at the end of storage was determined in the dry clotted cream A sample ( $2.16 \pm 0.15$  mg KOH / g fat). It has been reported that the acid value can reach 1.8 mg KOH / g and there is a distinctly inferior aroma [31, 32]. It was thought that the traditional drying method, which takes longer to dry samples than other methods causes faster lipolysis. Cakmakci and Hayaloglu [16] reported that the acid value of the dry clotted cream samples was  $1.69 \pm 0.61$  mg/ KOH g fat. It has been seen that the acid value results of the dry clotted cream samples on the first day were similar to these data.

While the peroxide values of the dry clotted cream samples were similar at the beginning of

in dairy products was limited to 2 meq O<sub>2</sub>/kg fat by Downey [33]. Pearson [34] reported that the peroxide value in rancid butter was 6.3 meq O<sub>2</sub>/kg fat of fat. It was observed that the dry clotted cream samples were below this limit. The peroxide values of the samples at the end of the storage, seen in the samples using the vacuum drying system were lower than the other samples. Zhou et al [35] reported that in a study comparing different drying methods, the lowest peroxide value was obtained with vacuum drying. The TBA values of the dry clotted cream samples produced in different drying systems varied between  $0.07 \pm 0.03$  and  $0.28 \pm 0.02$  mg malonaldehyde/kg fat during the storage period, and the highest change occurred in the dry clotted cream samples produced by the conventional method. TBA results in other samples have been found to be close to each other.

### 3.2.2. Results of free fatty acids

The free fatty acid results of the dry clotted cream samples produced by traditional, tray and vacuum drying systems are presented in Table 2. It is observed that there are difference in the fatty acid profile depending on the parameters during production, drying times and changes during storage. In all dried cream samples, palmitic, oleic and myristic acid were the dominant fatty acids while c10-heptadecanoic acid, tridecanoic acid and c-10-pentadecanoic acids were detected at lower levels. In the study conducted by the examination of the saturated fatty acid amounts in dry clotted cream samples showed that the sum of short-chain fatty acids in the dry clotted cream C samples decreased during the storage period and increased in the other sample groups. It was statistically determined that this difference was influenced by caprylic acid. In addition, the amount of caprylic acid determined in the dry clotted cream C sample was higher since the removal of some fatty acids through drying systems (tray and vacuum drying systems) takes a shorter time compared to the traditional system. In the study conducted by Tosun [15], the fatty acids contents of clotted cream samples (short,

medium and long chain) were determined as 5.23-5.87 %, 5.06 %-5.55 % and 52.44 %-53.92 %, respectively. It was noted that the total amount of unsaturated fatty acids decreased in the dry clotted cream B sample during storage but increased in other groups. Oleic acid, one of the monounsaturated fatty acids, and linoleic acid, one of the polyunsaturated fatty acids, were the cause of statistical difference between the groups. Free fatty acid composition and amount were mostly affected by raw material properties. It was also affected by both drying and storage [36]. Senel [37], it was reported that the decrease in the amount of total fatty acids was related to the catabolic reactions of microorganisms, that is, biochemical changes in the formation of aroma and flavor. It was also reported that volatile free fatty acids decreased with oxidation. During the removal of water in vacuum dryers, oxidation was prevented since there is no air in the environment. Prevention of oxidation was caused significant changes on fatty acids [38].

When evaluated in terms of fatty acids in both methods (vacuum and tray drying), the results obtained with the traditional method were found to be similar.

Table 2 Free Fatty Acid Profile of Dry Clotted Cream Samples (n: 3)

Methyl Ester	Fatty Acid	1 <sup>st</sup> day(*) (M ±SD)(%)			20 <sup>th</sup> day(*) (M ±SD)(%)		
		A(**)	B(**)	C(**)	A(**)	B(**)	C(**)
<b>C4:0</b>	Butyric	3.15±0.30	3.43±0.03	3.58±0.62	3.41±0.03	3.41±0.07	3.60±0.05
<b>C6:0</b>	Caproic	3.23±0.16	3.12±0.11	3.44±0.69	3.20±0.08	3.25±0.01	3.32±0.01
<b>C8:0</b>	Caprylic	2.02±0.19	2.20±0.02	2.35±0.22	2.12±0.04	2.19±0.08	2.31±0.05
<b>C10:0</b>	Capric	4.60±0.20	4.78±0.06	5.33±0.11	4.57±0.10	4.66±0.31	4.85±0.02
<b>C11:0</b>	Undecanoic	0.54±0.06	0.48±0.00	0.54±0.00	0.46±0.05	0.46±0.02	0.50±0.01
<b>C12:0</b>	Lauric	4.70±0.32	4.93±0.00	5.48±0.15	4.74±0.04	4.73±0.21	4.92±0.05
<b>C13:0</b>	Tridecanoic	0.14±0.02	0.12±0.00	0.12±0.01	0.12±0.00	0.13±0.01	0.12±0.00
<b>C14:0</b>	Myristic	12.82±0.86	13.41±0.02	15.03±1.19	13.22±0.12	12.85±0.56	13.32±0.02
<b>C14:1</b>	Myristoleic	1.48±0.41	1.13±0.01	1.57±0.43	1.83±0.01	1.08±0.05	1.12±0.01
	<b>Saturated<sup>1</sup></b>	<b>64.95</b>	<b>67.93</b>	<b>73.67</b>	<b>67.54</b>	<b>66.13</b>	<b>67.81</b>
<b>C15:0</b>	Pentadecanoic	1.13±0.01	1.13±0.01	1.11±0.03	1.12±0.02	1.07±0.03	1.11±0.01
<b>C15:1</b>	c-10-pentadecanoic	0.42±0.05	0.34±0.02	0.34±0.02	0.37±0.01	0.35±0.005	0.37±0.01
<b>C16:0</b>	Palmitic	25.18±1.94	26.45±0.39	29.41±3.96	26.56±0.13	25.62±0.85	26.03±0.16
<b>C16:1</b>	Palmitoleic	1.20±0.07	1.26±0.02	1.22±0.02	1.22±0.03	1.26±0.01	1.25±0.01
<b>C17:0</b>	Heptadecanoic	0.57±0.02	0.54±0.05	0.55±0.04	0.58±0.01	0.55±0.00	0.57±0.00
<b>C17:1</b>	c-10 heptadecanoic	0.15±0.03	0.18±0.00	0.14±0.05	0.19±0.05	0.16±0.02	0.18±0.05
<b>C18:0</b>	Stearic	6.84±0.38	7.31±0.02	6.71±0.23	7.42±0.09	7.17±0.11	7.13±0.20
<b>C18:1n9t</b>	Elaidic	1.82±0.58	1.24±0.01	1.08±0.03	1.30±0.02	1.23±0.03	1.24±0.07

Table 2 Free Fatty Acid Profile of Dry Clotted Cream Samples (n: 3) (Continue)

Methyl Ester	Fatty Acid	1 <sup>st</sup> day <sup>(*)</sup> (M ±SD)(%)			20 <sup>th</sup> day <sup>(*)</sup> (M ±SD)(%)		
		A(**)	B(**)	C(**)	A(**)	B(**)	C(**)
<b>C18:1n9c</b>	Oleic	15.21±0.37	15.96±0.21	15.55±0.80	16.19±0.08	15.55±0.11	15.74±0.40
<b>C18:2n6c</b>	Linoleic	1.81±0.04	1.83±0.05	1.67±0.02	1.77±0.00	1.68±0.06	1.73±0.02
<b>C18:3n39</b>	Linolenic	0.47±0.10	0.58±0.00	0.54±0.04	0.60±0.01	0.60±0.02	0.58±0.00
	<b>Monounsaturated<sup>2</sup></b>	<b>20.29</b>	<b>20.12</b>	<b>19.92</b>	<b>21.11</b>	<b>19.65</b>	<b>19.92</b>
	<b>Polyunsaturated<sup>3</sup></b>	<b>2.28</b>	<b>2.42</b>	<b>2.22</b>	<b>2.37</b>	<b>2.42</b>	<b>2.31</b>
	<b>Unsaturated<sup>4</sup></b>	<b>22.57</b>	<b>22.54</b>	<b>22.14</b>	<b>23.49</b>	<b>21.93</b>	<b>22.23</b>

\* a, b, c: Lower case letters indicate that the difference is statistically significant (p <0.05)

\*\* A: Traditionally dried Clotted Cream; B: Tray dried Clotted Cream; C: Vacuum dried Clotted Cream; M: Mean, SD:Standart deviation

1: Saturated: Total of Saturated Fatty Acids; C4: 0 + C6: 0 + C8: 0 + C10: 0 + C11: 0 + C12: 0 + C13: 0 + C14: 0 + C15: 0 + C16: 0 + C17: 0 + C18: 0

2: Monounsaturated: Total of Monounsaturated Fatty Acids; C14: 1 + C15: 1 + C16: 1 + C17: 1 + C18: 1

3: Polyunsaturated: Total of Polyunsaturated Fatty Acids; C18: 2 + C18: 3

4: Unsaturated: Total of Unsaturated Fatty Acids; C10: 1 + C14: 1 + C16: 1 + C17: 1 + C18: 1 + C18

### 3.3. Results of Texture Analysis

The measurement values of the hardness, springiness, cohesiveness, gumminess, chewiness and resilience properties of the dry clotted cream samples examined in this study are presented in Table 3. Although there are very few studies investigating the textural properties of dry clotted cream, it was found in this study that the sample produced by drying in a tray dryer (B) reached the highest hardness value in the end of storage. The fact that the products dried in the vacuum system were not as hard as the products in the tray drying system may have been caused by the loss of bubbles on the dry clotted cream surface during the vacuum process and a decrease in the structural strength. While the highest value was found in sample A (0.96), springiness values were

decreased in all samples during storage. The cohesiveness values of the dry clotted cream samples produced in different drying systems were determined to be between 0.17 and 0.45. The gumminess value in dry clotted cream samples were found to be between 98.25 N and 510.13 N. It was concluded that the dry clotted cream samples showed a change in parallel with the hardness values as it increased linearly. The chewiness values of the dry clotted cream samples were determined to be between 57.57 and 800.09, and group B showed the highest chewable property in the end of storage comparison to the other groups. While the C group (0.39 N) showed the highest level of resilience, it was observed that the dry clotted cream samples of the A and B groups were similar. These values were found to be close to those reported by Yıldırım et al. [39].

Table 3 Textural characteristics of Dry Clotted Cream Samples (n: 3)

Samples (**)	Hardness (N)	Springiness	Cohesiveness	Gumminess(N)	Chewiness	Resilience (N)
Day 1 (*) (M±SD)						
A	856.59±56.02 <sup>b</sup>	0.91±0.05 <sup>ab</sup>	0.25±0.08	211.25±55.17 <sup>cdf</sup>	198.76±62.60 <sup>b</sup>	0.09±0.01 <sup>b</sup>
B	973.02±95.24 <sup>b</sup>	0.54±0.06 <sup>b</sup>	0.38±0.01	327.79±32.02 <sup>b</sup>	182.42±39.28 <sup>b</sup>	0.14±0.01 <sup>b</sup>
C	421.34±120.13 <sup>c</sup>	0.57±0.13 <sup>b</sup>	0.34±0.05	134.41±16.51 <sup>ef</sup>	74.99±9.16 <sup>b</sup>	0.21±0.06 <sup>ab</sup>
Day 10 (*)						
A	845.74±55.32 <sup>b</sup>	0.83±0.08 <sup>b</sup>	0.28±0.01	245.20±32.28 <sup>bcd</sup>	208.20±46.39 <sup>b</sup>	0.11±0.02 <sup>b</sup>



Table 3 Textural characteristics of Dry Clotted Cream Samples (n: 3) (Continue)

Samples (**)	Hardness (N)	Springiness	Cohesiveness	Gumminess(N)	Chewiness	Resilience (N)
B	1121.91±195.01 <sup>ab</sup>	0.68±0.05 <sup>b</sup>	0.25±0.01	284.8±49.86 <sup>bc</sup>	480.07±320.02 <sup>a</sup>	0.10±0.01 <sup>b</sup>
C	421.84±131.51 <sup>c</sup>	0.68±0.09 <sup>b</sup>	0.29±0.01	103.97±5.72 <sup>f</sup>	72.19±14.62 <sup>b</sup>	0.17±0.06 <sup>ab</sup>
Day 20 (*)						
A	905.71±186.11 <sup>b</sup>	0.71±0.19 <sup>b</sup>	0.28±0.02	249.86±32.69 <sup>bcd</sup>	169.19±25.13 <sup>b</sup>	0.12±0.01 <sup>b</sup>
B	1342.50±237.69 <sup>a</sup>	0.65±0.05 <sup>b</sup>	0.31±0.01	422.15±87.98 <sup>a</sup>	284.55±80.32 <sup>ab</sup>	0.14±0.01 <sup>b</sup>
C	522.30±131.51 <sup>c</sup>	0.69±0.16 <sup>b</sup>	0.34±0.11	155.50±16.11 <sup>def</sup>	103.74±14.36 <sup>b</sup>	0.27±0.12 <sup>a</sup>

\* a, b, c: Lower case letters indicate statistically significant differences (p <0.05).

\*\* A: Traditionally dried Clotted Cream; B: Tray dried Clotted Cream; C: Vacuum dried Clotted Cream, M: Mean, SD: Standard deviation

### 3.4. Results of Color Analysis

L\*, a\* and b\* color values of dry cream samples produced in three different drying systems are given in the Table 4. When dry clotted cream samples were evaluated in terms of the b\* color value, statistically the group B sample was observed to decrease, and the group C dry clotted cream sample increased. Yildirim et al. [39] determined the average b\* values of the dry clotted cream sample to be 17.44. The results of the study were determined to be close to this value.

Table 4 Color properties of Dry Clotted Cream Samples

Samples (**)	L*	a*	b*
1 <sup>st</sup> day	M±SD	M±SD	M±SD
A	85.25±1.33	-3.44±0.21 <sup>abc</sup>	16.71±0.77 <sup>ab</sup>
B	85.88±0.90	-4.11±0.19 <sup>d</sup>	18.39±1.33 <sup>a</sup>
C	84.33±1.60	-3.61±0.11 <sup>ab</sup>	15.18±1.14 <sup>b</sup>
10 <sup>th</sup> day			
A	86.16±1.20	-3.19±0.22 <sup>a</sup>	17.09±1.10 <sup>ab</sup>
B	85.69±1.67	-3.92±0.35 <sup>cd</sup>	18.22±1.46 <sup>ab</sup>
C	86.56±1.38	-3.32±0.22 <sup>ab</sup>	16.00±1.15 <sup>ab</sup>
20 <sup>th</sup> day			
A	85.46±1.77	-3.35±0.17 <sup>abc</sup>	16.14±1.70 <sup>ab</sup>
B	84.99±1.09	-3.89±0.14 <sup>cd</sup>	18.11±1.08 <sup>ab</sup>
C	84.94±2.06	-3.76±0.40 <sup>bcd</sup>	16.44±1.50 <sup>ab</sup>

\* a, b, c: Lower case letters indicate statistically significant differences (p <0.05).

\*\* A: Traditionally dried Clotted Cream; B: Tray dried Clotted Cream; C: Vacuum dried; M: Mean; SD: Standard deviation

Although using the vacuum drying system took longer than the tray drying system, the b\*

value was found to be lower in these samples, so the vacuum effect caused the samples to be less yellow in color. However, no statistical difference was observed between the b\* values of the samples on the 10<sup>th</sup> and 20<sup>th</sup> days of storage. Silva and Moriera [40] stated that the vacuum drying method reduced the color deterioration in the samples due to the absence of oxygen during the process.

### 3.5. Results of Appearance Analysis

In our study, surface imaging process was performed on dry clotted cream samples produced in different drying systems and is presented in Figure 1. The appearance analysis of the dry clotted cream samples was only measured on day 1 of storage. The textural analysis showed that porosity was formed when milk was poured to cause frothing. Detailed information about this feature has been obtained through the appearance analysis. It was determined that the group B dry clotted cream sample had the highest porosity rate of 25.36±1.15 %, while the lowest level of porosity was achieved with 12.57±1.55 % in the sample dried in the vacuum dryer. It was found that the porosity decreased due to the effect of the vacuuming. In the study conducted by Atamer et al. [17], the microtextural structure of dry clotted cream samples was examined and it was reported that the protein

layer surrounding the oil bubbles maintained the shape of the adsorption layer during the drying phase and that the fat globules that rose during the cooling phase formed a structure characterized by the penetration of the air bubbles.

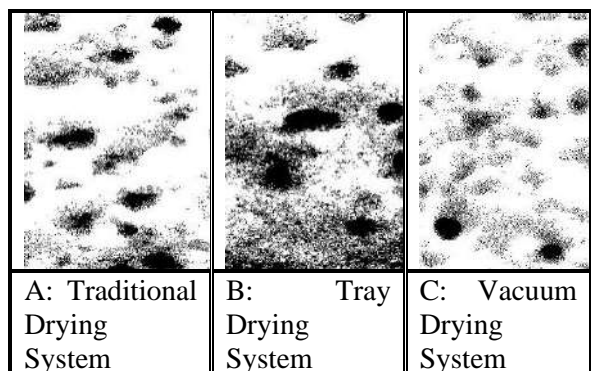


Figure 1 Images of Dry Clotted Cream Samples A; Traditional Drying System, B; Tray Drying System, C; Vacuum Drying System

### 3.6. Principal Component Analysis (PCA)

The sensory analysis results of dry clotted cream samples were analyzed by the principal component analysis (PCA) method. This test, which explained 57.34 % of the total variance,

is presented in Figure 2. The first major component explained 38.70 % of the total variance, while the second component explained 18.63 %. The eigenvalue value of the first main component was determined to be 7.35, and for the second component was determined to be 3.54. According to the distance of the first basic component from zero and having the same sign, the order of porous appearance was 0.29, the yellowish color was 0.24, the cuttability was 0.31, the animal malodor was -0.26, the pleasant smell was 0.31, the foreign taste -0.29, the milk taste 0.25, the flavorless taste was -0.31, the sour taste - 0.23, an oxidized taste was -0.27, and a stale taste was -0.28. The order of the second main component was 0.35 for a smooth appearance, 0.41 for an elastic structure, and -0.33 for a crumby structure. In the first 10 days of storage, it was concluded that samples A and B had an elastic, smooth appearance, were porous yellowish, had a cuttable structure and a distinctive pleasant odor. While sample C had a milk odor at the beginning, at the end of the storage period (20<sup>th</sup> day) together with the other samples A and B, it turned into a stale, sour and oxidized product with a bad odor

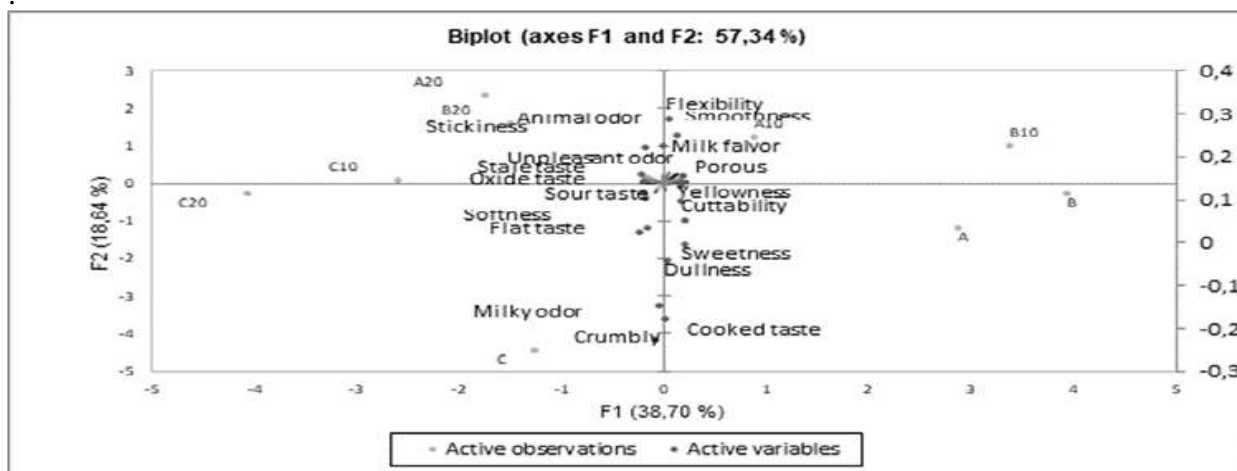


Figure 2 Principal Component Analysis Values of Dry Clotted Cream Samples A: Traditionally dried Clotted Cream; B: Tray dried Clotted Cream; C: Vacuum dried Clotted Cream, A10,B10,C10: Samples on the 10<sup>th</sup> day of storage A20,B20,C20: Samples on the 20<sup>th</sup> day of storage

### 3.7. Results of Microbiological Analysis

Coliform growth and yeast and mold growth were not observed in the dried cream samples obtained by drying in different drying systems.

## 4. CONCLUSIONS

In this study, dry clotted creams producibility were evaluated using a traditional method and using a vacuum dryer and tray drying systems. It was observed that the dry clotted cream samples produced in tray drying systems had the lowest pH, titratable acidity, and free fatty acid values. Samples produced in tray drying systems were the most yellow in color, had the hardest and most porous structure. Dry clotted cream samples produced in vacuum drying systems were noted to be samples with the lowest values in terms of peroxide and TBA numbers, which determined the oil oxidation. It was observed that the amounts of saturated, short, and medium chain fatty acid in dry clotted creams produced by vacuum drying system were higher than the other samples. It was observed that the samples produced by traditional drying were the most desirable group in the sensory evaluation in terms of structure, texture, and odor qualities. Based on the results found in this study, it was concluded that the production duration could be shortened by using tray and vacuum drying systems. In addition, it was observed that the tray drying system yielded better results than the traditional drying system. It was seen that the vacuum drying system is not a suitable technique for the production of dry cream in the industrial sense. Although this technique had positive effects on the shelf life of cream, it did not show positive effects on physical and sensory properties. However, in this study, it has been seen that a production similar to conventional production in industrial terms can be carried out in a shorter time by using a tray dryer.

### *Funding*

This study was financially supported by the Süleyman Demirel University Scientific Research Project Coordination Unit through project no FYL-2019-6928.

### *Conflict of nterest*

The authors have declared no conflicts of interest for this article.

### *Author Contributions*

The authors contributed equally to this work.

### *The Declaration of Ethics Committee Approval*

This study does not require ethics committee permission or any special permission.

### *The Declaration of Research and Publication Ethics*

The authors of the paper declare that they comply with the scientific, ethical and quotation rules of SAUJS in all processes of the paper and that they do not make any falsification on the data collected. In addition, they declare that Sakarya University Journal of Science and its editorial board have no responsibility for any ethical violations that may be encountered, and that this study has not been evaluated in any academic publication environment other than Sakarya University Journal of Science.

## REFERENCES

- [1] İ. Doymaz, C. Aktaş “Patlıcan Dilimlerinin Kurutma ve Rehidrasyon Karakteristiklerinin Belirlenmesi” Journal of The Faculty Engineering and Architecture of Gazi University, vol. 33 no. 3, pp. 833–841, 2018.
- [2] T. Kovacı, E. Dikmen, Ş. A. Şencan “Kurutma Sistemleri , Enerji Tüketimleri ve Ürün Kalitesine Etkileri ve Örnek

- Sistem Tasarımı” Teknik Bilimler Dergisi, vol.8, no.2, pp.25–39, 2018.
- [3] A. D. Yazıcı, M. Daş “Güneş Enerjisi Destekli Kurutma Sistemi İle Elma Ürününün Kurutulması ve Kurutma Değerlerinin Yapay Sinir Ağı İle Modellenmesi” Intenational Journal of Multidisciplinary Studies and Innovative Technologies, vol. 2, no. 1, pp 8–13, 2018.
- [4] E. Ozen, F. Kar “Farklı Teknikler Kullanılarak Domatesin Kurutulması” Fırat Üniversitesi Mühendislik Bilimleri Dergisi, vol. 30, no.1, pp. 47–57, 2018.
- [5] M. Ayaz, E. Dikmen, A. Ş. Şahin “Isı Pompalı Vakumlu Kurutma Fırınında Tıbbi Bitkilerin Kurutulması ve Kurutma Parametrelerinin Araştırılması” Süleyman Demirel Üniversitesi Teknik Bilimler Dergisi, vol. 6, no.1, pp. 1–11, 2016.
- [6] A. Emirmustafaoğlu, H. Coşkun “Kızartmalık Keş Üretim Teknolojisinin Optimizasyonu” Yüzüncü Yıl Üniversitesi Tarım Bilimleri Dergisi, vol. 27, no.3, pp. 357–369, 2017.
- [7] G. Ergene, S. Aslan “Chemical and sensory characteristics of dried Çökelek cheeses at different temperatures” Journal of Food Processing and Preservation, vol. 43, no. 6, pp. 1-8, 2019.
- [8] G. Kızılalp, İ. Polat, M. Urgan, N. Koca “Evaluation of İzmir Tulum cheese pieces by drying with tray drier at different air flow rates and temperatures”. En IDS 2018. 21st International Drying Symposium Proceedings. Editorial Universitat Politècnica de València. 1679-1685, 2018.
- [9] E. A. Anli “Possibilities for using microwave-vacuum drying in Lor cheese production“ International Dairy Journal, vol. 102, 104618, 2020.
- [10] S. Chudy, A. Makowska, M. Piatec, M. Krzywdzińska-Bartkowiak “Application of microwave vacuum drying for snack production: Characteristics of pure cheese puffs” International Journal of Dairy Technology, vol. 72, no.1, pp.82-88, 2019.
- [11] I. S. Hwang, K. B. Lee, Y. K. Shin, M. Y. Baik, B. Y. Kim, “Effect of drying and storage on the rheological characteristics of Mozzarella cheese” Food Science and Biotechnology, vol. 24, no. 6, pp. 2041–204, 2015.
- [12] S. Danviriyakul, D. J. McClements, W. W. Nawar, P.Chinachoti, Physical stability of spray dried milk fat emulsion as affected by emulsifiers and processing conditions. Journal of Food Science, vol.67 No.6, pp. 2183-2189, 2002.
- [13] P. Schuck, Milk Powder: Types and Manufacture. Encyclopedia of Dairy Sciences (2.Edition), Edited by Fuquay, J. W., Fox, P. F. , McSweeney, P. L. H. London, UK: Elsevier Academic Press 2011.
- [14] A. B Himmetağaoğlu, Z. Erbay, M. Çam “Süt yağının toza dönüştürülmesi ve krema tozu” Akademik Gıda vol.17, No.1, pp.72-80, 2019.
- [15] F. Tosun “Ekzopolisakkarit Üreten Laktik Kültürlerin Tereyağı, Yayı Tereyağı ve Kaymağın Kalite Özellikleri Üzerine Etkisi” Erciyes Üniversitesi Fen Bilimleri Enstitüsü, Doktora Tezi, pp. 194, Kayseri, 2016.

- [16] S. Cakmakci, A. Hayaloğlu, "Evaluation of the Chemical , Microbiological and Volatile Aroma Characteristics of Ispir Kaymak , A Traditional Turkish Dairy Product" *International Journal of Dairy Technology*, vol.64, no.3, pp.444–450, 2011.
- [17] M. Atamer "Tereyağı Teknolojisi" Sidaş Medya Ltd. Şti, pp. 169, Ankara, 2016.
- [18] Ş. Pamuk "Geleneksel Afyon Kaymağı Üretimi" *Atatürk Üniversitesi Veteriner Bilimleri Dergisi*, vol.12, no.1, pp. 84–84, 2017.
- [19] Anonymous "Ankara İl Kontrol Laboratuvar Müdürlüğü, Ham protein tayini Döküman Kodu: Yem" MT.004/P13, 2003.
- [20] AOAC "In Official Methods of Analysis of AOAC International" (Vol. 17). Washington DC:Association of Official Analytical Chemists, 2000.
- [21] A. Jha, A. Kumar, P. Jain, A. Kumar Gautam, P. Rasane, "Effect of Modified Atmosphere Packaging On The Shelf Life of Lal Peda" *Journal of Food Science and Technology*, vol. 52, no. 2, pp.1068-1074, 2015.
- [22] AOAC, "AOAC Official Method 996.06", revised 2001. In: (eds) *Official methods of analysis (18th edn.)*. AOAC International, Gaithersburg, MD, 2005
- [23] P. Karatepe, B. Patır "Eugenol ve Thymol'ün Pastörize Tereyağının Kimyasal , Mikrobiyolojik ve Duyusal Kalitesi Üzerine Etkisi" *Fırat Üniversitesi Sağlık Bilimleri Veteriner Dergisi*, vol. 26, no.1, pp. 35–46, 2012.
- [24] G. Dos Reis, B. Stroustrup, "A Principled, Complete, and Efficient Representation of C++". *Mathematic Computer Science* vol.5, pp.335–356, 2011.
- [25] H. T. Lawless, H. Heymann "Sensory Evaluation of Food Principles and Practices", 2nd Edition, XXIII, ISBN 978-1-4419-6488-5, 2010.
- [26] K. A. Halkman K A, Merck Gıda Mikrobiyolojisi Uygulamaları. Basak Matbaacılık Ltd. Şti, pp. 1-10, Ankara, 2005.
- [27] Z. Albay, B. Şimşek "Tarçın ve Tarçın Uçucu Yağı ile Üretilen Kaymakların Bazı Özelliklerinin Belirlenmesi" In Ö. D. Gürcü (Ed.), *Young Scholars Union Congress Proceeding and Abstarcts Book*, pp. 191–203 Prauge, 2019.
- [28] K. Kocaturk, Ö. Gökçe, F. Ergin, A. Küçükçetin, O. Gürsoy, "Geleneksel Yöntemlerle Üretilen ve Manda Kaymağı Olarak Pazarlanan Ürünlerin Bazı Özellikleri ile Konjuge Linoleik Asit İçerikleri" *Akademik Gıda*, vol.17, No.4, pp.476–484, 2019.
- [29] D. T. Kahyaoğlu, "İnek, Koyun ve Keçi Sütlerinden Üretilen Tereyağlarında Depolama Süresince Uçucu Bileşikler, Oksidasyon Stabilitesi ve Diğer Bazı Kalite Kriterlerinin Belirlenmesi", *Atatürk Üniversitesi Fen Bilimleri Enstitüsü, Doktora Tezi*, pp.191, Erzurum, 2014
- [30] Anonymous, "Türk Gıda Kodeksi Yönetmeliği, Krema ve Kaymak Tebliği", *Resmi Gazete*, 27.09.2003, 2003.
- [31] M. Atamer, E. Senel, A. A. Hayaloğlu, B. Özer, "Kuru Kaymağın Tekstürel Yapısı", *Akademik Gıda*, vol.14, no.2, pp.189–195, 2016.

- [32] M. Atamer, E. Sezgin, "Tereyağlarında Lipolitik ve Oksidatif Bozulmaların Saptanmasında Yararlanılan Asit ve Peroksit Değerler ile Aroma Arasındaki İlişki" *Gıda*, vol. 6, pp.329-334, 1984.
- [33] W. K. Downey, "Butter Quality", Published by An Foras Taluntais 19 Sadyamount Avenue Dublin4, Dairy Research and Review Series no. 7, pp.142, 1975.
- [34] D. Pearson, "The assessment of rancidity of oils on a common cholorm extract with special reference to TBA values" *Journal of the Associatin of Public Analyts*, vol.12, pp.73-76, 1974.
- [35] X. Zhou, H. E. J. Gao, M. Wang, S. Wang, "Comparative Analyses of Three Dehydration Methods on Drying Characteristics and Oil Quality of In-shell Walnuts" *Drying Technology*, vol.36, no.1, pp.477-490, 2018.
- [36] J. Yongsawatdigul, S. Gunasekaran "Microwave-vacuum drying of cranberries: Part II. Quality evaluation" *Journal of Food Processing and Preservation*, vol. 20 no.2, pp. 145- 156. 1996.
- [37] E. Senel, "Some Carbonyl Compounds and Free Fatty Acid Composition of Afyon Kaymagi (clotted cream) and Their Effects on Aroma and Flavor" *Grasas y Aceites*, vol.62, no.4, pp. 418–427, 2011.
- [38] R. Paez, N. Pensel, N. Sabbag, M. Taverna, A. Cuatrin, C. Zalazar, "Changes in free fatty acid composition during storage of whole milk powder" *International Journal of Dairy Technology*, vol. 59, No.4, pp. 236-241, 2006.
- [39] K. Yıldırım, Z. Albay, E. Capa, B. Simşek, "Determination of the Chemical, Microbiological and Textural Properties of Kuru Kaymak (Dry Clotted Cream)" In Ö. D. Gürcü (Ed.), *Young Scholars Union Congress Proceeding and Abstarcts Book* . pp. 292. Prauge, 2019
- [40] P. F. Silva, R. G. Moreira "Vacuum frying of high-quality fruit and vegetable-based snacks " *LWT – Food Science and Technology* vol.41, pp.1758-1767, 2008.